Multi-Electron Transfer To and From Organic Molecules

by

Christopher Batchelor-McAuley

Submitted to the University of Oxford

for the degree of

Doctor of Philosophy

Physical and Theoretical Chemistry

February 2012

Contents

Acknowledgments

First and foremost, thanks must go to RGC for his guidance, motivation and his seemingly ceaseless willingness to give up his time over the last 3.5 years. Qian Li also requires an extra special mention due to her extensive help and efforts in the production of much of this work. It's been a pleasure to be a part of the group and to have had the opportunity to work with so many people. Away from the lab, Carly Collier deserves a commendation for putting up with me over the last month and still being willing to proof read sections!

Finally though, to fulfil a promise,
much love and thanks go to J.S. Ransom.

Abstract

Herein, the influence of protonation and adsorption upon the redox and electrocatalysis of quinone species – specifically anthraquinone derivatives – is investigated.

Through the comparison of the measured rate constants of one-electron reductions of a family of quinones in acetonitrile at both graphite and gold electrodes, it was confirmed that the redox potential indirectly influences the rate of electron transfer in a manner consistent with the potential-dependence of the density of states. In aqueous media, the voltammetric response of both anthraquione-2-sulfonate (AQMS) and anthraquinone-2,6-disulfonate (AQDS) was measured over the full aqueous pH range. A model is provided which is able to describe not just the variation in the formal potential but also the peak height as a function of pH. Importantly, this model predicts that the formal potential for the first ($E^{\ominus}_{f1}$) and second ($E^{\ominus}_{f2}$) electron transfers are comparable in magnitude ($E^{\ominus}_{f2} - E^{\ominus}_{f1}$ equals -15mV for AQMS and -36mV for AQDS). This quantitative model is then further extended to consider the situation in which the system is not fully buffered, giving insight into the change of pH at the electrode surface during experimentation.

Adsorption to graphitic electrodes can impart a strong influence on the measured voltammetric response. It is demonstrated that through the pre-exposure of a newly prepared graphitic electrode to organic solvents, these adsorption processes can be predominantly blocked. Moreover, it is shown that the electroactivity of the electrode is not *significantly* altered. This thesis also highlights two cases in which adsorption of the electroactive species may be used to positive effect. First, the surface adsorption of anthraquinone-2-monosulfonate is studied on a graphite electrode, where it is demonstrated that the heterogeneity of the electrode surface may be probed through studying the electrochemical response of the adsorbed species. From this work it is concluded that the rate of electron transfer at the graphitic basal plane is 2-3 orders of magnitude lower than that observed on the edge plane sites. Second, the co-adsorption of DNA and anthraquinone-2-monosulfonate is used as an indirect method to measure the solution phase concentration of DNA (LOD = 8.8μM).

The reduced form of anthraquinone is also known to readily reduce oxygen. Through the use of a boron-doped diamond electrode it was possible to directly study the anthraquinone mediated reduction mechanism. Significantly, the voltammetric response indicates the reduction of the oxygen via the semi-quinone intermediate ($k_f = 4.8 \times 10^9$ mol^{-1} dm^3 s^{-1}) is over two orders of magnitude faster than the reaction involving the di-reduced form ($k_f = 1 \times 10^7$ mol^{-1} dm^3 s^{-1}). More importantly, this work provides voltammetric evidence for the existence of the semi-quinone species. This work is subsequently extended through the investigation of the poorly soluble anthraquinone derivative quinizarin. Not only is it possible to detect voltammetrically this biologically relevant species to concentrations as low as 5nM (100ppt), but the methodology also allows the electrochemistry of the quinizarin species to be probed, something which was not previously possible.

The research presented in this thesis comprises work published in the following articles, listed in order of appearance within the text:

- Batchelor-McAuley, C., Wildgoose, G.G. and Compton, R.G. *Biosensors and Bioelectronics* 2009, 24, 3183–3190
- Batchelor-Mcauley, C., Dickinson, E.J.F., Rees, N.V., Toghill, K.E. and Compton, R.G. *Analytical Chemistry* 2012, 84, 669-684
- Nissim, R., Batchelor-Mcauley, C., Henstridge, M.C., Compton, R.G. *Chemical Communications* 2012, 48, 3294-3296
- Batchelor-McAuley, C., Li, Q., Dapin, S.M. and Compton, R.G. *Journal of Physical Chemistry B* 2010, 114, 4094–4100
- Batchelor-Mcauley, C., Kozub, B.R., Menshykau, D. and Compton, R.G. *Journal of Physical Chemistry C* 2011, 115, 714–718
- Batchelor-Mcauley, C., Gonalves, L.M., Xiong, L., Barros, A.A. and Compton, R.G. *Chemical Communications* 2010, 46, 9037–9039
- Neumann, C.C.M., Batchelor-Mcauley, C., Downing, C. and Compton, R.G. *Chemistry - A European Journal* 2011, 17, 7320–7326
- Xiong, L., Batchelor-McAuley, C., Gonalves, L.M., Rodrigues, J.A. and Compton, R.G. *Biosensors and Bioelectronics* 2011, 26, 4198–4203
- Li, Q., Batchelor-Mcauley, C., Lawrence, N.S., Hartshorne, R.S. and Compton, R.G. *Chemphyschem* 2011, 12, 1255–1257
- Li, Q., Batchelor-Mcauley, C., Lawrence, N.S., Hartshorne, R.S. and Compton, R.G. *Chemical Communications* 2011, 47, 11426–11428
- Batchelor-McAuley, C., Dimov, I.B., Aldous, L. and Compton, R.G. *Proceedings of the National Academy of Sciences of the United States of America* 2011, 108, 19891–19895
- Batchelor-Mcauley, C. and Compton, R.G. *Journal of Electroanalytical Chemistry* 2012, 669, 73-81

Glossary of Symbols and Abbreviations

	Roman Characters	
A	area	cm^2
a_i	activity of species i	mol cm^{-3}
C	concentration	mol cm^{-3}
C_{dl}	double layer capacitance	μF cm^{-2}
D	diffusion coefficient	cm^2s^{-1}
E	cell potential	V
$E^{\ominus}$	electrode potential under standard conditions	V
$E_f^{\ominus}$	formal electrode potential	V
F	the Faraday constant = 96485.3 C mol^{-1}	
$\Delta G^{\ominus}$	change in Gibbs energy under standard conditions	J mol^{-1}
I	current	A
I_p	peak current	A
I_{ss}	steady-state current	A
K_{eq}	equilibrium constant	
k^o	heterogeneous rate constant	cm s^{-1}
k	rate constant	
n	total number of electrons passed	
n'	number of electrons passed prior to the RDS	
r	electrode radius	cm
R	the gas constant = 8.31447 J K^{-1} mol^{-1}	
R_s	solution resistance	Ω
t	time	s
T	temperature	K
	Greek Characters	
α	Butler-Volmer transfer coefficient for reduction	
α_{RDS}	the transfer coefficient for the RDS electron transfer	
β	Butler-Volmer transfer coefficient for oxidation	
Γ	surface coverage	mol cm^{-2}
η	overpotential	V
λ	reorganisation energy	eV
Λ	the Matsuda-Ayabe parameter or a dimensionless reorganisation energy	
ν	scan rate	V s^{-1}

Chapter 1

Introduction

In part due to the extensive work undertaken during the mid-twentieth century on *homogeneous* (solution phase) electron transfer by among others, H. Taube[1] and also as a result of their *relatively* simple and reproducible results, metal complexes are invariably used as paradigmatic cases for the illustration of *heterogeneous* (interfacial) electrochemical processes and techniques. It is upon these experimental systems that, via the work of R.A. Marcus,[2] a framework for the molecular description of electron transfer is based. Importantly, the electrochemical responses observed for non-metallic species can be, and regularly are, significantly more complicated.

Organic redox-active species play highly important roles within numerous biological processes, ranging from photosynthesis[3] to neurotransmission[4]. In many cases the effective electrochemical analysis of these compounds would be desirable, either for assessment of an analyte concentration or, alternatively, as a method by which to probe the kinetics and thermodynamics of a biological pathway. However, the use of electrochemical techniques is often hindered due to a lack of specificity and sensitivity, arising commonly from the indiscriminate nature of the electrochemical probe. It is these problems that this thesis aims to address. This is achieved through both investigating the fundamental electrochemical processes as-

sociated with the redox chemistry of quinones as a 'model' organic system and by developing new methodologies by which these species may be investigated. This introduction briefly discusses the techniques and materials used throughout the course of this research.

1.1 Fundamentals

1.1.1 The Electronic Structure of Solids

The resistivity of solids varies over thirty-two orders of magnitude, ranging from values as low as 10^{-10} ohm·cm for pure metals up to 10^{22} ohm·cm for good insulators. This represents one of the widest parameter ranges for any common physical property.[5] Within the field of interfacial electrochemistry the majority of work solely utilises metallic electrodes. The electronic properties of the electrode are, perhaps correctly, assumed to impart minimal influence upon the observed electrochemical response. However, this thesis shall be focussing not just upon the use of metallic electrodes, and consequently consideration of the electronic structures of these solids is imperative.

An understanding of the electronic nature of a material may be gained through recognition that the energy levels available for an electron in a solid are

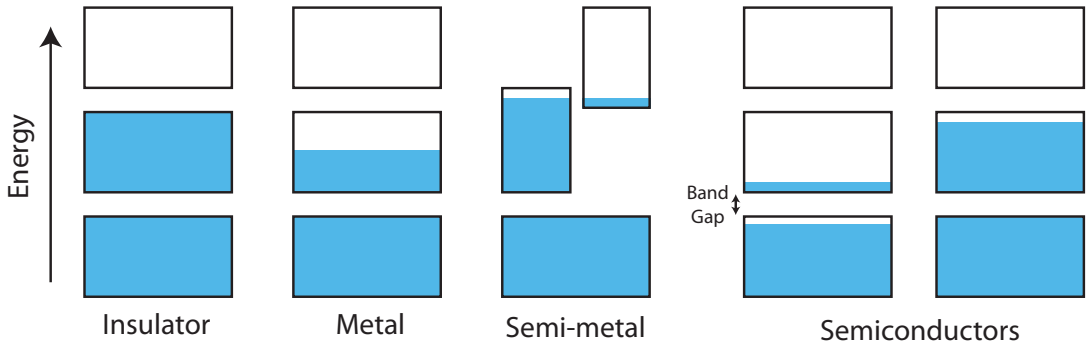

Figure 1.1: Schematic of the energy band structures of different solids. The boxes represent the allowed energy bands with the vertical axis representing increasing energy and shaded areas indicating the extent to which the energy band is filled. Figure adapted from Kittel.[5]

arranged into bands. Figure 1.1 depicts a schematic for the different physical cases. For cases in which the energy bands are either totally filled or empty the material is found to be insulating, alternatively if a band is approximately 10-90% occupied the material is metallic. Semi-metals and semiconductors represent cases where one or more band is partially filled. In regards to this thesis, the latter two cases are of particular note. It should also be highlighted that the distinction between a semiconductor and an insulator relates to the magnitude of the band gap such that a material is regarded as an *intrinsic* semiconductor when the band gap is small enough for electrons to be thermally excited to the higher energy band.

Apart from intrinsic semiconductors, materials may also be doped so as to increase a solid's conductivity. The energy level for the dopant is selected so as to be situated in the energy gap between the valence and conduction bands. Two cases may be considered here; either the dopant provides an unoccupied energy level above the valence band (n-type), or the dopant provides a filled energy level below the conduction band (p-type). Importantly for these *extrinsic* semiconductors, as the dopant concentration increases, a threshold value (n_c) may be reached inducing a metal-insulator transition, where at higher dopant levels the material is more metallic in nature.[6] Such heavily doped materials are commonly known as 'degenerate semiconductors.'

1.1.2 Capacitative Processes and the Double Layer

The application of a potential to an electrode in an electrolytic solution results in the build up of charge in the interfacial region. With a metallic electrode this charge is supported within a finite layer upon the surface, which is compensated for by an equal and opposite charge contained within a *diffuse* layer in the solution. To a first approximation this process may be regarded as being analogous to a capacitor in an electrical circuit. Hence, the charge held upon the interface may

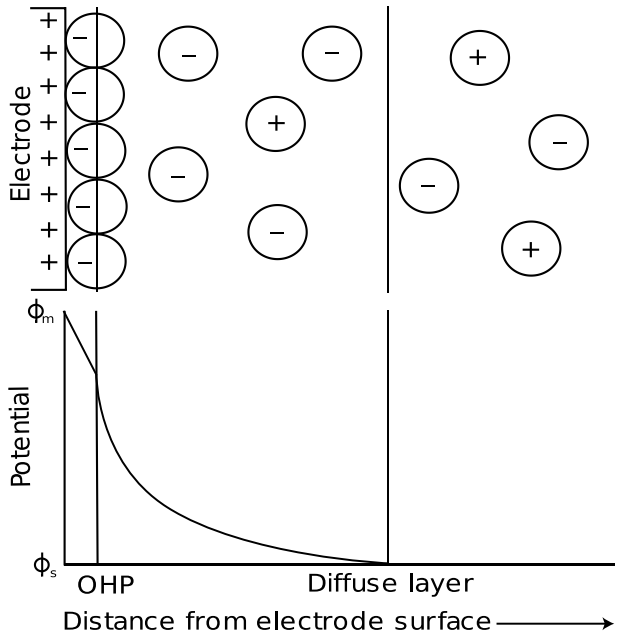

Figure 1.2: Schematic depicting the GCS model of the double layer and the variation of the potential as a function of distance, where ϕ_m and ϕ_s are the electrochemical potentials of the electrode and solution respectively.

be described by;

$$q_m = EAC_{dl} \tag{1.1}$$

where q_m is the charge upon the electrode in Coulombs, E is the potential applied across the interface in Volts, A is the surface area of the electrode (cm^2) and C_{dl} is the double layer capacitance measured in Farads per centimetre squared. Values of C_{dl} for real electrodes are found to be in the region of 10-40 μF cm^{-2}. Unlike an ideal capacitor, the value of C_{dl} for an electrochemical interface will vary as a function of potential.[7] In terms of experimentation it is illuminating to consider how the charge held upon the electrode varies as a function of time; this will be considered in a later section of this introduction.

The physical structure of the diffuse layer of charge held within the solution has received considerable attention over the years. Use of the Gouy-Chapman-Stern (GCS) model can, to a reasonable degree, explain the gross features of the

'double-layer'. Importantly here the ions in solution are taken to have a finite size and may only approach the electrode as close as their ionic radius. These ions may form a compact layer upon the electrode, designated as the 'Outer Helmholtz Plane' (OHP). Between the OHP and the electrode surface the potential drops linearly as a function of distance. Further out from the OHP the ions are contained within a diffuse layer, across which the potential drop may be viewed as decreasing in an exponential fashion. This variation in the potential as a function of distance from the electrode surface is shown schematically in Figure 1.2.

The extent of this double layer away from the electrode surface varies as a function of both potential and electrolyte concentration. Significantly, for experimental electrochemistry the double layer is compressed with increasing supporting electrolyte, such that, for a 0.1 M electrolyte solution (25°C) the double layer extends ∼10Å into solution, over such distances electron tunnelling may readily occur. In regards to Chapter 4, a second important conclusion of this model is that under conditions of low support the 'Potential of Zero Charge' - the point at which experimentally q_m is zero - may be measured as a minimum in the capacitance.

1.1.3 Faradaic Processes

Thermodynamics

For an electrode in a solution containing an electroactive species an equilibrium is established at the solid-liquid interface. Consider the simple case:

$$\mathrm{A}^{z}_{solution} + \mathrm{e}^{-}_{metal} \rightleftharpoons \mathrm{B}^{z-1}_{solution} \tag{1.2}$$

where A and B are species in solution with associated charges of 'z' and '$z-1$' respectively and e^{-} is an electron situated within the electrode. Depending on the relative *electrochemical* potentials of A, B and the electron prior to equilibration,

charge may either be transferred to or from the electrode on equilibration of the system. The electrochemical potential in a non-ideal solution differs from the chemical potential in that it takes into account the electrical energy of the species and may be defined as follows:

$$\mu_i = \mu_i^0 + RT \ln a_i + z_i F \phi \tag{1.3}$$

where μ is the electrochemical potential, μ^0 is the standard chemical potential, R is the gas constant, T is temperature, a_i is the activity of species i, z_i is the charge of species i, F is Faraday's constant and ϕ is the local electrostatic potential. In recognising that at equilibrium the electrochemical potentials for the products and reactants of Equation 1.2 are equal, then an expression for the difference in potential (E) for the metal (ϕ_{metal}) and solution ($\phi_{solution}$) phase is gained.

$$E = E^{\ominus} + \frac{RT}{F} \ln \left(\frac{a_{\mathrm{A}}}{a_{\mathrm{B}}} \right) \tag{1.4}$$

where $E^{\ominus}$ is the standard electrode potential. The above is the Nernst equation and provides a direct method of assessment of the thermodynamics of a system. However, due to most experiments being performed under high salt conditions the above form is normally adapted so as to be expressed in terms of concentrations not activities.

$$E = E_f^{\ominus} + \frac{RT}{F} \ln \left(\frac{[\mathrm{A}]}{[\mathrm{B}]} \right) \tag{1.5}$$

where $E_f^{\ominus}$ is the formal electrode potential. This is achieved via the assumption that the ionic strength and hence the activity coefficients of the species are (relatively) constant during experimentation.

Kinetics

Again looking at the simple example of a one electron reduction as outlined in Equation 1.2 and recognising that the current may be described via the equation below:

$$I = I_a + I_c = nFAj \tag{1.6}$$

where I is the net current passed, I_a and I_c are the anodic and cathodic currents respectively and j is the flux at the interface. We may define the current for the reduction (I_c) and oxidation (I_a) reactions as being equal to,

$$I_c = -FAk_{red}[\mathrm{A}] \tag{1.7}$$

$$I_a = FAk_{ox}[\mathrm{B}] \tag{1.8}$$

where k_{red} and k_{ox} are the electron transfer rate constants for the reduction and oxidation respectively. Classically the rate of electron transfer may be described via the well-known Butler-Volmer equation, as shown in Equations 1.9 and 1.10 for a one electron process:

$$k_{red} = k^0 exp\left[-\frac{\alpha F}{RT}\eta\right] \tag{1.9}$$

$$k_{ox} = k^0 exp\left[\frac{\beta F}{RT}\eta\right] \tag{1.10}$$

where k^0 is the standard electrochemical rate constant, α and β are the transfer coefficients and η is the overpotential ($E - E_f^{\ominus}$). These equations may be derived from the use of 'transition state theory.' The transfer coefficients (α and β) indicate the position of the transition state between reactants and products, where their sum is, for a one electron case, unity.[7] The newly introduced 'standard electrochemical rate constant' (k^0) represents the magnitude of k_{red} and k_{ox} at the formal potential. Importantly, this value of k^0 can be used as a guide to the 're-

versibility' or 'irreversibility' of a given redox couple. It should be highlighted that the above equations are presented for the case of a one electron transfer and that the discussion of the correct forms for multiple electron transfers is reserved until Chapter 12. Combining Equations 1.7, 1.8, 1.9 and 1.10 together yields the full expression for the rate of electron transfer as a function of potential:

$$I = FAk^0 \left(exp \left[\frac{+\beta F \eta}{RT} \right] [B] - exp \left[\frac{-\alpha F \eta}{RT} \right] [A] \right) \tag{1.11}$$

Two points should be made about this equation. First, for situations in which k^0 is large – such that the ratio of I/k^0 may be regarded as zero – then the equation collapses to that of the Nernst equation (1.5). Second, at very negative or positive overpotentials one of the exponential terms will be effectively zero. For example, at very negative overpotentials the recorded current is equal to:

$$I = -FAk^0 exp \left[\frac{-\alpha F \eta}{RT} \right] \tag{1.12}$$

where a plot of $\ln |I|$ versus η will yield a straight line, with a gradient proportional to the transfer coefficient. Such a form of graphical analysis is commonly referred to as a Tafel plot, the results of which readily allows the position of the transition state for an irreversible electron transfer to be experimentally determined.

Even given its successful application in a wide variety of experimental cases, problems with the Butler-Volmer formulation do exist. Primarily, Equation 1.11 does not predict a maximum rate of electron transfer. As the overpotential tends towards infinity so does the rate of electron transfer, which is physically unrealistic. Modern improvements upon this formulation have been achieved through the application of Marcus theory. Historically, Marcus theory was developed for *homogeneous* electron transfer. Its main premise is the assumption that the atomic configuration and the solvation shell of the reactants and products may be de-

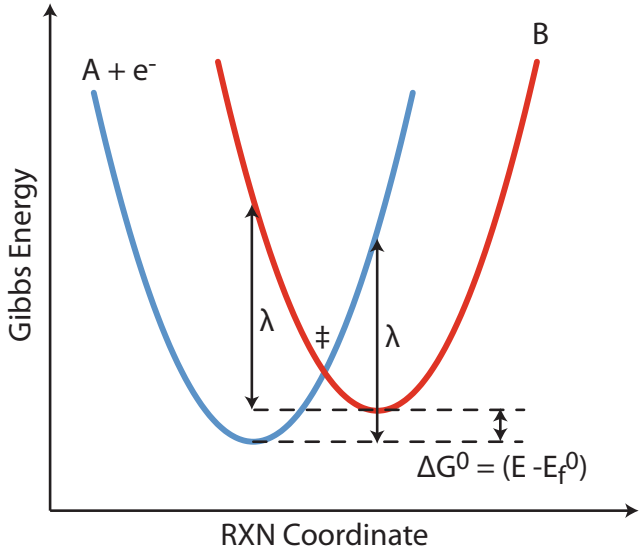

Figure 1.3: Gibbs energy curves as a function of the reaction coordinate for an electron transfer reaction according with the Marcus-Hush Model

scribed via parabolae. The curvature of the parabolae are described via the reorganisation energy (λ). This parameter represents the energy required to change the atomic configuration and the solvation shell of the reactants to being equal to that of the products in the absence of an electron transfer. Figure 1.3 is a schematic for the Gibbs energy curves for the electron transfer as a function of the reaction coordinate. In order for the electron transfer to occur the reactants must be thermally excited up to a transition state (‡). Upon reaching this transition state the electron transfer may occur without the loss or gain of energy (a radiationless transition). The energy required to reach the transition state ($\Delta G^{\ddagger}$) is described via the reorganisation energy.

The main prediction of this theory is that for highly thermodynamically driven reactions the rate of electron transfer is found to decrease with increasing overpotential. This effect is known as the 'inverted region' but such effects are *not* observed for electron transfer at *metallic* electrodes. This arises due to the presence of a continuum of electronic energy levels within the material. Consequently, at

high overpotentials the energy level of a redox species is able to overlap with a level within the metal away from the fermi energy. Thus, experimentally a levelling off of the rate of electron transfer is observed where excess energy is dissipated as heat. The expressions for the Marcus-Hush formalisation of electron transfer are presented in Chapter 4. As a final point it is of interest that for semiconductor electrodes it is possible to observe the inverted region, due to the limited number of energy levels available. This was experimentally demonstrated through the use of a zinc oxide electrode substrate.[8]

1.2 Electrochemical Cells

Up until this point the discussion presented within this introduction has been solely focused upon the reaction occuring at a single electrode surface. However, in order to experimentally study an electrochemical system a closed circuit is required, which necessitates at least two electrodes. For a two electrode cell as depicted in Figure 1.4, the potential difference is being equal to:

$$\text{potential difference} = (\phi_m - \phi_s)_{\text{electrode 1}} - (\phi_m - \phi_s)_{\text{electrode 2}} + IR_s \qquad (1.13)$$

where the first and second terms are the potential difference at the first and second electrode interfaces respectively. The third term is the ohmic drop through the solution, with R_s being the solution phase resistance. Commonly, the second electrode is a *reference* electrode which has a well defined potential and is relatively stable; examples for aqueous setups include the *saturated calomel electrode* and the *silver/silver chloride* electrode. Assuming non or minimal current is passed, this enables the potential difference at the electrode of interest to be assessed. However, if we pass a current through this system then Faradaic processes occur at the electrode interfaces and thus there will be an associated change in the

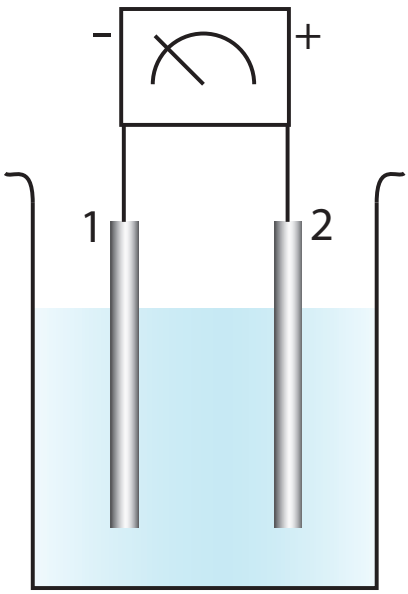

Figure 1.4: Schematic for a two electrode setup, with the voltammeter measuring the potential difference of two electrodes in an electrolytic solution.

concentration of species adjacent to the electrode. Further, we know from Equation 1.5 that the formal potential for a species will vary as a function of concentration, consequently in passing a current through the system the potential held at the reference electrode will no longer be a constant. Moreover, the term for the Ohmic drop (IR_s) through solution will also be a variable as a function of the current. In order to study an electrochemical reaction of interest at an electrode surface a three electrode set up is required.

The three electrode system comprises of a working electrode, a counter electrode and a reference electrode. The working electrode is the electrochemical interface of interest and the potential at this surface is held relative to the reference electrode. Effectively no current is passed between these two electrodes, hence minimising the value of the Ohmic drop in solution and ensuring that the potential at the reference electrode does not vary during experimentation. However, a current is passed between the working and counter electrode. This experimental system is

controlled through the use of a potentiostat, allowing the potential applied to the working electrode to be varied as a function of time.

As a final point on electrochemical measurements, within non-aqueous media the selection of suitable reference electrode systems is more limited, with a *silver-silver nitrate* electrode being one of the few viable options.[9] This silver-silver nitrate electrode is not without problems, in as much as it is light sensitive and so requires regular cleaning and renewal. Consequently, within non-aqueous media it is not uncommon to utilise a *pseudo* reference such as a clean silver wire. Problematically, such electrodes are prone to potential drift and so the extraction of thermodynamic data must be undertaken with some level of caution. To overcome this problem, an 'internal' reference commonly a stable redox couple like ferrocene/ferrocenium, may be utilised. The internal reference allows the pseudo reference electrode to be calibrated during each experiment, although it should be noted that this methodology is not always applicable due to interaction of the internal reference with the electrochemical system of interest.

1.3 Mass-Transport

Before looking further at the electrochemical experiments utilised within this work it is necessary to provide some information regarding the mass-transport of species in solution. There are three forms of mass-transport that may affect electrochemical reactions of solution phase species, namely: migration, convection and diffusion. In the majority of experiments, migration (the movement of ions within an electric field) is avoided through the use of high concentrations of supporting electrolyte. In such cases of 'high support' – as utilised throughout this research – the electric field is confined to a region close to the electrode interface. Only a limited number of studies have broached the problem of electrochemical experiments under 'low support,' partly because such systems require a large amount of computation

and theory in order to extract physically significant information.[10] Convection, on the other hand, has a far more prominent role within the literature and represents movement due to physical means. Broadly, this form of mass-transport may be characterised as being either 'natural' or 'forced.' Natural convection arises due to small thermal or density differences in the solution, causing movement in an unpredictable manner. Hence, it is generally preferable to avoid natural convection.[11] Consequently, experiments at macroelectrodes are limited to being, at maximum, ∼20 seconds in length. However, forced convection historically plays a dominant role within the field in the form of *hydrodynamic* experiments. Such work encompasses, amongst others, rotating disk, wall-jet and flow cell systems (channel and tubular).[12] In all cases the convective flow at the electrode surface is reproducible and relatively easily understood. Within this work mass-transport for solution phase species is limited to being diffusion only; the gain of which is that the results are readily analysable. The remainder of this section presents an understanding of diffusion.

Diffusion occurs due to a system maximising its entropy. Consequently, in the presence of a concentration gradient there is a net flux towards the region of lower concentration. Mathematically, diffusion is aptly described via the use of Fick's laws. Fick's first law states that at a given point the flux (j) is proportional to the diffusion coefficient (D) times by the concentration gradient[13]. In one dimension (x) this may be written as:

$$j = -D\frac{\partial[i]}{\partial x} \tag{1.14}$$

where $[i]$ is the concentration of species i. From this Fick's second law may be derived;

$$\frac{\partial[i]}{\partial t} = D\frac{\partial^2[i]}{\partial x^2} \tag{1.15}$$

which describes how the concentration varies as a function of time (t); see Appendix A.1 for a derivation. Importantly, the value of D gives a measure of how far a molecule can travel during a period of time. More precisely, the root mean squared displacement in one dimension is given by,

$$\sqrt{\langle x^2 \rangle} = \sqrt{2Dt} \tag{1.16}$$

Further, it should be noted that the diffusion coefficient is highly temperature dependent, where it is commonly described as exhibiting Arrhenius type behaviour. Generally, values of D for solution phase species are in the range of 1-10$\times 10^{-6}$ cm^2 s^{-1} (25°C). Within aqueous solutions the diffusion of both protons and hydroxide ions are notable exceptions, where both species have significantly higher values due to the so called 'Grotthuss' mechanism.[14] However, it is important to highlight that diffusion in solutions is a slow process. After one second the root mean squared displacement of a molecule with a diffusion coefficient of 1×10^{-5} cm^2 s^{-1} will only be 50 μm.

This section shall now look towards more practical uses of Equations 1.15 and 1.16. Consider the experimental situation where an electrode is submerged into a solution containing an electroactive species A, at time equals zero ($t = 0$) the potential is jumped to a value at which A is reduced to B, via a one electron transfer. Experimentally this is equivalent to the recording of a chronoamperogram. Assuming that the potential is of a large enough magnitude that the electron transfer is *not* the rate determining step then, through the use of Equation 1.16 the concentration of species A may be defined both as a function of time and distance from the electrode as shown below,[15]

$$[\mathrm{A}]_x = [\mathrm{A}] \operatorname{erf}\left(\frac{x}{2\sqrt{Dt}}\right) \tag{1.17}$$

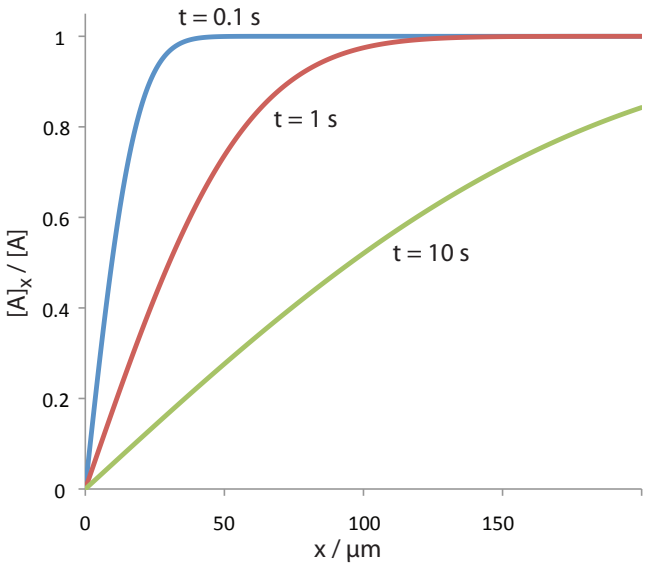

Figure 1.5: Concentration profiles at varying times after a potential step D = 1×10^{-5} cm^2s^{-1}.

where 'erf' is the error function, $[A]_x$ is the concentration of species 'A' at a distance x from the electrode and [A] is the bulk concentration (derivation of this is equation is provided within Appendix A.2). Figure 1.5 depicts the concentration profiles as defined by Equation 1.17 for species A at varying times after the potential step. Further, from use of this equation we may also define a 'diffusion layer,' representing the distance from the electrode where, at a given time, the concentration is equal to 99.7% of the bulk solution. In one dimension this corresponds to a value of $3 \cdot \sqrt{\langle x^2 \rangle}$. Moreover, the differential of Equation 1.17 with respect to the distance x from the electrode allows via the use of Fick's first law (Equation 1.15) an expression for the current as a function of time to be provided and this result is the well-known Cottrell equation:[16]

$$I = \frac{FA\sqrt{D}[A]}{\sqrt{\pi t}} \tag{1.18}$$

where A is the geometric area of the electrode. It is of particular note that this expression tends to zero as time goes to infinity.

These results as presented are for a *linear* diffusion regime as found for experiments at macroelectrodes (radius $\gtrsim$1 mm). However, for situations in which the distance diffused by the species is of the same order of magnitude (or larger) than the dimensions of the electrode, the concentration profiles and hence the current response is altered. Such a situation is commonly encountered with the use of microelectrodes. For these systems the electrode surface is not uniformly accessible. In order to be able to describe the diffusion to a microelectrode, a two dimensional coordinate system is required. Due to the electrode being of the same order of magnitude or smaller than the diffusion layer thickness, the diffusion to the electrode surface may be described as being 'radial'. Radial diffusion leads to more efficient mass-transport to the electrode surface and consequently higher diffusional current densities are observed at the electrode surface. However, this two dimensional diffusion problem is not analytically solvable. The current at the microelectrode during chronoamperometry may be described empirically by the Shoup and Szabo equation as expressed below:[17]

$$I = 4F[\mathrm{A}]Drf(\tau) \tag{1.19}$$

$$f(\tau) = 0.7854 + 0.4431\tau^{-0.5} + 0.2146\exp\left(0.39115\tau^{-0.5}\right) \tag{1.20}$$

where

$$\tau = \frac{Dt}{r^2} \tag{1.21}$$

and r is the radius of the electrode. At short times this gives a Cottrellian type response, i.e. linear diffusion, whereas at long times the equation reduces to:

$$I_{ss} = 4F[\mathrm{A}]Dr \tag{1.22}$$

Equation 1.22 is the steady-state current at a microdisc, which highlights an

important difference between the two diffusional cases. For situations in which the electrode dimensions are significantly larger than the diffusion layer thickness ($r >> \sqrt{\langle x^2 \rangle}$) then diffusion to the electrode may be viewed as being linear and the current during a chronoamperomogram decreases towards zero as a function of time. Conversely, for a microelectrode where the dimension of the electrochemical interface are comparable or smaller than the diffusion layer thickness then a chronoamperomogram decreases to reach a steady state value at long times. This reflects the more efficient mass transport to the electrode surface.

1.4 Voltammetry

During the course of the previous sections the experimental technique of chronoamperometry has been introduced. The following section considers the case in which the potential is swept linearly as a function of time. Although, as will be demonstrated, this technique is a powerful tool, the convolution of the time and potential domains leads to complex results. In fact, for the case of a diffusional species the current time response is not analytically tractable.[18] Before moving to this more complex system we shall briefly consider first the influence of capacitance upon a voltammogram, and second the voltammetric response of a surface bound species.

For a linear sweep voltammogram the potential held upon the electrode (E) is equal to the scan rate (Vs^{-1}) multiplied by time (s). For a cyclic voltammogram a second sweep is performed after the first scan, reversing the scan direction and returning the potential held upon the electrode back to its original value. As discussed earlier in its most basic form the electrochemical interface, in the absence of electroactive species, can be viewed as acting in an analogous manner to a capacitor in an RC circuit. The measured capacitive current may be defined as

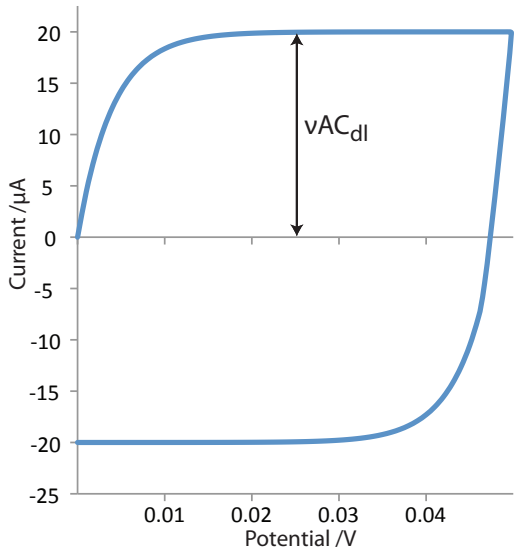

Figure 1.6: Simulated cyclic voltammogram showing the expected response of an electrode where the charging current is taken to be equivalent to an RC circuit. $R = 200\ \Omega$, $AC_d = 2\ \mu F$ and $\nu = 10\ \mathrm{Vs}^{-1}$

being equal to:

$$I = \nu AC_{dl}\left[1 - \exp\left(\frac{-t}{R_s AC_{dl}}\right)\right] \tag{1.23}$$

see Appendix A.3 for a derivation. Consequently at times significantly larger than the product $R_s AC_{dl}$ the measured current is equal to νAC_{dl}. Figure 1.6 depicts the current expected for an RC circuit as a function of applied potential (E), where the scan rate has been set at $10\mathrm{Vs}^{-1}$, R_s is 200 Ω and AC_{dl} is 2 μF. This method of measurement of an electrode's capacitance is used experimentally in Chapter 4 for assessment of the variation in the capacitance as a function of potential.

For a surface bound electroactive species which can undergo a one-electron transfer as described by Equation 1.24, the total surface coverage of the redox species is equal to the sum of the surface coverages of the reduced and oxidised forms.

$$\mathrm{A}_{\mathrm{adsorbed}} + \mathrm{e}^-_{\mathrm{metal}} \rightleftharpoons \mathrm{B}_{\mathrm{adsorbed}} \tag{1.24}$$

Further, if the species are non-interacting upon the electrode surface and the rate

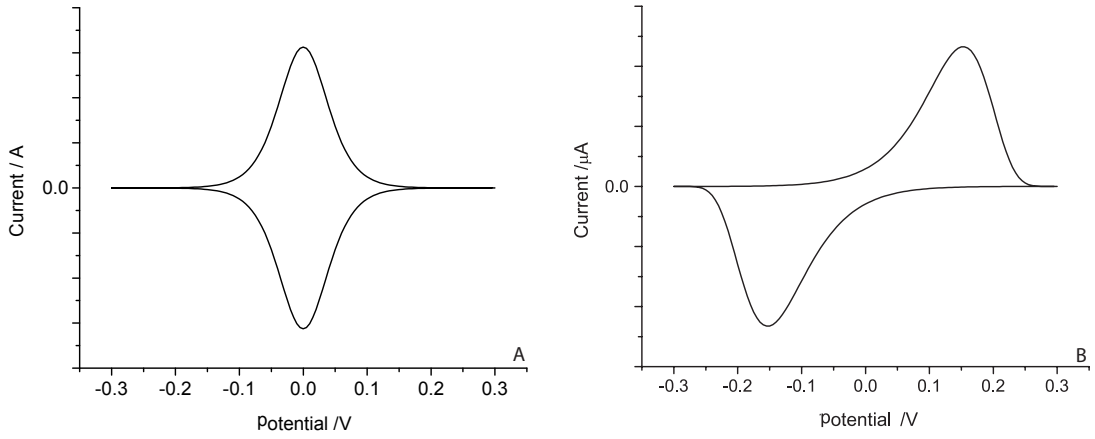

Figure 1.7: Idealised cyclic voltammetric response of A) a reversible and B) an irreversible surface bound species.

of electron transfer is sufficiently large, such that the surface coverage of the electroactive species are at equilibrium, then Figure 1.7 A depicts the expected form of the voltammetric response. Of note is the symmetric nature of the waves where the peak positions are situated at the formal potential for the redox couple. Importantly, for such systems the total surface coverage of the electroactive species is readily determined through measurement of the Faradaic charge passed during the voltammetric experiment. This procedure is of particular importance in Chapter 9.

Due to the finite nature of the rate of electron transfer, as the scan rate is increased the electron transfer becomes *relatively* slower over the time frame of the experiment. Consequently, at high scan rates the surface coverages of species A and B are not at equilibrium and hence can not be described via the Nernst equation. For such situations the electron transfer is termed 'irreversible' and Figure 1.7 B depicts the expected response for such a system. A marked difference is observed from the reversible example. First, the wave shape is no longer Gaussian. Second, the peak currents for the forward and backward wave do not occur at the same potential. It is highlighted that the formal potential for the electron transfer may still be estimated through measurement of the mid-point potential, although the

peaks may not be equi-distant from the formal potential depending on the value of the transfer coefficient. The variation of the peak positions as a function of scan rate provides a method by which the rate of electron transfer may be readily assessed. Commonly, the peak position is plotted versus the natural log of the experimental scan rate from which the rate of electron transfer may be assessed and for such analysis the peak-to-peak separation must be at least 200 mV, for a one electron transfer.[19]

For a diffusional species the definition of an electrochemical process as being 'reversible' or 'irreversible' is more complex. Not only is it dependent upon the scan rate and the rate of electron transfer (as for the diffusionless case), but importantly the rate of mass-transport to and from the electrode surface is influential. The reversible situation dictates that the concentrations of the reduced and oxidised species are at equilibrium at the electrode surface; however if the rate of mass-transport is high then it is feasible for the redox species to be removed from the electrode surface prior to reaching equilibrium. This factor is most influential upon the observed voltammetric response at microelectrodes; as already noted the mass-transport to microelectrodes is more efficient. Equally for the reaction products the mass-transport away from the electrode is also efficient, leading to divergent diffusion. As a result the *apparent* reversibility for a redox couple at a microelectrode is strongly dependent upon the diffusion coefficient of the redox species and the electrode size. This point is exemplified further within Chapter 4. Whilst discussing microelectrodes it should also be noted that their voltammetric wave shape differs significantly from that observed at a macroelectrode. Experimentally a sigmoidal waveform is observed with no back-peak.

Figure 1.8 depicts the simulated voltammetric response for a diffusional species at a macroelectrode. On the forward wave for all three cases as depicted three distinct regions may be observed. First, at low overpotentials no Faradaic

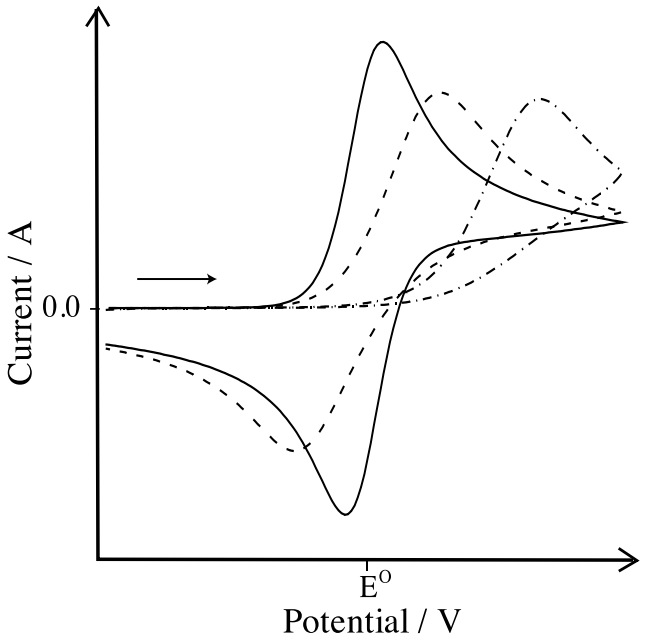

Figure 1.8: The simulated voltammetric response for a diffusional species at a macroelectrode. The solid line depicts a fully reversible electron transfer, the dashed line is a quasi reversible electron transfer and the dot-dashed line is an irreversible electron transfer. The arrow indicates the scan direction.

current is passed, as the electrode potential is insufficient to induce electron transfer. Second, as the potential increases, a near exponential increase in the current is measured. For the reversible case this relates to the Nernstian formation of the product at the electrode surface. Alternatively, for the irreversible situation the increase in current follows the Butler-Volmer equation (1.11). Third, as the current increases further, depletion of the electroactive species at the electrode surface results in the appearance of a peak; at this potential and at higher values the current is diffusion limited. On the reverse scan for the reversible species, a back-peak is observed relating to the re-oxidation or reduction of the formed product at the electrode surface. Conversely, no back peak is observed for the irreversible situation. In the irreversible limit, due to the high overpotential required for the reverse reaction to occur, upon reaching the appropriate potential the product has had sufficient time to diffuse away from the electrode. The quasi-reversible case

represents a situation between these two limits.

Analytically, voltammetric waves are commonly quantified in terms of their peak heights and peak-to-peak separation. As before for the surface bound case, the variation of the peak-to-peak separation as a function of scan rate allows the rate of electron transfer to be readily determined. It is of interest that even for a fully reversible case the peak-to-peak separation is non-zero ($\sim$59mV for a one electron transfer at 25°C). This reflects the influence of the mass-transport upon the system, where the peak occurs at the potential at which the concentration of the electroactive species adjacent to the electrode surface is zero. The use of the voltammetric peak height as a diagnostic tool, via use of the Randles-Ševčík equation, shall be discussed in greater depth in both Chapters 5 and 12.

1.5 Electrode Materials

As alluded to at the beginning of this Introduction, the electronic structures of solids vary enormously. This final section of this introduction looks in more detail at the properties of both graphite and boron doped diamond, both of which are used as electrode materials within this thesis.

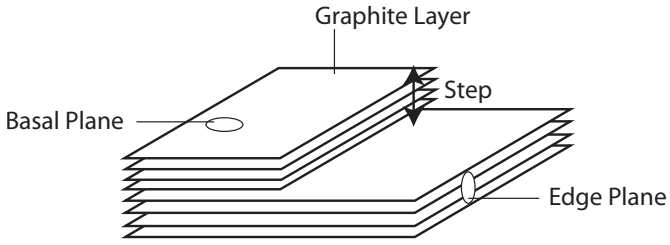

Figure 1.9: Schematic of the material structure of graphite highlighting the layered structure which exhibits both basal and edge plane sites.

1.5.1 Semi-Metallic: Graphite

The structure of graphite comprises of layers of sp2 carbon arranged into a hexagonal lattice. Conduction occurs through the overlapping p-orbitals present perpendicular to the carbon planes. A schematic of the material's structure is shown in Figure 1.9. Importantly, graphite is a semi-metallic material with the valance and conduction bands overlapping at the fermi level. The density of states for graphite at its fermi level is approximately 5% that of gold on a per volume basis.[20,21] The influence of the material's electronic structure upon its electrochemical response is investigated within Chapter 4.

The layered structure of graphite leads to the observed properties being highly anisotropic. Significantly, in terms of electrochemistry the conduction parallel and perpendicular to the planes is reported to differ by a factor of between 10^2-10^4.[22] Furthermore, the surface densities of states at the edge and basal plane sites are found to differ significantly. This difference can be observed experimentally through the use of scanning tunnelling microscopy.[23] Consequently, the properties of a graphitic electrode are altered depending upon the crystal alignment. In general, lower rates of electron transfer are observed for electrodes in which the lattice layers are aligned parallel to the electrode surface (basal) as opposed to perpendicular (edge).[24] The difference in electrochemical activity of the basal and edge plane electrodes is explored further in Chapter 8.

1.5.2 Semiconductor: Boron-Doped Diamond

In the absence of doping, diamond has a wide band gap of 5.5 eV and the addition of boron provides an unoccupied energy level situated 0.37 eV above the top edge of the valence band.[25] It is theoretically predicted that upon reaching a threshold dopant concentration (n_c) the conductivity of the solid will increase rapidly. This occurs at the point at which the groundstate wavefunctions for neighbouring

dopant atoms overlap significantly, forming a continuous energy band throughout the structure. For boron-doped diamond this metal-insulator transition is predicted to occur at a dopant level of 4.5×10^{20} atoms per cm^{-3}; importantly, this result has been confirmed experimentally.[26] The boron-doped diamond utilised within this work is reported to have an *average* boron concentration of $\sim2\times10^{20}$ atoms cm^{-3}.[27] As shall be discussed, this relatively low value may impart a significant effect upon the material's electrochemical response.

The boron-doped diamond surface is known to be heterogeneous, exhibiting areas of high and low conductivity. This variation in the surface activity is perhaps best demonstrated by studying metal deposition onto the electrode surface. Figure 1.10 depicts a representative scanning electrochemical microscopy image of a nickel nanoparticle modified boron doped diamond surface, clearly showing the different electroactive domains. This variation in the electroactivity of the surface has been ascribed as being related to the grain-dependent uptake of boron during manufacturing.[28] Consequently, given that the reported boron concentration is comparable to the value for n_c, it would seem credible that the large variation in the surface activity is directly related to the electronic structure of the material.

It is worth noting that although the conduction of boron-doped diamond may be described as being *metallic* in nature, due to the material being a degenerate semiconductor, this does not necessarily imply that the electrochemical properties are expected to be equivalent to that of a metal. Certainly, the dopant band is likely only to be of the order of 0.2 V in width.[29] Thus, it may be predicted that the density of states for the material at the fermi level will be of the order of 1×10^{21} states eV^{-1} cm^{-3}, as compared to a value of 1.65×10^{22} states eV^{-1} cm^{-3} for gold. Furthermore, experimentally the rate of electron transfer at boron-doped diamond electrodes is regularly found to be significantly lower. In fact it is this lower rate of electron transfer that shall be exploited within Chapters 10 and 11

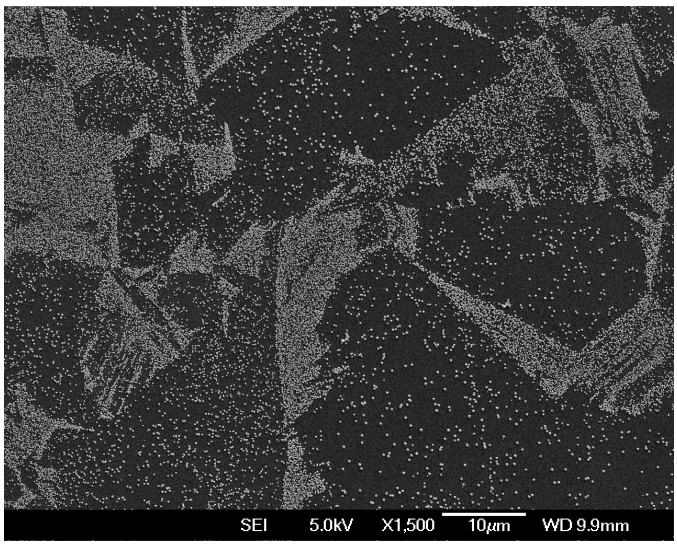

Figure 1.10: SEM image of a nickel modified boron doped diamond electrode, showing the different electroactive domains

so as to allow selective reduction of a species at the electrode surface.

This chapter has provided a brief outline of the theoretical basis underpinning this thesis. The following chapter provides a review of the state-of-the-art methods for electrochemical DNA detection.

References

[1] Taube, H. *Angew. Chem. Int. Ed.* **1984**, *23*, 329–339.

[2] Marcus, R. A. *Angew. Chem. Int. Ed.* **1993**, *32*, 1111–1121.

[3] Gray, H. B.; Winkler, J. R. *Ann. Rev. Biochem.* **1996**, *65*, 537–561.

[4] Amatore, C.; Arbault, S.; Guille, M.; Lemaître, F. *Chem. Rev.* **2008**, *108*, 2585–2621.

[5] Kittel, C. *Introduction to Solid State Physics 8th Ed.*; Wiley Int. Ed., 2005.

[6] Ashcroft, N.; Mermin, N. D. *Solid State Physics*; Harcout, Inc, 1976.

[7] Bard, A. J.; Faulkner, L. R. *Electrochemical methods: fundamentals and applications*; Wiley, 2001.

[8] Hamann, T. W.; Gstrein, F.; Brunschwig, B. S.; Lewis, N. S. *J. Am. Chem. Soc.* **2005**, *127*, 7815–7824.

[9] Kolthoff, I. M.; Thomas, F. G. *J. Phys. Chem.* **1965**, *69*, 3049–3058.

[10] Belding, S. R.; Limon-Petersen, J. G.; Dickinson, E. J. F.; Compton, R. G. *Angew. Chem. Int. Ed.* **2010**, *49*, 9242–9245.

[11] Amatore, C.; Pebay, C.; Thouin, L.; Wang, A.; Warkocz, J.-S. *Anal. Chem.* **2010**, *82*, 6933–6939.

[12] Rees, N. V.; Compton, R. G. *Russ. J. Electrochem.* **2008**, *44*, 368–389.

[13] Fick, A. *Poggendorff's Annel. Physik.* **1855**, *94*, 59–86.

[14] Agmon, N. *Chem. Phys. Lett.* **1995**, *244*, 456–462.

[15] Compton, R. G.; Banks, C. E. *Understanding Voltammetry 2nd Ed.*; Imperial College Press, 2011.

[16] Cottrell, E. G. *Z. Physik. Chem.* **1902**, *44*, 385.

[17] Shoup, D.; Szabo, A. *J. Electroanal. Chem.* **1982**, *140*, 237.

[18] Nicholson, R. S.; Shain, I. *Anal. Chem.* **1964**, *36*, 706–723.

[19] Laviron, E. *J. Electroanal. Chem.* **1979**, *101*, 19–28.

[20] Dahn, J. R.; Reimers, J. N.; Sleigh, A. K.; Tiedje, T. *Phys. Rev. B* **1992**, *45*, 3773–3777.

[21] McCreery, R. L. *Chem. Rev.* **2008**, *108*, 2646–2687.

[22] Chung, D. D. L. *J. Mat. Sci.* **2002**, *37*, 1475–1489.

[23] Niimi, Y.; Matsui, T.; Kambara, H.; Tagami, K.; Tsukada, M.; Fukuyama, H. *Appl. Surf. Sci.* **2005**, *241*, 43–48.

[24] Banks, C.; Compton, R. *Analyst* **2006**, *131*, 15–21.

[25] Yokoya, T.; Nakamura, T.; Matsushita, T.; Muro, T.; Takano, Y.; Nagao, M.; Takenouchi, T.; Kawarada, H.; Oguchi, T. *Nature* **2005**, *438*, 647–650.

[26] Klein, T.; Achatz, P.; Kacmarcik, J.; Marcenat, C.; Gustafsson, F.; Marcus, J.; Bustarret, E.; Pernot, J.; Omnes, F.; Sernelius, B. E.; Persson, C.; Ferreira da Silva, A.; Cytermann, C. *Phys. Rev. B* **2007**, *75*, 165313.

[27] *http://www.windsor-ltd.co.uk/Boron-Doped-Diamond.html*.

[28] Wilson, N.; Clewes, S.; Newton, M.; Unwin, P.; Macpherson, J. *J. Phys. Chem. B* **2006**, *110*, 5639–5646.

[29] Baskaran, G. *J. Supercond. Nov. Magn.* **2008**, *21*, 45–49.

Chapter 2

Electrochemical Methods of DNA Detection- A Review

The review presented within this chapter comprises material used in two published reviews: *Biosensors and Bioelectronics* 2009, 24, 3183–3190 and *Analytical Chemistry* 2012, 84, 669–684.

First isolated by Friedrich Miescher in 1869, deoxyribonucleic acid (DNA) is one of the most fundamental molecules to biological life. As a consequence of Oswald T. Avery's work during the 1940s it was shown that DNA is responsible for the storage and transfer of a cell's genetic information.[1] Following this a substantial body of work was focused on determining the structure of DNA, culminating in the paper by Watson and Crick in 1953 in which the classical double helix form was proposed.[2] This paper provided the first model for a major macromolecular cellular component, allowing a basis for new theories for a variety of cellular biological processes.[3] Over the last fifty years intensive work has gone into elucidating the role of DNA within a wide variety of biological fields. During the late 1990's the Human Genome Project was established with the aim to identify all of the 20,000-25,000 genes present in human DNA. With the knowledge of how these genes affect us, there is an ever increasing demand for simple and reliable methods for their analysis.

Importantly it is the genetic mutations within our genetic code which allows us, as a species to evolve, but which also lead to a multitude of diseases.[4] Single-nucleotide polymorphisms (SNPs) are a common form of genome variation where there is a single alteration to the base sequence, which may lead to the adaptation of a gene's given function. The ability of a DNA biosensor to be able to differentiate between a fully complementary sequence and one in which there is a single change is obviously of great importance. Current commercial (non-electrochemical) methods for DNA testing are restricted by the need for extensive sample treatment undertaken by skilled personnel. Alternative systems, that will allow the miniaturisation of these procedures enabling the production of portable point-of-care devices able to screen for a number of genetic disorders, are desired. Due to the comparative ease with which electrochemical methods may be miniaturised and the lower associated costs, they may enable this objective to be fulfilled.

This review aims to look first, at the underlying physicochemical properties of DNA and its hybridisation and second, how present electrochemical methods approach the problem of DNA detection. These methodologies may broadly be characterised as 'non-labelled' or 'labelled' procedures. Of the former type, systems include the direct oxidation or reduction of the DNA, surface capacitance measurements or the use of 'Nanopore' technology. Labelled approaches tend to be more involved and commonly utilise a redox active species, which may be bound to the DNA either chemically or via intercalation. The variation of the voltammetric response of this redox species is used to electrochemically characterise the DNA hybridisation event.

2.1 DNA Structures and Hybridisation

The classic double helix structure of double stranded DNA (dsDNA) is well known and is easily recognised not just within the scientific community. Although com-

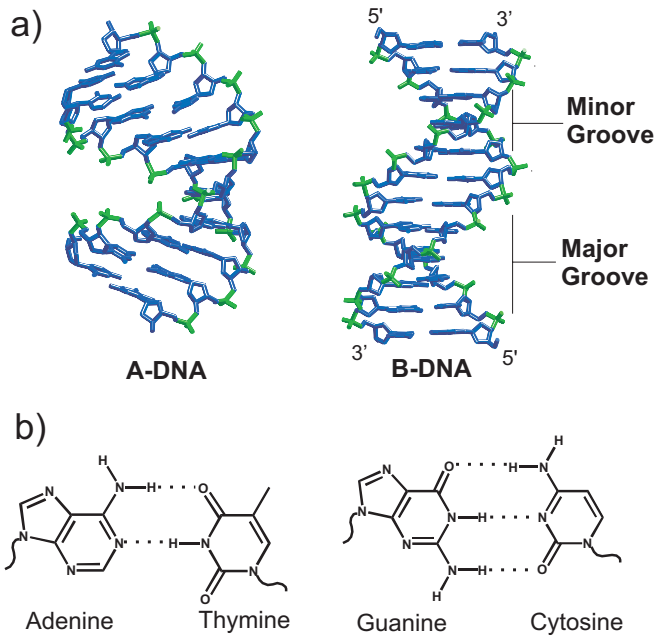

Figure 2.1: a) Diagram showing the crystal structure of A-DNA and B-DNA (crystal structures obtained from the nucleic acid database.[5] b) Chemical structures of the 'Watson and Crick' paired bases; adenine and thymine, and guanine and cytosine.

mon, the double helix is not the only possible configuration for DNA to take, with some configurations being radically different to the Watson and Crick proposed structure.[3] In physiological conditions A-DNA, B-DNA (Watson and Crick structure) and Z-DNA have all been observed. Figure 2.1, a) shows the crystal structures for two DNA sequences with 'A' and 'B' configurations b) depicts the structure of the nucleobase pairs present within DNA. The conformation assumed by a length of DNA is dependent on a variety of factors including, the base pair sequence[6] and the supporting environment.[7,8] These three conformations (A, B and Z) all consist of two antiparallel strands bound together through hydrogen bonding. Unlike the other two major conformations Z-DNA differs in exhibiting a left-handed double helical structure, this structure is found to often occur with G-C rich sequences in high salt conditions.[9] With B-DNA the interwinding of the DNA strands leads to a structure in which there is two distinct grooves spiralling around the DNA duplex as labelled within Figure 2.1.

DNA is a semiflexible polyelectrolyte. Due to the charged nature of polyelectrolytes, within solution their flexibility and conformation differs to that of an uncharged polymer. Coulombic repulsions between the phosphate groups of the DNA backbone results in its flexibility and structure being dependent on the supporting salt concentration. Through heating dsDNA and breaking the weak hydrogen bonds the two strands may be separated (denatured). The thermodynamic stability of dsDNA is frequently quoted as the melting temperature (T_m), at which 50% of the sample has denatured.[10] It has long been known that this property is dependent on the length, make up of the sample, and is also solvent dependent. For longer sequences of DNA it is possible to estimate the T_m purely through the percentage of guanine and cytosine base pairs present, but for shorter lengths, this is less applicable and a more rigorous approach has to be utilised in which the effect of the sequence is taken into account. In these so called nearest neighbour (NN) approximations the summation of the energies between the adjacent bases results in a value for the melting temperature.[11] This work on the NN model is reviewed by SantaLucia,[12] in which the results of seven studies are compared, allowing the author to present a unified NN model.

On cooling ssDNA in the presence of a complementary sequence, the process of denaturation may be reversed where the bases pair together to form dsDNA (hybridisation). It is possible for strands of DNA that are not fully complementary to pair but the number of mismatches affects the stability of the dsDNA and consequently lowers the melting temperature. The effect of single base pair mismatch on the stability of the dsDNA is of significance for biosensors, such that the difference in thermodynamic stability can be used to differentiate between closely related sequences. Early work by Bonner *et al.*[13] demonstrated that for DNA strands in solution that are ∼150 bases long, a 10°C reduction in the Tm corresponded to approximately a 10% mismatch of bases. More importantly for shorter DNA

sequences the presence of single base pair mismatch can have a significant and measurable influence upon the hybridisation temperature. For example, Wallace *et al.*[14] used oligionucleotides varying in length from 14-20 bases and observed that a single base pair mismatch reduced the Tm by upto 5°C.

Knowledge of the kinetics of hybridisation is an important factor for consideration when designing or improving a DNA biosensor.[15] In bulk solution the hybridisation reaction may be viewed as being second order where the rate is dependent on the solvent, length of strand and complexity of the sequence.[11] For longer DNA sequences the time for hybridisation equilibrium ($T_{1/2}$) can be very long with $T_{1/2}$ for a target human genome being 41 days.[16] Even with shorter probe molecules the time required to reach equilibrium may be in the region of 1-2 days.[17] These long periods can be restricting in nature and consequently many hybridisation experiments may not have been performed under equilibrium conditions. As such the optimum sensitivity for a procedure will have not been achieved. In order to overcome this restraint work has focused on finding conditions in which the kinetics of hybridisation are accelerated.[18]

For many DNA analytical methods the probe molecule is fixed to a surface be it an electrode or a glass plate. The conformation assumed by a DNA sequence while attached to an electrode surface is dependent upon the strength of the interactions between the interface and DNA strand. Lemeshko *et al.* showed that, at least for DNA on a charged surface, an asymmetrical non-helical DNA duplex can be the preferred structural isomer under standard biochemical conditions ($90mM$ sodium carbonate, 5× Denhardt's buffer solution, pH 9.5, for 12mer targets).[19] Within the literature the use of a gold-sulfur bond is commonly utilised to affix DNA to an Au electrode surface. This is achieved via formation of a self-assembled monolayer of thiolated ssDNA. To reduce non-specific adsorption of the DNA to the gold surface, the electrode is also commonly co-modified with 6-mercapto-1-

hexanol (MCH). The use of MCH was first reported by Levicky *et al.*.[20] The exact role of the MCH has been under debate, work by Lao *et al.*[21] showed that even after treatment of an Au surface with MCH it is not possible to fully remove all non-specific DNA:surface interactions. Further work by Dharuman *et al.*[22] used dilutants of various chain length to elucidate the mechanism by which these compounds control non-specific DNA-Au interactions, highlighting the important role of their hydrophilic/hydrophobic nature.

Beyond structure, the kinetics of hybridisation are also greatly altered when the probe molecule is attached to a surface. In this case the density of the probe on the surface has a significant effect.[15] For probes that are well spaced and non-interacting, Erickson *et al.* provided a model for the kinetic behaviour of DNA hybridisation which accounts for both direct hybridisation from bulk solution and hybridisation after an initial non-specific adsorption step. Further, this model has been verified experimentally.[23] It should be noted that the thermodynamics of the hybridisation process will also be altered when the DNA is affixed to a surface. By adapting the NN model through use of the Langmuir isotherm it is possible to show the correlation between ΔG in solution and the hybridisation intensities for DNA attached to a surface.[24]

2.2 Electrochemical Sensing Methods

In general an electrochemical DNA sensor comprises of a biorecognition component and a transducer, which converts the hybridisation event or presence of DNA at the surface into a measurable electrical signal, alternative to this are systems which utilise 'Nanopore' technology. The present methods can be broadly divided into two main groups; labeled and label-free systems. Labeled methods use a redox active compound to transduce the hybridisation event. The electroactive molecule may be attached to the electrode, DNA, or be present in solution. Com-

pounds that associate with DNA generally bind to the minor or major groove on dsDNA, intercalate between the two strands, or binding to the exposed bases on ssDNA. Label-free systems either detect the hybridisation event through a change in the physical properties of the recognition layer or alternatively, in the case of 'Nanopore' systems the blockage of the ionic current allows measurement of the size and hence character of the DNA traversing the pore.

The following sections aim to give an outline of the wide variety of methods that have to date been employed to electrochemically detect specific DNA sequences. As these methods improve, work has begun to be focused beyond the detection of a single DNA sequence; a number of papers which are directed at multi-analyte detection are highlighted in the final section.

2.2.1 Label-Free Methods

Direct Redox

One of the first electrochemical approaches to the detection of DNA involved the direct reduction of guanine at a dropping mercury electrode.[25] This was later developed through the use of adsorptive transfer stripping voltammetry, allowing the differentiation between ds and ss DNA, with associated limits of detection below 0.1 μg/ml.[26] Although allowing high sensitivity the use of mercury is problematic due to DNAs high affinity for adsorption leading to non-specific binding. Paleček *et al.* circumvented this through having a separate surface upon which the DNA is hybridised (in this case magnetic beads) and another surface upon which the oxidation of the sample occurs.[27] The use of magnetic beads has been applied to a number of different systems and presents a number of advantages over using a single biorecognition/electrode surface. The properties of the hybridisation surface can be readily optimised to allow efficient binding of the DNA without incurring non-specific adsorption; furthermore, the hybridised product can then be easily

separated from the original sample before detection takes place.[28] For many of the DNA sensors based on guanine oxidation, the hybridisation event is confirmed by a marked increase in the guanine signal resulting from an increase of the analyte at the surface. This is inherently problematic, due to the requirement of having a known and consistent response from the unhybridised probe. One method for avoiding this problem is through substitution of guanine with inosine (a closely related base which is oxidised at a different potential) in the probe strand, therefore any guanine peak observed is due to hybridised DNA.[29] Although useful, substitution with inosine does lead to a loss in specificity due to inosine's ability to bind to adenine, thymine or cytosine.

Due to the health concerns associated with mercury and the fact that its use is restricted in a number of countries,[30] work has also focused on the development and investigation of other suitable electrode materials. Carbon is of particular note due to being both inexpensive and relatively chemically inert. Recent work has highlighted the benefits of graphite based electrodes for the oxidation and electroanalytcial detection of DNA over other forms of carbon.[31]

Nanopore Technology

Since its inception in 1996[32] nanopore technology and specifically its application towards DNA sequencing has developed significantly. Broadly, the technique comprises of applying a voltage across a nanopore containing membrane. Due to the potential difference an ionic current is induced, the measured current is proportional to the rate of flux of ions through the pore. When DNA (or other molecule of interest) traverses the pore the rate of ionic flux decreases. This process is commonly termed *ionic current blockade* (ICB). The modulation of the current is proportional to the extent to which the pore is obstructed. The variation is detectable and may be related to the either the DNA sequence traversing the pore

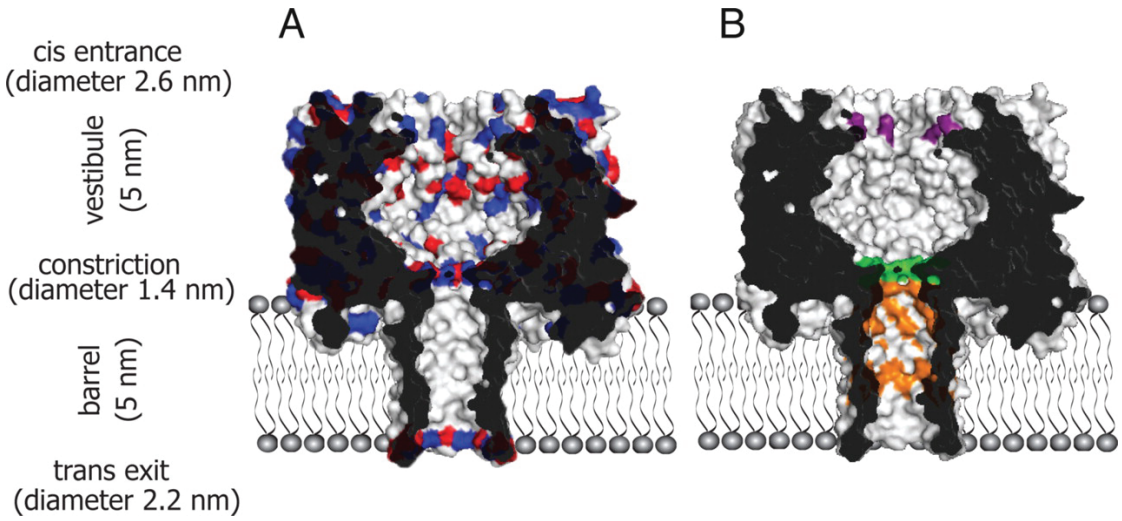

Figure 2.2: Sections through the αHL nanopore (PDB: 7AHL). (A) Charge distribution in the WT αHL nanopore. Positively charged amino acids of αHL are coloured in blue and negatively charged amino acids in red. (B) Sites in the αHL nanopore modified in this work. Lys-8 is in purple. The constriction formed by the ion pair Glu-111/Lys-147 is coloured in green. Met-113, Thr-115, Thr-117, Gly-119, Asn-121, Asn-123 and Thr-125 are in orange. Proc. Nat. Acad. Sci. 105 (2008)19720–19725, Copyright (2008) National Academy of Sciences, USA.

or the analyte of desired detection.

Work to date can be roughly classified as either being based around a biological or solid-state pore. Biological systems comprise of a lipid bilayer that is traversed by a pore containing protein (commonly, staphylococcal α-hemolysin (αHL), Figure 2.2).[33] Conversely, the materials used for the formation of solid-state pores are far more diverse, ranging from carbonous materials such as graphene[34] and carbon nanotubes[35] to inorganic membranes, including; SiN,[36,37] SiO_2[38] and TiN.[39] Although biological pores potentially offer greater atomic precession within the pore itself - in part due to the ability to fine tune the lumen of the protein[40,41] - solid-state approaches hold an advantage in their higher durability and the greater ease with which they may be incorporated into an electronic device.[42] Significantly, recent work by Hall *et al.* has demonstrated the possibility of combining the two approaches through the insertion of a αHL protein into a solid-state support.[43] For both procedures spatial resolution of the nucleotides (separation of $\sim$0.4 nm) is a

significant issue arising predominantly from the fact that at any one time multiple bases straddle the pore, all of which contribute to the measured ICB.[44] Consequently a large amount of work within the literature is limited to differentiating between single and double stranded DNA,[45,46] or alternatively focuses upon the detection of DNA modifications. Seminal work by the Bayley group has achieved the identification and sequencing of continuous bases but this procedure requires the presence of an exonuclease enzyme to cleave individual nucleotides. Only single bases traverse the nanopore at any one time and thus this circumvents issues regarding resolution.[47]

Due to the inherent issues relating to the resolution, in part due to the commonly high translocation rates (a 3kbp DNA strand may be translocated through a 8±2 nm pore in a few hundreds of μs)[48] of the DNA sequence through only measuring the ionic current blockade, it has been suggested that the applicability and accuracy of the procedure may be enhanced through application and measurement of tunnelling currents across the nanopore, so that the individual bases will modulate the measured current cf. scanning tunnelling microscopy.[49] Further, due to the high interest in graphene and on the basis of its high electrical conductivity, a few authors have suggested that graphene may be a suitable nanopore support (trans-electrode) across which the tunnelling current may be measured.[34,50] Promising developments have also been made in a similar direction where the current through a graphene sheet forming part of a nanochannel has been modulated via its π-π stacking with the nucleotides.[51]

Other Non-labelled Methods

The use of novel conducting polymers has been the focus of much interest, allowing the hybridisation process to be directly monitored through measurement of the substances resistance without the requirement of redox probes. Work by

Korri-Youssoufi *et al.* provided one of the first examples of this methodology. A functionalised polypyrrole surface was produced through electropolymerisation, to this an amino-substituted oglionucleotide was attached via chemical substitution of a N-hydroxyphthalimide group on the polymer surface. The modified electrode was incubated with various concentrations of the complementary strand, and upon hybridisation, a decrease in the current density was observed.[52] This behaviour has been ascribed to the steric blocking of counter-ions by the hybridised surface.

Impedance spectroscopy allows the complex electrical resistance of a system to be analysed. Due to its sensitivity toward changes in both bulk and surface properties it lends itself well for applications in biosensors.[53] Analysis of the polymer surface with EIS shows changes attributed to the rearrangement of the electrode surface.[54,55] The use of EIS is not limited to new polymer materials, the modification and subsequent hybridisation event has been followed at a number of interfaces using this analytical method. Shrestha *et al.* supported ellipsoidal Pr_6O_{11} particles on indium tin oxide (ITO) modified with oligonucleotides. In the impedance spectra a notable shift is observed on hybridisation as a result of the biorecognition process.[56] Alternatively a novel approach was taken by Vagin *et al.* who looked at the effect of DNA hybridisation at a liquid-liquid interface, showing that the formation of the duplex caused a decrease in ion transfer resistance which could be monitored through impedance spectroscopy.[57] The general use of EIS for biosensing applications (including nucleic acid sensing) has been recently reviewed by Lisdat *et al.*.[53]

2.2.2 Labeled Approaches

A large number of techniques involving labeled systems require the modification of the target DNA strand. Consequently, such procedures are not directly applicable for use as DNA sensors, thus, such work shall not be reviewed in the following

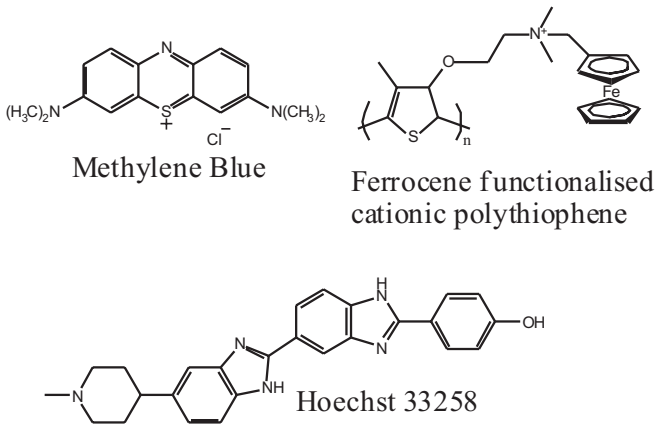

Figure 2.3: Chemical structures of selected redox labels.

sections.

Groove Binders and Redox Indicators

Post the publication of Bard's paper in the late 1980s regarding the use of voltammetric techniques for the characterisation of the binding nature of certain redox species to DNA,[58] a swathe of mimetic papers have been produced with varying degrees of insight. However, redox active metal complexes that preferentially bind to either dsDNA or ssDNA have been successfully employed to measure DNA hybridisation. One example is $[Co(phen)_3]^{3+}$ which associates selectively and reversibly to dsDNA. Upon hybridisation the pre-concentration of the metal complex in the DNA layer adjacent to the electrode surface causes an increase in the electrochemical signal.[59] In a similar procedure Zhang *et al.* used the cadmium compound $[CdL_2(H_2O)_2](NO_3)_2$ where L=N-(2-pyridinylmethyl)benzamide, this complex also preferentially binds to dsDNA.[60]

Other redox active metal and non-metal containing compounds are also applicable for this application. Figure 2.3 shows the chemical structures of Hoechst 33258, Methylene Blue (MB) and the organometallic ferrocene functionalised cationic polythiophene. Hoechst 33258 is a commonly used organic DNA dye, this molecule

binds to the minor groove on dsDNA and was used in the fabrication of a microelectrode array.[61] MB, another organic dye, not only acts as a DNA intercalator as per its role in charge transfer experiments,[62] but it has also been shown to strongly associate with ssDNA. Upon DNA hybridisation the decrease in indicator electrochemical peak current reflects the extent of the duplex formation. This procedure was successfully used by Erdem *et al.* in the detection of short DNA segments (21-mer oglionucleotides) related to the hepatitis B virus (HBV).[63]

In order to improve sensitivity and selectivity new compounds have been developed -some with multiple metal centres[64]- Floch *et al.* synthesised a ferrocene functionalised cationic polythiophene transducer. This compound associates with the anionic phosphate backbone of DNA through electrostatic interactions. By using a PNA probe (neutral backbone), the formation of the PNA/DNA duplex can be followed by the increase in metal complex concentration close to the electrode surface.[65] A recent review of the transition metal complexes available for DNA binding is provided by Li *et al.*.[66]

Charge Transfer

The charge transfer ability of DNA is of great interest. Efficient long-range electron transfer has been shown to occur through base pair stacking, over distances of up to 35 Å. Consequently the use of DNA as a 'molecular wire' for nanostructured systems has been investigated.[67] The mechanism for electron transfer is still under debate but it has been shown that the transfer occurs through the π-stacked bases of the duplex. This property has the potential to allow high selectivity toward a given sequence.[68] Work by Wain *et al.* has advanced this technique by demonstrating how 'scanning electrochemical microscopy' can be utilised to image localised DNA spots situated on a single gold electrode, thereby circumventing the requirement for the use of individually addressable electrodes for the detection of

multiple sequences.[69]

Although methylene blue is commonly used within such charge transfer systems other intercalators have been studied, for example, work by Gooding *et al.* used the dsDNA intercalating compound anthraquinone-2,6-disufonate (AQDS) as a redox probe. When the sensor is hybridised with a fully complementary target and then incubated with AQDS long range electron transfer is observed, targets with a single base mismatch give a greatly decreased AQDS redox signal. In this work the negative dipole of the MCH, apart from avoiding non-specific binding of the DNA to the electrode surface, also plays a secondary role by serving to block the gold electrode surface from direct redox of the AQDS via electrostatic repulsion.[70] This system was later improved so as to allow in situ testing thus avoiding the requirement to repeatedly wash the electrode. This improvement stems from the lower value of E_c (reduction electrode potential) for the intercalated AQDS, this change in redox potential is reported to be a result of the stabilisation of the reduced form of the probe. Through use of square wave voltammetry a limit of detection of 0.5 nM was obtained.[71]

Sandwich Methods

Many of the labeled methods discussed above suffer from large background noise due to non-specific binding of the redox probes either to the electrode or the unintended DNA form. To overcome this problem methods involving signal amplification have been developed; however, many of these involve the direct modification of the target DNA. An alternative procedure known as the 'sandwich' method has resulted in a number of highly sensitive experimental systems. Here the target DNA acts as a bridging molecule between the capture probe (bound to the electrode surface) and a signal probe (a ssDNA sequence bound to an indicator molecule), this method requires the occurrence of two hybridisation events. A generalised

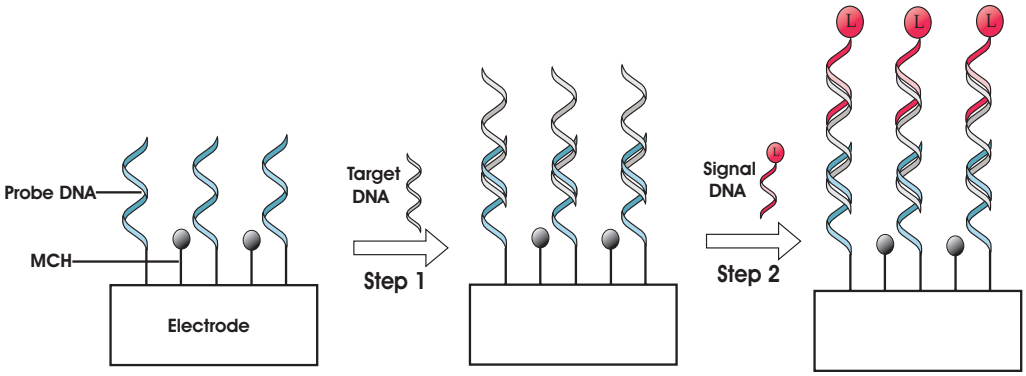

Figure 2.4: Schematic of the 'sandwich' method of DNA sensing. A ssDNA modified electrode is hybridised with a target DNA sequence (Step 1) and then a labeled signal sequence (Step 2). The presence of the redox probe at the electrode surface signifies the binding of the target DNA.

schematic for this procedure is shown in Figure 2.4. A ssDNA modified electrode is produced, as previously mentioned MCH is often employed to avoid unspecific binding of the DNA to the electrode surface. Step 1 involves the hybridisation of the electrode with the target DNA, this event is then followed by a second hybridisation with the signal DNA. The signal DNA may be modified with various labels (often either enzymatic or nanoparticulate in nature). These indicators serve to highly enhance the transduced signal.

Both horse radish peroxidase (HRP) and glucose oxidase (GOx)[72] are common enzymatic labels. Alfonta *et al.* amplified the sensing of oligonucleotide-DNA binding using liposomes labeled with biotin and the enzyme horseradish peroxidase (HRP). The HRP is associated to the signal probe through an avidin bridge. The HRP enzyme biocatalyses the oxidation of 4-chloro-1-naphthol to produce an insoluble product at the electrode surface. The insulation of the electrode surface was measured through impedance spectroscopy with an associated limit of detection of 0.65 pM.[73] Recent work has removed the requirement for the use of biotin through the direct cross-linking of the signal DNA with the HRP enzyme.[74] In an analogous method to Alfonta's work, Won *et al.* replaced the use of a labeled signal probe with a biotin tagged anthraquinone. The anthraquinone acted as a DNA

intercalator and to this a polymeric streptavidin/polymerase complex was bound. Again the biocatalysed production of an insoluble product allowed the hybridisation event to be followed through measurement of the electrodes insulation.[75]

The instability of enzymes can be a hindrance to their use, methods employing nanoparticles generally exhibit better long term stability. Attachment of streptavidin modified gold nanoparticles to biotin labeled signal probes allowed detection of the hybridisation event through dissolution of the gold tag followed by measurement of the gold concentration via stripping voltammetric analysis.[76] Zhang *et al.* produced gold nanoparticles modified with a large number of signal probes. Here $[Ru(NH_3)_6]^{3+}$ was used as a redox active indicator, this positively charged metal complex is electrostatically attracted to the anionic phosphate backbone of the DNA molecule. The hybridisation of one probe to the target strand brings a large number of probe strands (and consequently ruthenium complexes) into close proximity with the electrode and subsequently a large analytical signal is observed.[77] An alternative approach has also been employed by Umek *et al.*[78] in which the signal probe is labelled with ferrocene. This work has lead to the production of the 'eSensor,' which was one of the first commercially available electrochemical assays for DNA mutations.

Labelled Probe

The physical change in structure of DNA upon duplex formation has been used in a number of experimental systems to transduce the hybridisation event, via labelling of the distal end of the DNA probe with an electroactive compound. Unhybridised ssDNA acts as a polymer (when in high salt conditions) and the redox compound is able to come into close proximity with the electrode surface, consequently an electrochemical signal may be recorded. When hybridised, the dsDNA structure is 'rod-like' (provided the contour length of the DNA is less

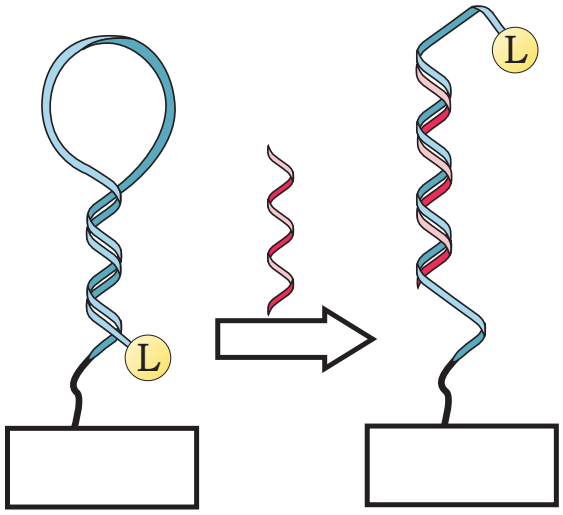

Figure 2.5: Schematic of the 'stem and loop' method of DNA detection. Hybridisation of the target DNA sequence to the probe strand, decreases the electrochemical signal due to re-orientation of the redox label away from the electrode surface.

than the associated persistence length) orientating the electroactive centre further away from the electrode surface.[79,80] This method has been improved upon by use of 'stem-loop' DNA probes which improve the sensitivity of the system by ensuring the close proximity of the redox centre to the electrode surface in the unhybridised state.[81] A generalised schematic for the system is shown in Figure 2.5. Again hybridisation results in a conformational change moving the redox centre away from the electrode. This method, although sensitive, is susceptible to false positive results due to the detection of the target DNA being measured as a decrease in the observed electrochemical signal. Work has been focused on the development of systems in which a 'signal-on' effect is observed with hybridisation. Grinstaff *et al.* produced a DNA-PEG-DNA triblock probe, where hybridisation causes a large conformational change which orientates the electroactive label closer to the electrode surface.[82] In a similar manner, Heeger *et al.* produced a system utilising a DNA pseudoknot probe, in the unhybridised form the probe holds the

redox label away from the electrode surface. The DNA probe does this through base pairing with itself in two regions, hybridisation causes a large conformational change, orientating the label close to the electrode. This method had an associated limit of detection of 2 nM, a level of sensitivity that allowed its use for detection of DNA in blood serum.[83]

2.3 Arrays and Multianalyte Detection

A number of electrochemical based systems have demonstrated the ability to be both sensitive and selective toward a specific hybridisation event. Although much progress is still being made in this area, attention has begun to be focused on production of sensors capable of the detection of multiple analytes. Many electrochemical sensing methods differentiate between fully complementary targets and those with a single base pair mismatch through their difference in thermodynamic stability, this is often achieved via comparison of signal intensities. This methodology can impart a reasonable level of signal separation between closely related sequences provided optimal hybridisation conditions are used. When applying these methods to array systems difficulties arise as duplex binding energies for adjacent probe sequences (i.e. for different genes) may vary significantly more than the differential binding energies of a particular probe with its complementary versus mutated test sequence.[62]

Electrochemical limits of detection at stationary electrodes is often restricted to micro-molar analyte concentrations. In order to improve the signal-to-noise ratio Hintsche *et al.* have investigated the use of interdigitated microelectrodes in a flow-cell system. This work focused on the amperometric detection of the analyte through redox-cycling, allowing the detection limit to be improved by more than an order of magnitude.[84] This system has been applied to the detection and quantification of a variety of pathogenic RNA and DNA sequences including Escherichia[85]

and Herpes viruses.[86] In both of these examples biotin labelled signal probes are conjugated with alkaline phosphatase. The presence of the alkaline phosphatase liberates the electrochemical mediator p-aminophenol. Measurement of the analyte is achieved through amperometric techniques involving a multipotentiostat. In order to miniaturise and reduce costs work has also been aimed at producing systems in which electrodes may be multiplexed so as to allow the voltammetric response to be measured via a simple mono or bipotentiostat.[87]

Pioneering work by Wang *et al.* utilised magnetic beads modified with three different ssDNA probes, with the aim of producing an electrochemical systems able to detect multiple analytes. A labeled DNA 'sandwich' method was used with the signal probes being modified with nanocrystals of different compositions. These nanocrystals had been previously shown to give distinct voltammetric stripping signals. The hybridisation of the targets was simultaneously tested for and could be differentiated between, by the separate voltammetric peaks.[88] The use of arrays in systems analogous to current florescent experimental procedures have shown promising results. Mascini *et al.* localised different ODN strands through 'spotting' onto a gold electrode. The hybridisation event was developed by use of biotinylated signalling probe which was then bound to streptavidin-alkaline phosphatase conjugate. The subsequent biocatalysed reaction changed the conductance of the electrode surface, which allowed imaging of the array by scanning electrochemical microscopy (SECM).[89] Multianalyte detection has not been limited to DNA targets, Harper *et al.* produced a sensor on which both genomic and proteomic analytes were tested. The method was able to simultaneously perform electrochemical detection of a DNA sequence related to the breast cancer BRCA1 gene and the human cytokine protein interleukin-12, which is a substantial component in the immune system response and attack of tumour cells.[90]

In general single-use sensors have several advantages, such as avoidance of

contamination, constant sensitivity and reproducibility. Much would be gained through the production of an electrode which could be mass produced and subsequently easily tuned to the detection of a variety of analytes. One such scheme involved the use of a silane anchor on an indium tin oxide surface. To this differing dynamic ligands could be attached through a disulphide bond. The use of a disulphide bond imparted further use as it allowed selective removal of the ligands via either electrochemical or chemical methods.[91] Further to this, Pavlovic *et al.* have produced a microfluidic electrochemical device that supports in situ electrode cleaning, preparation, selective DNA probe immobilisation, sequence-specific target detection, and efficient regeneration of sensing pixels.[92]

2.4 Conclusions

This review has highlighted the physical aspects of DNA, specifically looking at the thermodynamics and kinetics of hybridisation with the aim of elucidating how these properties may be controlled and used in the detection of DNA sequences. Continuing from this the main approaches to electrochemical DNA sensing have been discussed with reference to recent work in the corresponding fields. As further research is produced in this area ever more sensitive and selective methods for DNA detection are being sought.

References

[1] Dahm, R. *Hum. Gen.* **2008**, *122*, 565–581.

[2] Watson, J. D.; Crick, F. H. C. *Nature* **1953**, *171*, 737–738.

[3] Macgregor Jr., R. B.; Poon, G. M. K. *Comp. Bio. Chem.* **2003**, *27*, 461–467.

[4] Brookes, A. J. *Gene* **1999**, *234*, 177–186.

[5] Berman, H. M.; Olson, W.; Beveridge, D. L.; Westbrook, J.; Gelbin, A.; Demeny, T.; Hsieh, S.-H.; Srinivasan, A. R.; Schneider., B. *Biophys. J.* **1992**, *63*, 751–759.

[6] Hays, F. A.; Teegarden, A.; Jones, Z. J. R.; Harms, M.; Raup, D.; Watson, J.; Cavaliere, E.; Ho, P. S. *Proc. Natl. Acad. Sci. USA* **2005**, *102*, 7157–7162.

[7] McConnell, K. J.; Beveridge, D. L. *J. Mol. Biol.* **2000**, *304*, 803–820.

[8] Saenger, W.; Hunter, W. N.; Kennard, O. *Nature* **1986**, *324*, 385–388.

[9] Rich, A.; Nordheim, A.; Wang, A. H. J. *Annu. Rev. Biochem.* **1984**, *53*, 791–846.

[10] Watterson, J.; Piunno, P. A. E.; Krull, U. J. *Anal. Chim. Acta* **2002**, *469*, 115–127.

[11] Wetmur, J. G. *Crit. Rev. Biochem. Mol. Biol.* **1991**, *26*, 227–259.

[12] SantaLucia Jr., J. *Proc. Natl. Acad. Sci. USA* **1998**, *95*, 1460–1465.

[13] Bonner, T. I.; Brenner, D. J.; Neufeld, B. R.; Britten, R. J. *J. Mol. Bio.* **1973**, *81*, 123–135.

[14] Wallace, R. B.; Shaffer, J.; Murphy, R. F.; Bonner, J.; Hirose, T.; Itakura, K. *Nucleic Acids Res.* **1979**, *6*, 3543–3557.

[15] Hagan, M. F.; Chakraborty, A. K. *J. Chem. Phys.* **2004**, *120*, 4958–4968.

[16] Carletti, E.; Guerra, E.; Alberti, S. *Trends Biotechnol.* **2006**, *24*, 443–448.

[17] Halperin, A.; Buhot, A.; Zhulina, E. B. *J. Phys. Conden. Matter* **2006**, *18*, S463–S490.

[18] Ku, W. C.; Lau, W. K.; Tseng, Y. T.; Tzeng, C. M.; Chiu, S. K. *Biochem. Biophys. Res. Commun.* **2004**, *315*, 30–37.

[19] Lemeshko, S. V.; Powdrill, T.; Belosludtsev, Y. Y.; Hogan, M. *Nucleic Acids Res.* **2001**, *29*, 3051–3058.

[20] Levicky, R.; Herne, T. M.; Tarlov, M. J.; Satija, S. K. *J. Am. Chem. Soc.* **1998**, *120*, 9787–9792.

[21] Lao, R.; Song, S.; Wu, H.; Wang, L.; Zhang, Z.; He, L.; Fan, C. *Anal.Chem.* **2005**, *77*, 6475–6480.

[22] Dharuman, V.; Hahn, J. H. *Sens. Actuator B* **2007**, *127*, 536–544.

[23] Erickson, D.; Li, D.; Krull, U. J. *Anal. Biochem.* **2003**, *317*, 186–200.

[24] Weckx, S.; Carton, E.; De Vuyst, L.; Van Hummelen, P. *J. Phys. Chem. B* **2007**, *111*, 13583–13590.

[25] Paleček, E. *Nature* **1960**, *188*, 656–657.

[26] Paleček, E. *Anal. Biochem.* **1988**, *170*, 421–431.

[27] Paleček, E.; Billová, S.; Havran, L.; Kizek, R.; Mičulková, A.; Jelen, F. *Talanta* **2002**, *56*, 919–930.

[28] Paleček, E.; Fojta, M. *Talanta* **2007**, *74*, 276–290.

[29] Ozkan, D.; Erdem, A.; Kara, P.; Kerman, K.; Meric, B.; Hassmann, J.; Ozsoz, M. *Anal. Chem.* **2002**, *74*, 5931–5936.

[30] Engle, M. In *Dynamics of Mercury Pollution on Regional and Global Scales*; Pirrone, N., Mahaffey, K. R., Eds.; Springer, 2005.

[31] Gonçalves, L. M.; Batchelor-McAuley, C.; Xiong, L.; Barros, A. A.; Compton, R. G. *Electroanalysis* **2011**, *23*, 583–587.

[32] Kasianowicz, J. J.; Brandin, E.; Branton, D.; Deamer, D. W. *Proc. Nat. Acad. Sci. USA* **1996**, *93*, 13770–13773.

[33] Ma, L.; Cockroft, S. L. *ChemBioChem* **2010**, *11*, 25–34.

[34] Garaj, S.; Hubbard, W.; Reina, A.; Kong, J.; Branton, D.; Golovchenko, J. A. *Nature* **2010**, *467*, 190–193.

[35] Liu, H.; He, J.; Tang, J.; Liu, H.; Pang, P.; Cao, D.; Krstic, P.; Joseph, S.; Lindsay, S.; Nuckolls, C. *Science* **2010**, *327*, 64–67.

[36] Van Den Hout, M.; Hall, A. R.; Wu, M. Y.; Zandbergen, H. W.; Dekker, C.; Dekker, N. H. *Nanotechnology* **2010**, *21*, 115304.

[37] Vlassiouk, I.; Apel, P. Y.; Dmitriev, S. N.; Healy, K.; Siwy, Z. S. *Proc. Nat. Acad. Sci. USA* **2009**, *106*, 21039–21044.

[38] Shin, J. W.; Lee, J. Y.; Lee, D. U.; Oh, D. H.; Kim, D. H.; Kim, T. W.; Cho, W. J.; Jin, S. *Nanotechnology* **2009**, *20*, 075703.

[39] Harrer, S.; Waggoner, P. S.; Luan, B.; Afzali-Ardakani, A.; Goldfarb, D. L.; Peng, H.; Martyna, G.; Rossnagel, S. M.; Stolovitzky, G. A. *Nanotechnology* **2011**, *22*, 275304.

[40] Luo, Y.; Egwolf, B.; Walters, D. E.; Roux, B. *J. Phys. Chem. B* **2010**, *114*, 952–958.

[41] Li, W. W.; Claridge, T. D. W.; Li, Q.; Wormald, M. R.; Davis, B. G.; Bayley, H. *J. Am. Chem. Soc.* **2011**, *133*, 1987–2001.

[42] Chen, Z.; Jiang, Y.; Dunphy, D. R.; Adams, D. P.; Hodges, C.; Liu, N.; Zhang, N.; Xomeritakis, G.; Jin, X.; Aluru, N. R.; Gaik, S. J.; Hillhouse, H. W.; Brinker, C. J. *Nat. Mater.* **2010**, *9*, 667–675.

[43] Hall, A. R.; Scott, A.; Rotem, D.; Mehta, K. K.; Bayley, H.; Dekker, C. *Nat. Nanotechnol.* **2010**, *5*, 874–877.

[44] Branton, D. et al. *Nat. Biotechnol.* **2008**, *26*, 1146–1153.

[45] Gyarfas, B.; Abu-Shumays, R.; Wang, H.; Dunbar, W. B. *Biophys. J.* **2011**, *100*, 1509–1516.

[46] Balagurusamy, V. S. K.; Weinger, P.; Ling, X. S. *Nanotechnology* **2010**, *21*, 335102.

[47] Clarke, J.; Wu, H. C.; Jayasinghe, L.; Patel, A.; Reid, S.; Bayley, H. *Nat. Nanotechnol.* **2009**, *4*, 265–270.

[48] Li, J.; Talaga, D. S. *J. Phys. Condens. Mat.* **2010**, *22*, 454129.

[49] Huang, S.; He, J.; Chang, S.; Zhang, P.; Liang, F.; Li, S.; Tuchband, M.; Fuhrmann, A.; Ros, R.; Lindsay, S. *Nat. Nanotechnol.* **2010**, *5*, 868–873.

[50] Bayley, H. *Nature* **2010**, *467*, 164–165.

[51] Min, S. K.; Kim, W. Y.; Cho, Y.; Kim, K. S. *Nat. Nanotechnol.* **2011**, *6*, 162–165.

[52] Korri-Youssoufi, H.; Garnier, F.; Srivastava, P.; Godillot, P.; Yassar, A. *J. Am. Chem. Soc.* **1997**, *119*, 7388–7389.

[53] Lisdat, F.; Schäfer, D. *Anal. Bioanal. Chem.* **2008**, *391*, 1555–1567.

[54] Peng, H.; Zhang, L.; Spires, J.; Soeller, C.; Travas-Sejdic, J. *Polymer* **2007**, *48*, 3413–3419.

[55] Gautier, C.; Cougnon, C.; Pilard, J. F.; Casse, N. *J. Electroanal. Chem.* **2006**, *587*, 276–283.

[56] Shrestha, S.; Yeung, C. M. Y.; Mills, C. E.; Lewington, J.; Tsang, S. C. *Ange. Chem. - Int. Ed.* **2007**, *46*, 3855–3859.

[57] Vagin, M. Y.; Trashin, S. A.; Karyakin, A. A.; Mascini, M. *Anal. Chem.* **2008**, *80*, 1336–1340.

[58] Carter, M. T.; Rodriguez, M.; Bard, A. J. *J. Am. Chem. Soc.* **1989**, *111*, 8901–8911.

[59] Millan, K. M.; Saraullo, A.; Mikkelsen, S. R. *Anal. Chem.* **1994**, *66*, 2943–2948.

[60] Zhang, S.; Tan, Q.; Li, F.; Zhang, X. *Sens. Actuator B* **2007**, *124*, 290–296.

[61] Choi, Y.-S.; Lee, K.-S.; Park, D.-H. *Curr. Appl. Phys.* **2006**, *6*, 777–780.

[62] Kelley, S. O.; Boon, E. M.; Barton, J. K.; Jackson, N. M.; Hill, M. G. *Nucleic Acids Res.* **1999**, *27*, 4830–4837.

[63] Erdem, A.; Kerman, K.; Meric, B.; Akarca, U. S.; Ozsoz, M. *Anal. Chim. Acta* **2000**, *422*, 139–149.

[64] Sato, S.; Tsueda, M.; Watanabe, S.; Ohtsuka, K.; Takenaka, S. *Nucleic Acids Symp. Ser.* **2008**, *52*, 239–240.

[65] Le Floch, F.; Ho, H. A.; Harding-Lepage, P.; Bédard, M.; Neagu-Plesu, R.; Leclerc, M. *Adv. Mater.* **2005**, *17*, 1251–1254.

[66] Li, F.; Chen, W.; Tang, C.; Zhang, S. *Talanta* **2008**, *77*, 1–8.

[67] Priyadarshy, S. *Synth. React. Inorg. Met. -Org. Chem.* **2007**, *37*, 353–356.

[68] Kelley, S. O.; Barton, J. K. *Science* **1999**, *283*, 375–381.

[69] Wain, A.; Zhou, F. *Langmuir* **2008**, *24*, 5155–5160.

[70] Wong, E. L. S.; Gooding, J. J. *Anal. Chem.* **2003**, *75*, 3845–3852.

[71] Wong, E. L. S.; Gooding, J. J. *Anal. Chem.* **2006**, *78*, 2138–2144.

[72] Elena, D.; Oscar, R.; Arantzazu, N. *Anal. Chem.* **2004**, *76*, 3132–8.

[73] Alfonta, L.; Singh, A. K.; Willner, I. *Anal. Chem.* **2001**, *73*, 91–102.

[74] Wang, Z.; Yang, Y.; Leng, K.; Li, J.; Zheng, F.; Shen, G.; Yu, R. *Anal. Lett.* **2008**, *41*, 24–35.

[75] Won, B. Y.; Lee, D. W.; Shin, S. C.; Cho, D. Y.; Lee, S. S.; Yoon, H. C.; Park, H. G. *Biosens. Bioelectron.* **2008**, *24*, 665–669.

[76] Wang, J.; Xu, D.; Kawde, A. N.; Polsky, R. *Anal. Chem.* **2001**, *73*, 5576–5581.

[77] Zhang, J.; Song, S.; Wang, L.; Pan, D.; Fan, C. *Nat. Protoc.* **2007**, *2*, 2888–2895.

[78] Umek, R. M.; Lin, S. W.; Vielmetter, J.; Terbrueggen, R. H.; Irvine, B.; Yu, C. J.; Kayyem, J. F.; Yowanto, H.; Blackburn, G. F.; Farkas, D. H.; Chen, Y. P. *J. Mol. Diag.* **2001**, *3*, 74–84.

[79] Mearns, F. J.; Wong, E. L. S.; Short, K.; Hibbert, D. B.; Gooding, J. J. *Electroanalysis* **2006**, *18*, 1971–1981.

[80] Ricci, F.; Lai, R. Y.; Plaxco, K. W. *Chem. Comm.* **2007**, *36*, 3768–3770.

[81] Fan, C.; Plaxco, K. W.; Heeger, A. J. *Proc. Natl. Acad. Sci. USA* **2003**, *100*, 9134–9137.

[82] Immoos, C. E.; Lee, S. J.; Grinstaff, M. W. *J. Am. Chem. Soc.* **2004**, *126*, 10814–10815.

[83] Xiao, Y.; Qu, X.; Plaxco, K. W.; Heeger, A. J. *J. Am. Chem. Soc.* **2007**, *129*, 11896–11897.

[84] Hintsche, R.; Paeschke, M.; Woflenberger, U.; Schnakenberg, U.; Wagner, B.; Lisec, T. *Biosens. Bioelectron.* **1994**, *9*, 697–705.

[85] Elsholz, B.; Wörl, R.; Blohm, L.; Albers, J.; Feucht, H.; Grunwald, T.; Jürgen, B.; Schweder, T.; Hintsche, R. *Anal. Chem.* **2006**, *78*, 4794–4802.

[86] Nebling, E.; Grunwald, T.; Albers, J.; Schäfer, P.; Hintsche, R. *Anal. Chem.* **2004**, *76*, 689–696.

[87] Hintsche, R.; Albers, J.; Bernt, H.; Eder, A. *Electroanalysis* **2000**, *12*, 660–665.

[88] Wang, J.; Liu, G.; Merkoçi, A. *J. Am. Chem. Soc.* **2003**, *125*, 3214–3215.

[89] Palchetti, I.; Laschi, S.; Marrazza, G.; Mascini, M. *Anal. Chem.* **2007**, *79*, 7206–7213.

[90] Harper, J. C.; Polsky, R.; Wheeler, D. R.; Dirk, S. M.; Brozik, S. M. *Langmuir* **2007**, *23*, 8285–8287.

[91] Moore, E. J.; Curtin, M.; Ionita, J.; Maguire, A. R.; Ceccone, G.; Galvin, P. *Anal. Chem.* **2007**, *79*, 2050–2057.

[92] Pavlovic, E.; Lai, R. Y.; Wu, T. T.; Ferguson, B. S.; Sun, R.; Plaxco, K. W.; Soh, H. T. *Langmuir* **2008**, *24*, 1102–1107.

Chapter 3

Experimental

All reagents were purchased from Aldrich (Gillingham, UK) and were used as received without further purification. All solutions were prepared using deionised water of resistivity not less than 18.2 MΩ·cm at 298 K (Viviendi water systems, UK). Electrochemical measurements were recorded using a computer controlled μII-Autolab or PGSTAT 12 potentiostat (EcoChemie) with a standard three electrode configuration. A platinum wire (99.99% GoodFellow, Cambridge, UK) counter electrode and, in aqueous media, a saturated calomel reference electrode (SCE, Radiometer, Copenhagen, Denmark) completed the cell assembly. Alternatively for experiments in acetonitrile an Ag wire was used as a pseudo reference electrode. Unless stated otherwise experiments were carried out at 20 ± 2°C, the work presented in Chapter 4 was performed in a thermostated water bath at 25±0.1°C.

3.1 Aqueous Buffers

The following buffers were used; pH 0-2 (HCl, 0.1M KCl), pH 3 (0.1M citric acid, 0.1M KCl), pH 4-5 (50mM acetic acid, 50mM sodium acetate, 0.1M KCl), pH6-8 (50mM monobasic potassium phosphate, 50mM dibasic potassium phosphate, 0.1M KCl), pH 9-10 (0.1M disodium tetraborate, 0.1M KCl), pH 11 (50mM phenol, 50mM phenoxide, 0.1M KCl) and pH 12-13 (NaOH, 0.1M KCl), concentrated

NaOH or HCl was used to adjust the pH to the desired level. The pH of the solution was measured using a pH213 Microprocessor pH meter (Hanna Instruments, Leighton Buzzard, UK).

3.2 Working Electrodes

The polycrystalline gold disk working electrode used, was of 1.6mm (BASi Technicol, USA) or 25μm (Cypress Systems Ltd, Massachusetts, USA) in diameter. The Au electrodes were polished using alumina slurries of decreasing size from 3.0-0.1 μ m (Buehler Micropolishing II, USA) with the electrode briefly sonicated between each polishing step to remove any adhered alumina microparticles. The boron-doped diamond (BDD) disk electrodes, diameter 3.1 mm, were purchased from Windsor Scientific (Slough, UK) and were polished on alumina (1.0, 0.3 μm, Buehler), rinsed, and sonicated for 1 min in deionized water between each experiment. The edge plane pyrolytic graphite (EPPG) disk electrode (4.9 mm diameter, Le Carbone, Ltd. Sussex, UK), was fabricated in house and was contained in a teflon casing.

Chapter 4

Electrode Kinetics at Carbon Electrodes and the Density of Electronic States

Although widely used, the electrochemical response of carbon and specifically graphite electrodes are complex and generally poorly understood. First, the surface is heterogenous in nature presenting both edge and basal plane sites.[1] These two sites exhibit significantly different rates of electron transfer; this point shall be expanded further in Chapter 8. Second, the material is semi-metallic and consequently the electronic structure differs from that of other commonly used electrode materials.[2] This latter point has had limited attention within the literature, with the majority of articles focussing on the surface heterogeneity and its implications for mass-transport to the electrode. This chapter aims to systematically investigate if the graphitic electronic structure influences the observed electrochemical response via comparison to results recorded at a gold electrode. This is achieved through studying the voltammetric response of a family of quinone species. The work presented within this chapter has been published in *Chemical Communications* 2012 48 3294–3296; R. Nissim should be recognised for her contribution in obtaining the experimental results, further thanks are necessary to M.C. Henstridge for producing of the simulation software.

In non-aqueous media quinones are known to exhibit two one-electron reduc-

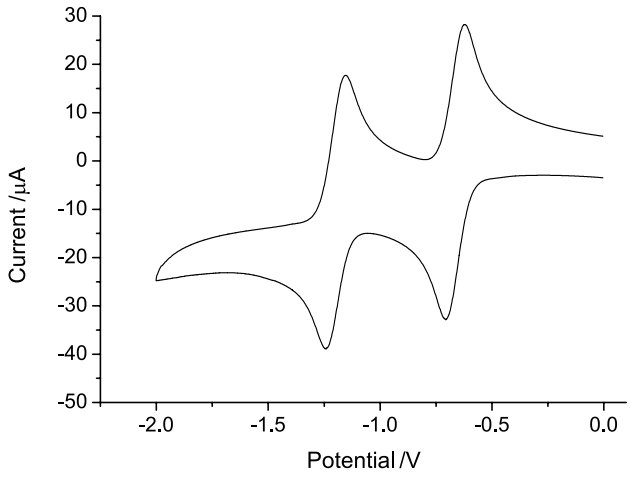

Figure 4.1: The voltammetric response of 1mM anthraquinone in acetonitrile (0.1 M TBAP at 100 mVs^{-1} vs Ag ref.) measured at a glassy carbon macroelectrode.

tions, where the potential difference between the first and second electron transfer is in the order of hundreds of millivolts.[3] A representative voltammogramm for the reduction of anthraquinone in acetonitrile (0.1M TBAP, at 100 mVs^{-1}) is shown in Figure 4.1. It should be noted that in protic media the reduction mechanism is dramatically different, as shall be outlined in the following two chapters.

Marcus provided[4,5] the first molecular based model of electron transfer and subsequently this theory has been applied widely in studies of homogeneous electron transfer. The quantitative application to heterogenous electron transfer and to the electrochemical rate constant has been made in principle using the work of Hush[6] and through the use of Fermi's Golden rule.[7] Whilst Marcus-Hush theory has successfully been applied to heterogeneous electron transfer to species immobilised on electrode surfaces, the application to diffusional processes is presently under critical examination.[8] Whilst work has focused on reorganisation energies[9,10] and their molecular description[11] few studies have considered the electrode properties – in particular the density of states – and the comparison between different electrode materials.

In terms of probing the validity of the Marcus-Hush theory the fact that

the density of states (DOS) of graphite varies significantly as a function of energy with a minimum at the fermi level[12] is of potentially great value. As such, if the electron transfer is non-adiabatic then the rate of electron transfer should vary as a function of redox potential. In order to test this, the current work compares the rate of electron transfer for a family of quinone species, with formal potentials ranging over greater than 1V, at both carbon and gold microdisc electrodes. It is assumed that the density of states for gold is effectively invariant over the potential range studied.[13,14]

For a diffusional outer-sphere electron transfer process where the energy levels of the electrode are considered as a continuum - and through the use of Fermi's golden rule - one may obtain the following Marcus-Hush expressions for describing the reductive (k_{red}) and oxidative (k_{ox}) rate constants[8];

$$k_{red} = k^o e^{-(1/2)\theta \frac{I(\theta,\Lambda)}{I(0,\Lambda)}} \tag{4.1}$$

$$k_{ox} = k^o e^{+(1/2)\theta \frac{I(\theta,\Lambda)}{I(0,\Lambda)}} \tag{4.2}$$

where k^o is the standard electrochemical rate constant, $\theta = F(E - E_f^{\ominus})/RT$ and $\Lambda = (F/RT)\lambda$. Within these equations $E_f^{\ominus}$ is the formal electrode potential, λ is the reorganisation energy, F the Faraday constant (96,485 C mol^{-1}), R the gas constant 8.314 J K^{-1} mol^{-1}, T the absolute temperature, K. $I(\theta, \Lambda)$ is an integral:

$$I(\theta, \Lambda) = \int_{-\infty}^{\infty} \frac{\exp[-(\varepsilon - \theta)^2/4\Lambda]}{2\cosh[\varepsilon/2]} \mathrm{d}\varepsilon \tag{4.3}$$

The standard electrochemical rate constant (k^o) is defined as[8]

$$k^o = \frac{(2\pi)^2 \rho \mathrm{H}_{DA}^{o2}}{\beta h \sqrt{4\pi\Lambda}} exp\left[-\frac{\Lambda}{4}\right] I(0, \Lambda) \tag{4.4}$$

where ρ is the density of electronic states in the electrode material H_{DA}^{o} is the

electronic coupling matrix at the closest distance of approach and β is its associated electronic coupling attenuation coefficient. Consequently, if we assume that the dimensionless reorganisation energy (Λ) and the electronic coupling attenuation coefficient (β) are independent of the electrode material then the ratio of the standard rate constant for a carbon (C) and gold (Au) electrode is;

$$\frac{k^o_{\mathrm{C}}}{k^o_{\mathrm{Au}}} = \frac{\rho_{\mathrm{C}}\mathrm{H}^{o2}_{DA(\mathrm{C})}}{\rho_{\mathrm{Au}}\mathrm{H}^{o2}_{DA(\mathrm{Au})}} \tag{4.5}$$

Given further the assumption that the densities of states for gold is effectively constant as a function of potential over the experimental range[14] then the variation in the ratio should mirror the variation in the carbon electronic density of states. The validity of this conclusion is experimentally verified below.

4.1 Results and Discussion

Measurement of the standard electrochemical rate constants for a family of quinone species; anthraquinone (AQ), p-benzoquinone (BQ), chloro-p-benzoquinone (CBQ), dichloro-p-benzoquinone (DCQ) and dichloro-dicyano-p-benzoquinone (DDQ), was achieved through the measurement of the steady-state current at a microelectrode in an acetonitrile solution (0.1 M tetra-n-butyl ammonium perchlorate [TBAP]). Microelectrodes provide a relatively facile method by which the rate of simple quasi-reversible electron transfer processes may be assessed.[15] Under steady-state conditions the 'reversibility' or 'irreversibility' of a given electrochemical system is related to the standard rate of electron transfer (k^o), the diffusion coefficient of the species and the electrode size. For accurate determination of the diffusion coefficient the radius of the microelectrode requires precise assessment, this was achieved experimentally through calibration of the electrode via measurement of the steady state limiting current for a 1 mM solution of ferrocene in acetonitrile,

with a known literature diffusion coefficient of 2.43×10^{-5} cm^2s^{-1} (25°C).[16] From calibration of the electrodes the radius of the carbon and gold microdiscs was found to be 5.61 ± 0.43 $\times 10^{-6}$ m and 4.96 ± 0.02 $\times10^{-6}$ m respectively, where the errors on the radii represents the variation in the electrode size between polishings. The electrodes were re-calibrated prior to each experiment. Throughout experimentation, a pseudo Ag reference electrode was used, consequently the measured formal potentials for the redox species was found to be only approximately constant. However, given that the electrochemical species are quasi-reversible in nature it is possible to determine the rate of electron transfer via assessment of the voltammetric wave width.[15]

As discussed in the introduction of this chapter, in non-aqueous media the reduction of quinone species occurs via two one-electron electrochemical processes, such that the first voltammetric wave is the reduction of the quinone species to the semiquinone.[17] In order to extract physically significant data regarding the rates of electron transfer for the five quinone species, the one-electron voltammetric waves were fitted to a simulated voltammetric response provided by an in house program. The quantification of the accuracy of the fitting and hence the accuracy of the obtained values was achieved through measurement of the difference in current between the experimental and simulated responses. This difference in current was expressed as a *mean scaled absolute deviation* (MSAD). The MSAD is defined as,

$$\% \text{ MSAD} = \frac{1}{n}\sum_{n}\left|\frac{i_{\text{exp}} - i_{\text{sim}}}{i_{\text{exp}}}\right| \times 100 \tag{4.6}$$

where i_{exp} and i_{sim} are the experimental and simulated currents respectively and n is the number of data points. Since the points of the simulated voltammetry are not necessarily aligned at the same potential values as those of the experimental voltammetry, spline interpolation was used to calculate i_{sim} at the potentials of the

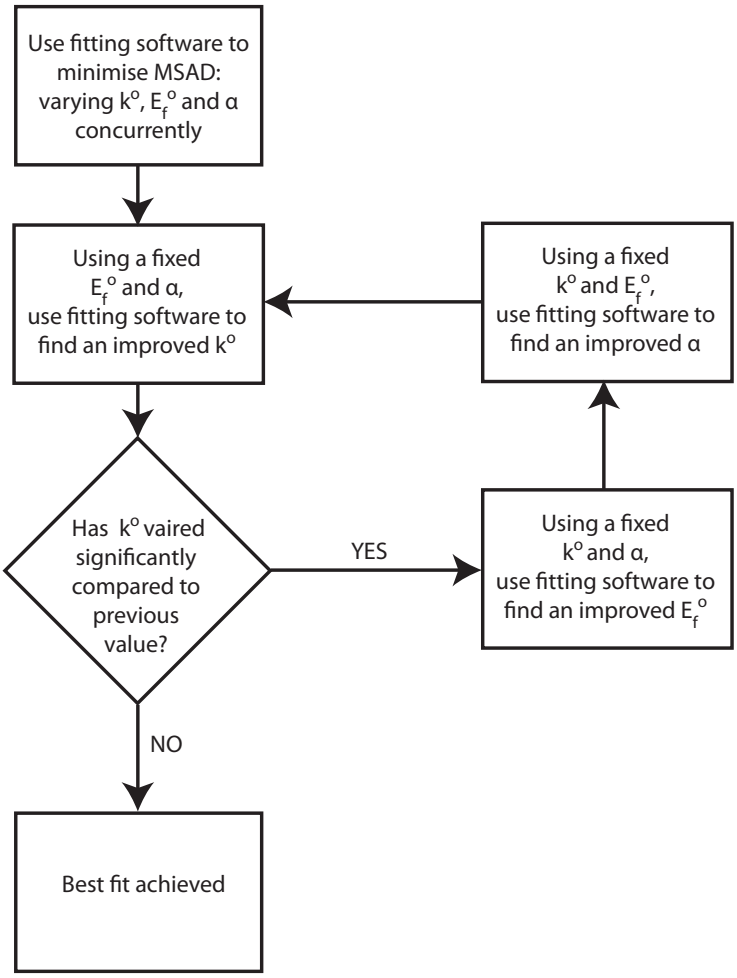

Figure 4.2: Flow chart depicting the procedure utilised in order to find the best fit for the experimental results.

experimental points. Additionally a narrow strip of the experimental voltammetry near $i = 0$ was omitted from the MSAD calculations because dividing by a very small value of i_{exp} yields a very large value of MSAD even if $i_{\text{exp}} - i_{\text{sim}}$ is small. The MSAD values at each point considered are then averaged to yield a final value of average MSAD per point. In order to obtain the best fit for each of the voltammetric responses the procedure as outlined in Figure 4.2 was followed. Here a direct search method was undertaken so as to find the minimum in the MSAD value.

The plots shown in figures 4.3, 4.4, 4.5, 4.6 and 4.7 depict the voltammetric

response for AQ, BQ, CBQ, DCQ and DDQ respectively, on both a gold and carbon microdisc. Also depicted in figures 4.3, 4.4, 4.5, 4.6 and 4.7 is the variation in the MSAD for the fitting of the simulation to the experimental results as a function of the simulated k^o.

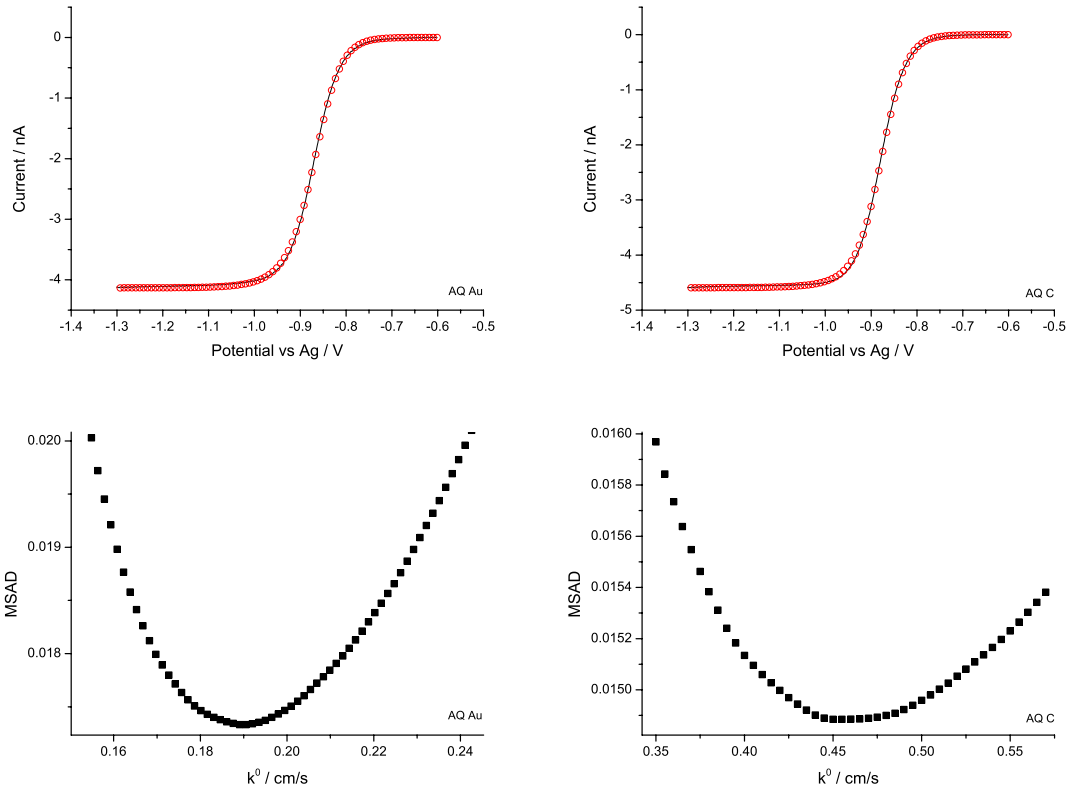

Figure 4.3: Experimental (line) and simulated (circles) best fits for the reduction of AQ (1mM) on both a gold (left) and carbon (right) microdisc at a scan rate of 25 mVs^{-1} [0.1M TBAP, 25°C, vs. Ag pseudo ref]. Also depicted (below voltammetry) is the plot of MSAD versus the value of k^o used within the simulation.

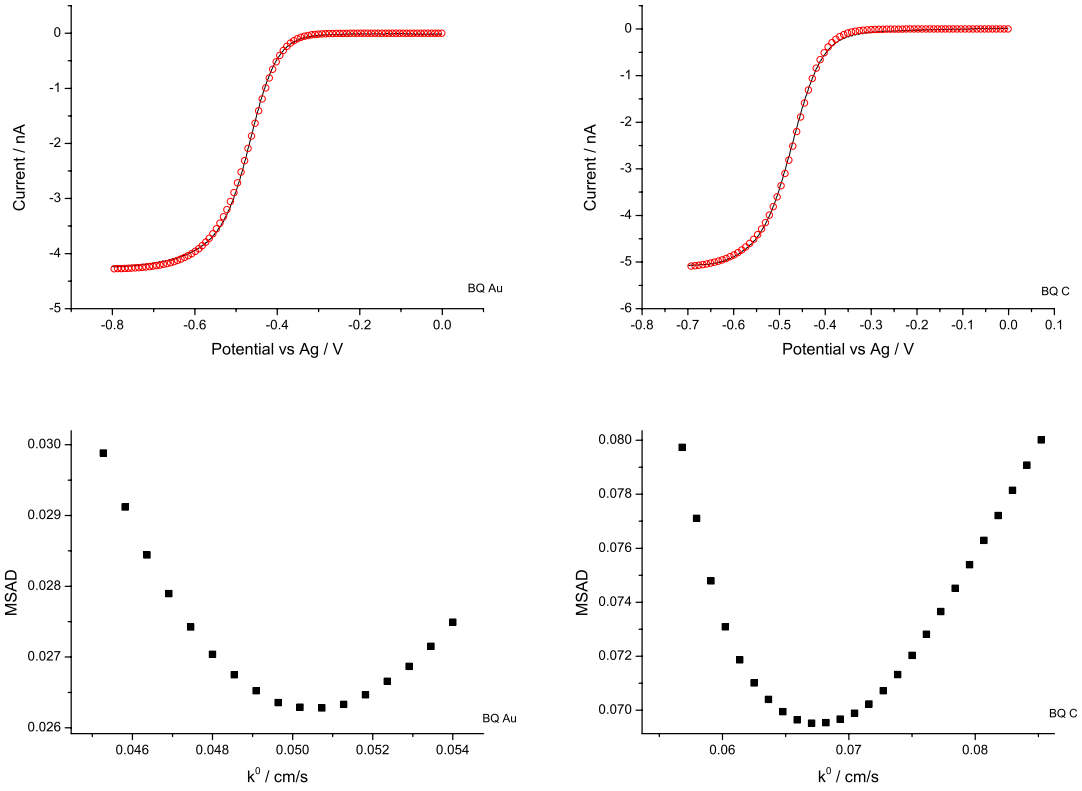

Figure 4.4: Experimental (line) and simulated (circles) best fits for the reduction of BQ (1mM) on both a gold (left) and carbon (right) microdisc at a scan rate of 25 mVs^{-1} [0.1M TBAP, 25°C, vs. Ag pseudo ref]. Also depicted (below voltammetry) is the plot of MSAD versus the value of k^o used within the simulation.

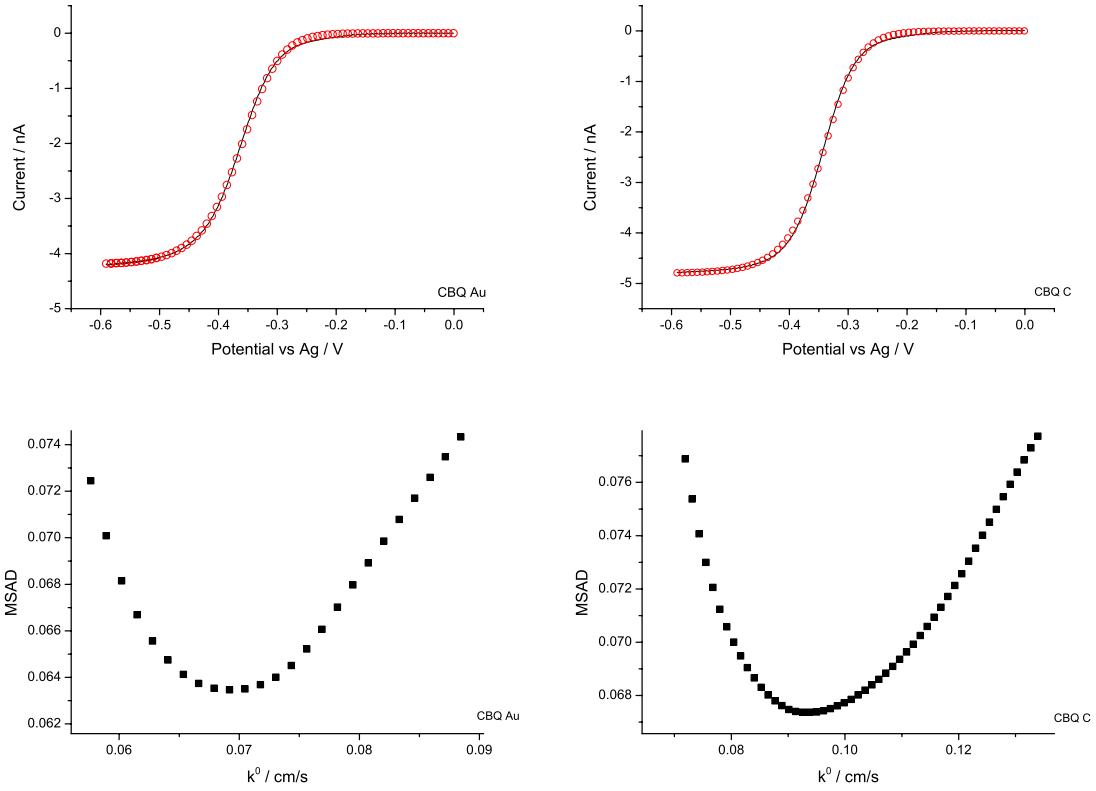

Figure 4.5: Experimental (line) and simulated (circles) best fits for the reduction of CBQ (1mM) on both a gold (left) and carbon (right) microdisc at a scan rate of 25 mVs^{-1} [0.1M TBAP, 25°C, vs. Ag pseudo ref]. Also depicted (below voltammetry) is the plot of MSAD versus the value of k^o used within the simulation.

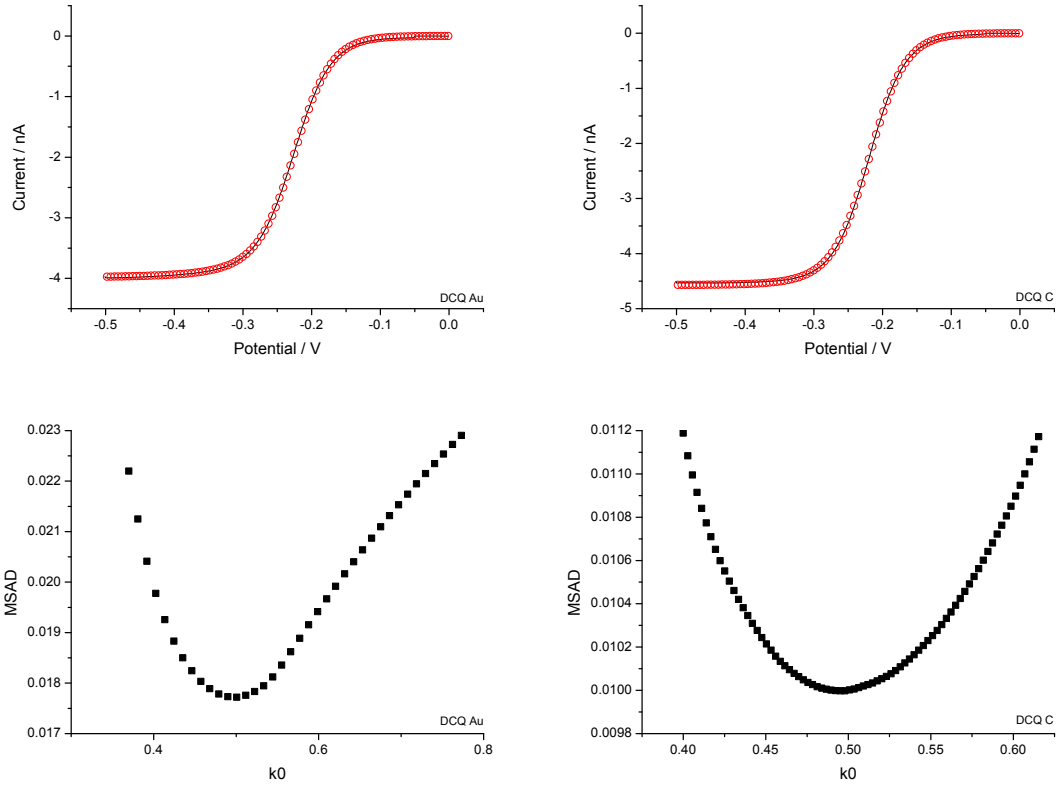

Figure 4.6: Experimental (line) and simulated (circles) best fits for the reduction of DCQ (1mM) on both a gold (left) and carbon (right) microdisc at a scan rate of 25 mVs^{-1} [0.1M TBAP, 25°C, vs. Ag pseudo ref]. Also depicted (below voltammetry) is the plot of MSAD versus the value of k^o used within the simulation.

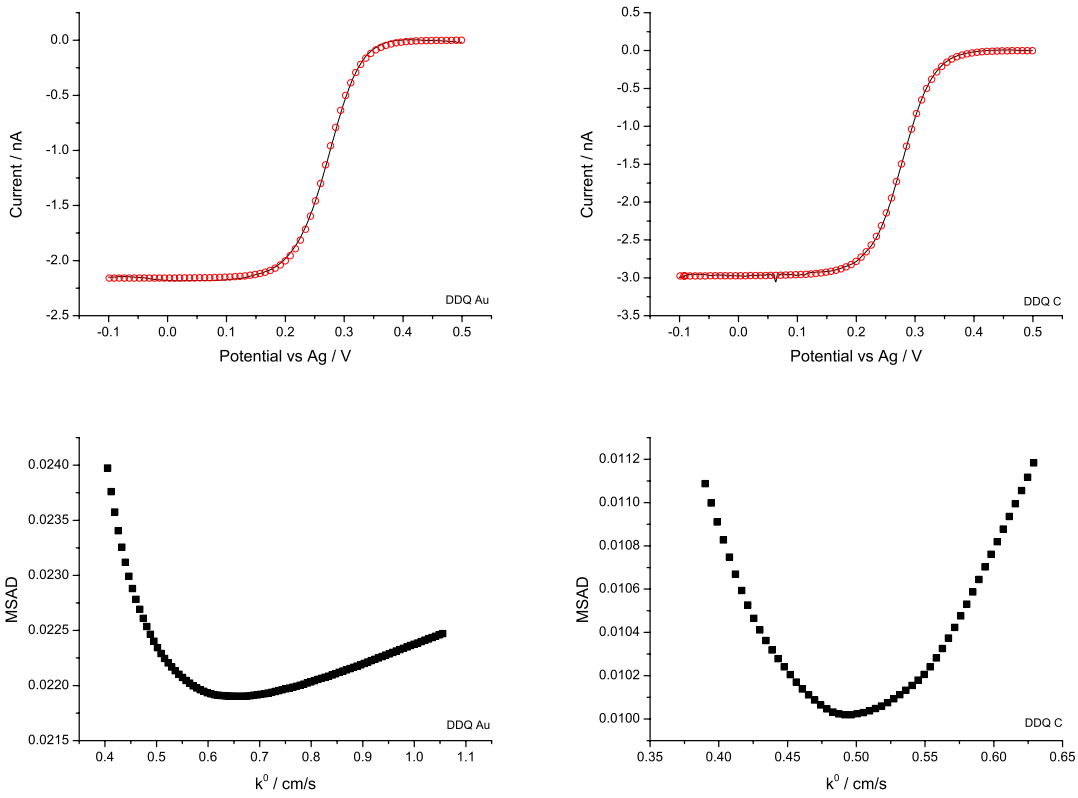

Figure 4.7: Experimental (line) and simulated (circles) best fits for the reduction of DDQ (1mM) on both a gold (left) and carbon (right) microdisc at a scan rate of 25 mVs^{-1} [0.1M TBAP, 25°C, vs. Ag pseudo ref]. Also depicted (below voltammetry) is the plot of MSAD versus the value of k^o used within the simulation.

The minimum in the MSAD versus k^o plots represents the best fit. Further, from these plots the *relative* errors in the k^o may be assessed, where the values quoted represent the k^o value where the MSAD is +10% greater than the minimum. In all experimental cases the fit of plot of MSAD versus k^o is asymmetric about the minimum, this is most apparent in the case of the reduction of DDQ on a gold electrode. This asymmetry arises due to the fact that at the high rates of electron transfer the influence of the electron transfer rate decreases, as the system tends towards the fully reversible (Nernstian) limit. Consequently the errors for the simulated best fit k^os within the text are given different upper and lower bounds. Table 4.1 provides the values for the best-fits i.e. the minimum in the MSAD plots. It should also be highlighted that although the values of alpha have been stated, due to the system being close to the reversible limit, alpha does not have a significant influence upon the simulated voltammetry. If error bars are applied to the simulated alpha values in an analogous manner to that done for the standard rates of electron transfer the variation will on average be $\alpha \pm 0.05$ units.

As can be seen a good agreement between the simulated and experimental results is achieved, as evidenced by the low MSAD values. It should be commented that these quinone species in *aqueous* media at a carbon electrode might be expected to exhibit surface adsorption.[18] However, as recently demonstrated and as will be discussed further in Chapter 7, the presence of acetonitrile can effectively block surface adsorption of electroactive species at graphitic materials.[19] Furthermore, given the high degree of fit and absence of 'pre' or 'post' voltammetric waves – which would be indicative of a surface bound species – it is reasonable to conclude that an outer-sphere electron transfer process is operative. Table 4.2 provides the experimental potentials for the reduction processes versus the pseudo silver reference and gives the confidence intervals (based on the MSAD) for the measured rates of electron transfer.

		Au micro	C micro
AQ			
	k^0 (cm s^{-1})	0.191	0.450
D = 2.43 × 10^{-5} cm^2 s^{-1}	alpha	0.584	0.489
	MSAD	0.0173	0.0149
BQ			
	k^0 (cm s^{-1})	0.0507	0.0670
D = 2.18 × 10^{-5} cm^2 s^{-1}	alpha	0.468	0.477
	MSAD	0.0263	0.0695
CBQ			
	k^0 (cm s^{-1})	0.0694	0.0930
D = 2.16 × 10^{-5} cm^2 s^{-1}	alpha	0.575	0.6
	MSAD	0.0635	0.06737
DCQ			
	k^0 (cm s^{-1})	0.501	0.495
D = 1.97 × 10^{-5} cm^2 s^{-1}	alpha	0.385	0.515
	MSAD	0.0177	0.010
DDQ			
	k^0 (cm s^{-1})	0.668	0.496
D = 1.47 × 10^{-5} cm^2 s^{-1}	alpha	0.498	0.453
	MSAD	0.0219	0.010

Table 4.1: Best-fit experimental values obtained from fitting of the simulated data. Where, D is the diffusion coefficient k^o is the rate of electron transfer.

Redox species	E_f^o vs Ag /V	k^o_{Au} /cm s^{-1}	k^o_C /cm s^{-1}
AQ	-0.86±0.03	$0.19^{+0.04}_{-0.03}$	$0.45^{+0.32}_{-0.11}$
BQ	-0.44±0.03	$0.051^{+0.006}_{-0.005}$	$0.067^{+0.014}_{-0.009}$
CBQ	-0.34±0.03	$0.069^{+0.013}_{-0.010}$	$0.093^{+0.031}_{-0.022}$
DCQ	-0.22±0.03	$0.50^{+0.10}_{-0.09}$	$0.50^{+0.11}_{-0.09}$
DDQ	0.27±0.03	$0.67^{+1.28}_{-0.27}$	$0.50^{+0.12}_{-0.10}$

Table 4.2: Experimentally measured formal potential ($E_f^{\ominus}$ vs. pseudo Ag ref) and standard rates of electron transfer (k^o) for the reduction of the quinone species for both gold and carbon electrodes. Error in the formal potential represents the variation of the pseudo reference electrode and the errors for standard rates of electron transfers represent +10% MSAD.

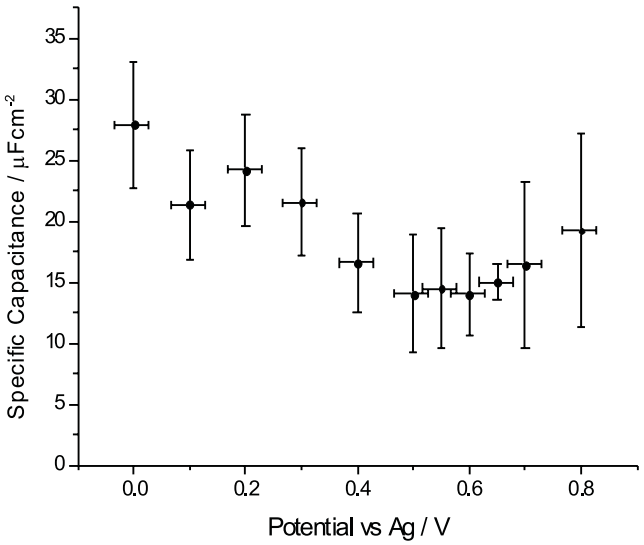

Figure 4.8: The variation in the capacitance for the carbon fibre microelectrode as a function of potential versus a pseudo Ag reference electrode. Capacitance was measured via cyclic voltammetry in an acetonitrile solution containing 0.1mM TBAP. The minimum indicates the position of the PZC.

Next, the potential of zero charge (PZC) for the carbon electrode was estimated. To a reasonable degree of accuracy, in the absence of adsorption, the electrochemical PZC correlates to the fermi level of the electrode.[20] The PZC (vs. the Ag pseudo reference) was measured for the carbon microelectrode via assessment of the capacitance through the use of cyclic voltammetry over a limited potential range (50mV) with a relatively high scan rate of 2 Vs^{-1}, in a solution containing 0.1mM TBAP. The results of this is shown in Figure 4.8, where a distinct minimum corresponding to the PZC is observed at $\sim$+0.55V vs. Ag, this value is comparable to that previously reported for a 'highly ordered pyrolytic graphite' electrode in an acetonitrile solution, $\sim$+0.59V vs. Ag (corrected). These later experiments were performed in a solution containing 0.2 M tetra-n-propylammonium tetrafluoroborate.[20]

The carbon fibre used within the microelectrode is a mesophase pitch-based material, consequently the carbon has a highly orientated molecular structure and is comprised of high crystallinity graphite.[21] The properties of the carbon fibre

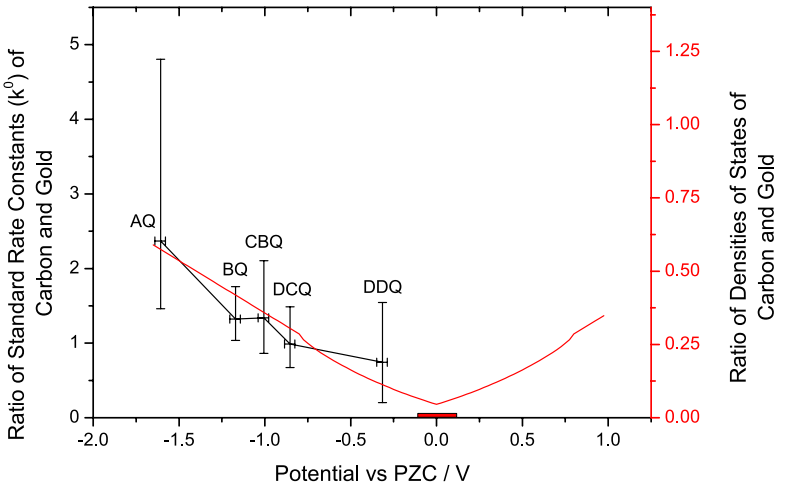

Figure 4.9: Left hand axis: The ratio of the standard electrochemical rate constants for carbon and gold, for the reduction of the quinone species as a function of the formal potential (vs PZC, where the red error on the x-axis represents the error in the known position of the PZC). Right hand axis: the ratio of theoretical densities of states of carbon and gold as a function of energy (plotted as a potential difference at the electrode interface).

may therefore to a first approximation be equated to that of highly ordered pyrolytic graphite. Hence, the density of electronic states should vary significantly as a function of potential at values close to the Fermi level. Using an analytical expression for the variation in the graphitic densities of states[22] and a value of 0.28 states atom^{-1} eV^{-1} for the density of states in gold,[13] it is possible to provide an estimate for the value of ρ_C/ρ_{Au}. This ratio is depicted as a function of potential in Figure 4.9. It should be emphasised that the ratio of the DOS has not been expressed on a per atom but on a per volume basis, so as to allow direct comparison between the two materials. Also depicted in Figure 4.9 is the ratio of standard electrochemical rate constants for the one electron reductions of quinonal species, as a function of potential (corrected to versus PZC). Given that the experimental data was measured versus an Ag pseudo reference the error for the experimental data in the x-direction mirrors the estimated variation in the reference potential.

Figure 4.9 shows a clear correlation between the theoretical ratio of the densities of states for the two materials and the measured ratio of the standard

electrochemical rate constants. Considering Equation 4.5 it can be seen that on the basis of the current theory this difference in the scaling of the two ratios likely represents the value of $H^{o2}_{DA(C)}/H^{o2}_{DA(Au)}$. Consequently, this data implies that the electronic coupling of the quinone species to the electrode surface is a factor of two greater for carbon than gold. In light of the work by Gosavi and Marcus[14] this result may not be unjustified owing to the likely different nature of the atomic orbitals involved in the electron transfer for the two cases.

4.2 Conclusions

In conclusion this work has successfully demonstrated that the redox potential may indirectly influence the electrochemical rate constant of an electroactive species on a carbon based electrode, such that, the variation in the standard electrochemical rate constant mirrors the variation in the density of electronic states of carbon. Further, from this analysis it is also shown that the electronic coupling of the quinone species is greater with the carbon substrate. This work opens up the possibility of further investigation, of fundamental studies of heterogenous electron transfer at carbon electrodes, with implications for the investigation of Marcus-Hush theory.

The following chapter studies the electrochemical response of quinones, specifically anthraquinone mono and di-sulfonate in aqueous media. The voltammetric response differs significantly as compared to that found in organic media, as utilised in this chapter.

References

[1] Banks, C. E.; Compton, R. G. *Analyst* **2006**, *131*, 15–21.

[2] Gerischer, H. *Electrochim. Acta* **1990**, *35*, 1677–1699.

[3] Izutsu, K. *Electrochemistry in Nonaqueous Solutions, 2nd Ed.*; Wiley, 2009.

[4] Marcus, R. A.; Sutin, N. *Biochim. Biophys. Acta* **1985**, *811*, 265–322.

[5] Marcus, R. A. *J. Chem. Phys.* **1956**, *24*, 966–978.

[6] Hush, N. S. *J. Chem. Phys.* **1958**, *28*, 962–972.

[7] Feldberg, S. W. *Anal. Chem.* **2010**, *82*, 5176–5183.

[8] Henstridge, M. C.; Laborda, E.; Rees, N. V.; Compton, R. G. *Electrochim. Acta* **2011**, in press.

[9] Weber, K.; Creager, S. E. *Anal.Chem.* **1994**, *66*, 3164–3172.

[10] Moser, J.; Grätzel, M. *Chem. Phys.* **1993**, *176*, 493–500.

[11] Wu, Q.; Van Voorhis, T. *J. Phys. Chem. A* **2006**, *110*, 9212–9218.

[12] Niimi, Y.; Matsui, T.; Kambara, H.; Tagami, K.; Tsukada, M.; Fukuyama, H. *Appl. Surf. Sci.* **2005**, *241*, 43–48.

[13] McCreery, R. L. *Chem. Rev.* **2008**, *108*, 2646–2687.

[14] Gosavi, S.; Marcus, R. A. *J. Phys. Chem. B* **2000**, *104*, 2067–2072.

[15] Mirkin, M. V.; Bard, A. J. *Anal. Chem.* **1992**, *64*, 2293–2302.

[16] Wang, Y.; Rogers, E. I.; Compton, R. G. *J. Electroanal. Chem.* **2010**, *648*, 15–19.

[17] Quan, M.; Sanchez, D.; Wasylkiw, M. F.; Smith, D. K. *J. Am. Chem. Soc.* **2007**, *129*, 12847–12856.

[18] Duvall, S. H.; McCreery, R. L. *J. Am. Chem. Soc.* **2000**, *122*, 6759–6764.

[19] Batchelor-McAuley, C.; Gonçalves, L. M.; Xiong, L.; Barros, A. A.; Compton, R. G. *Chem. Comm.* **2010**, *46*, 9037–9039.

[20] Gerischer, H.; McIntyre, R.; Scherson, D.; Storck, W. *J. Phys. Chem.* **1987**, *91*, 1930–5.

[21] Matsumoto, T. *Pure & Appl. Chem.* **1985**, *57*, 1553–1562.

[22] Dahn, J. R.; Reimers, J. N.; Sleigh, A. K.; Tiedje, T. *Phys. Rev. B* **1992**, *45*, 3773–3777.

Chapter 5

Voltammetric Characterisation of DNA Intercalators across the Full pH Range: Anthraquinone-2,6-disulfonate and Anthraquinone-2-sulfonate

The work presented in this chapter was published in the *Journal of Physical Chemistry B* 2010, 114, 4094–4100; the assistance of both Q. Li and S. Dapin should be noted in the collection of the experimental data.

As described in Chapter 2, a widespread strategy for electrochemical DNA detection is the utilisation of an electrochemical label which may bind to DNA. Whilst metal nanoparticles[1] and enzymes[2–4] have been used in this context the most commonly adopted label is that of a redox active molecule, especially ones which either intercalate between two adjacent base pairs or else interact with the DNA major or minor groove.[5] For intercalation flat, planar molecules are appropriate and examples include both organic compounds[6] and metal complexes,[7] of these the use of anthraquinone derivatives[8] is of particular interest. Work varies in complexity, from situations where the anthraquinone has been specifically modified for the purpose of being a DNA hybridisation indicator,[9] to analyses that simply involve adding of the reagent to the solution containing DNA. The later method

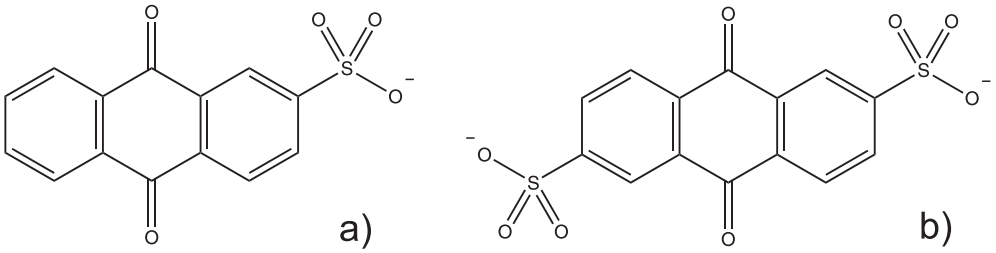

Figure 5.1: The structures of a) anthraquinone-2-sulfonate (AQMS) and b) anthraquinone-2,6-disulfonate (AQDS).

has the considerable advantage that prior labelling of reagents is unnecessary and the method is therefore 'universal' in nature.[10] Wong and Gooding[11] utilised the charge transfer ability of DNA to produce a sequence specific DNA sensor, whereby anthraquinone-2,6-disulfonic acid (AQDS) acted as a redox probe. The reductive redox signal decreased in the presence of C-A or G-A base pair mismatches. This methodology was further developed to allow in situ testing using anthraquinone-2-sulfonic acid (AQMS), this is possible due to the observed shift in electrochemical potential for the DNA bound form of the intercalator.[8,12]

The use of anthraquinone (AQ) derivatives, notably the sulfonate and disulfonate salts, is commonly necessitated in aqueous media due to the low water solubility of the underivatised form, viz. anthraquinone itself (6.5 μmol dm^{-3}).[13] The chemical structures of AQMS and AQDS are shown in Figure 5.1. Unlike in the previous chapter where the reduction of anthraquinone proceeded via two one-electron reductions, within aqueous media the two electron transfers occur during a single voltammetric feature. Further, under buffered acidic conditions and sufficiently driving negative potentials, the reduction of AQ or its derivatives, proceeds via a two-proton, two-electron process;

$$\mathrm{AQ} + 2\mathrm{H}^+ + 2\mathrm{e}^- \rightleftharpoons \mathrm{AQH}_2 \tag{5.1}$$

However, under other conditions (i.e. solutions of differing pH or supporting electrolyte) the process can, at least in principle, stop at a lower protonated or oxidation state. Moreover, even if the process is overall a 2-electron, 2-proton system the precise mechanism, i.e. the sequence of the addition of electrons and protons, can be pH dependent. Accordingly, the voltammetric signals seen for reaction 5.1 will be expected to, and in fact do, vary considerably with pH. Furthermore, there is evidence that with the case of sulfonated anthraquinones, these molecules can interact with cations present in solution,[14,15] this point shall be expanded upon in further in Chapter 10. It follows that the use of reaction 5.1 as a voltammetric probe is highly medium (solvent and electrolyte) dependent. Work done with the intercalation of anthraquinone derivatives into DNA, has generally been undertaken in buffered media at around neutral pH. At these levels of proton concentration, the reduction of the AQ derivative will result in the formation of the fully protonated form (due to the associated pK_a values) and will likely follow a complex mechanistic pathway, involving the mono-protonated semiquinone radical.

In the present chapter, the quantitative characteristics of the redox of anthraquinone-2,6-disulfonic acid and anthraquinone-2-sulfonic acid over the full pH range are presented. The variation in the peak potential and current is shown to vary significantly and has been successfully modelled, to describe the mechanistic rates, as a function of pH ($0 < pH < 13$). From a physical electrochemical perspective, we believe these studies to be the first case of a 'scheme of squares' analysis of a $2H^+$, $2e^-$ reaction over a full pH range of pH $0-13$. As the proton concentration is varied, the electrochemical reduction mechanism is shown to change from a simple EE process at high pH, then as the pH is lowered to around 10 an EECC mechanism predominately operates, at lower pH (4-7) an ECEC process occurs and finally at low pH (around pH 1) the reduction follows an CECE type mechanism. It should be noted here that in accordance with the Testa-Reinmuth

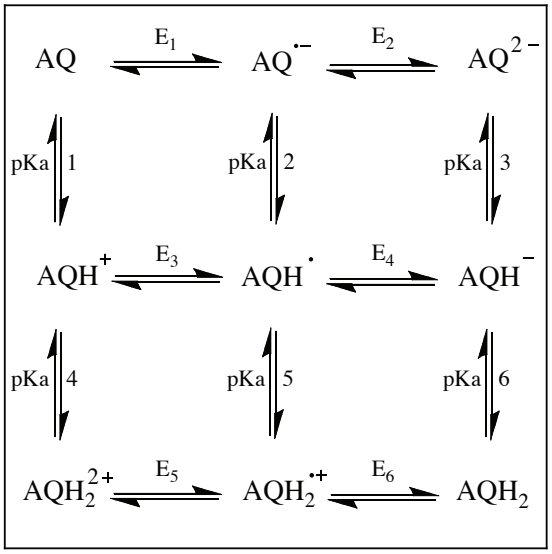

Figure 5.2: Generalised 'scheme of squares' for the anthraquinone $2H^+, 2e^-$ redox system.

nomenclature,[16] an 'E' step corresponds to an electron transfer and a 'C' represents a chemical process, such as a protonation as for the present example. The change in mechanism is a result of various protonated intermediates becoming involved in the electrochemical reaction as the pH is lowered, this is due to their differing acid dissociation constants.

5.1 Theory

Due to quinones being present in a number of biological systems, their electrochemical properties have long been studied. A theoretical description of the $2H^+$, $2e^-$ system was first proposed by Jacq,[17] this 'scheme of squares' model is based upon the assumption that the electron transfers are the rate limiting steps and that the protonations are at equilibrium. A generalised scheme for the anthraqinone redox system is presented in Figure 5.2. The mechanistic pathway taken is heavily dependent upon the associated pK_a values of the intermediate species and the pH of the local environment. Jacq's work was later developed by Laviron[18] where it was demonstrated that, where the transfer coefficient (α) is 0.5 and all diffusion

coefficients are equal, this scheme behaves as a simple reaction with two successive one-electron transfers with *apparent* rate constants and standard potentials. This has been applied to the analysis of the kinetics of p-benzoquinone reduction on a platinum electrode.[19] A complete scheme of squares has been approximately *calculated* for AQDS by Rosso et al.[20] by conversion of electron affinities in the gas phase to reduction potentials, but the values obtained are not realistic for media involving hydrogen bonding, the calculated potentials for the first and second electron transfer differ by 107 mV, in such a case at high pH two consecutive one-electron transfers would be observed, as per aprotic media; experimentally in aqueous media one peak is observed.

The electrochemical response of quinones differs greatly between protic and aprotic media, in which they tend to show one and two electron waves respectively. This incongruous behaviour was explained by Quan et al.[21] whom demonstrated the role of hydrogen bonding in stabilising the reduced dianion form of the quinone. Recent work has also aimed to apply the 'scheme of squares' to the simulation and analysis of the redox behaviour of flavin adenine dinucleotide, but this work was only focused on a limited pH range (5-9). Moreover, the analysis did not involve the use of the diprotonated oxidised or the unprotonated reduced forms, pK_a values were specifically chosen so that they did not contribute to the overall observed current. Furthermore, the simulation is simplified by the assumption that all electron transfer rate constants are arbitrarily high, with a value of 10^4 cm s^{-1} being used universally. Comparison of this work to experimental data was exclusively limited to the position of the peak potential of the reductive wave[22,23] and ignored the magnitude of the voltammetric waves, their shapes and their widths.

5.2 Experimental

5.2.1 Modelling

Simulations for the current investigation was carried out using the commercial software package DIGISIM® (version 3.0, BASi Technicol, USA). Digisim is based on a fully implicit finite difference (IFD) method as proposed by Rudolph.[24,25] For both AQDS and AQMS three of the pK_a values within the scheme have been reported by a number of groups, Gamage et al.[15] provides a table of known values. Table 5.1 gives the values used within this work taken from the literature for simulation purposes, note the pK_a value used for the AQMS semiquinone is marginally higher than the given literature values due to improved simulation results. All protonations were assumed to be fully buffered, consequently the following equilibrium can be used within DIGISIM®;

$$\begin{aligned} \mathrm{B} &\rightleftharpoons \mathrm{A} \\ K_{eq} &= \frac{K_a}{[\mathrm{H}^+]} \end{aligned}$$

Here A is the unprotonated form, B the protonated form and K_a is the actual acid dissociation constant for the species B. Realistic rate constants must be used within the simulation, as such the rate constant for protonation must and can be no larger than 1×10^{10} dm^3 mol^{-1} s^{-1} (diffusion limited), it can also be shown that with the equilibrium used above, the the rate constant for protonation depend on the proton concentration. Within the model, all diffusion coefficients were set as equal and values taken were those measured from the steady-state current at a microdisk electrode; see section below for further explanation. Further, all electron transfer coefficients, α, were set as 0.5.

5.2.2 Diffusion Coefficient Determination

The diffusion coefficients of both AQDS and AQMS were determined via two methods, first, via the use of the Randles-Ševčík equation for peak current of a reversible electron transfer at a macroelectrode and, second, via use a microelectrode and calculation of the diffusion coefficient from the limiting current. Solutions containing 0.1M NaOH, 0.1M KCl and either 1mM AQDS or AQMS were prepared (pH 12.6). Cyclic voltammetry was run on a gold macroelectrode from -0.4 V to -0.75 V (vs SCE) at varying scan rates from 50 mVs^{-1} to 500 mVs^{-1} (results not shown). The reductive peak current was plotted against the square root of the scan rate, through use of the Randles-Ševčík equation for a reversible n electron process (Equation 5.2).[26]

$$i_p = (2.69 \times 10^5) A D^{0.5} C \nu^{0.5} n^{1.5} \tag{5.2}$$

Here i_p is the peak current (*amperes*), A the area of the electrode (cm^2), D is the diffusion coefficient (cm^2s^{-1}), C is the bulk concentration of the analyte (moles cm^{-3}), ν is the scan rate (Vs^{-1}) and n is the total number of electrons transferred. It is possible to estimate the *apparent* diffusion coefficients for AQDS and AQMS as being 2.0×10^{-6} cm^2 s^{-1} and 2.9×10^{-6} cm^2 s^{-1}. Note these diffusion coefficients are discussed below and the true values are found to be quite different in the light of microelectrode experiments, resulting from the inapplicability of Equation 5.2 to the process is of interest.

Prior to measurement of the anthraquinone diffusion coefficients via use of a microdisc, the microdisc electrode requires accurate calibration. The radius of gold microdisk electrode was characterised via electrochemical methods, a solution containing 2mM ferrocene and 0.1M tetra-n-butylammonium perchlorate in acetonitrile was prepared, through performing chronoamperometry and using the

equation developed by Shoup and Szabo[27] the radius of the electrode was accurately determined (not shown). This electrode was then voltammetrically scanned, at 5 mVs^{-1} in the above pH 12.6 solutions and the limiting current for each species measured (not shown). Equation 5.3 describes the steady-sate current at a microdisk electrode,[26] this was used to determine the diffusion coefficient, values of 5.2×10^{-6} cm^2 s^{-1} and 4.7×10^{-6} cm^2 s^{-1} were found for AQDS and AQMS.

$$i_{ss} = 4nFDCr \tag{5.3}$$

The notation used is the same as above but here i_{ss} is the steady-state current (amperes) at the microelectrode, F is the Faraday constant and r is the radius of the electrode (cm). There is a large discrepancy between the two methods outlined (microelectrode vs. macroelectrode), for measuring the diffusion coefficients. The Randles-Ševčík equation for a multi-electron transfer is based upon the assumption that the electron transfer rate is high and that the second electron transfer is sufficiently driven, so as the two redox processes occur concurrently. These assumptions do not hold for the case in question, as such, the use of the Randles-Ševčík equation underestimates the values of D. In particular the close but not equal values of the redox potentials for the first and second electron transfer, leads to the cyclic voltammetry showing a diffusional process but not one which is quantitatively consistent with Equation 5.2. For systems involving the transfer of multiple electrons, in which the subsequent electron transfer steps are not sufficiently driven, there is a significant error when the Randles-Ševčík equation is used for the analysis of the diffusion coefficients involved. This arises due to the increased probability of the intermediate species diffusing away from the electrode surface before being further oxidised or reduced, causing a decrease in the peak current. This point is expanded upon within Chapter 12.

The measurement of the diffusion coefficients via the use of the microdisc is more accurate, due to the methodology not being influenced by the associated electron transfer kinetics or separation between two redox potentials. Accordingly, the limiting current at the microdisc electrode is controlled by the diffusion of AQ and at sufficiently negative potentials is a full two electron process. As such the values obtained from the microdisc experiment were used in the theoretical model.

5.3 Results and Discussion

The electrochemical response of AQDS and AQMS was examined over the full aqueous pH range as shown in Figures 5.3 a) and c). For both species 1mM solutions were prepared in buffered media, cyclic voltammetry was run in a cathodic direction from an upper potential of +0.2 V to -0.9 V (vs SCE) at a scan rate of 100 mV s^{-1}, as can be clearly seen from the plots appropriate potential limits were chosen for each pH. It was not possible to measure the voltammetry of AQMS below pH 1, due to the low solubility of the species in this medium.

At high pH i.e. above pH 12, both anthraquinone derivatives should exhibit a simple EE process with no coupled homogeneous reactions (protonations), between, before or after the electron transfer steps, this allows the values of E_1 and E_2 and the associated electron transfer rates to be obtained through fitting. As the pH is decreased the reduction product changes from the unprotonated, to the monoprontonated and finally to the diprotonated form as the respective pK_as are reached. This change in equilibrium causes a Nernstian shift in the observed $E_f^{\ominus}$ for the redox couple. If the simulation is limited to an EECC mechanism then at higher proton concentrations (below about pH 6) the back-peak (oxidative wave) decreases in size, as the shift in equilibrium towards the protonated forms promotes *apparent* irreversibility. A similar situation was found by Streeter et al.[28] where the instability of the reduced 2,6-diphenylpyrylium cation led to an appar-

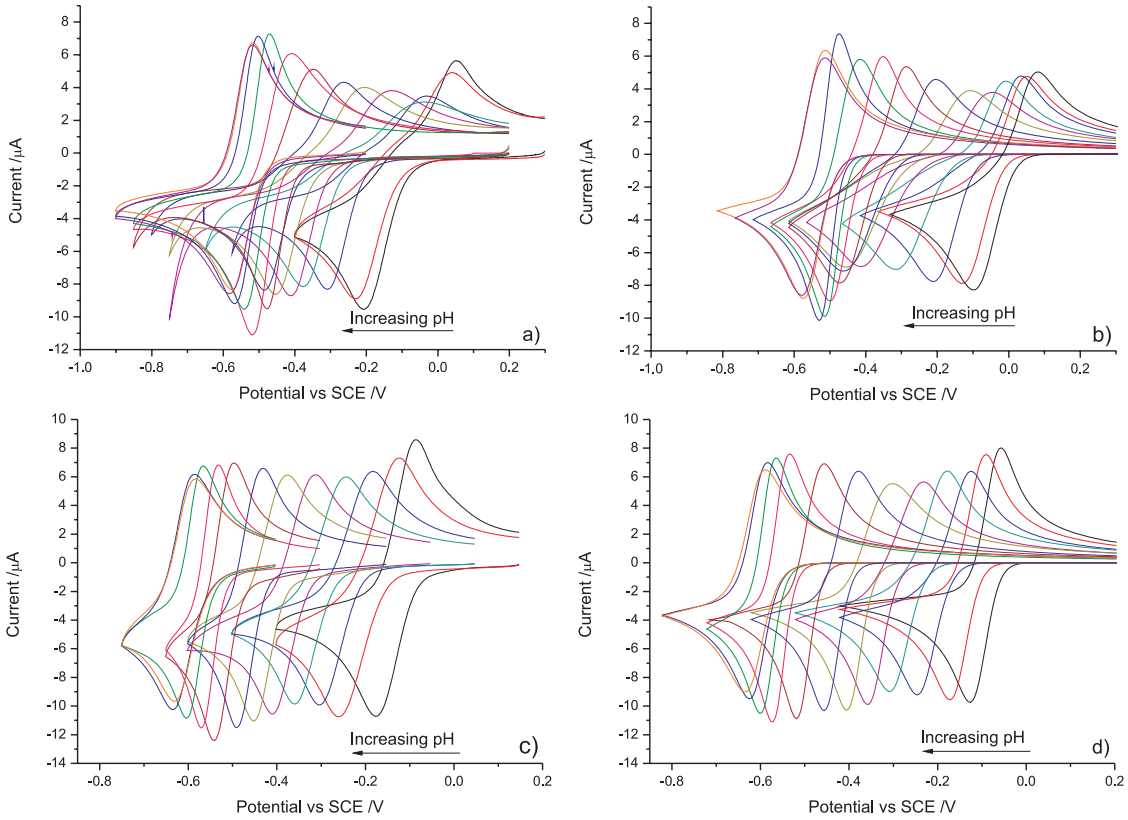

Figure 5.3: Overlaid cyclic voltammetry for 1mM AQDS (a + b) and 1mM AQMS (c + d), over the full aqueous pH range 1-13 (0.1M buffer); experimental (a + c) and simulated (b + d) results are plotted separately. Colour code: black (pH 1), red (pH 2), light blue (pH 3), dark green (pH 4), dark pink (pH 5), light green (pH 6), dark blue (pH 7), dark red (pH 8), dark pink (pH 9), green (pH 10), dark blue (pH 11), orange (pH 12) and purple (pH 13).

	AQDS	AQMS
pK_a 1	0	0.84
pK_a 2	3.2^a	4.3^a
pK_a 3	10.5^a	11^a
pK_a 5	4.8	3.12
pK_a 6	7.6^a	7.6^a

Table 5.1: pK_a values used within this work as labelled on Figure 5.2, ^{a} values are taken from work by Gamage et al.[15], others are calculated from optimised standard potentials used with the simulations.

ent irreversible electrochemical response. This point shall be further emphasised and investigated in Chapter 12. So as to allow a description of the anthraquinone sulfonate derivative redox system at lower pH other mechanistic pathways must be included. The issue of apparent irreversibility of the EECC mechanism is predominately solved through the inclusion of $AQH_2^{\cdot+}$, $AQH^{\cdot}$ and AQH^+ as intermediates. If the intermediates $AQH_2^{\cdot+}$ and AQH^+ are not included within the simulation it is not possible to produce a system in which a good fit is obtained over the full pH range, this arises due to the ECEC mechanism becoming more irreversible in nature at higher proton concentrations. We assume that because of the extreme difficulty of doubly protonating AQ – such that AQH_2^{2+} in an unknown species in aqueous solution (to the best of the author's knowledge) – the e^-, H^+ sequence by which AQ is reduced to AQH_2 does not involve the AQH_2^{2+} as an intermediate within the embraced pH range of this study. This model was then optimised to give a best fit, the two major fitting characteristics considered were peak position and peak current. Table 5.1 gives the acid dissociation constants used within this work, with the literature values clearly labelled. Table 5.2 gives the optimised values for the potentials and electron transfer rates for the two AQ derivatives. The overlaid simulated voltammetry obtained from these values is depicted in Figure 5.3 for both AQDS (b) and AQMS (d).

It can be seen from Figure 5.3 and from the values given in Table 5.2 that the overpotential associated with the AQDS redox system is larger than that for

Redox couple	Standard potential (V vs SCE)	Electron transfer rate (cms^{-1})
	AQDS	
E_1	-0.529	0.025
E_2	-0.565	0.1
E_3	-0.340	1.0
E_4	-0.134	10
E_6	+0.029	0.019
	AQMS	
E_1	-0.606	10
E_2	-0.621	0.38
E_3	-0.400	10
E_4	-0.227	10
E_6	+0.038	10

Table 5.2: Values for the standard potentials and electron transfer rates obtained from the optimised simulation for both AQDS and AQMS.

AQMS. The sulfonate groups present have a negative charge at all pHs tested due to having a pK_a value of around -9. As a consequence, when the system undergoes a two electron reduction, the result is a highly charged 4- ion. Gamage et al.[14] demonstrated through x-ray crystallography that there is a likely interaction between the sulphonate and quinone oxygen groups. Hence, the relatively large overpotential present for the AQDS reduction probably originates from a change in shape between either the quinone and semiquinone or seminquinone and hydroquinone species.[26]

The simulation was optimised so as to get a best fit with experiment, the primary criteria being the peak position (V) and peak height (A), Figure 5.4 shows the comparison between these two measurements. A good fit was obtained over the full pH range; improvement of the fit through the use of an MSAD measurement was not attempted due to the large number of variables which may leading to non-realistic results being obtained. As observed by Conant et al.[29] the addition of a sulfonate group in either the 1 or 2 position adjacent to a quinone oxygen

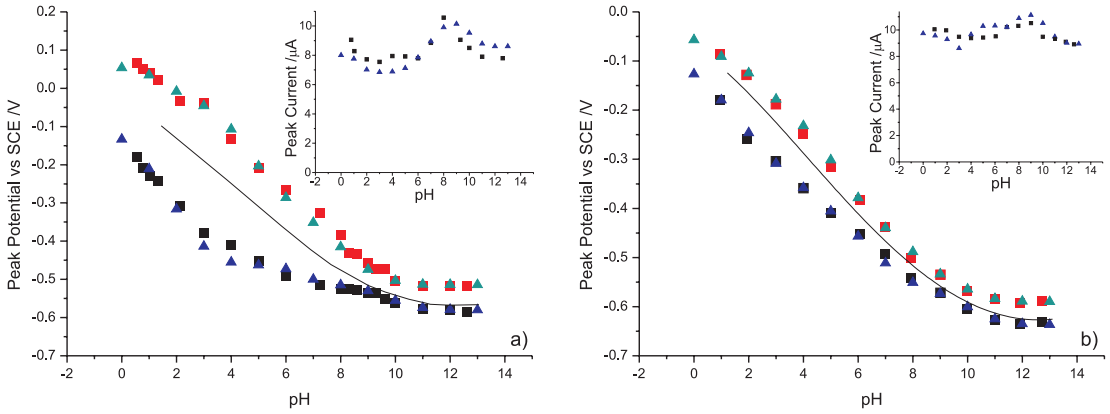

Figure 5.4: Comparison of experimental (exp) and simulated (sim) results for a) AQDS and b) AQMS. Main plots show peak potential versus pH; reductive peak, black squares (exp) and blue triangles (sim), oxidative peak, red squares (exp) and green triangles (sim). The black line represents the E_o values as taken from work by Conant et al..[29] Insets depict the variation of peak height with pH for both experimental (black squares) and simulated (blue triangles). Errors: magnitude of square point represents the error for the experimental data in the y-axis.

causes a shift of around +40mV of the $E_f^{\ominus}$ due to the electron withdrawing nature of the added sulfonate group. This observation is born out in practice, with the $E_f^{\ominus}$ values provided by Conant et al.[29] (plotted as a black line in Figure 5.4) being in good agreement with the experimental results. Quantitative agreement was possible between simulation and experiment with the assumption of equal diffusion coefficients for all the anthraquinone species, provided some unusual features of the system were recognised. Moreover, in the absence of this recognition no fits were possible across the pH range. The first unusual factor is that the rapid protonation seen at low pH following electron transfer can promote the electrochemical *irreversibility* of couples, which are normally thought to show rapid electron transfer (i.e. quinone/semiquinone; semiquinone/hydroquinone). This factor influences both the wave shape and the voltammetric peak-to-peak separation. A second unusual factor is the close similarity of the formal potentials of the two couples; this leads to the cyclic voltammetry showing diffusional characteristics but with the peak current unrelated to the usual expressions for simple n electron reversible or irreversible behaviour. Finally, the pK_as of the quinone, semiquinone and hy-

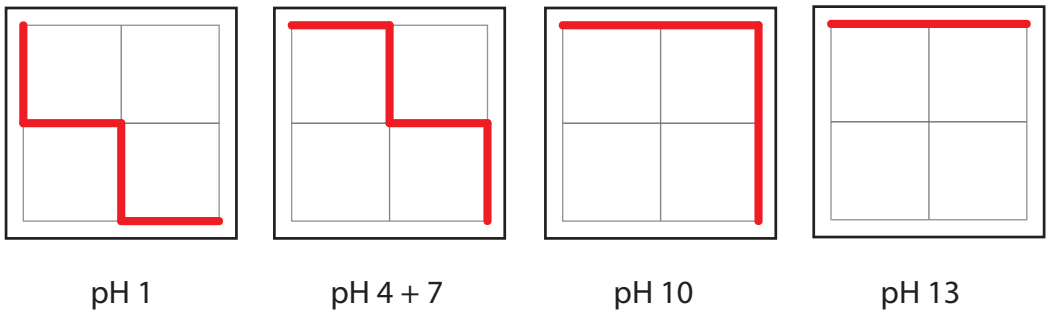

Figure 5.5: Scheme showing the major mechanistic pathways for both AQDS and AQMS at varying pH. Horizontal movement represents electron transfer and vertical represents proton transfer, as per Figure 5.2.

droquinone do not necessarily show comparable trends to each other, so that the model needs to consider a wide range of pK_a parameters to identify a correct fit.

The model provided, allows assessment of the dominating mechanistic pathway for the reduction of the two compounds at various pH, this is achieved through selectively 'switching off' pathways within the scheme. Due to the similarities in the pK_a values for the two species, at the pHs selected the same mechanistic pathways operate for both compounds. Figure 5.5 gives a graphical representation of these mechanisms, here horizontal movement indicates an electron transfer and vertical movement represents a proton transfer, as per Figure 5.2. It is of importance to note that although these are the dominant pathways at each pH, other mechanistic routes may contribute to the observed current, certainly in regions between the selected pH's multiple routes may occur concurrently. The relative contributions to the peak current of each pathway is also not only dependent upon the equilibrium position for each protonation but importantly for AQDS the relative rates of electron transfer will also have an effect. It is also of worth noting that the forward and back reaction routes may not be the same as it is possible for the rate determining electron transfer step to change with potential.

5.4 Conclusions

For the first time a 'scheme of squares' model has been used to produce an accurate description of a $2H^+$, $2e^-$ redox system over the full pH range with direct comparison to experimentally produced cyclic voltammetry. This analysis has provided quantitative information on the pK_as and $E_f^{\ominus}$s involved within the systems and allowed the dominant mechanistic routes to be resolved at varying pH, subsequently this greater understanding will provide a basis upon which more sensitive and sophisticated DNA hybridisation sensors can be developed. The model demonstrates how the pK_a values of the anthraquinone intermediates dominate the observed voltammetry, the change in proton concentration not only causes a Nernstian shift in the measured electrochemical potential for the redox couple but also results in changes in the mechanistic pathway. At high pH a simple EE process is found to occur, as the pH decreases the formation of other protonated species becomes possible, around pH 10 the mechanism is shown to be an EECC process, at pH 4-7 the redox process follows an ECEC route and finally in acidic conditions (around pH 1) the mechanism is shown to likely follow a CECE process.

References

[1] Zhang, J.; Song, S.; Wang, L.; Pan, D.; Fan, C. *Nat. Protoc.* **2007**, *2*, 2888–2895.

[2] Wang, Z.; Yang, Y.; Leng, K.; Li, J.; Zheng, F.; Shen, G.; Yu, R. *Anal. Lett.* **2008**, *41*, 24–35.

[3] Elena, D.; Oscar, R.; Arantzazu, N. *Anal. Chem.* **2004**, *76*, 3132–8.

[4] Alfonta, L.; Singh, A. K.; Willner, I. *Anal. Chem.* **2001**, *73*, 91–102.

[5] Choi, Y. S.; Lee, K. S.; Park, D. H. *Curr. Appl. Phys.* **2006**, *6*, 777–780.

[6] Erdem, A.; Kerman, K.; Meric, B.; Akarca, U. S.; Ozsoz, M. *Anal. Chim. Acta* **2000**, *422*, 139–149.

[7] Carter, M. T.; Rodriguez, M.; Bard, A. J. *J. Am. Chem. Soc.* **1989**, *111*, 8901–8911.

[8] Wong, E. L. S.; Mearns, F. J.; Gooding, J. J. *Sens. Actuators B* **2005**, *111-112*, 515–521.

[9] Kowalczyk, A.; Nowicka, A. M.; Jurczakowski, R.; Niedzialkowski, P.; Ossowski, T.; Stojek, Z. *Electroanalysis* **2010**, *22*, 49–59.

[10] Castaño Álvarez, M.; Fernández-Abedul, M.; Costa-García, A. *Electrophoresis* **2007**, *28*, 4679–4689.

[11] Wong, E. L. S.; Gooding, J. J. *Anal. Chem.* **2003**, *75*, 3845–3852.

[12] Wong, E. L. S.; Gooding, J. J. *Aust. J. Chem.* **2005**, *58*, 280–287.

[13] Zhong, C.; Hu, Q. *J. Pharm. Sci.* **2003**, *92*, 2284–2294.

[14] Gamage, R. S. K. A.; Peake, B. M.; Simpson, J. *Aust. J. Chem.* **1993**, *46*, 1595–1604.

[15] Gamage, R. S. K. A.; McQuillan, A. J.; Peake, B. M. *J. Chem. Soc. Farad. Trans.* **1991**, *87*, 3653–3660.

[16] Testa, A. C.; Reinmuth, W. H. *Anal. Chem.* **1961**, *33*, 1320–1324.

[17] Jacq, J. *J. Electroanal. Chem.* **1971**, *29*, 149–180.

[18] Laviron, E. *J. Electroanal. Chem.* **1983**, *146*, 15–36.

[19] Laviron, E. *J. Electroanal. Chem.* **1984**, *164*, 213–227.

[20] Rosso, K. M.; Smith, D. M. A.; Wang, Z.; Ainsworth, C. C.; Fredrickson, J. K. *J. Phys. Chem. A* **2004**, *108*, 3292–3303.

[21] Quan, M.; Sanchez, D.; Wasylkiw, M. F.; Smith, D. K. *J. Am. Chem. Soc.* **2007**, *129*, 12847–12856.

[22] Malinowski, E.; Barber, M. J.; Whitaker, G. T.; Smith, E. T. *J. Chemometr.* **2007**, *21*, 520–528.

[23] Smith, E. T.; Davis, C. A.; Barber, M. J. *Anal. Biochem.* **2003**, *323*, 114–121.

[24] Rudolph, M. *J. Electroanal. Chem.* **1991**, *314*, 13–22.

[25] Rudolph, M. *J. Electroanal. Chem.* **1992**, *338*, 85–98.

[26] Compton, R. G.; Banks, C. E. *Understanding Voltammetry*; World Scientific Publishing, Singapore, 2007.

[27] Shoup, D.; Szabo, A. *J. Electroanal. Chem.* **1982**, *140*, 237–245.

[28] Streeter, I.; Jenkinson, S.; Fleet, G. W. J.; Compton, R. G. *J. Electroanal. Chem.* **2007**, *600*, 285–293.

[29] Conant, T. B.; Kahn, H. M.; Fieser, L. F.; Kurtz Jr., S. S. *J. Am. Chem. Soc.* **1922**, *44*, 1383–1396.

Chapter 6

Voltammetric Responses of Surface-Bound and Solution-Phase Anthraquinone Moieties in the Presence of Unbuffered Media

The work in the previous chapter considered the voltammetric responses of both anthraquinone-2,6-disulfonate (AQDS) and anthraquinone-2-sulfonate (AQMS) in a fully buffered aqueous environment. This chapter continues by considering the electrochemical response of AQMS and surface bound anthraquinone, under conditions of *low* buffering. Specifically, the author highlights how under certain aqueous conditions two voltammetric reduction waves for anthraquinone may be observed. In contrast to the previously discussed results in non-aqueous media, the two voltammetric peaks presented in the following work are *not* a result of a large difference in formal potential for the first and second electron transfer. In this present work, the voltammetric response is a result of the change in the pH adjacent to the interface during the voltammetric scan. Moreover, the magnitude of the pH change is illuminated through simulation. The work presented herein was published in the article '*Journal of Physical Chemistry C* 2011, 115, 714–718.' The help of B.R. Kozub is highlighted for her aiding the production of the modified carbon electrode and recording its response in low buffered media.

Numerous redox processes involve the coupled transfer of both protons and electrons.[1] Within biological systems pH gradients are utilised within a cell for the energy conversion and storage.[2] Attempts to chemically mimic biological functions have also focused on the use of protonation as a source of energy.[3,4] Apart from these more complex examples, changes in pH have also recently been used within the literature for both the exploration of electrochemical mechanisms[5] and as a method of controlling the rate of chemical reactions.[6] The study of the influence on the local pH of these reactions at an electrode interface has been probed using methods such as interferometry,[7] Raman spectroscopy[8] and the fluorescence of pH sensitive probes.[9,10] Of the species able to undergo multiple electron and proton transfers anthraquinone and its derivatives have been well studied as model systems. As discussed in the previous chapter, theoretical descriptions of the $2H^+, 2e^-$ system may be achieved through the use of a 'scheme of squares' mechanism. A generalised scheme for the redox behaviour of anthraquinone (AQ) was presented in Figure 5.2. Recent work by Quan *et al.* demonstrated how the somewhat incongruously large difference in redox behaviour for quinones in protic and non-protic media may be explained in terms of hydrogen bonding of the reduced dianion species.[11] This was understood through the investigation of the influence of the concentration of buffer present in the electrolyte solution upon the observed voltammetry. Voltammetric simulations based upon the 'scheme of squares' for two-proton, two-electron systems are surprisingly limited within the literature with examples mainly focusing on buffered systems over limited pH ranges.[12,13] However, Guo *et al.* have undertaken a quantitative analysis of the voltammetric response of $[\alpha 2 - Fe(OH_2)P_2W_{17}O_{61}]^{7-/8-}$, which undergoes a $1H^+, 1e^-$ transfer. This species was studied in conditions of limited concentrations of buffer;[14] proton consumption during the redox process was clearly demonstrated to cause a second voltammetric feature.

Carbon electrodes present a rich variety of oxygen functionality upon their surface.[15] Certainly for some redox species these oxygen species may impart a strong influence upon the electron transfer process.[16] However, these groups also provide numerous routes by which redox active species maybe bound to the electrode surface. Chemical modification may be achieved through a variety of methods but the use of diazonium salt chemistry is widely employed.[17] As a result of their highly reactive nature diazonium salts allow the production of surfaces with high surface coverages. The use of anthraquinone modified carbon electrodes has previously been utilised for the production of reagentless electrochemical pH probes, able to accurately measure the pH of buffered media across a large range of pHs.[18,19] A recent review of the use of carbon derivatised carbon materials for pH measurement has been undertaken by Kahlert.[20] The effect of low buffered media upon these pH probes has not been investigated and as will be shown, the voltammetric response is significantly altered.

The cyclic voltammetry of anthraquinone monosulfonate is shown to exhibit two waves under conditions of low buffer concentrations. This system is demonstrated to be readily simulated providing quantitative information about the variation in the local pH adjacent to the electrode. Furthermore, the modification of a graphitic electrode with anthraquinone moieties is achieved through the use of diazonium salt chemistry. This modified electrode is voltammetrically characterised and shown to be highly reversible with the peak potentials for the redox feature varying in a Nernstian manner. The response of this electrode in conditions of limited buffer also exhibits significant proton consumption, as a result of the high surface loading. As such, this work provides physical insight into how surface bound anthraquinone under conditions of limited buffering exhibits a distorted voltammetric response involving split waves; this result is analogous to that found for solution-phase anthraquinone. Hence, this demonstrates that a

significant change in the pH of the solution adjacent to the electrode is occurring as a result of consumption of protons during the electrochemical experiment.

6.1 Experimental Methods

6.1.1 Synthesis of Anthraquinone-2-diazonium Tetrafluoroborate

Anthraquinone-2-diazonium tetrafluoroborate was synthesized according to the method developed by Milner.[21] 0.5 g of 2-aminoanthraquinone (Sigma–Aldrich, Gillingham, U.K.) was added to 0.4 g of nitrosonium tetrafluoroborate (ca 50% molar excess) (Sigma–Aldrich, Gillingham, U.K.) in 50 ml of dichloromethane (DCM) (Fisher Scientific, Loughborough, U.K.). The slurry was kept in an ice–water bath. It was stirred for 1 h and after which the DCM was removed under vacuum. The resulting anthraquinone-2-diazonium tetrafluoroborate product was stored at -5°C.

6.1.2 Modification of EPPG Electrode with 2-Anthraquinone Groups

The polished 'edge plane pyrolytic graphite' (EPPG) electrode was immersed in a stirred solution of ca. 0.04 g of synthesized anthraquinone-2-diazonium tetrafluoroborate product in 25 ml of water for about 30 minutes. The solution of diazonium salt was prepared using deionized water cooled to the temperature below 5°C. After that the EPPG electrode modified with 2-anthraquinone groups (AQ-2 modified EPPG) was rinsed with acetonitrile, DMF and deionised water to remove any unreacted salt.

6.1.3 Modelling

The DIGISIM® based model presented in this chapter differs from that provided in the previous due to requiring that the proton concentration is finite. Protonation

steps were modelled as

$$A + H^+ \rightleftharpoons B \qquad\qquad K = \frac{[B]}{[A][H^+]}$$

to enable the system to be fully equilibrated at all points the rate of the protonation was set as being larger than 1×10^{10} $mol^{-1}dm^3s^{-1}$. This simplification ensures that it is unnecessary to include all of the possible mechanistic pathways leading to a change in the level of protonation of the intermediate species. Included within the simulation was the self-ionisation of water, where the concentration of water was set as 55.56 M and the value of K_w taken as 1.0×10^{-14} mol^2 dm^{-6}.[22] Control of the pH of the system was modelled through the inclusion of 0.1M buffer (as per the experimental section).

The values used for the standard potentials, electron transfer rates and pK_as associated with the solution phase AQMS system were taken from the work presented in the previous chapter. Further, the diffusion coefficient was set as being $4.7\times$ 10^{-6} cm^2 s^{-1}, as measured from the reductive steady-state current at an Au microdisc electrode in aqueous media. The diffusion coefficient of the proton varies between 5.0×10^{-5} and 9.3×10^{-5} cm^2 s^{-1} depending on the ionic strength of the solution,[23] but in accordance with the theoretical value as given by from the Grothus mechanism[24] and from experimental work by Unwin[25] a value of 7×10^{-5} cm^2 s^{-1} was used within the simulations. In reference to the nomenclature used within this text the double reduced and unprotonated form of anthraquinone is referred to as the dianion species (AQ^{2-}). As such in the case of AQMS this ignores the charge associated with the sulfonate group, this is done in order to simplify the discussion and ease direct comparison between the solution phase and surface bound species.

6.2 Results and Discussion

6.2.1 Solution Phase Voltammetry of AQMS

The cyclic voltammetric response of 1mM AQMS at a gold macro electrode was measured in aqueous media containing varying concentrations of HCl as depicted in Figure 6.1 a). The voltammetric response of AQMS has previously been shown to be a reversible $2H^+, 2e^-$ system and to exhibit near Nernstian behaviour across the full aqueous pH range. From the literature, the pK_a values (25°C) associated with the reduced form are found to be 7.6 and 11,[26] consequently below ca. pH 7 the peak potentials for the voltammetry varies with 59mV/pH and above pH 11 the system is found to be insensitive to the proton concentration. In the presence of 4mM HCl the reduction of 1mM AQMS is found to exhibit one voltammetric feature (at -0.21 V vs. SCE), corresponding to the transfer of $2H^+$ and $2e^-$. As the concentration of protons is decreased to 0.25 mM a second voltammetric feature is apparent at a higher potential. In the case where no HCl has been added to the electrolyte, a single voltammetric feature is observed at -0.59 V (vs. SCE). This observed behaviour may be explained as being a result of the consumption of protons upon reduction of the anthraquinone species. When under conditions of limited buffering, the reduction process may alter the pH adjacent to the electrode. As such in the case of 0.25 mM HCl the reduction of AQMS is effectively limited by the availability of the protons. In the absence of protons the reduction proceeds via the formation of the dianion species (AQ^{2-} in Figure 5.2), this reduction occurs at -0.59 V (vs. SCE) as evidenced by the voltammetric response of AQMS in the absence of HCl. Note that the second voltammetric wave observed for the 0.25 mM HCl does not occur at exactly -0.59 V (vs. SCE) and this is likely as a result of the formation of equilibrium concentrations of dianion, monoprotonated and diprotonated species.[11]

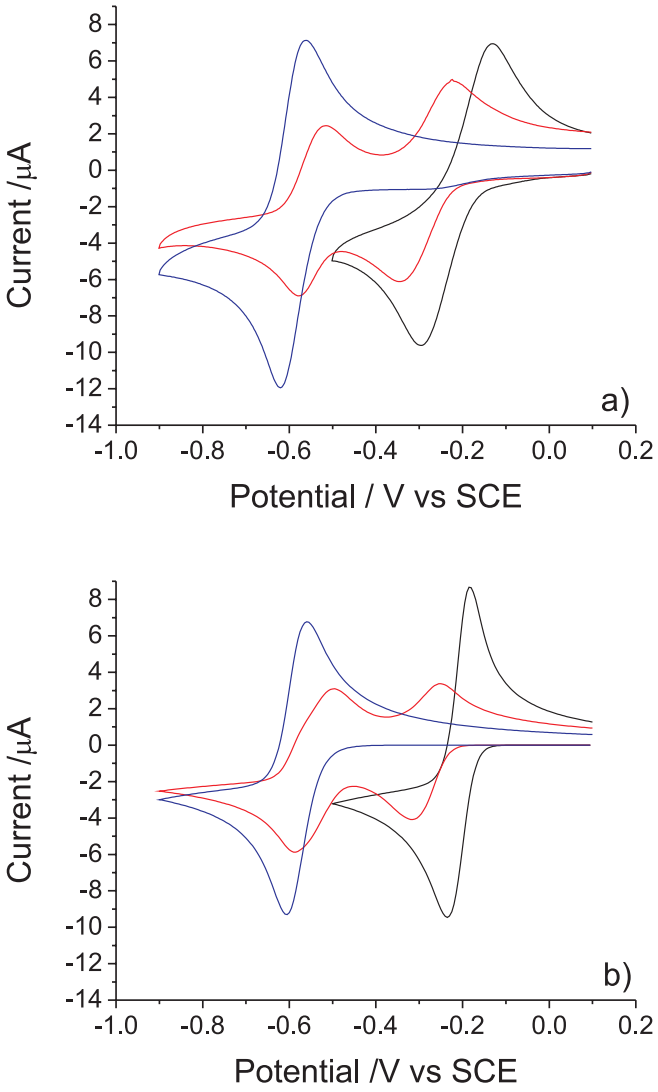

Figure 6.1: The cyclic voltammetric response of 1mM AQMS in the presence of a finite solution phase proton concentration- as controlled through decreasing concentrations of HCl (black, 4mM; red 0.25mM; blue 0mM) for both a) experimental and b) simulated results at a scan rate of 100mVs^{-1}.

6.2.2 Modelling of the Solution Phase Voltammetry

Modelling of the voltammetric response of 1mM AQMS at a gold macro electrode was under taken so as to allow quantitative information to be obtained about the extent of change in pH at, and adjacent to, the electrode in aqueous solutions containing low buffer concentrations. The simulation used was based upon that given from the previous chapter, using the same thermodynamic parameters. Further details of how this current model differs, so as to allow the proton concentration to be limited, are given within the Experimental section. As can be seen the voltammetric simulation results closely follow that found experimentally (Figure 6.1). It should be noted that the second peak observed in 0.25 mM HCl shows a shoulder on the voltammetric wave which is not observed experimentally. It is surmised that this is due to a further possible mechanistic pathway by which the reduced product may equilibrate which is not present within the simulation. Further, as a result of assuming that the protonations are fully equilibrated the simulated voltammetry has a smaller peak-to-peak separation than is experimentally found. A least squared methodology was not used to improve the simulated voltammetric response, this is as a result of the inherent number of variables present in the system and as such use of this methodology may lead to obtaining non-physically correct values. It is of significance that this simulation is able to accurately predict (as a function of pH) the shift in voltammetric response from that of a one voltammetric feature to that of two waves. Hence this leads to the confirmation that the model is accurately able to describe the proton concentrations at and adjacent to the electrode surface.

For the three proton concentrations outlined above (4mM, 0.25mM and 0mM) the simulation was used to describe the variation in the pH adjacent to the electrode surface. Figure 6.2 depicts the results obtained at the switching potentials. As can be seen in relatively high proton concentrations the reduction

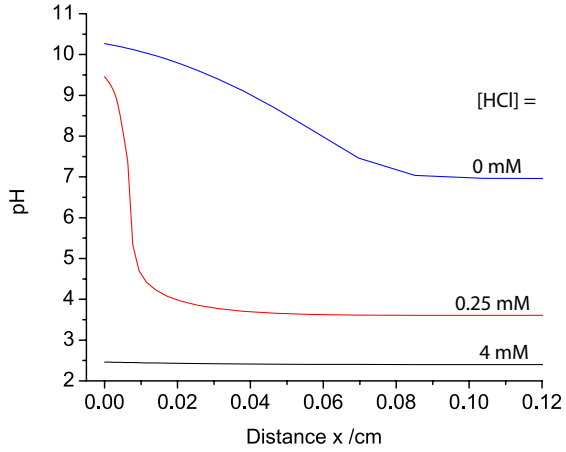

Figure 6.2: The theoretical variation of the pH with distance from the electrode at the switching potentials for the cyclic voltammetry depicted in Figure 6.1 b).

of the anthraquinone species has little influence upon the levels of acidity adjacent to the electrode. As the initial proton concentration is decreased to 0.25 mM a significant change in the pH of the solution occurs at distances close to the electrode surface, where the pH at the electrode interface is roughly 5-6 pH units greater than that of the bulk solution. This region of high pH is confined to a layer close to the electrode interface (< 0.01 cm). In the case where no HCl is present in the solution, a significant alteration in the solution pH occurs at distances further from the electrode (< 0.08 cm). This simulation clearly demonstrates how due to the transfer of protons to the electrochemically reduced species the pH adjacent to the electrode is significantly altered. Hence, systems based on such chemistry for the measurement of pH are going to be significantly influenced by the buffer concentrations and will not give readily analysable results.

6.2.3 Surface Bound Anthraquinone

The the cyclic voltammetry of an AQ-2 modified EPPG electrode was run from 0.0V to -1.0V (vs SCE) in buffers of various pH from 1-14 (Figure 6.3). The cyclic voltammetry exhibits a large surface bound wave, which is ascribed as being a

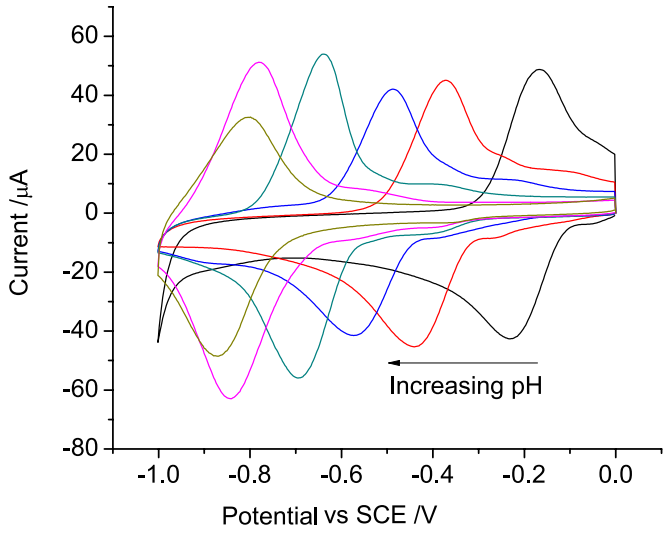

Figure 6.3: The cyclic voltammetry of an AQ-2 modified EPPG electrode in fully buffered media (0.1M) with varying pH (1-14), scan rate of 100mVs^{-1}. Colour code: black (pH 1), red (pH 4), blue (pH 6.7), green (pH 9), purple (12) and light green (pH 14).

$2H^+, 2e^-$ process. From the geometric area of the EPPG electrode it is possible to estimate that a full monolayer of vertically aligned anthraquinonal groups leads to a surface coverage of 1.9×10^{14} molecules cm^{-2}. This value is based on the crystal structure data (assuming a = 2c, space group P21/a)[27] and molar volume of 159 cm^3 mol^{-1} [28] where one anthraquinone molecule occupies the area of 51.2 Å^2 (taken as the projection of an AQ crystal with its ab-plane 30° away from the electrode surface). However, this value for the maximum surface coverage is an underestimate due to the actual surface area of the electrode being greater than its geometric area as a result of the surface not being atomically flat. Certainly, through the use of an adsorbed-transfer method as developed by Qian *et al.* the surface coverage of horizontally aligned anthraquinone species was found to be 4.5×10^{14} molecules cm^{-2} on an EPPG electrode surface.[29] Hence from analysis of the voltammetry it is concluded that the anthraquinone modified EPPG electrode has a high surface coverage of anthraquinonal groups ($1.3 \pm 0.1 \times 10^{15}$ molecules cm^{-2}). Due to this high surface coverage there is a distinct possibility that the modification of the surface with anthraquinone may have lead to the formation

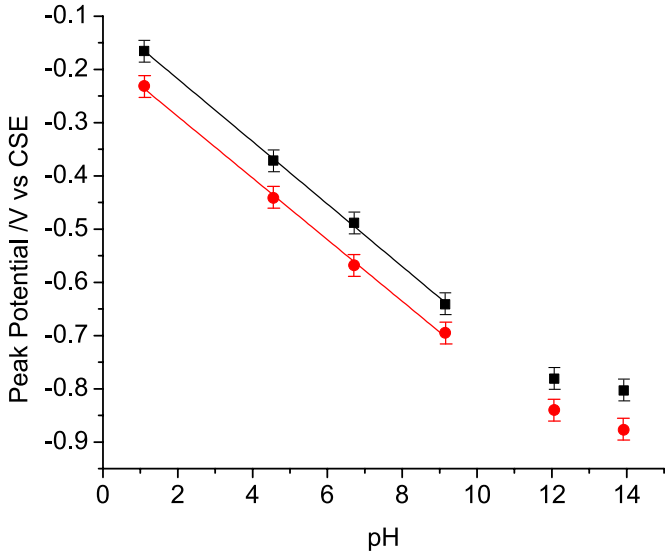

Figure 6.4: A plot of peak potentials (reductive red and oxidative black) for an AQ-2 modified EPPG electrode in fully buffered media (0.1M) of varying pH. The associated cyclic voltammetry is depicted in Figure 6.3. The lines represent the lines of best fit for both the reductive and oxidative peak positions as a function of pH. Error: from five repeat modifications the peak potential is found to vary by ±15 mV.

of multilayers. At all pHs the voltammetric peak-to-peak separation is non-zero (∼70 mV) whereas for an *ideal* fully reversible surface bound species the peak-to-peak separation is expected to be zero. Figure 6.4 depicts the variation of the peak potentials for the AQ-2 modified EPPG with pH, below pH 9 the reductive and oxidative peaks are found to vary with -59 mV/pH and -58 mV/pH respectively. These values are very close to those expected for a fully reversible two electron two proton system as given by the Nernst equation (59 mV/pH; 25°C), thus suggesting that although the peak-to-peak separation is larger than expected for an ideal surface bound species the system is reversible in nature and the non zero peak-to-peak separation is likely a result of the surface bound species being non-ideal.[30,31] Above pH 9 the gradient for the plot of peak potential versus pH deviates away from being that of a two-proton, two-electron system. This is a result of the pH being greater than the pK_as associated with the doubly reduced anthraquinone species (pK_a3 and pK_a6 as shown on Figure 5.2).

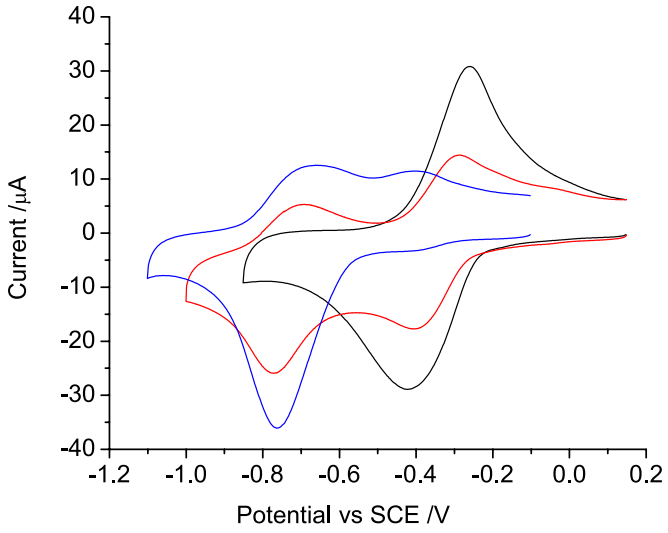

Figure 6.5: The cyclic voltammetry an AQ-2 modified electrode in the presence of a finite solution phase proton concentration as controlled through the concentration of HCl (black, 0.3 mM; red, 0.1 mM; blue, no HCl).

It is of interest that it is also possible to modify the EPPG surface with AQ-1 (AQ-1 is the result of using 1-aminoanthraquinone for the formation of the diazonium salt). The mid-point potentials for the voltammetric response of both AQ-2 and AQ-1 modified EPPG electrodes occur at the same potential below pH 12 (within experimental error). Although the reduction of these species is thermodynamically similar, the AQ-1 exhibits a less reproducible wave which also shows a greater peak-to-peak separation. Consequently for this present study AQ-2 modified EPPG electrodes were used for the experimental investigation of the influence of low buffered media.

The influence of low proton concentrations upon the voltammetry of the AQ-2 modified EPPG electrode was investigated. Figure 6.5 depicts the recorded voltammetric response of the AQ-2 modified electrode in 0.3, 0.1 and 0 mM HCl at a scan rate of 100 mVs^{-1}. As for the fully buffered species the voltammetric response of the modified electrode in 0.3 mM HCl exhibited as single two electron two proton feature at -0.34 V (vs. SCE). As the proton concentration is further reduced (0.1 mM HCl) a second voltammetric feature becomes apparent. This

second voltammetric feature occurs at the same potential (-0.73 V vs. SCE) as that found for the reduction of the surface bound AQ in the absence of HCl. It should be noted that for the response at 0.3 mM HCl although only one voltammetric wave is observed the peak is significantly distorted from that expected for a fully buffered system where the peak-to-peak separation is measured as 159mV as opposed to 67mV for the fully buffered system and the mid-point potential has been shifted negatively by $\sim$12 mV. This result is analogous to that found for the solution phase species and demonstrates how, in the case of high surface coverages of redox active species involving the transfer for protons the measured voltammetry is significantly altered in low buffering conditions. From the simulation it can be seen that for the solution phase species when the concentration of the buffer is less than twice that of the AQMS significant deviations are observed in the voltammetry. As such, for the present experimental case with 1 mM AQMS, concentrations of less than 2mM HCl exhibit voltammetry which is distorted from that of a fully buffered system. In comparison it is observed experimentally that for the surface bound species concentrations of $\leq$5 mM HCl lead to distorted peaks, where the voltammetric peak-to-peak separation is increased and there is a shift in the apparent mid-point potential. This occurs as a result of the relatively high levels of proton consumption adjacent to the electrode and hence alteration of the local environment. This result is significant, as it highlights how pH measurements based on such a methodology are restricted to the use of media in which there is a relatively high concentration of buffer. Furthermore, as a proof-of -concept it demonstrates how such a modified electrode may be used to effectively control the pH adjacent to an electrode surface.

6.3 Conclusions

This work has demonstrated through the use of a solution phase species which may undergo a $2H^+, 2e^-$ process how the measured voltammetry is significantly

altered when under conditions of low buffering, as exemplified through the use of anthraquinone monosulfonate. As a result of proton consumption upon reduction of the electro-active species the pH adjacent to the electrode is altered leading to, in some situations, the observation of two voltammetric features. The response for the AQMS system in low buffered aqueous media has been modelled through the use of the commercially available software package DIGISIM®. Through the use of these simulations it was possible to ascertain that the pH adjacent to the electrode may be altered by up to 5-6 pH units as compared to that of the bulk solution.

Further, the modification of an EPPG electrode with anthraquinone groups was achieved through the use of diazonium salt chemistry. This modified electrode was shown to exhibit near reversible behaviour in fully buffered aqueous media. In the case of the use of low buffered media the voltammetry of the surface bound species altered significantly, leading to the observation of split voltammetric waves, in a manner analogous to that found for the solution phase species. This distortion is a result of the significant consumption of protons during the electrochemical experiment. As such, it is concluded that this modified electrode may cause a significant shift in pH adjacent to the electrode interface. This is of importance due to the use of similar methodologies for the voltammetric measurement of pH. Further, it is demonstrated as a proof-of-concept that such modified electrodes may be used for the effective control of the pH adjacent to an electrode.

References

[1] Costentin, C. *Chem. Rev.* **2008**, *108*, 2145–2179.

[2] Porcelli, A. M.; Ghelli, A.; Zanna, C.; Pinton, P.; Rizzuto, R.; Rugolo, M. *Biochem. Biophys. Res. Commun.* **2005**, *326*, 799–804.

[3] Bacljić, J. D.; Balzani, V.; Credi, A.; Silvi, S.; Stoddart, J. *Science* **2004**, *303*, 1845–1849.

[4] Ashton, P. R.; Ballardini, R.; Balzani, V.; Baxter, I.; Credi, A.; Fyfe, M. C. T.; Gandolfi, M.; Gomez-Lopez, M.; Martnez-Daz, M. .-V.; Piersanti, A.; Spencer, N.; Fraser Stoddart, J.; Venturi, M.; White, A. J. P.; Williams, D. J. *J. Am. Chem. Soc.* **1998**, *120*, 11932–11942.

[5] Henstridge, M. C.; Wildgoose, G. G.; Compton, R. G. *J. Phys. Chem. C* **2009**, *113*, 14285–14289.

[6] Johnson, E. K.; Adams, D. J.; Cameron, P. J. *J. Am. Chem. Soc.* **2010**, *132*, 5130–5136.

[7] Pawliszyn, J. *Anal. Chem.* **1992**, *64*, 1552–1555.

[8] Ozeki, T.; Irish, D. E. *J. Electroanal. Chem.* **1990**, *280*, 451–455.

[9] Rudd, N. C.; Cannan, S.; Bitziou, E.; Ciani, I.; Whitworth, A. L.; Unwin, P. R. *Anal. Chem.* **2005**, *77*, 6205–6217.

[10] Cannan, S.; Douglas Macklam, I.; Unwin, P. R. *Electrochem. Commun.* **2002**, *4*, 886–892.

[11] Quan, M.; Sanchez, D.; Wasylkiw, M. F.; Smith, D. K. *J. Am. Chem. Soc.* **2007**, *129*, 12847–12856.

[12] Smith, E. T.; Davis, C. A.; Barber, M. J. *Anal. Biochem.* **2003**, *323*, 114–121.

[13] Malinowski, E. R.; Barber, M. J.; Whitaker, G. T.; Smith, E. T. *J. Chemometr.* **2007**, *21*, 520–528.

[14] Guo, S. X.; Feldberg, S. W.; Bond, A. M.; Callahan, D. L.; Richardt, P. J. S.; Wedd, A. G. *J. Phys. Chem. B* **2005**, *109*, 20641–20651.

[15] McCreery, R. L. *Chem. Rev.* **2008**, *108*, 2646–2687.

[16] Holloway, A. F.; Wildgoose, G. G.; Compton, R. G.; Shao, L.; Green, M. L. H. *J. Solid State Electrochem.* **2008**, *12*, 1337–1348.

[17] Pinson, J.; Podvorica, F. *Chem. Soc. Rev.* **2005**, *34*, 429–439.

[18] Wildgoose, G. G.; Pandurangappa, M.; Lawrence, N. S.; Jiang, L.; Jones, T. G. J.; Compton, R. G. *Talanta* **2003**, *60*, 887–893.

[19] Leventis, H. C.; Streeter, I.; Wildgoose, G. G.; Lawrence, N. S.; Jiang, L.; Jones, T. G. J.; Compton, R. G. *Talanta* **2004**, *63*, 1039–1051.

[20] Kahlert, H. *J. Solid State Electrochem.* **2008**, *12*, 1255–1266.

[21] Milner, D. J. *Synth. Commun.* **1992**, *22*, 73–82.

[22] Harned, H. S.; Hamer, W. J. *J. Am. Chem. Soc.* **1933**, *55*, 2194–2206.

[23] Henstridge, M. C.; Wildgoose, G. G.; Compton, R. G. *Langmuir* **2010**, *26*, 1340–1346.

[24] Choi, P.; Jalani, N. H.; Datta, R. *J. Electrochem. Soc.* **2005**, *152*, A1548–A1554.

[25] Macpherson, J. V.; Unwin, P. R. *Anal. Chem.* **1997**, *69*, 2063–2069.

[26] Gamage, R. S. K. A.; McQuillan, A. J.; Peake, B. M. *J. Chem. Soc. Farad.Trans.* **1991**, *87*, 3653–3660.

[27] Prakash, A. *Acta Crystallogr.* **1967**, *22*, 439–440.

[28] *Calculated using Advanced Chemistry Development (ACD/Labs) Software V11.02 (©1994–2011 ACD/Labs).*

[29] Li, Q.; Batchelor-McAuley, C.; Lawrence, N. S.; Hartshorne, R. S.; Compton, R. G. *New J. Chem.* **2011**, *35*, 2462–2470.

[30] Honeychurch, M. J.; Rechnitz, G. A. *Electroanalysis* **1998**, *10*, 285–293.

[31] Laviron, E. *J. Electroanal. Chem.* **1979**, *100*, 263–270.

Chapter 7

Controlling Voltammetric Responses by Electrode Modication; Using Acetone to Tailor the Properties of Graphitic Electrodes

In the previous chapter the electrode surface was chemically modified via the use of diazonium salt chemistry; the work presented here looks alternatively at the physisorption of electroactive species onto graphitic electrodes. Specifically, how the pre-adsorption of organic solvents onto graphitic electrodes influences the observed voltammetric response. The work presented in this chapter was published in *Chemical Communications* 2011, 46, 9037–9039; the assistance of both L.M. Gonçalves and L. Xiong in completion of this work is recognised and appreciated.

Graphite is known to be comprised of both basal and edge plane sites.[1] It is generally accepted that the rate of electron transfer is greater at the edge plane sites and that their surface density strongly influences the observed voltammetry.[2,3] It has been reported that organic solvents such as acetonitrile can modify graphitic surfaces, but in the case of highly ordered pyrolytic graphite (HOPG) a large change in the electron transfer kinetics is observed.[4] Work by McCreery *et al.* has suggested that adsorption is generally strongest at the edge plane sites as a result of their more polar nature.[5,6] This is in contrast to more recent work focused on

the adsorption of the nucleobases to graphite electrodes which suggests that the degree of adsorption is strongly influenced by the surface coverage of basal plane sites.[7,8]

Acetone is a polar organic molecule and is known to adsorb from the gas phase to the basal plane sites of graphite; this adsorption has been studied under high vacuum using surface techniques such as optical differential reflectance (ODR).[9,10] This chapter highlights how through the pre-adsorption of acetone to a graphite electrode, the subsequent adsorption of aromatic molecules from solution is effective blocked, without significantly affecting the substrates electro-activity. As a consequence of this pre-adsorption of acetone the measured voltammetric signals for two aromatic based molecules (anthraquinone monosulfonate [AQMS] and ferrocene dimethanol) is shown to be almost purely diffusional in contrast to the adsorptive behaviour seen in the absence of acetone.

7.1 Results and Discussion

The pre-adsorption of acetone was achieved through rinsing of the alumina slurry polished edge plane pyrolytic graphite (EPPG) electrode with acetone and allowing the electrode to dry under ambient conditions, the acetone used was newly purchased and of analytical reagent ($\geq$ 99.5%) grade. It should be noted that although the observed difference between the modified and unmodified electrodes are ascribed as being due to the adsorption of acetone to the electrode surface, due to impurities naturally occurring within the acetone it is feasible that the observed different voltammetric responses is a result of these contaminants. The differing response for this modified electrode towards four different aqueous redox probes was investigated (Figure 7.1). As can be seen for ruthenium (III) hexaamine which is known to be reduced via an outer-sphere mechanism no change in the voltammetric signal occurs with the addition of acetone. The oxidation of ferrocyanide is

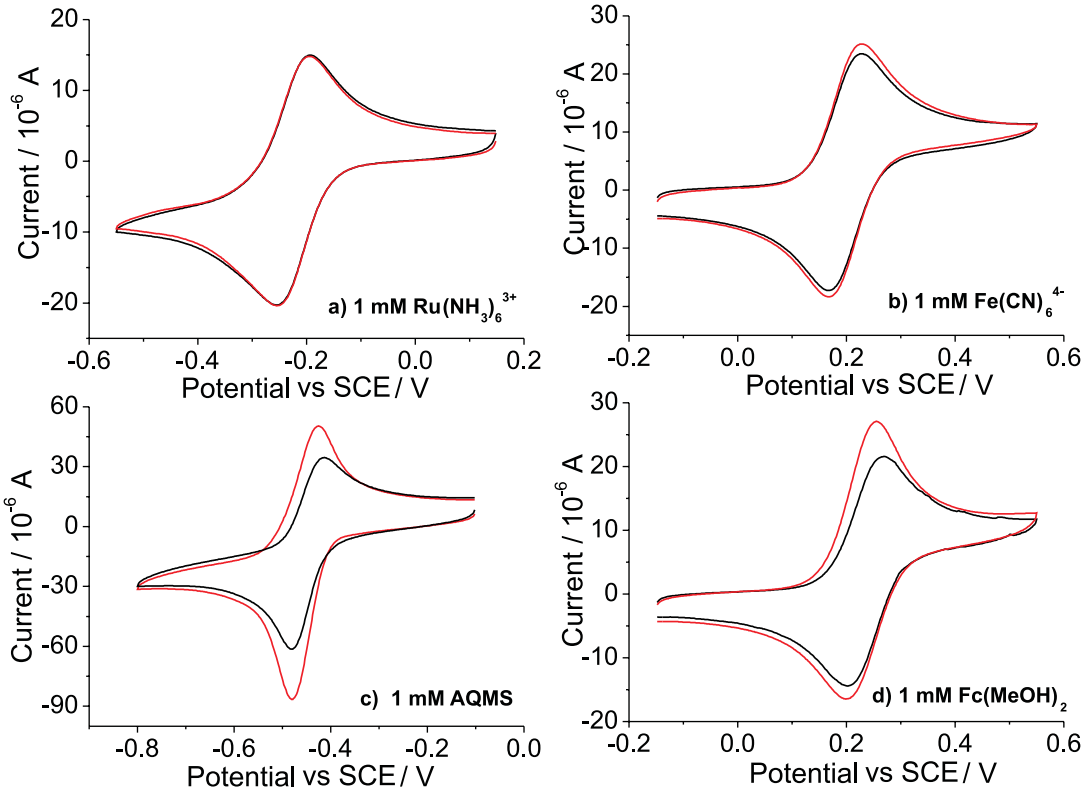

Figure 7.1: Cyclic voltammograms of different redox probes (1 mM) in 0.1 M aqueous phosphate buffer pH 6.8, recorded at EPPG electrode with (black solid line) and without (red solid line) acetone at a scan rate of 50 mV; a) ruthenium (III) hexaamine b) ferrocyanide c) AQMS and d) ferrocene dimethanol.

known to exhibit surface-sensitivity,[11] here the presence of acetone causes a minimal decrease in peak height. Note that under comparable experimental conditions the acetone modification of a 'basal plane pyrolytic graphite' electrode leads to significant distortions of the ferrocyanide voltammetric response. This it has been concluded is related to the weaker binding of the bridging ion complex required for the electron transfer to proceed.[12] Further, the results from Xiong *et al.*[12] combined with the present work strongly implies that it is predominantly the 'edge' plane sites that are electroactive towards ferrocyanide. Whereby, due to the lower density of 'edge' sites on the basal plane electrodes, the electrode is inherently more sensitive to the pre-adsorption of organic solvents. For the EPPG electrode the minimal variation in the voltammetic response towards the redox of both ruthenium (III) hexaamine and ferrocyanide implies that the surface is not significantly altered with pre-adsorption of acetone. The results found for both AQMS and ferrocene dimethanol contrast; in both cases significant decreases in the measured peak current occurs.

For a fully reversible diffusion only species the peak current (i_p) may be described by the Randles-Ševčík equation as given below.[13]

$$i_p = (2.69 \times 10^5) A D^{0.5} C \nu^{0.5} n^{1.5} \tag{7.1}$$

where A is the area of the electrode surface in cm^2, D is the diffusion coefficient of the species in $cm^2\ s^{-1}$, C is the bulk concentration of the species in mol cm^{-3} and ν is the scan rate in V s^{-1}. For a fully reversible surface bound species the peak current is given by,[13]

$$i_p = \frac{n^2 F^2}{4RT} \nu A \Gamma \tag{7.2}$$

where Γ is the surface coverage with units of mol cm^{-2}. As such a common method for differentiating between surface bound and diffusional systems is through the

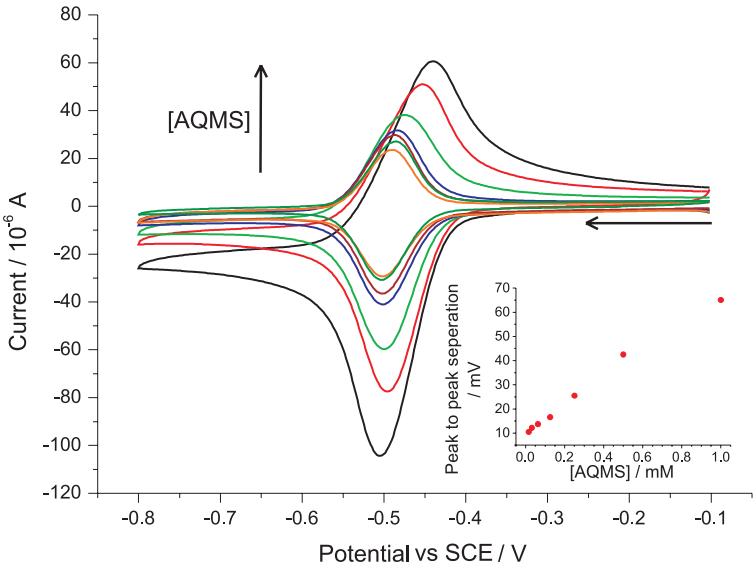

Figure 7.2: Cyclic Voltammograms from increasing concentrations of AQMS recorded at a EPPG electrode in 0.1 M aqueous phosphate buffer pH 6.8 at a scan rate of 50 mV from -0.1V to -0.8V (vs SCE). From lowest to highest peaks: 1/64 mM (orange), 1/32 mM (dark green), 1/16 mM (maroon), 1/8 mM (blue), 1/4 mM (green), 1/2 mM (red), 1 mM (black). Inlay: peak to peak separation dependence with the AQMS concentration.

analysis of the peak current dependency with the scan rate. Where a plot of $\log|i_p| vs \log|\nu|$ will be a straight line, of gradient 0.5, for a purely diffusional system and a gradient of 1 for indicates a purely adsorbed process. Gradients lying between 0.5-1 represent mixed systems where the value is indicative of the level of contribution from the two environments.[14]

The sulfonate derivatives of anthraquinone are well known examples of electro-active species which readily adsorb on to graphite surfaces.[5,15] At low bulk solution concentrations of AQMS, the measured voltammetric signal is predominantly that of a surface bound species, as the concentration is increased this response becomes more diffusional in nature. Figure 7.2 depicts the varying response of AQMS on an EPPG electrode with increasing concentration. The shift from an adsorbed signal to that of a more diffusional response is easily exemplified by measuring the increase in peak-to-peak separation with concentration (Figure

7.2 inlay).

The variation of the peak current for 1mM AQMS was measured as a function of square root of scan rate for both a blank and acetone modified electrode (Figure 7.3 a). The unmodified electrodes shows clear deviations away from linearity suggesting appreciable levels of adsorption and a plot $\log|i_p| vs \log|\nu|$ gives a straight line of gradient 0.57. The apparent diffusion coefficient measured from this data yields a value of $9.7 \pm 0.5 \times 10^{-6}$ cm^2 s^{-1} this value is far greater than that found in the literature where the *true* diffusion coefficient for AQMS in aqueous solution is reported as 4.7×10^{-6} cm^2 s^{-1}.[16] This is comparable to the value found for the acetone modified electrode where the plot of peak current versus square root of scan rate is found to be near linear and the apparent diffusion coefficient is measured as $4.7 \pm 0.3 \times 10^{-6}$ cm^2 s^{-1}; further a plot of $\log|i_p| vs \log|\nu|$ is found to give a straight line of gradient 0.51. However, as discussed in Chapter 5 due to the first and second electron transfer for the reduction of AQMS occuring at comparable potentials, the direct application of Equation 7.1 to this system is not possible. Consequently, from a plot of square root of scan rate versus peak height one would expect to measure an *apparent* diffusion coefficient of 2.9×10^{-5} cm^2 s^{-1}. Hence, given the above information it must be concluded that *most* but not all of the AQMS has been blocked from adsorbing to the electrode surface.

Conversely, for 1mM ferrocene dimethanol at a modified electrode (Figure 7.3 b) the results do indicate that the ferrocene dimethanol has been fully blocked from adsorbing. The blank electrode gives an apparent diffusion coefficient of $8.8 \pm 0.4 \times 10^{-5}$ cm^2 s^{-1}, this is far greater than the true diffusion coefficient as reported in the literature as being 6.4×10^{-6}cm^2 s^{-1}.[17] In comparison the acetone modified electrode yields a measured diffusion coefficient of $5.8 \pm 0.2 \times 10^{-6}$ cm^2 s^{-1}. Hence, the measured peak currents are within experimental error ($\leq$5%) of that expected from the diffusion only system. Further, a plot of $\log|I| vs \log|\nu|$

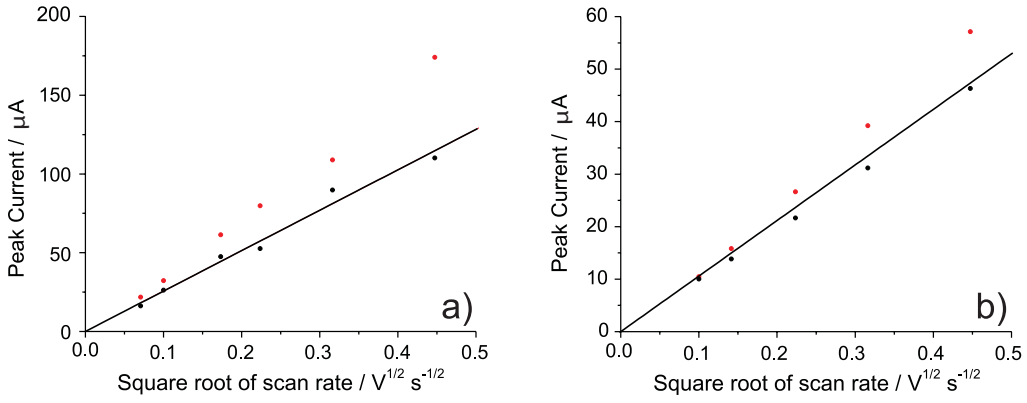

Figure 7.3: Peak current dependence with the square root of scan rate for a) AQMS and b) ferrocene dimethanol recorded on an EPPG electrode in 0.1 M aqueous phosphate buffer solution pH 6.8. Red points: unmodified electrode; black points: acetone modified electrode and the solid line is the expected value for a purely diffusional response.

for the blank and modified electrodes yield straight lines of gradients 0.58 and 0.50 respectively. Given that in both experimental cases (AQMS and ferrocene dimethanol) the acetone modification leads to a significant decrease in peak current and also corresponding decrease in the measured $\log|I| vs \log|\nu|$, it seems credible that the acetone is serving to effectively block further adsorption to the electrode.

It is surmised that the blocking of the adsorption without significantly adversely affecting the electrode's activity – as evidenced by the lack of shift in the peak-to-peak separation – may result from the differing roles of the edge and basal plane sites upon the electrode, where the edge planes are responsible for the observed electro-activity and the basal planes provide the adsorption sites. An alternative hypothesis is that the acetone provides a thin adsorbed layer across which electron tunnelling may occur, such that, for the case in question adsorption of the species would not be a pre-requisite for electron transfer.

The adsorption of AQMS from 1mM bulk solution clearly leads to a high surface coverage of the anthraquinone species on the surface. This adsorption can also be shown to be reasonably irreversible as even when an EPPG electrode with adsorbed AQMS is transferred to a blank buffer solution the AQMS redox couple

is still observed, this is not the case with ferrocene dimethanol. The adsorption of ferrocene dimethanol to the electrode surface leads to a lower surface coverage (as compared to AQMS) and is also reversibly adsorbed. As such in the case of ferrocene dimethanol the use of an analogous transfer experiment will not show the presence of any surface adsorbed species. Consequently, the use of acetone has clearly resolved the influence of the surface adsorption of the ferrocene dimethanol species to the electrode: something that was not previous possible. This arises as a result of the pre-adsorbed acetone blocking subsequent adsorption of the analyte to the electrode surface. It is of further interest to note that experimentally the change in peak height for the oxidative and reductive peaks for 1mM ferrocene dimethanol (Figure 7.1 d) with and without acetone modification of the EPPG electrode is not symmetrical where the oxidative peak is more significantly reduced, as such through comparison with work by Wopschall and Shain, it can be concluded that the oxidised form of ferrocene dimethanol is more weakly adsorbed upon the graphite surface.[18]

7.2 Conclusions

In conclusion this work has demonstrated that through use of this simple modification it is possible to effectively moderate the adsorption of aromatic species to the electrode substrate. The resulting signals are nearly purely diffusional in nature. Further through the use of the redox couples ruthenium hexaamine and ferrocyanide it is clear that the electro-activity of the graphite electrode has not been significantly adversely affected by the presence of the acetone.

References

[1] Banks, C. E.; Compton, R. G. *Anal. Sci.* **2005**, *21*, 1263–1268.

[2] Banks, C. E.; Moore, M. R.; Davies, T. J.; Compton, R. G. *Chem. Comm.* **2004**, *10*, 1804–1805.

[3] Banks, C. E.; Davies, T. J.; Wildgoose, G. G.; Compton, R. G. *Chem. Comm.* **2005**, 829–841.

[4] Liu, Y.; Freund, M. S. *Langmuir* **2000**, *16*, 283–286.

[5] McDermott, M. T.; Kneten, K.; McCreery, R. L. *J. Phys. Chem.* **1992**, *96*, 3124–3130.

[6] McDermott, M. T.; McCreery, R. L. *Langmuir* **1994**, *10*, 4307–4314.

[7] Li, Q.; Batchelor-McAuley, C.; Compton, R. G. *J. Phys. Chem. B* **2010**, *114*, 7423–7428.

[8] Gonçalves, L. M.; Batchelor-McAuley, C.; Barros, A. A.; Compton, R. G. *J. Phys. Chem. C* **2010**, *114*, 14213–14219.

[9] Kwon, S.; Vidic, R.; Borguet, E. *Surf. Sci.* **2003**, *522*, 17–26.

[10] Kwon, S.; Russell, J.; Zhao, X.; Vidic, R. D.; Karl Johnson, J.; Borguet, E. *Langmuir* **2002**, *18*, 2595–2600.

[11] Kawiak, J.; Kulesza, P. J.; Galus, Z. *J. Electroanal. Chem.* **1987**, *226*, 305–314.

[12] Xiong, L.; Batchelor-McAuley, C.; Ward, K. R.; Downing, C.; Hartshorne, R. S.; Lawrence, N. S.; Compton, R. G. *J. Electroanal. Chem.* **2011**, *661*, 144–149.

[13] Bard, A. J.; Faulkner, L. R. *Electrochemical methods : fundamentals and applications*, 2nd ed.; Wiley: New York, 2001.

[14] Laviron, E.; Roullier, L.; Degrand, C. *J. Electroanal. Chem.* **1980**, *112*, 11–23.

[15] Ta, T. C.; Kanda, V.; McDermott, M. T. *J. Phys. Chem. B* **1999**, *103*, 1295–1302.

[16] Batchelor-McAuley, C.; Li, Q.; Dapin, S. M.; Compton, R. G. *J. Phys. Chem. B* **2010**, *114*, 4094–4100.

[17] French, R. W.; Collins, A. M.; Marken, F. *Electroanalysis* **2008**, *20*, 2403–2409.

[18] Wopschall, R. H.; Shain, I. *Anal. Chem.* **1967**, *39*, 1514–1527.

Chapter 8

Anthraquinone Monosulfonate Adsorbed on Graphite Shows Two Very Different Rates of Electron Transfer: Surface Heterogeneity due to Basal and Edge Plane Sites

In the previous two chapters work focused on the two routes by which graphitic electrodes maybe modified namely, chemi and physi-adsorption. In the latter case it was demonstrated how through the use of organic solvents the adsorption to the electrode may be minimised. Alternatively, this chapter will look towards how adsorption of an electroactive molecule and the voltammetric responses of the adsorbed species can allow greater insight into the electrochemical nature of the surface. This work was published in '*Chemistry- A European Journal* 2011, 17, 7320–7326'. The assistance of C.C.M. Neumann in the recording of the electrochemical responses is appreciated, further thanks are given to C. Downing for the production of the SEM images and D. Menshykau for his insights into modelling surface bound species.

The graphitic surface is heterogeneous in nature comprising both basal and edge plane sites. Depending upon how the graphitic material is aligned an electrode may either be predominantly basal or edge plane in character.[1] It is of note

that the electroactivity of carbon nanotubes are often interpreted with respect to macroscopic carbon, where the sidewalls are compared to the basal planes of graphite and the tube ends are approximated as being akin to the edge plane sites.[2] For graphite, although it is generally accepted that the rate of electron transfer is greater at the edge plane sites, debate still exists as to how relatively electroactive the basal sites are. McCreery *et al.* concluded that, depending upon the electrode history and experimental conditions the electron transfer rate constants measured for the two sites can differ by up to a factor of 10^5 and further the density of edge plane sites will have a large influence upon the observed voltammetry.[3,4] More recently Banks *et al.* demonstrated that for diffusional species the rate of electron transfer for the basal plane site may be viewed as effectively negligible as electrolysis initially takes place preferentially at the edge plane sites in linear sweep voltammetry.[5,6] This can be juxtaposed with work by Edwards *et al.* who with the use of a thin layer film, interpreted the redox of ruthenium hexaamine on the basal plane sites of highly ordered pyrolytic graphite as being nearly fully reversible.[7] Similar results have also been found by Bond *et al.* who analysed a sub-monolayer coverage of adsorbed porphyrin on a basal plane surface, finding the resulting voltammetric response to be near ideal and highly reversible in nature.[8] Furthermore, work on well defined single walled carbon nanotubes has shown the basal sidewalls to have considerable activity.[9–11] Apart from kinetics the two sites also differ in terms of adsorption; for anthraquinone disulfonate, adsorption has been shown to be strongest on edge plane graphite and the presence of the edge planes sites may influence the adsorption on basal plane sites adjacent to the edge defect.[12,13] More recent work has highlighted how the adsorption of the nucleobases adenine and guanine occurs primarily upon the basal plane plateaux.[14,15]

The redox chemistry of quinones is well documented and is known to be a $2H^+, 2e^-$ process, where under most experimental conditions the electron and

proton transfers may be viewed as occurring consecutively.[16] This reaction mechanism is usually described in terms of a 'scheme of squares' (Figure 5.2) as first proposed by Jacq,[17] as discussed in more detail in Chapter 5. The mechanistic route is highly dependent upon the associated pK_as and the pH of the solution.

This present work investigates the characteristics of anthraquinone-2-monosulfonate adsorbed upon graphitic surfaces across the full aqueous pH range (1-12). Two distinct adsorption sites are clearly resolved and are attributed as being related to the basal and edge planes. Through modelling of this diffusionless system via the use of the 'scheme of squares' mechanism as presented in Chapter 6, quantitative information about the kinetics and thermodynamics of the process is provided. It is found that both the pK_as and the rates of electron transfer for the species in the two adsorption sites differs significantly; the voltammetric feature attributed as being 'basal' in nature exhibits electron transfer kinetics which are significantly slower than than those found for the 'edge' plane sites by 2-3 orders of magnitude. Moreover, from a physical electrochemical perspective we believe this is the first case of a 'scheme of squares' analysis for a $2H^+$, $2e^-$ system over the full pH range for a diffusionless system. The insight gained has important implications for electrochemical systems involving surface-bound species on graphite surfaces, highlighting that electron transfer occurring at the basal plane site should not be viewed as negligible, albeit much slower than 'reversible'.

8.1 Experimental

8.1.1 Modelling

The model presented within this chapter is based upon that used within Chapter 5 and 6, but in the present case the model was adapted so as to take into account that the redox species are confined to the electrode surface. For a thin-layer cell under

conditions where the concentration profiles of all the species present are uniform with respect to the distance from the electrode, the resulting response is equivalent to that for an adsorbed species in which there are no interactions between adsorbate molecules.[18] This approximation was used in the present work to simulate the behaviour of adsorbed quinone using a thin layer of depth 1×10^{-8} m, so ensuring that over the timescale of the simulated experiment all concentration profiles are effectively uniform. Protonation steps were modelled as

$$\mathrm{A} + \mathrm{H}^+ \rightleftharpoons \mathrm{B} \qquad\qquad K = \frac{[\mathrm{B}]}{[\mathrm{A}][\mathrm{H}^+]}$$

where the bimolecular protonation step was set as being diffusionally controlled with a value of 1×10^{10} mol^{-1} dm^3 s^{-1}. Included within the simulation was the self ionisation of water, where the concentration of water was set as 55.56 M and the value of K_w taken as 1.0×10^{-14} mol^2 dm^{-6}.[19] Control of the pH of the system was modelled through the inclusion of 0.1 M buffer (as per the experimental section). The experimentally observed system is known to be fully buffered as such due to the possibility of including only a finite quantity of buffer within the simulation it is necessary to ensure that the concentration of the electroactive speices present within the simulation is substantially lower than the concentration of buffer. To this end the initial concentration of the anthraquinone species was set as 1 mM so as to ensure that in all cases the system was fully buffered. Further a mechanistic pathway allowing direct protonation and deprotonation of the anthraquinone species via the buffer was included. Due to being modelled as a thin-layer the electron transfer rates were entered as those for a diffusional species i.e. with the units cm s^{-1}. These values are readily converted to those for a surface bound species by division by the depth of the cell used. As shown below, where for a simple

electrochemical reduction of

$$\mathrm{A} + \mathrm{e}^- \rightleftharpoons \mathrm{B}$$

for a surface bound species the rate is given by

$$\frac{\mathrm{d}\,\Gamma_\mathrm{A}}{\mathrm{d}\,t} = k_s \Gamma_\mathrm{A} e^{-\alpha\Theta}$$

where Γ_A is the surface coverage of A, t is time, k_s is the surface rate constant, α is the transfer coefficient and Θ is the dimensionless overpotential. The dimensionless overpotential is equal to $\eta F/RT$. For a species confined to a thin-layer,

$$D \left.\frac{\partial[\mathrm{A}]}{\partial z}\right|_0 = k_o[\mathrm{A}]e^{-\alpha\Theta}$$

where D is the diffusion coeffiecient, $[A]$ is the concentration of species A, z is the distance perpendicular to the electrode, k_o is the diffusional rate constant and all other symbols are the same as above. Hence, where the concentration profiles across the thin-layer are uniform,

$$\frac{\partial \Gamma_\mathrm{A}}{\partial t} = D \left.\frac{\partial[\mathrm{A}]}{\partial z}\right|_0$$

and given

$$\Gamma_\mathrm{A} = [\mathrm{A}] \left(\frac{mol}{m^3}\right) l_o(m) = \frac{mol}{m^2}$$

where l_o is the depth of the thin-layer then

$$k_s \Gamma_\mathrm{A} e^{-\alpha\Theta} = k_o[\mathrm{A}]e^{-\alpha\Theta}$$

$$k_s l_o = k_o$$

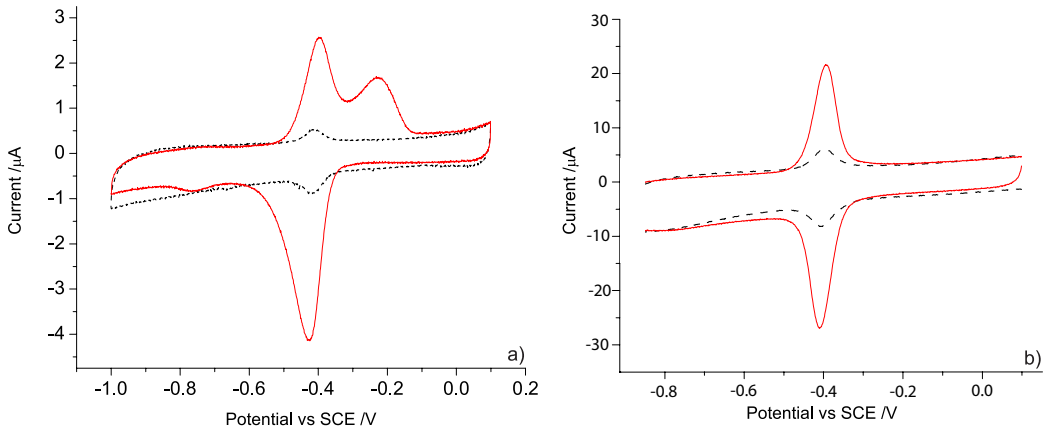

Figure 8.1: The representative voltammetric response for a BPPG (a) and EPPG (b) electrode with (solid) and without (dotted) pre-adsorbed AQMS at pH 5.25 (50mM acetate buffer adjusted with conc. NaOH, 0.1M KCl).

8.2 Results and Discussion

8.2.1 The Voltammetric Response of Surface Bound AQMS

The cyclic voltammetric response of AQMS physisorbed onto a BPPG and EPPG electrode was measured in buffered media across the full aqueous pH range (1-12), from 0.05 – -1.0 V at a scan rate of 100 mVs^{-1}. Figure 8.1 shows a representative voltammogram, demonstrating the influence of pre-adsorbed AQMS upon the electrochemical response for both a BPPG and EPPG electrode at pH 5.25. Clearly for both electrodes the large voltammetric feature can be ascribed as being due to the presence of physisorbed anthraquinone moieties. It is of further note and interest that a small voltammetric feature is observed in the absence of adsorbed AQMS, this feature is a result of quinonal groups intrinsically present upon the electrode surface.[20] Figure 8.2 depicts the cyclic voltammetry of four representative pHs of 2, 4, 7 and 10 on both a BPPG (a) and EPPG (b) electrode. The surface coverage of AQMS as measured voltammetrically is found to be $\sim 1 \times 10^{14}$ molecules cm^{-2} for the BPPG electrode (of which $\sim 3 \times 10^{13}$ molecules cm^{-2} are ascribed as being upon the basal plane) and $\sim 2 \times 10^{14}$ molecules cm^{-2} for the EPPG electrode. These results are in reasonable agreement to the coverage of edge plane sites upon

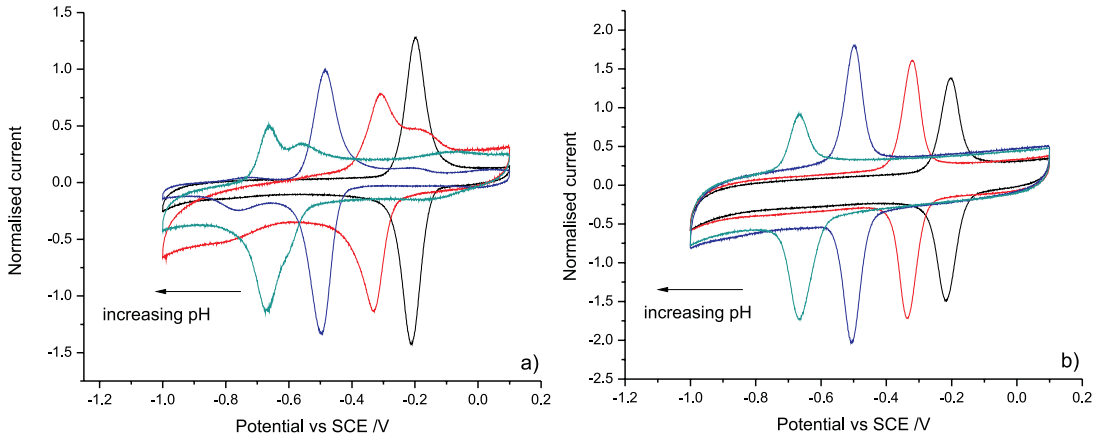

Figure 8.2: The cyclic voltammetric (100 mVs^{-1}) response of AQMS adsorbed on a BPPG (a) and EPPG (b) electrode in buffered aqueous media of pH 2.0 (black), 4.5 (red), 7.0 (blue) and 10.0 (green). Current has been normalised with respect to peak area for ease of comparison.

the BPPG electrode as shown in the SEM images (Figure 8.3). From the SEM images it can be clearly seen that the BPPG surface comprises of between 10-20% coverage of high density edge plane defect sites, this value neglects the likely large number of edge plane defects present upon the basal plane plateau with smaller step heights, these smaller defects are not apparent due to the image resolution.

Due to variation in the coverage of the adsorbed species between experiments there is some fluctuation ($\sim$ 30% for the BPPG electrode) in the absolute peak current of the AQMS signal. This relatively large fluctuation in the observed voltammetry is likely due to the fact that the voltammetric response for graphitic electrodes is strongly influenced by the surface coverage of the edge plane sites. Further, the number of edge plane sites present will vary with each electrode preparation. As such, for ease of comparison, the data in Figure 8.2 is normalised with respect to the Faradaic charge passed. Between pHs 1 and 9, the surface adsorbed species for both the EPPG and BPPG electrodes are found to be relatively stable, with only minimal loss of material during repeated voltammetric cycling. At higher pHs, where the reduced product is either the mono or dianion, which is more water soluble than the diprotonated reduced species, greater loss of material

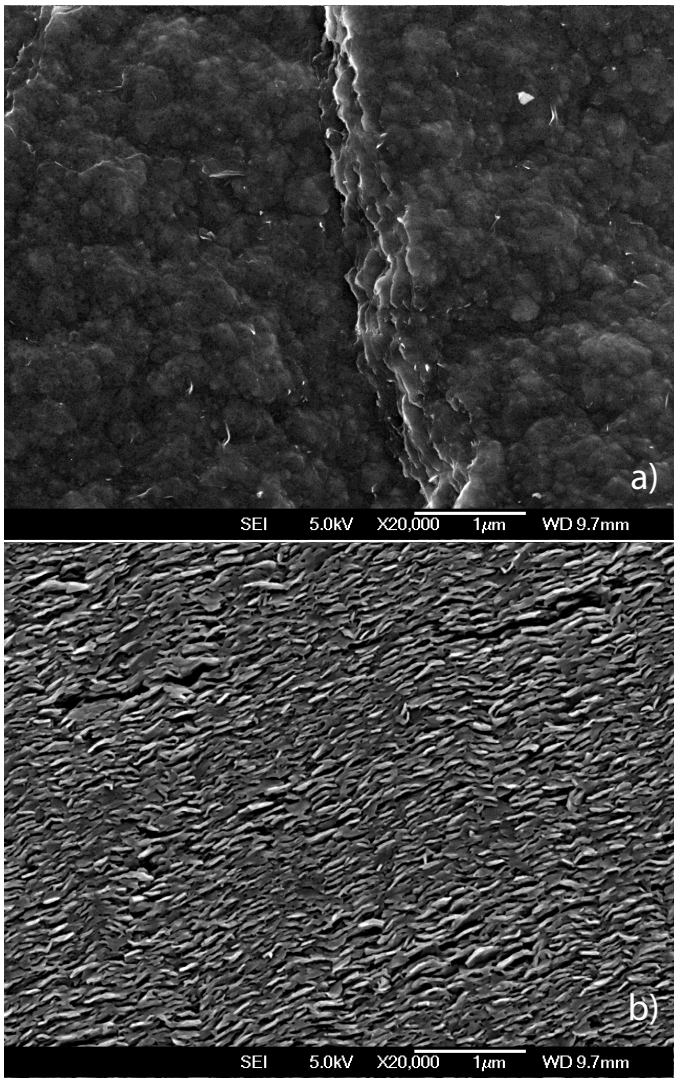

Figure 8.3: SEM image of a BPPG (a) and EPPG (b) electrode.

is observed during experimentation, as evidenced by the reduced magnitude of the oxidation peak on the reverse scan.

On the EPPG electrode, AQMS shows a clearly defined reversible redox couple with a peak-to-peak separation of less than 10mV. The peak width at half peak height for an ideal surface adsorbed species is expected to be $90.6/n$ mV (25°C), where 'n' is the number of electrons transferred,[21] for the EPPG electrode with adsorbed AQMS the measured peak width is found to consistently lie between 57 and 64 mV. Although this is larger than theoretically expected this difference is likely mainly a result of the second electron having a higher standard potential than the first. Furthermore, the shift in both the forward and back peak position as a function of pH, is almost Nernstian i.e. the peak currents shift with approximately 59 mV/pH (25°C).

The cyclic voltammetry associated with AQMS adsorbed on a BPPG electrode is more complex than that found for the EPPG. The predominant redox feature is found to occur at the same potential, but the peak width at half peak height is far larger (ranging from 67 to 98 mV) and furthermore the width is found to vary with pH. It can be clearly seen that at certain pHs a shoulder is observed upon the main voltammetric peak. Also at higher potentials (-0.76 V vs SCE) an unassigned irreversible voltammetric feature is also observed, the potential of this feature did not vary with pH; as such it is assumed that it is not associated with the system of interest.

Through varying the switching potential of the cyclic voltammogram it was possible to determine that at all pHs the cause of the broader voltammetric peak and the appearance of a distinct shoulder for the BPPG electrode with adsorbed AQMS was the result of two overlapping redox signals. This is exemplified in Figure 8.4 which depicts the cyclic voltammetric response of AQMS at pH 6, on a BPPG surface where the switching potential has been varied between -0.45V and

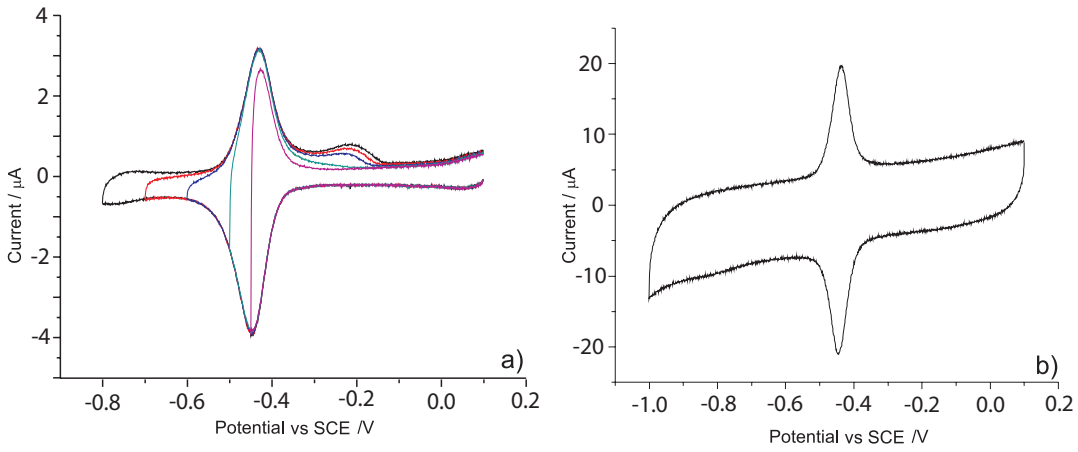

Figure 8.4: The cyclic voltammetry of AQMS adsorbed on a BPPG (a) electrode in pH 6 buffer, with varying switching potential (-0.45 – -0.8 V vs SCE) and (b) depicts the cyclic voltammetry for AQMS adsorbed on to an EPPG electrode in pH6 buffer (100 mVs^{-1}).

-0.80 V (vs SCE). The shoulder observed on the oxidative back peak is resolved as being related to an obscured reductive peak that occurs at a similar potential to the main voltammetric feature. Figure 8.4 (b) shows the cyclic voltammetry of AQMS on an EPPG electrode at pH 6, no voltammetric features apart from the main redox signal are observable. Further, it is of particular note that a greater peak current is measured on the EPPG electrode as compared to the BPPG electrode (noting that their geometric areas are equal), hence it is possible to conclude that the voltammetric feature common to both electrodes is directly related to the electro-reduction and oxidation of AQMS adsorbed on or adjacent to the edge plane site. Further, as a direct consequence it is reasonable to assume that the second voltammetric feature observed purely on the BPPG electrode is most likely due to the electro-reduction and oxidation of AQMS at the basal plane sites. It is fair to assume that this latter redox couple is purely related to the basal plane site and not basal plane sites adjacent to an edge plane defect as this environment should also be present upon the EPPG electrode.

In order for more quantitative information to be obtained from this experimental data it is necessary to resolve the two potentially closely related redox

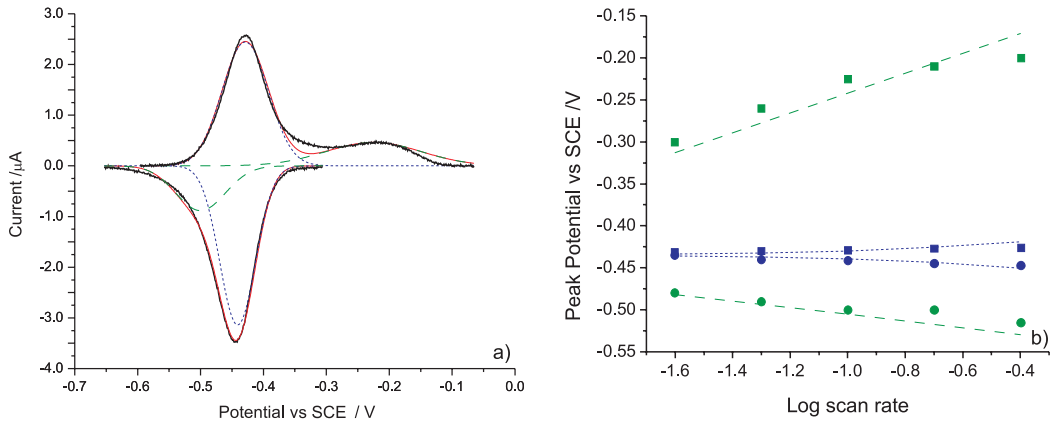

Figure 8.5: (a) The background subtracted voltammetry for AQMS adsorbed on a BPPG electrode, showing the Gaussian peak fitting, the dotted blue line is the fitting of the 'edge plane' redox couple, the dashed green line is the fitting of the 'basal plane' redox couple and the solid red line is the summation of these two sets of curves. Experimentally obtained data is shown as a solid black line. (b) depicts the variation of the deconvoluted peak positions with scan rate; circle and square points represent the experimentally obtained reduction and oxidation peak potentials respectively and the lines indicate the peak positions obtained from the theoretical model.

couples. This was achieved through the Gaussian fitting of the forward and backward peaks. The best fit was obtained through minimising the route mean squared difference between the experimental and Gaussian fitted curves. An example of the this fitting is shown in Figure 8.5, where the two redox couples are clearly marked. So as to be consistent the areas (charge passed) under the oxidative and reductive features were kept equal (within experimental error). The peak positions of these resolved voltammetric signals gives insight into the kinetics and thermodynamics associated with the system. Figure 8.5 (b) plots the peak positions for the basal and edge plane features as a function of scan rate (at pH 6). Figure 8.6 plots the reductive and oxidative peak positions as a function of pH for both the basal (a) and edge (b) plane redox couple. Below pH 3 it is not possible to accurately resolve the two redox couples as they occur at similar potentials. Similarly for pHs 9 and 9.5 resolution of the forward reductive wave is not achievable.

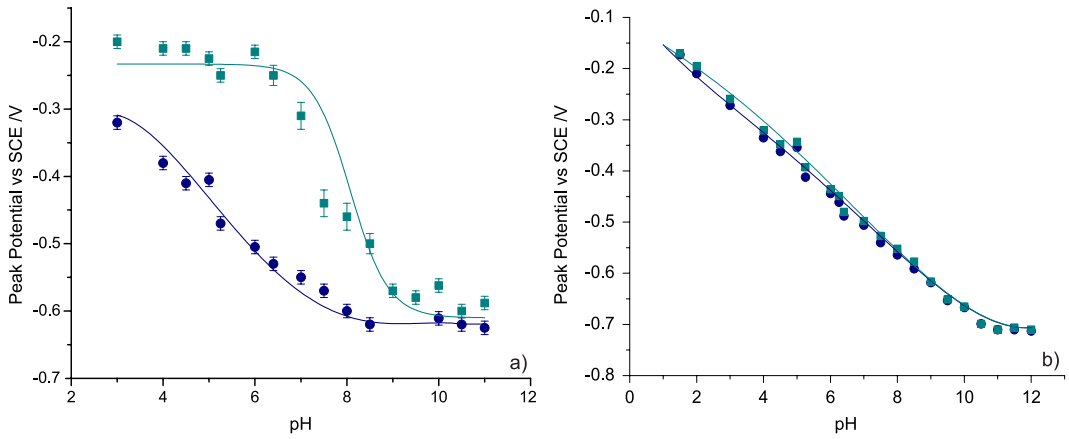

Figure 8.6: Peak potentials for AQMS adsorbed on a BPPG (a) and EPPG (b) electrode as a function of pH. The circle and square points represent the experimentally obtained reduction and oxidation peak potentials respectively and the lines indicate the peak positions obtained from the theoretical model.

8.2.2 Simulation

For the experimental examples in Chapter 5, three of the pK_as for the species had been reported within the literature. However, adsorption of a species on to a surface is known to have a significant influence upon its acidity.[22] Consequently, in order to proceed further with simulation of the present experimental example the values of pK_{a3} and pK_{a6} (cf. Figure 5.2) require assessment. For both pairs of peaks (edge and basal) an estimation of the equilibrium potential (E_{eq}) is possible through measurement of the mid point potential (E_m), where the mid point potential is the potential equidistant from the reductive and oxidative peak potentials. Through the use of the Nernst equation it is possible to obtain an expression through which both pK_{a3} and pK_{a6} (as labelled on Figure 5.2) may be estimated.[23]

$$E_m \approx E_{eq} = C + \frac{RT}{2F} \ln\left([\mathrm{H}^+]^2 + K_{a3}[\mathrm{H}^+] + (K_{a3} \cdot K_{a6})\right) \tag{8.1}$$

where C is a constant, R is the ideal gas constant, T is temperature and F is the Faraday constant. Fitting of Equation 8.1 to the experimentally obtained mid-point potentials enables pK_{a3} and pK_{a6} for the basal plane site to be measured

as 9.6 ± 0.35 and 9.00 ± 0.4 respectively, whereas for the edge plane site values of 10.8±0.18 and 10.4±0.20 as found from the EPPG electrode and values of 10.9±0.5 and 10.5±0.40 from the deconvoluted values obtained from the BPPG. Noting that the errors associated with the values for the BPPG electrode are larger as a result of the inaccuracies incurred through the process of Gaussian fitting. These values may be directly compared to those for the solution phase species which are found to be 11 and 7.6.[24] These shifts in the associated pK_a values likely represent the differing electronic and steric interactions of the AQMS with the electrode substrate.[22] From comparison with the redox chemistry of AQMS in the solution phase,[24] it is reasonable to assume that for both cases although the standard potentials for electron transfers E_1 and E_2 are similar in value, E_2 will be marginally higher cf. solution phase AQMS; for the purposes of simulation this difference (E_1 - E_2) was set as 10mV. Use of a larger potential separation would lead significantly larger peak widths. With this assumption it is possible to provide realistic values for E_1 and E_2 for both redox couples. This is achieved through assessment of the value of mid-point potential (E_m as defined earlier) at high pH, where the reaction is a direct $2e^-$ process. Moreover, under such conditions the redox couple associated with the basal plane site is found to have a mid-point potential of -0.62 V (vs SCE) which is less than that associated with the edge plane site (-0.705 V vs SCE). This significant difference in potential is directly related to the relative binding energies of AQMS to the two sites. Estimation of the adsorption energy is achieved through comparison to the solution phase value for the redox couple, -0.614 V (vs SCE). It is not possible to directly calculate the the Gibbs energy of adsorption from these two potentials, but the difference between the Gibbs energy of adsorption for the oxidised and reduced species can be obtained. Hence it is estimated that the Gibbs energy of AQMS (non-reduced) adsorption to the edge plane site is an order of magnitude greater than that for the basal plane site ($\sim$ 23 kJ mol^{-1}).

As such this large discrepancy in the binding energy provides explanation as to the small magnitude of the basal plane voltammetric peak given that on a BPPG electrode the basal plane sites have a larger surface coverage; adsorption on the latter is energetically less favored. This result is not in contradiction to that found by Ta *et al.* who performed in situ studies of the adsorption of anthraquinone disulfonate on highly ordered pyrolyic graphite.[25] Adsorption of the AQMS to the basal planes still occurs but due to being transferred to a solution containing no AQMS and due to the lower Gibbs energy of adsorption to the basal plane sites, in this experiment lower surface coverages result.

To simplify the modelling process AQH_2^{2+} is neglected as an intermediate because of the extreme difficulty of doubly protonating AQ; AQH_2^{2+} is an unknown species in aqueous solution (to the best of the authors knowledge). Consequently the e^-, H^+ sequence by which AQ is reduced to AQH_2 is assumed not to involve AQH_2^{2+} as an intermediate within the embraced pH range of this study. Hence through optimisation of the model within the bounds of the above constraints it is possible to provide a full mechanistic analysis of the system based upon the 'scheme of squares'. These optimised values are given within Table 8.1. The variation in the peak potentials associated with these models closely fit those found experimentally, as depicted by the solid lines in Figure 8.6. Although electron transfer rates are provided for all electron transfers it is only the rate of rate determining steps which maybe accurately assessed. The invariance in the position of the oxidative wave for the BPPG site between roughly pH 3 and 6 is strongly indicative of a ECCE process where the second electron transfer is rate determining in nature. The marked shift in the oxidative peak potential between pH's 7 and 9 for the basal plane site is as a result of the change of mechanism due to the effective 'switching-off' of the equilibrium for the formation of $AQH_2^{\cdot+}$ (BPPG: $pK_{a5} = 6.4$) at high pH, the position of this shift is also influenced to a degree by the associated rates of

redox couple	standard potential vs. SCE (V)	electron transfer rate (s^{-1})
	basal plane site	
E_1	-0.615	1000
E_2	-0.625	10
E_3	-0.304	100
E_4	-0.279	10
E_6	-0.131	15
	edge plane site	
E_1	-0.7	$> 10^4$
E_2	-0.71	$> 10^4$
E_3	-0.404	$> 10^4$
E_4	-0.368	$> 10^4$
E_6	-0.108	$> 10^4$

Table 8.1: Values for the standard potentials and electron transfer rates obtained from the optimised simulation for both the basal plane site and the edge plane site. The assocaited pK_as maybe readily calculated from use of Hess's law with the above thermodynamic information and the experimentally measured values for pK_a3 and pK_a6.

electron transfer. Due to the fact that the redox couple AQMS appears as nearly fully reversible on the edge plane site it is not possible to differentiate between the rates of electron transfer for each electrochemical step as such the values provided for this system in Table 8.1 represent the value at which the simulated voltammetry does not not deviate from being fully reversible (i.e. a near non-zero peak-to-peak separation). Of importance is the fact the provided model also successfully fits the peak positions as a function of the scan rate (Figure 8.5 (b)). It can be confidently stated that the numerical analysis shows that there is at least 2-3 orders of magnitude difference between the electron transfer rates for AQMS adsorbed on the edge plane site as compared to the basal pane site.

8.3 Conclusions

This work has successfully investigated the voltammetric response of AQMS adsorbed onto graphitic surfaces, where two dominant adsorption sites have been identified and attributed as related to the basal and edge plane sites. The voltam-

metric couples have been resolved so as to provide information relating to both the kinetics and thermodynamics of the species in each environment. Importantly this analysis has allowed it to be shown that the rate of electron transfer at the basal plane site is significant but still lower than that for the edge plane site by 2-3 orders of magnitude. These insights have importance to a number of electrochemical investigations, demonstrating that for surface bound species on graphitic surfaces the electrochemistry associated with the basal plane site should not be neglected. Further, this result may help explain some of the anomalous results found within the literature pertaining to the electrochemistry of single walled carbon nanotubes.

References

[1] Banks, C. E.; Compton, R. G. *Anal. Sci.* **2005**, *21*, 1263–1268.

[2] Dumitrescu, I.; Unwin, P. R.; MacPherson, J. V. *Chem. Comm.* **2009**, 6886–6901.

[3] Robinson, R. S.; Sternitzke, K.; McDermott, M. T.; McCreery, R. L. *J. Electrochem. Soc.* **1991**, *138*, 2412–2418.

[4] Rice, R. J.; McCreery, R. L. *Anal. Chem.* **1989**, *61*, 1637–1641.

[5] Banks, C. E.; Davies, T. J.; Wildgoose, G. G.; Compton, R. G. *Chem. Comm.* **2005**, 829–841.

[6] Banks, C. E.; Moore, M. R.; Davies, T. J.; Compton, R. G. *Chem. Comm.* **2004**, *10*, 1804–1805.

[7] Edwards, M. A.; Bertoncello, P.; Unwin, P. R. *J. Phys. Chem. C* **2009**, *113*, 9218–9223.

[8] Fleming, B. D.; Bond, A. M. *Electrochim. Acta* **2009**, *54*, 2713–2719.

[9] Heller, I.; Kong, J.; Heering, H. A.; Williams, K. A.; Lemay, S. G.; Dekker, C. *Nano Lett.* **2005**, *5*, 137–142.

[10] Dumitrescu, I.; Unwin, P. R.; Wilson, N. R.; Macpherson, J. V. *Anal. Chem.* **2008**, *80*, 3598–3605.

[11] Dudin, P. V.; Unwin, P. R.; Macpherson, J. V. *J. Phys. Chem. C* **2010**, *114*, 13241–13248.

[12] McDermott, M. T.; Kneten, K.; McCreery, R. L. *J. Phys. Chem.* **1992**, *96*, 3124–3130.

[13] McDermott, M. T.; McCreery, R. L. *Langmuir* **1994**, *10*, 4307–4314.

[14] Gonçalves, L. M.; Batchelor-McAuley, C.; Barros, A. A.; Compton, R. G. *J. Phys. Chem. C* **2010**, *114*, 14213–14219.

[15] Li, Q.; Batchelor-McAuley, C.; Compton, R. G. *J. Phys. Chem. B* **2010**, *114*, 7423–7428.

[16] Huynh, M. H. V.; Meyer, T. J. *Chem. Rev.* **2007**, *107*, 5004–5064.

[17] Jacq, J. *J. Electroanal. Chem.* **1971**, *29*, 149–180.

[18] Laviron, E. *J. Electroanal. Chem.* **1972**, *39*, 1–23.

[19] Harned, H. S.; Hamer, W. J. *J. Am. Chem. Soc.* **1933**, *55*, 2194–2206.

[20] Thorogood, C.; Wildgoose, G.; Crossley, A.; Jacobs, R.; Jones, J.; Compton, R. *Chem. Mat.* **2007**, *19*, 4964–4974.

[21] Honeychurch, M. J.; Rechnitz, G. A. *Electroanalysis* **1998**, *10*, 285–293.

[22] Masheter, A. T.; Abiman, P.; Wildgoose, G. G.; Wong, E.; Xiao, L.; Rees, N. V.; Taylor, R.; Attard, G. A.; Baron, R.; Crossley, A.; Jones, J. H.; Compton, R. G. *J. Mater. Chem.* **2007**, *17*, 2616–2626.

[23] Conant, T. B.; Kahn, H. M.; Fieser, L. F.; Kurtz Jr., S. S. *J. Am. Chem. Soc.* **1922**, *44*, 1383–1396.

[24] Batchelor-McAuley, C.; Li, Q.; Dapin, S. M.; Compton, R. G. *J. Phys. Chem. B* **2010**, *114*, 4094–4100.

[25] Ta, T. C.; Kanda, V.; McDermott, M. T. *J. Phys. Chem. B* **1999**, *103*, 1295–1302.

Chapter 9

Co-adsorption on Graphitic Surface for the Indirect Electrochemical Detection and Quantification of DNA

Having broached, within this thesis, how graphite surfaces may be modified through the use of both electroactive and non-electroactive species; demonstrating how these adsorption processes can yield information regarding the electrode interface. The present chapter turns to present an experimental situation in which surface adsorption can be used for analytical purposes. Specifically, the co-adsorption of AQMS and DNA is studied, highlighting how the solution phase DNA concentration can be determined through indirect assessment of the concentration of surface adsorbed DNA. The work presented within this chapter was published in the article *Biosensors and Bioelectronics* 2011, 26, 4198-4203. The work of both L. Xiong and L.M. Gonçalves towards production of the results is appreciated.

The direct electrochemical detection of DNA typically involves the redox of the purine bases (guanine and adenine). The reduction and oxidation are known to be irreversible and as such analysis is necessarily destructive towards the analyte.[1] Mercury is commonly employed within these systems due to the favourable adsorption of DNA to its surface, resulting in readily analysable results. The use

of mercury is somewhat problematic for the application of these systems outside of the laboratory due to the regulation of its use.[2] As such the development of alternative electrochemical methods would be advantageous. The direct oxidation of DNA has been investigated upon a number of materials including, but not limited, to boron doped diamond,[3] glassy carbon,[4] gold[5] and carbon paste electrodes.[6]

The oxidative mechanism of the purine bases has been predominantly studied in the solution phase on pyrolytic graphite electrodes.[7,8] It has been shown that the oxidation of guanine proceeds via the transfer of 4 H^+ and 4 e^- while adenine oxidation involves the transfer of 6 H^+ and 6 e^- both mechanisms are complex in nature and involve multiple coupled chemical steps.[7] Due to inherent experimental difficulties, little work has focused on the mechanisms associated with guanine and adenine oxidation when situated within DNA. The electrochemical response of DNA, on electrode surfaces other than mercury, is often hindered due to the observed low peak currents; this is likely as a result of poor electrical connectivity of the DNA to the electrode or as a consequence of low levels of adsorption.[3,9,10] A number of studies have utilized carbon nanotubes for the oxidation of DNA, in part to improve the observed electro-analytical signal.[11,12]

Screen printed electrodes find use within the field of electroanalytical chemistry due to having more consistent surfaces than graphitic electrodes and hence allow more reproducible and analytically useful results to be obtained.[13] A wide range of organic and aromatic species are known to readily adsorb on to graphitic surfaces including the derivatives of anthraquinone,[14] the nucleobases (adenine and guanine),[15,16] capsaicin[17] and porphyrin.[18] As demonstrated in Chapters 7 and 8 AQMS adsorbs to the electrode surface and gives a readily analysable redox signal. DNA also readily adsorbs to graphitic surfaces but as demonstrated in the recent article by Gonçalves et al. the direct analysis of its oxidative voltammetric response is not of immediate analytical use.[10] This present work studies the

co-adsorption of DNA and anthraquinone monosulphonate on to an edge-plane pyrolytic graphite electrode (EPPG). The adsorption of the DNA to the electrode surface is effectively irreversible (over the time-scale of the experiment) and the surface coverage can be indirectly measured through the quantity of co-adsorbed AQMS. It is demonstrated that this methodology when combined with the use of screen printed mutliwalled carbon nanotubes (SPE-CNTs) provides a facile method by which the concentration of a DNA sample may be analysed.

9.1 Experimental

The DNA used was of around 2000 base pairs in length and all concentrations within the text are stated as being per base pair. Different concentrations of DNA were diluted from a 10 mM DNA stock solution. The molarity for the base pairs of DNA was determined by assuming an average relative molecular mass of one base pair to be 675 g/mol. Unless specified, 30 μM AQMS solutions were used throughout the experiment.

As an alternative to the standard setup, some of the following work required that the cell arrangement was replaced by a commercially available multiwalled carbon nanotube screen printed electrode (SPE-CNT; IJ Cambria Scientific, Burry Port, UK) with a built-in carbon counter electrode and an Ag/AgCl reference electrode. A 50 μL drop of a DNA solution was deposited onto the working electrode surface. The drop was removed after 6 min accumulation of DNA on the surface and the electrode was then rinsed with deionised water. A droplet of 30 μM AQMS was placed on the SPE-CNT, ensuring that all electrodes were covered by the solution. The cyclic voltammetry was recorded after 5 min. Figure 9.1 depicts a schematic outlining the procedure undertaken.

Variation in the voltammetric response for the SPE-CNTs was experimentally characterised. The average peak height for the reduction of AQMS on the

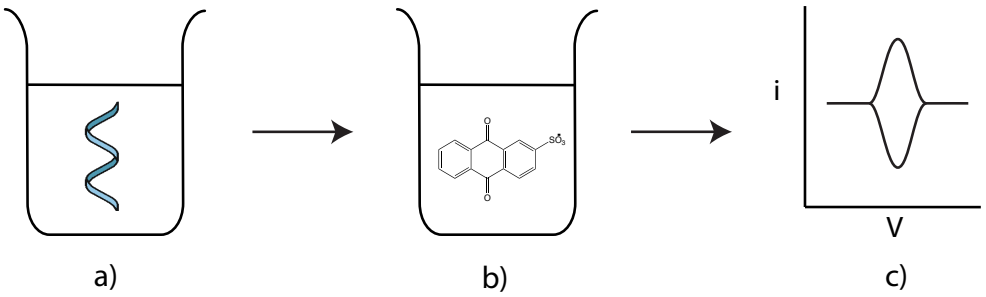

Figure 9.1: Schematic flow diagram for the co-adsorption of DNA and anthraquinone monosulfonate, a) the polished EPPG electrode is submerged in a 5 mM solution of DNA for a variable length of time (0–24 h), (b) the electrode is removed and submerged in a 30μM solution of AQMS for 5 min. Finally (c) the cyclic voltammetry of the modified electrode is run in the AQMS containing solution.

SPE-CNT is 1.68×10^{-5} A (following the procedure outlined above), with a standard deviation of 3.20×10^{-6}A. These values were obtained from the experiment being performed over two different days; in total 10 sets of data experimental data were used. All the experiments were carried out at pH 6.8 and at room temperature with the variation no more than 2 K.

9.2 Results and Discussion

Due to its relatively large size the diffusion coefficient of high molecular weight DNA is small. For DNA comprising of 2000 base pairs the the diffusion coefficient has been measured as being 4.06 ± 0.17 $\times10^{-8}$ cm^2 s^{-1}.[19] Consequently the use of diffusional voltammetry for the analytical assessment of a DNA concentration is inherently limited. The voltammetric response for high molecular weight DNA may be improved through the pre-adsorption of DNA to the electrode surface.[10] The direct oxidation of pre-adsorped DNA was studied at a graphite surface. A clean EPPG electrode was submerged into a 5mM DNA solution overnight in the absence of light and then transferred to a 0.1M PBS solution. The electrode was voltammetrically swept in an anodic direction from +0.4 to +1.4 V (vs. SCE) at

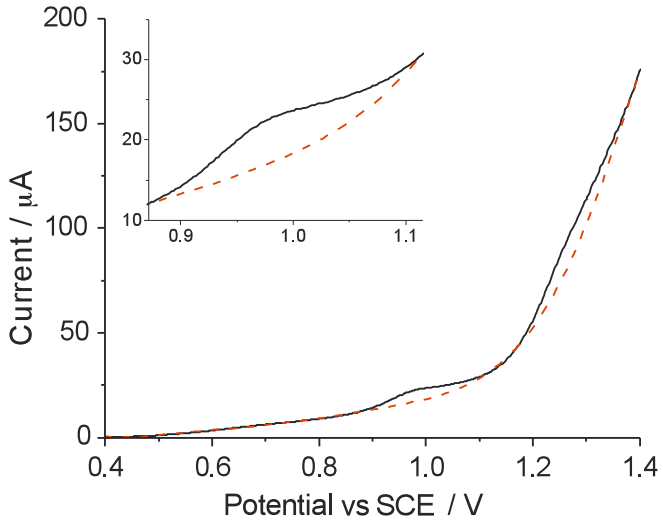

Figure 9.2: Polynomial fit for the oxidation of adsorbed DNA on an EPPG electrode in 0.1M PBS. Adsorption was performed overnight from a solution of 5mM DNA, inlay depicts a magnified view of the guanine oxidation signal.

a scan rate of 100mVs^{-1}, the resulting voltammogram is depicted in Figure 9.2.

The voltammetric peaks are found to be broad and ill defined, such that the subtraction of the background via the use of a 7th order polynomial is required to aid analysis.[10] As can be seen from Figure 9.2, two faradaic process are observed during the anodic sweep of the voltammetric scan. These two peaks situated at +0.97 and +1.28 V (vs. SCE) can be ascribed as being due to the oxidation of the DNA present upon the electrode surface. From the literature it is known that the oxidation of solution phase guanine and adenine bases exhibit characteristic peaks at +0.66 and +0.96V (vs. SCE) at pH 6.8 as recorded at a bare EPPG electrode.[10,16] Taking into account the fact that the guanine and adenine bases are in different local environments when contained within the DNA, as compared to the solution phase, we assign these peaks at +0.97 and +1.28V (vs. SCE) as being related to the guanine and adenine oxidations respectively.

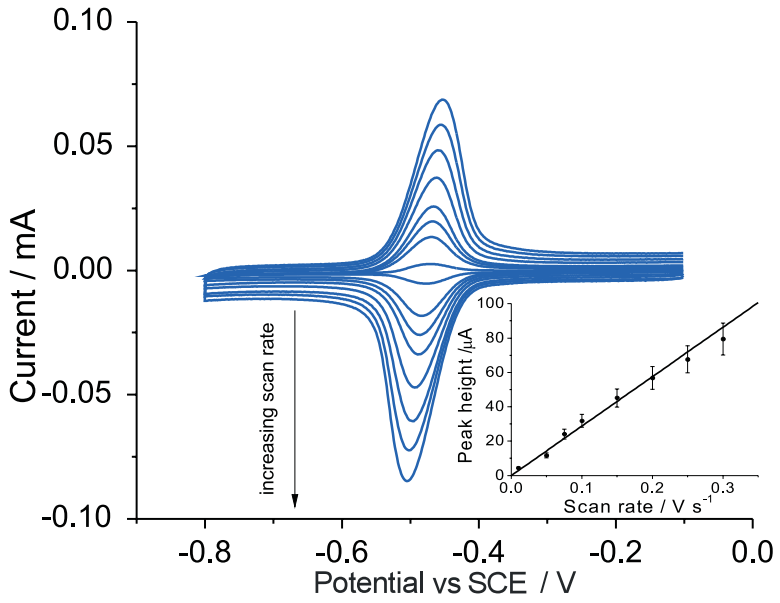

Figure 9.3: Cyclic voltammograms of 30μM AQMS in 0.1M PBS (pH 7) recorded at an EPPG electrode at variable scan rate 10-300 mVs^{-1}. Inlay: plot of peak current vs. scan rate.

9.2.1 Investigation of the AQMS Voltammetric Response

It is clear that although adsorption significantly enhances the electrochemical signal for the oxidation of DNA, the measured response is still minimal and as such its use for quantifying DNA concentrations is analytically challenging. AQMS, as demonstrated in Chapters 7 and 8, is known to readily adsorb to graphite surfaces and exhibits a well-defined surface voltammetric peak at low solution phase concentrations. The cyclic voltammetric response of a 30μM AQMS solution, over a potential range of -0.1 to -0.8 V (vs. SCE) at an EPPG electrode (after 5mins accumulation time), is depicted in Figure 9.3. A large voltammetric feature is observed at -0.49 V (vs. SCE) corresponding to the AQMS redox. Further the peak current for the wave was found to vary linearly as a function of scan rate (inlay), indicating that the AQMS is surface bound.[20] The time dependency of the magnitude of the voltammetric peak was also investigated as a function of accumulation time (not shown), where after 5 mins the surface concentration was found to be maximised. The surface coverage of the adsorbed AQMS was analysed

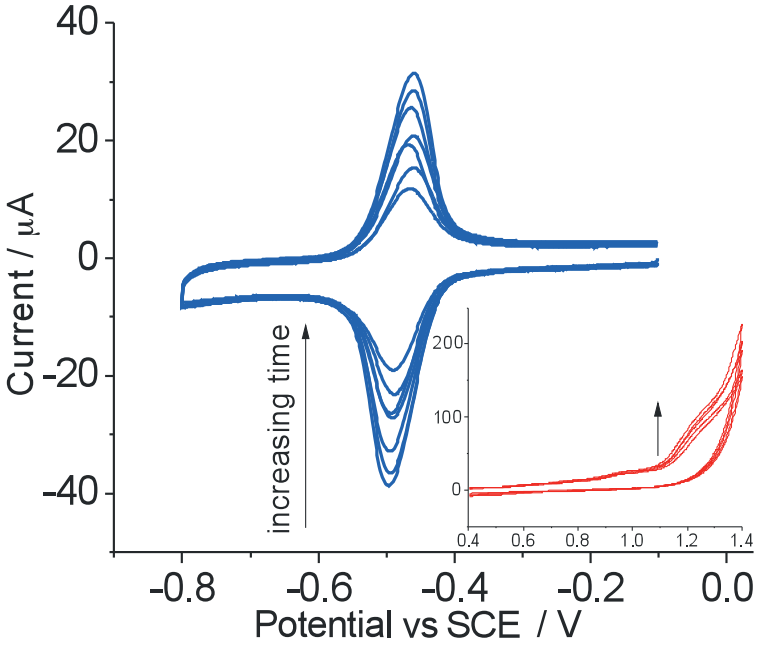

Figure 9.4: Cyclic voltammograms of the reduction of AQMS (30μM) recorded on an EPPG electrode in the presence of co-adsorbed DNA. DNA had been adsorbed from a 5mM solution for varying periods of time ranging from 10s to 2h. Inlay: the cyclic voltammograms of the direct oxidation of the adsorbed DNA in 0.1M PBS.

via the use of a transfer experiment, where the EPPG electrode was submerged in a 30 μM AQMS and transferred to a PBS in order to perform the voltammetric experiment. A surface coverage of 2.3±0.35 $\times$ 10^{14} molecules cm^{-2} was obtained, thus suggesting the formation of a near monolayer coverage (cf. Chapter 8).

9.2.2 DNA and AQMS Competitive Adsorption

Two sets of parallel analyses are introduced in this section in order to allow the indirect measurement of the DNA concentration via the co-adsorption of AQMS. First, the cyclic voltammetric response for the oxidation of DNA upon the EPPG electrode was studied as a function of accumulation time. An EPPG electrode was submerged into a 5mM DNA for a variable length of time and then subsequently transferred into PBS, following which an anodic cyclic voltammogram which was recorded at a scan rate of 100 mV s^{-1}, Figure 9.4 inlay. As can be seen

the voltammetric peak current for the oxidation of the adsorbed DNA, although poorly defined, increases as a function of the DNA accumulation time. Second, the influence of the pre-adsorption of DNA upon the subsequent AQMS adsorption was investigated. The EPPG electrode was exposed to the 5mM DNA solution for a variable period of time, after which the electrode was removed and submerged in a 30μM AQMS solution. The AQMS was allowed to accumulate for a period of 5 minutes prior to the cyclic voltammetry being run. The voltammetric results of this experiment can be seen in Figure 9.4. It can be seen that the formal potential for the reduction of AQMS does not vary as a function of DNA adsorption time. Consequently, this lack of shift in the redox potential implies that the AQMS is directly bound to the electrode surface and does not interact with the DNA. From Figure 9.4 it may also be noted that the DNA pre-adsorption time has a significant influence upon the measured AQMS peak height. Further, the AQMS peak current is more sensitive to the DNA surface coverage than the direct oxidative (DNA) peak current.

Figure 9.5 shows the variation in the peak current for the reduction of AQMS and the oxidation of the DNA as a function of DNA adsorption time, where for both species the maximum DNA surface coverage is found to occur after approximately two hours of DNA adsorption. Moreover, an inverse relationship between the two peak currents is observed. The DNA adsorbs upon the electrode surface irreversibly and due to the fact that the low concentrations of AQMS used results in an 'adsorptive' response it may be assumed that the total surface coverage for co-adsorbed AQMS and DNA is *effectively* constant. This approximation may be expressed as $\Gamma_{\text{total}} = \Gamma_{\text{DNA}} + \Gamma_{\text{AQMS}}$, where Γ_{total} is a constant, Γ_{DNA} is the surface coverage of DNA and Γ_{AQMS} is the surface coverage of AQMS. Hence, the AQMS adsorptive signal can be used to indirectly determine the quantity of DNA upon the electrode surface. It should be noted that Γ_{total} varies between subsequent

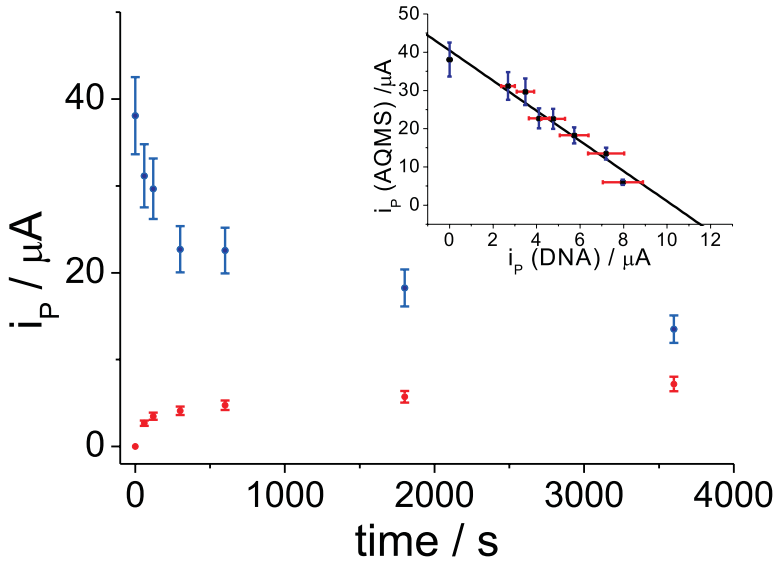

Figure 9.5: Dependency the peak current on the DNA adsorption time. Red points indicate the oxidation of DNA adsorbed on the EPPG electrodes in 0.1M PBS and blue points are the reduction of AQMS on the DNA modified EPPG electrodes. Inlay: plot of the peak current for the reduction of AQMS vs. the peak current for the oxidation of DNA at the same DNA adsorption times.

polishings of the electrode.

The inlay of Figure 9.5 shows the linear correlation between the peak current for the reduction of the AQMS and the peak current for the DNA oxidative wave. It should be noted that information regarding low DNA surface coverages (peak current $\leq 2\ \mu A$ which is equivalent to an accumulation time of ≤ 1 min) is not presented, this is due to the fact that the peak current for the DNA oxidation could not be satisfactorily and reproducibly measured, even though a change in the AQMS reduction signal can be observed. Further, at long accumulation time ($\geq$ 2h) the adsorbed AQMS signal shows a non-zero peak current ($I_p = 5.7\times 10^{-6}$ A). Hence, it is concluded that even at maximum DNA adsorption there are still unoccupied sites available for AQMS adsorption which are not available for the DNA. This non-zero peak current may also be relating to a small diffusional current as a result of the low AQMS concentrations used experimentally.

9.2.3 Analytical use of SPE-CNT's

The voltammetric performance of the 'carbon nanotube screen printed electrodes' (SPE-CNT) was investigated. The whole of the SPE-CNT electrode surface was covered with a drop (50 μL) of 30 μM AQMS under an argon atmosphere. First, the reductive peak current was measured as a function of adsorption time, it was found that maximum adsorption was achieved after 5 minutes. The resulting voltammetric response was found to be predominantly adsorptive in nature. The forward and back peaks for the AQMS reduction exhibit relatively high symmetry with a peak-to-peak separation of 18 mV, an indication of the electrochemical reaction being nearly reversible. The direct oxidation of pre-adsorbed DNA was also studied at the SPE-CNTs, where by a 50 μL droplet of 10mM DNA was deposited onto the working electrode for 2 hours. Upon running the cyclic voltammogram from +0.4 to +1.4V (vs. SCE) at a scan rate of 100 mVs^{-1} an ill-defined signal was observed for the direct oxidation of the DNA. These results for the SPE-CNT, with both AQMS and DNA, are analogous to those obtained for the EPPG electrode.

Due to the layered structure of graphite, there are both basal and edge plane sites present on the electrode. During polishing the graphite electrode, a random number of these sites are exposed on the surface. Thus, the adsorptive sites for both DNA and AQMS may vary, this variation is reflected in the fluctuation of the peak current for the reduction of the AQMS, which upon the EPPG electrode is found to vary by up to 16%. Due to this variation in the electrode surface the use of the EPPG electrode for analytical purposes is limited. In comparison, SPE-CNTs provide a far more consistent surface where the variation in the peak current for the reduction of AQMS was found to fluctuate by no more than 6.2%.

The influence of the DNA adsorption upon the AQMS signal on the SPE-CNT was investigated. Experimentally a 50 μL droplet of DNA solution (variable concentration) was left on the working electrode for 6 minutes after which the

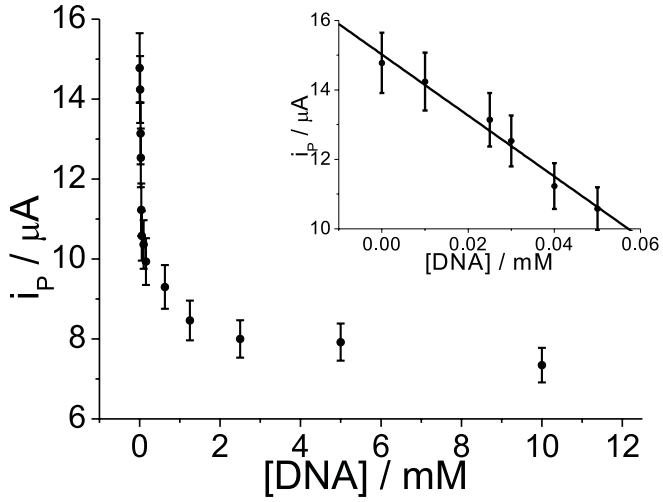

Figure 9.6: Plot of peak current of AQMS vs. DNA solution concentration on a SPE-CNT. The corresponding cyclic voltammograms were run in a range of -0.1 to -0.8V, a scan rate of 100 mVs^{-1}. Inlay: magnification of 0-0.05 mM DNA region.

electrode was rinsed with deionised water. Then a drop of 30 μM AQMS was placed on to the DNA modified SPE-CNT electrode in an oxygen free environment. The cyclic voltammetry for the AQMS reduction was run in a cathodic direction from -0.1 to -0.8V (vs. SCE) at a scan rate of 100 mVs^{-1}. The plot of of the peak current for the reduction of AQMS vs. DNA solution concentration is shown in Figure 9.6, where the experimental data set has been recorded on different electrodes for each concnetration. Again with increasing surface coverage of DNA (this time due to an increasing DNA concentration) the AQMS signal is found to decrease, moreover, at low DNA concentrations a near linear dependency is recorded (inlay). Within this linear range (0-0.05 mM DNA) a limit of detection (LOD) of 8.8 μM – as measured per base pair and is equivalent to 5.9 μg/mL – was determined through the use of the three sigma method. It should be noted that the sensitivity of this system may be improved through the use of longer DNA adsorption times. Longer experimental adsorption times were not used within this work due to being unnecessary for proof of concept; further, this ensured that the analysis was short enough to be readily employed analytically.

9.3 Conclusions

Through the voltammetric analysis of co-adsorbed DNA and AQMS on both EPPG and SPE-CNT electrodes, this work has demonstrated how the adsorption of DNA to the electrode surface may be readily quantified through the voltammetric analysis of the co-adsorbed anthraquinone species. Further this result highlights how when adsorbed upon the surface the two species are non-interacting as evidenced by lack of observed shift in the formal potential for either species. Through the use of this methodology it is possible to obtain a LOD for the quantification of the DNA solution phase concentration as 8.8 μM.

References

[1] Paleçek, E. *Electroanalysis* **2009**, *21*, 239–251.

[2] Engle, M. *Dynamics of Mercury Pollution on Regional and Global Scales* **2005**,

[3] Oliveira, S. C. B.; Oliveira-Brett, A. M. *J. Electroanal. Chem.* **2010**, *648*, 60–66.

[4] Brett, C. M. A.; Oliveira Brett, A. M.; Serrano, S. H. P. *J. Electroanal. Chem.* **1994**, *366*, 225–231.

[5] Pang, D. W.; Qi, Y. P.; Wang, Z. L.; Cheng, J. K.; Wang, J. W. *Electroanalysis* **1995**, *7*, 774–777.

[6] Wang, J.; Flechsig, G. U.; Erdem, A.; Korbut, O.; Gründler, P. *Electroanalysis* **2004**, *16*, 928–931.

[7] Dryhurst, G.; Elving, P. J. *J. Electrochem. Soc.* **1968**, *115*, 1014–1020.

[8] Dryhurst, G.; Pace, G. F. *J. Electrochem. Soc.* **1970**, *117*, 1259–1264.

[9] de-los Santos-Álvarez, P.; Lobo-Castañón, M. J.; Miranda-Ordieres, A.; Tuñón Blanco, P. *Anal. Chem.* **2002**, *74*, 3342–3347.

[10] Gonçalves, L.; Batchelor-Mcauley, C.; Xiong, L.; Barros, A. A.; Compton, R. G. *Electroanalysis* **2011**, *23*, 583–587.

[11] Wang, J.; Kawde, A. N.; Musameh, M. *Analyst* **2003**, *128*, 912–916.

[12] Wu, K.; Fei, J.; Bai, W.; Hu, S. *Anal. Bioanal. Chem.* **2003**, *376*, 205–209.

[13] Choudry, N. A.; Kampouris, D. K.; Kadara, R. O.; Banks, C. E. *Electrochem. Comm.* **2010**, *12*, 6–9.

[14] Ta, T. C.; Kanda, V.; McDermott, M. T. *J. Phys. Chem. B.* **1999**, *103*, 1295–1302.

[15] Gonçalves, L. M.; Batchelor-Mcauley, C.; Barros, A. A.; Compton, R. G. *J. Phys. Chem. C* **2010**, *114*, 14213–14219.

[16] Li, Q.; Batchelor-Mcauley, C.; Compton, R. G. *J. Phys. Chem. B* **2010**, *114*, 7423–7428.

[17] Kachoosangi, R. T.; Wildgoose, G. G.; Compton, R. G. *Analyst* **2008**, *133*, 888–895.

[18] Fleming, B. D.; Bond, A. M. *Electrochim. Acta* **2009**, *54*, 2713–2719.

[19] Liu, M. K.; Giddings, J. C. *Macromolecules* **1993**, *26*, 3576–3588.

[20] Bard, A. J.; Faulkner, L. R. *Electrochemical Methods: Fundamentals and Applications* **1980**,

Chapter 10

Semiquinone Intermediates in the Two Electron Reduction of Quinones in Aqueous Media and their Exceptionally High Reactivity Towards Oxygen Reduction

The simulations within this thesis for the voltammetric response of the anthraquinone species have all been predicated on the basis that the first and second electron transfers occur at comparable potentials (solution phase AQMS, $E^{\ominus}_{f,2} - E^{\ominus}_{f,1} = -15mV$). This has been evidenced in part on the experimental peak height being less than that predicted by the Randles-Ševčík equation when calculated using the diffusion coefficient obtained from the use of a micro-disc electrode. As a direct consequence of this difference in the formal potentials, it is predicted that during the course of the voltammetric scan the concentration of the semi-quinone intermediate will be appreciable at the electrode surface. Hence, this chapter aims to provide voltammetric evidence for the presence of the semi-quinone species through investigation of the electrochemical mechanism for anthraquinone mediated oxygen reduction. Furthermore, this work is then extended to demonstrate how the stability of the semi-quinone intermediate may be tuned through altering the supporting electrolyte. The work presented herein was published in the

two articles '*Chemphyschem* 2011, 12, 1255–1257' and '*Chemical Communications* 2011, 47, 11426-11428.' Moreover, this work was completed through a partnership with Q. Li.

The quinone mediated reduction of oxygen is of great importance, both biologically and industrially. Hydrogen peroxide is commercially produced via the catalytic reduction of 2-alkyl anthraquinone with approximately 2.2 million metric tonnes being annually produced worldwide in this way.[1] Beyond industry, a prime example of quinones for medicinal use lies with the anthracycline antibiotics. Anthracycline antibiotics are powerful chemotherapeutic drugs and are employed against a variety of cancers. Although highly successful their use is in part limited due to their high cardiotoxicity.[2] Over the last decade it has been proposed that this toxicity is directly related to, and is a result of, the biological redox cycling of the quinone moiety within the anthracycline molecule, leading to the production of reactive oxygen species.[3,4] Understanding the mechanism for oxygen reduction is therefore imperative not only for the optimisation of industrial processes but also to aid development of more suitable chemotheraputic drugs.

The direct electrochemical investigation of organic molecules and their interaction with oxygen is often hindered by the direct reduction of oxygen at the electrode, hence the voltammetric response of interest has to be carefully resolved from that of the background. Here we demonstrate that this issue is circumvented through the use of a boron-doped diamond electrode (BDD). This is achievable due to the very large overpotential required for oxygen reduction at a BDD interface. Another important factor is the experimentally low capacitance values measured at the BDD surface, this may arise either due to the fact that BDD is a semiconductor (albeit highly doped $\sim$0.1%) or it may also be related to its near atomically flat surface.[5] From studying the voltammetric response of anthraquinone at a BDD electrode in both the presence and absence of dissolved oxygen it is possible to

clearly elucidate the complex mechanistic process highlighting the remarkable potency of the semiquinone intermediate in the production of superoxide.

10.1 Experimental

10.1.1 Modelling

Modelling of the catalytic reduction of oxygen at neutral pH was based in part upon the following mechanistic steps;

$$\mathrm{AQMS^{-\cdot}} + \mathrm{O_2} \rightleftharpoons \mathrm{AQMS} + \mathrm{O_2^{-\cdot}} \tag{10.1}$$

$$\mathrm{AQMSH^-} + \mathrm{O_2} \rightleftharpoons \mathrm{AQMS} + \mathrm{HO_2}^- \tag{10.2}$$

where reaction 10.1 is the one electron reduction of oxygen to form superoxide via the semi-quinone intermediate ($\mathrm{AQMS^{-\cdot}}$). It is important to recognise that the one electron reduction of oxygen by the di-protonated form of the AQMS is not thermodynamically favourable and hence is not included within the reaction scheme. For the oxygen species the following reaction scheme was used as the basis for all thermodynamic calculations:

$$\begin{aligned}
\mathrm{O_2} + \mathrm{e^-} &\rightleftharpoons \mathrm{O_2^{-\cdot}} && E_{O1} = -0.4212\mathrm{V\ vs\ SCE} \\
\mathrm{O_2^{-\cdot}} + \mathrm{H^+} &\rightleftharpoons \mathrm{HO^{\cdot}} && pK_a = 4.88 \\
\mathrm{HO^{\cdot}} + \mathrm{e^-} &\rightleftharpoons \mathrm{HO_2}^- && E_{O2} = +0.5369\mathrm{V\ vs\ SCE} \\
\mathrm{HO_2}^- + \mathrm{H^+} &\rightleftharpoons \mathrm{H_2O_2} && pK_a = 11.62
\end{aligned}$$

The above thermodynamic values were obtained from the literature where they have been corrected for the experimental pH and against a SCE reference electrode.[6] Note that no direct reduction of the oxygen species is possible on the BDD electrode such that for E_{O1} and E_{O2}, $\mathrm{k}_s = 0.0\ \mathrm{cm\ s^{-1}}$. The following pathway was

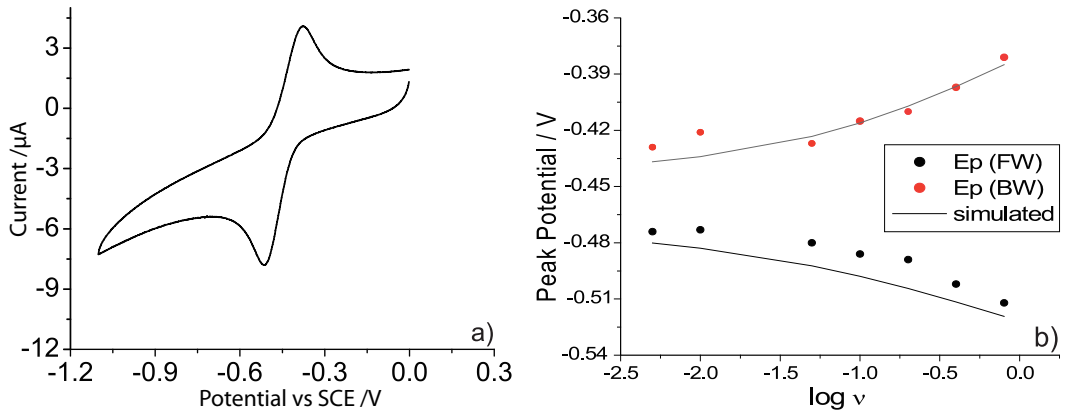

Figure 10.1: Cyclic voltammetry of 50 μM AQMS at 800mVs^{-1} (a), figure (b) shows the variation of the peak positions with scan rate.

also included so as to allow disproportionation of the superoxide species to occur;

$$2HO_2^{\cdot} \rightarrow O_2 + H_2O_2$$

This disproportionation was set to occur at a diffusion limited rate. Using this full model the voltammetric response was fitted to that found experimentally through varying the values of the forward rate constants for the rates for Reactions 10.1 and 10.2. Note that the thermodynamic values for the formal potentials and pK_as associated with the reduction of the AQMS were the same as used previously. The concentration of a saturated oxygen solution was found to be 1.24 mM[7] and has an associated diffusion coefficient of 1.77×10^{-5} cm^2 s^{-1} in aqueous solution.[8]

10.2 Results and Discussion

10.2.1 Studies at Neutral pH; the High Reactivity of Semi-quinone

The cyclic voltammetric response of 50 μM and 500 μM anthraquinone monosulfonate (AQMS) was investigated at a BDD electrode in an aqueous oxygen free solution (pH 6.74) at various scan rates. Figure 10.1 depicts a representative experimental voltammogram for 50 μM AQMS. A clear voltammetric wave is recorded at

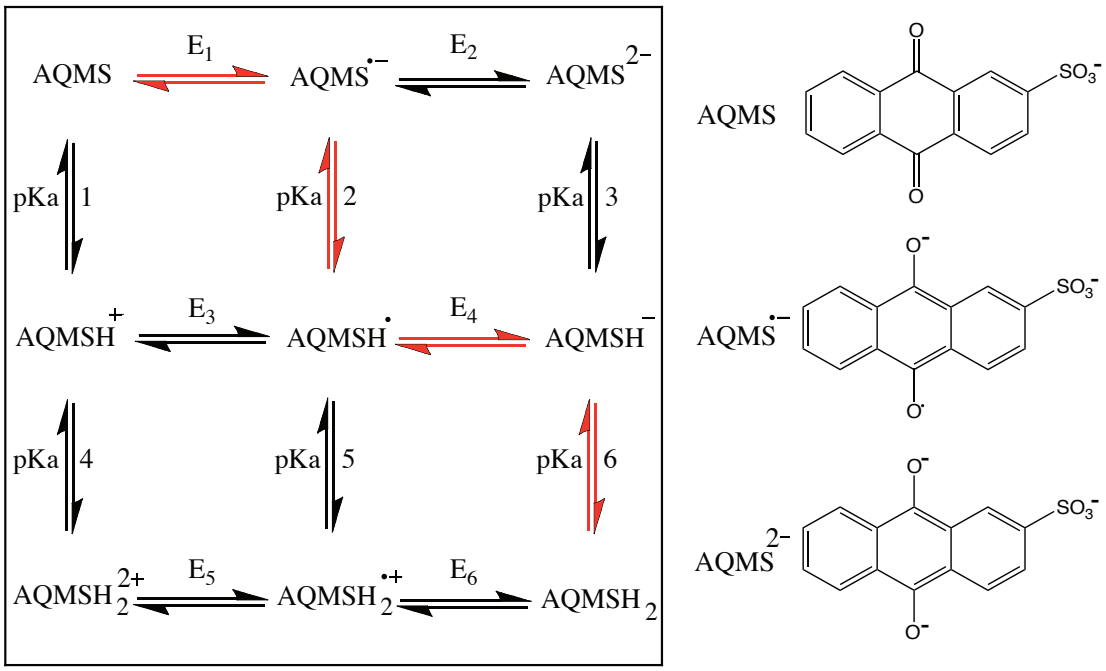

Figure 10.2: Schematic representation of the 'scheme of squares' model for the reduction of anthraquinone with the main mechanistic pathway at this pH highlighted in red. Adjacent are the unprotonated structures of the unreduced, monoreduced and direduced forms of the anthraquinone species.

-0.45 V (vs SCE), it is of note that the relatively low concentration of the AQMS used and high scan rate leads to the background (capacitative) current appearing superficially large. This electrochemical system was modelled through use of the commercially available software package DIGISIM®. At the experimental pH (6.74) the dominant pathway for the reduction of the anthraquinone species will be an ECEC type mechanism, as highlighted on Figure 10.2. It is fair to assume that the thermodynamic properties of the system (pK_as and potentials) are intrinsic to the AQMS and are not perturbed by the BDD surface (an outer-sphere electron transfer mechanism) but the kinetic parameters i.e. the rates of electron transfer may be altered due to being inherently linked to the density of electronic states present within the electrode. Consequently, the fit of the experimental voltammetry was achieved through variation of the rates of electron transfer for E_1 and E_4, where values of 10 and 5 cm s^{-1} were used. Figure 10.1 (b) depicts the variation

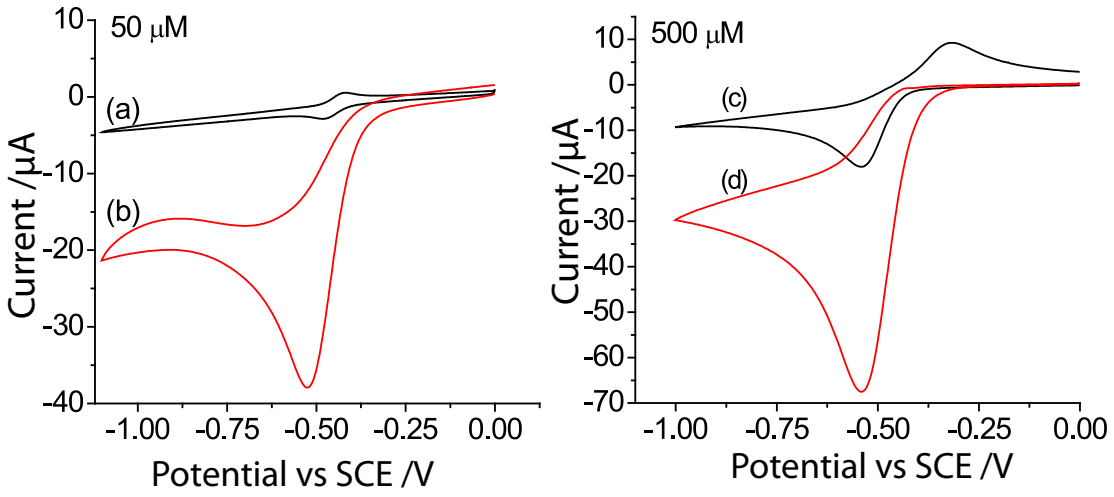

Figure 10.3: Comparison of the voltammetries of 50 μM and 500 μM AQMS in both the absence (a, c) and presence (b, d) of oxygen.

in the AQMS peak potential (experimental and simulated) as a function of scan rate.

The voltammetric response for the reduction of AQMS is markedly different in an oxygen saturated solution. The comparison between the reduction of AQMS (50 μM and 500 μM) in the presence and absence of oxygen is depicted in Figure 10.3. Further, over the potential range of study there is no significant reduction of either oxygen or hydrogen peroxide on the BDD electrode. It is of importance that at a concentration of 50 μM AQMS *not* all of the oxygen has been consumed, as evidenced by the lower peak height than that found for the 500 μM AQMS; hence, the rate limiting step is the redox of the AQMS species. In general the adsorption of species to BDD electrodes is reported to be weak, in part due to the 'low polarizability of the material.'[9] Combined with the fact that the voltammetric response of the anthraquinone is found to be purely diffusional in nature as evidenced through the variation in the peak current with scan rate; it is assumed that the influence of adsorption upon the catalytic response is *minimal*. Hence, it is not inappropriate to approximate the electron transfer as being an outer sphere mechanism. This assumption is further corroborated by the fact the redox poten-

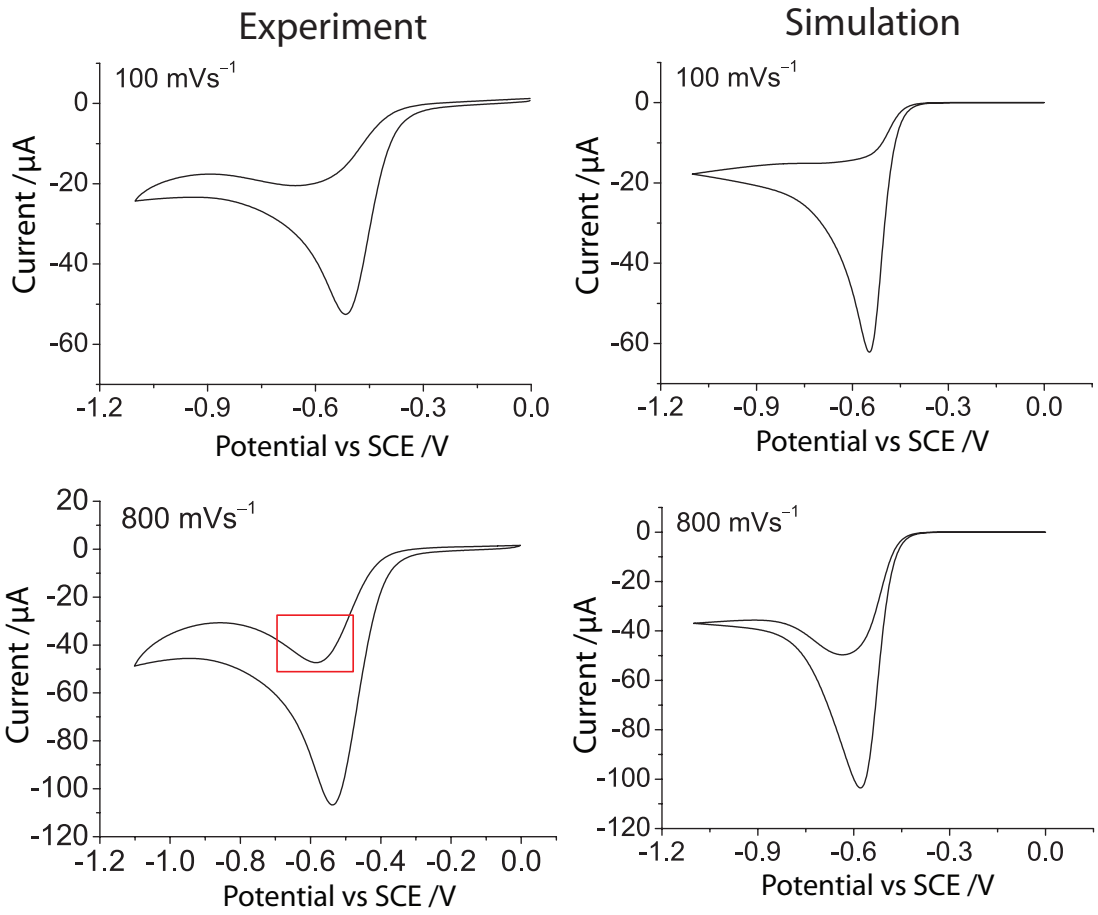

Figure 10.4: Comparison of the experimental and simulated voltammetry of 50 μM AQMS in the presence of oxygen at two different scan rates. The red square highlights the observed unusual 'reverse' peak.

tials for the anthraquinone species are found to be unaltered from those measured on a gold electrode.

The AQMS mediated electrochemical reduction of oxygen is known but the mechanistic pathway is not.[10,11] Overall, at pHs below $\sim$ 8, the process is known to lead to the two proton two electron reduction of oxygen leading to the formation of hydrogen peroxide. Figure 10.4 depicts the voltammetric response of 50 μM AQMS in an oxygen saturated solution at two different scan rates, 100mVs^{-1} (a) and 800mVs^{-1} (b). As can be seen from Figure 10.4, the observed voltammetric response shows a single irreversible wave at -0.55 V (vs. SCE). This voltam-

metric feature is attributed to the catalytic reduction of oxygen via the reduced anthraquinone. Of particular significance is the experimentally observed peak on the reverse scan (as highlighted via the red square in Figure 10.4). This feature is highly unusual and indicates a pathway for oxygen reduction which is non-operational at high over potentials.

For multi-electron transfers it is often assumed that the subsequent electron transfers after the first electron are highly driven and hence it is possible to analyse the obtained results using the well known classical equations.[12] In the case of many organic molecules this assumption does not necessarily hold, and as demonstrated for anthraquinone the potentials for the first and second electron transfer are likely comparable. As a direct result of this, at lower over potentials significant levels of the intermediate species (for example semiquinone) are produced and are able to diffuse away from the electrode surface. During a voltammetric experiment as the over potential is increased the rate of electron transfer for both steps increases such that at high over potential minimal levels, if any, of the intermediate will be produced. Hence, from the above results it is reasonable to conclude that the observed 'reverse' peak (red square in Figure 10.4) is related to the formation of the semiquinone species at lower overpotentials and its catalytic reduction of oxygen.

Within the full scheme as outlined within the experimental, this superoxide radical is able to undergo series of reactions including protonation and disproportionation which leads to the reformation of O_2 and the production of H_2O_2. Reaction 10.2 is the two-electron, one-proton reduction of oxygen to the monoprotonated peroxide ion via reaction with the monoprotonated direduced form of anthraquinone ($AQMSH^-$). Within this reaction scheme the di-reduced diprotonated form of anthraquinone ($AQMSH_2$) and the protonated semiquinone ($AQMSH^{\cdot}$) are not reactive towards oxygen. This is likely physically realistic as it is known that at pH 3.13, where both pK_a6 and pK_a2 (as defined on Figure 10.2)

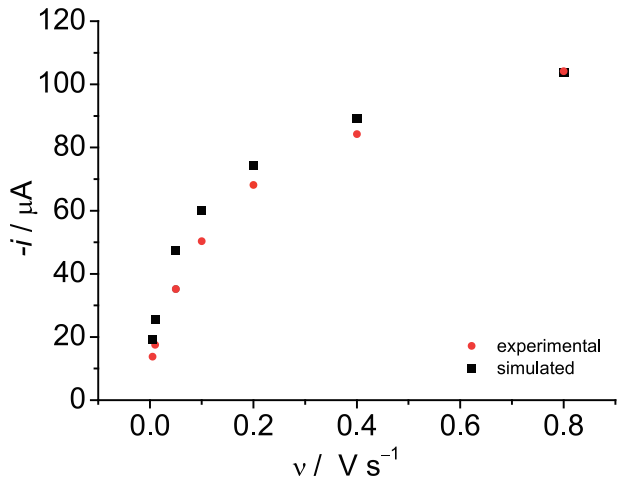

Figure 10.5: Comparison of the experimental and simulated peak currents for the reduction of AQMS in the presence of oxygen.

will lie heavily towards the production of $AQMSH_2$ and $AQMSH^{\cdot}$ respectively, *no* catalytic oxygen reduction is observed.

Applying the mechanism above to that for the reduction of anthraquinone, it is possible to obtain a high level of agreement between experiment and simulation, where the rate constants for Reaction 10.1 and 10.2 are 4.8×10^9 mol^{-1} dm^3 s^{-1} and 1×10^7 mol^{-1} dm^3 s^{-1}. The author highlights that the rate of reaction between the semiquinone and oxygen is over two orders of magnitude greater than the corresponding reaction between the di-reduced form and oxygen. The comparison of the voltammetry is shown in Figure 10.4, and Figure 10.5 depicts how the variation in the catalytic peak height varies with scan rate for both experimental and simulated results.

10.2.2 Studies at High pH; the Influence of Ion Pairing

In aprotic solvents the reduction of quinonal species follows a simple two electron reduction, where the second electron is significantly thermodynamically more difficult than the first (as demonstrated in Chapter 4). It is recognised that a

number of factors can also govern the relative positions of E_1 and E_2, for instance ion pairing, nonspecific solvation, and molecular structures etc.[13] As previously demonstrated (Chapter 5) the reduction of AQMS in aqueous media at high pH follows a simple EE mechanism. In order to investigate the influence of ion pairing upon the voltammetric response it is imperative that the pH is suitably controlled, this is achievable through the use of hydroxide salts.

The influence of supporting electrolyte upon reduction of anthraquinone-2-sulfonate (AQ) in aqueous media is investigated here. The electrochemical reduction of AQ was carried out in a fully supported (0.1 M electrolyte) and oxygen-free aqueous solution on a macro-gold electrode. Alkali metal cations are regularly used within aqueous media as part of the supporting electrolyte and/or buffer. The identity of the cation was varied down the periodic table from from sodium to rubidium, where it was found that for all cases a single voltammetric wave is observed at -0.65 V (vs. SCE). Alternatively, tetraalkylammonium salts find extensive use within aprotic media due to the relatively low degree to which they ion pair.[14] However, under aqueous conditions these cations can impart a significant influence upon the voltammetric response.[15] The voltammetric response for a 0.5 mM AQMS aqueous solution supported with varying proportion of the tetra-n-butylammonium hydroxide (TBAOH) and tetra-methylammonium hydroxide (TMAOH) was investigated at a gold macroelectrode. The cyclic voltammetric responses (Figure 10.6) demonstrate a trend of splitting one wave into two when the proportion of TBAOH increases from 0 to 100%. In the presence of 100% TMAOH, the relatively small ΔE results in a single $2e^-$ reduction wave. While keeping the pH environment and ionic strength unchanged, the increasing proportion of TBA^+ cations gradually causes E_1 and E_2 to separate; consequently resulting in two resolvable $1e^-$ reduction waves. Similar results are obtained if the length of the alkyl chain is varied.

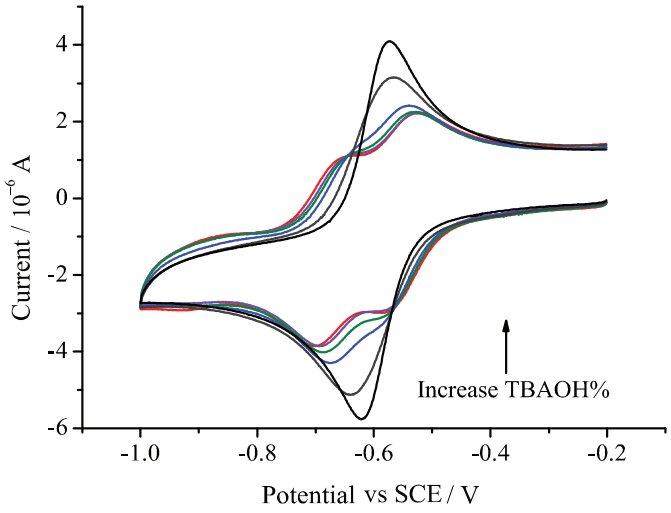

Figure 10.6: Cyclic voltammograms of 500 mM AQ/H2O supported with ([TMAOH] + [TBAOH]) = 0.1 M at 100 mV s^{-1} on an Au electrode. The proportion of TBAOH increases from 0 (black), 20 (brown), 40 (blue), 60 (green), 80 (violet) to 0% (red).

Importantly, with the use of TBAOH the difference between the formal potentials for the first and second electron transfer is found to be 138 mV; however the formal potential for the two electron transfer is only altered by 18 mV i.e. the decrease in the formal potential for the second electron transfer is almost equivalent to the increase in the value for the first electron transfer. Also of significance is that the diffusion coefficient for the AQMS, as measured from the steady state current at a microdisc electrode, is found to vary as a function of the supporting electrolyte as shown in Table 10.1. This implies that the TBAOH is ion pairing to the unreduced form of the AQMS to a significant degree. From this it is reasonable to conclude that the semiquinone species is stabilised due to ion pairing to the supporting electrolyte. A proposed structure for this ion paired complex is depicted in Figure 10.7. Noting that it is the addition of the sulphonate group to the anthraquinone structure that indirectly leads to the stabilisation of the semiquinone, the influence of the presence of TBA^+ upon the aqueous reduction of both anthraquinone and AQDS will likely be significantly different.

As demonstrated through controlling the concentration of the TBA^+ cation

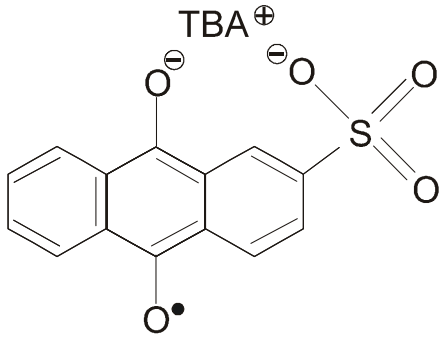

Figure 10.7: Proposed structure for the ion paired semi quinone intermediate.

Electrolyte (I = 0.1 M)	100% TBAOH	(60+40)% TBAOH + TMAOH	(20+80)% TBAOH + TMAOH	100% TMAOH	100% KOH
D / 10^{-6} cm^2s^{-1}	3.0	3.5	4.1	5.3	5.7

Table 10.1: Experimentally obtained diffusion coefficients of AQMS via steady-state currents.

it is possible to effectively 'tune' the potentials at which the first and second electron transfers occur, hence at high concentrations of TBAOH the concentration of the semiquinone formed at the electrode should be greater (due to the larger difference in potential between the first and second electron). It is important to note that due to the difference in formal potential between E_1 and E_2 this implies the feasibility of comproportionation occurring between the AQMS and $AQMS^{2-}$ species; however the voltammetric current system is blind to this mechanism. Previous work by Andrieux and Savéant showed under the conditions of fast electron transfers and equal diffusion coefficients of both parent and reduced species comproportionation mechanism is unobservable in conventional voltammograms.[16] This said, physically one predicts a significant increase in the concentration of the semiquinone species adjacent to the electrode surface.[17]

The influence of the presence of TBA^+ upon the AQMS mediated oxygen reduction was studied in order to help corroborate the conclusion that the observed shift in formal potentials is due to the relative stabilisation of the semiquinone intermediate. The electrochemical reduction of saturated oxygen was carried out

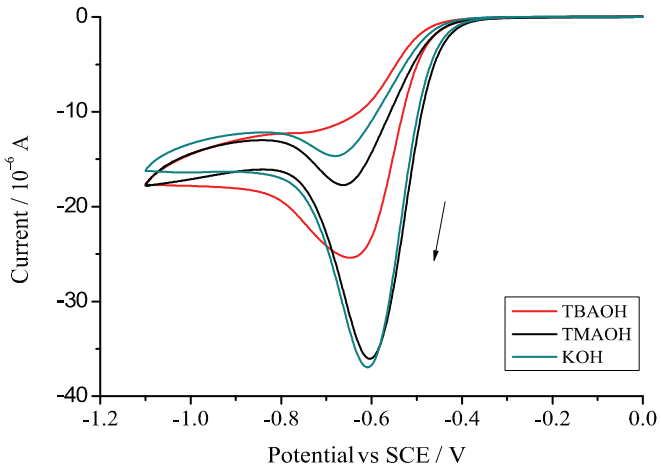

Figure 10.8: Cyclic voltammograms of oxygen reduction on BDD electrode (at 50 mVs^{-1}) in the presence of 5 mM AQ/H2O with various 0.1 M supporting electrolytes: TBAOH (red line), TMAOH (black line), and KOH (green line).

in a 5 μM AQMS aqueous solution supported by 0.1 M hydroxide salt with various counter-cation sizes. The voltammetric responses, depicted in Figure 10.8, show one irreversible wave for all three supporting electrolyte systems. Due to the lack of protonation of the reduced AQMS at the current pH, the electron transfer reaction between the quinone and oxygen are likely as follows;

$$\mathrm{AQMS}^{\cdot -} + \mathrm{O_2} \rightleftharpoons \mathrm{AQMS} + \mathrm{O_2^{\cdot -}} \tag{10.3}$$

$$\mathrm{AQMS}^{2-} + \mathrm{O_2} + \mathrm{H_2O} \rightleftharpoons \mathrm{AQMS} + \mathrm{HO_2^-} + \mathrm{OH^-} \tag{10.4}$$

As before, the mediated reduction at low over potentials likely proceeds via Equation 10.3, whereas at more negative over potentials the reduction proceeds via equation 10.4. Interestingly the current at high over potentials is – given the concentration of AQMS is an order of magnitude lower – *larger* as compared to the results obtained at lower pH. Hence, it would appear that protonation of the reduced species decreases the rate of electron transfer to oxygen. As can be seen from Figure 10.8, the use of TBAOH as the supporting electrolyte has a significant effect, where the peak current for the mediated reduction is significantly reduced

as is the 'reverse' peak. The decrease in the magnitude of the catalysed peak current likely reflects in part the decrease in the diffusion coefficient of AQMS in the presence of TBAOH. The diffusion coefficient in the presence of TBAOH is roughly 50% less than that found with alkali cations. Hence, on this basis the peak current may be predicted to decrease by ∼30% as observed experimentally (cf. $I_p \propto D^{0.5}$ with the assumption that the catalysed peak current is proportional to the concentration of AQMS able to diffuse to the electrode surface, this is however a major oversimplification as it ignores the influence of the oxygen concentration). However, importantly the corresponding decrease in the measured 'reverse' peak likely indicates that the reactivity of the semiquinone species has been correspondingly reduced as compared to the non-ion paired form.

10.3 Conclusions

Up to this point within the thesis the voltammetric simulations provided have been predicated on the basis that the formal potentials for the first and second electron transfer occurring at comparable potentials. Evidence for this was provided experimentally through the study of the measured peak current, which was found to be significantly smaller than would be expected if the two electron transfers were concerted. As a direct result of this, it is also predicted that a significant concentration of the semiquinone species will be formed at the electrode surface during the voltammetric scan. Evidence for the presence of the semiquinone species – and hence the validity of the simulation used – is provided within this chapter through studying the distinctive voltammetry associated with the mediated reduction of oxygen.

Experimentally, it is shown that under conditions where the oxygen in solution is in a large excess over the AQMS, such that the rate determining step is the reaction between the oxygen and the AQMS, a large and irreversible reduction

wave is observable. Importantly, in this situation the peak current is not related to the total consumption of the oxygen adjacent to the electrode. Alternatively, this voltammetric peak is explained in terms of the differing reactivites of the mono and di-reduced forms of the AQMS towards oxygen. The concentration of the semiquinone intermediate being produced is at a maximum at low over potentials during the voltammetric scan; hence, the mechanistic pathway relating to the one-electron reduction of oxygen via the semi quinone is observed to 'switch off' at higher voltages but returns at low overpotentials on the reverse voltammetric sweep. At neutral pH the simulation results provided directly demonstrate that the observed 'reverse' peak is a result of the higher reactivity of the semiquinone intermediate and the non-zero concentration of oxygen present at the electrode surface on the back sweep.

At higher pH the reactivity of the direduced form appears to be greater, as evidenced by the relatively large mediated current, implying that the protonation of the species decreases its reactivity. Furthermore, it is demonstrated that the formal potentials for the two electron transfer can be tuned through the use of alkylammonium cations. The cause of this change in the thermodynamics is ascribed as being due to ion pairing. Voltammetric evidence for the ion pairing is provided through study of the oxygen mediated reduction, whereby the reactivity of the semiquinone species is found to be reduced in the presence of the tetrabutlyammonium cation.

The search for optimal oxygen reduction catalysts can be seen to be dependent on finding a quinone/semiquinone/hydroquinone system in which the semiquinone is formed over a wide potential window and hence in which the two electron reductions are relatively more widely separated in aqueous solution. Similar conclusions may relate to the toxicity of anthracycline antibiotics, allowing the minimisation of the production of reactive oxygen species in biological systems,

this latter point shall be expanded upon in the following chapter.

References

[1] Melada, S.; Rioda, R.; Menegazzo, F.; Pinna, F.; Strukul, G. *J. Catal.* **2006**, *239*, 422–430.

[2] Minotti, G.; Menna, P.; Salvatorelli, E.; Cairo, G.; Gianni, L. *Pharmacol. Rev.* **2004**, *56*, 185–229.

[3] Singal, P. K.; Iliskovic, N. *N. Engl. J. Med.* **1998**, *339*, 900–905.

[4] Menna, P.; Salvatorelli, E.; Minotti, G. *Chem. Res. Toxicol.* **2010**, *23*, 6–10.

[5] Toghill, K. E.; Wildgoose, G. G.; Moshar, A.; Mulcahy, C.; Compton, R. G. *Electroanalysis* **2008**, *20*, 1731–1737.

[6] Koppenol, W.; Stanbury, D.; Bounds, P. *Free Radical Bio. Med.* **2010**, *49*, 317–322.

[7] Millero, F.; Huang, F.; Graham, T. *J. Solution Chem.* **2003**, *32*, 473–487.

[8] Han, P.; Bartels, D. M. *J. Phys. Chem.* **1996**, *100*, 5597–5602.

[9] McCreery, R. *Chem. Rev.* **2008**, *108*, 2646–2687.

[10] Seinberg, J. M.; Kullapere, M.; Maeorg, U.; Maschion, F. C.; Maia, G.; Schiffrin, D. J.; Tammeveski, K. *J. Electroanal. Chem.* **2008**, *624*, 151–160.

[11] Tammeveski, K.; Kontturi, K.; Nichols, R. J.; Potter, R. J.; Schiffrin, D. J. *J. Electroanal. Chem.* **2001**, *515*, 101–112.

[12] Bard, A. J.; Faulkner, L. R. *Electrochemical methods : fundamentals and applications*, 2nd ed.; Wiley: New York, 2001.

[13] Izutsu, K. *Electrochemistry in Nonaqueous Solution*; Wiley, 2009.

[14] Wain, A.; Wildgoose, G.; Heald, C.; Jiang, L.; Jones, T.; Compton, R. *Journal of Physical Chemistry B* **2005**, *109*, 3971–3978.

[15] Gamage, R. S. K. A.; McQuillan, A. J.; Peake, B. M. *J. Chem. Soc. Farad. Trans.* **1991**, *87*, 3653–3660.

[16] Andrieux, J. M., C. P.; Savéant *J. Electroanal. Chem.* **1970**, *28*, 339.

[17] Belding, S. R.; Limon-Petersen, J. G.; Dickinson, E. J. F.; Compton, R. G. *Angew. Chem. Int. Ed.* **2010**, *49*, 9242–9245.

Chapter 11

The Electrochemistry of Quinizarin Revealed Through its Mediated Reduction of Oxygen

Developing on from the work presented in the previous chapter, this current work aims to demonstrate how the mediated oxygen reduction pathway can be used to both investigate low concentrations of a quinone species and further provide biologically relevant information. This work was presented as an article in the *Proceedings of the National Academy of Sciences of the United States of America* 2011, 108, 19891-19895. The time and efforts of I.B. Dimov towards the production of the experimental results is both recognised and appreciated.

The anthracycline antibiotic family is known to contain some of the most effective chemotherapeutic drugs available; however, their use is hindered by their well-documented cardiotoxicity.[1,2] Although this toxicity is multifactorial, it is predominantly related to the production of reactive oxygen species (ROS) via interaction of the quinone functionality with iron (ferritin).[3] A large body of evidence exists implicating the production of ROS as being the primary cause of cardiomyopathy.[1] However, there has been a lack of success to date in improving clinical outcomes through the use of antioxidants and iron-selective chelators as cardiovascular protectants.[4] Significantly, recent research has also focused on the possibility of direct quinone mediated ROS production (Figure 11.1A). Within the heart the

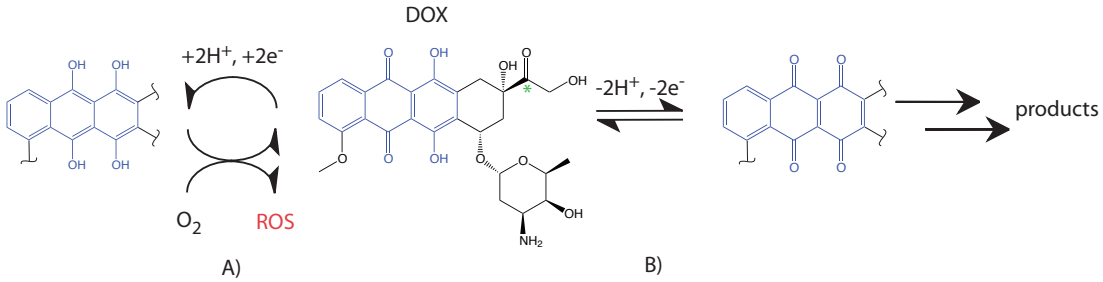

Figure 11.1: Schematic showing the structure of Doxorubicin (DOX) and highlighting the QZ moiety (blue). Systems A) and B) are the reduction and oxidation of the QZ moiety respectively, degradation pathway is not shown (cf. the text). The C-13 carbon has been labeled on the DOX species with a green star.

presence of H_2O_2, as formed from the reductive anthracycline redox cycling, may lead to degradation of the anthracycline species through its mediated oxidation via myoglobin (Figure 11.1B). Post oxidation, it is proposed that the molecule chemically decomposes leading to loss of its redox properties.[5] On the basis of this mechanistic route it has been proposed that finding a chemical species which enhances the rate of degradation of the anthracycline antibiotic within the heart may prove to be an effective cardioprotectant.[6] This work focuses on the chemistry of quinizarin (QZ), which is the redox-active moiety present in a variety of anthracycline antibiotics, including doxorubicin (DOX) as depicted in Figure 11.1.

The majority of the proposed mechanistic routes leading to necrosis of cardiomyoctes are related not to anti-tumoral activity (notably DNA intercalation and topoisomerase II inhibition) but commonly cite the involvement of the redox properties of the quinone moiety. As such one may expect electrochemistry to provide significant insights into the processes occurring. In fact this point was realised as early as 1979, when the newly produced 5-iminoduanorubicin was investigated electrochemically in order to confirm its lower reactivity towards oxygen reduction as compared to its parent molecule.[7] The further development and use of electrochemical techniques for investigation of the fundamental properties of

antharcycline antibiotics and their mimetics has been highly limited. It should be noted that the use of 5-iminodaunorubicin was clinically unsuccessful due to its increased myelotoxicity.[8]

Of the electrochemical methodologies available, voltammetry is a powerful experimental tool providing information about both the kinetics and thermodynamics of a system.[9] This said, the use of such procedures for investigating biologically relevant systems is often hampered due to sensitivity and selectivity issues and it may be this which has hindered their wider use within pharmacology. Limitation in sensitivity may be understood in terms of the magnitude of the capacitative current relative to the faradaic current; for a metallic macro-electrode the limit of detection for a diffusion only system is often confined to micro-molar concentrations, whereby at lower concentrations the faradaic current of interest will be smaller than the background capacitative current.[9] Given the large number of electroactive species present within most biological systems, voltammetric procedures are somewhat indiscriminate leading to complex results. These problems are in part overcome in this chapter in the same manner as the previous chapter- through the use of a BDD electrode. Importantly, for the present chapter the BDD electrode has been polished using an alumina slurry; the use of commercially available diamond polishing sprays was found to significantly reduce the level of adsorption to the electrode surface.

For the anthracycline antibiotics their electrochemical activity derives from the QZ moiety present within their structures (Figure 11.1, highlighted in blue). Hitherto, direct electrochemical study of this moiety has been restricted due to its relatively low solubility within aqueous media (2-5μM).[10] To date work studying the responses of quinones within aqueous media have regularly required addition of charged substitutents so as to enhance the solubility of the species and hence increase the analytical signal cf. the previous chapters.[11,12] However, as highlighted

the presence of these charged substituents can result in significant alterations of the quinones redox chemistry. This present study demonstrates how by harnessing the QZ mediated catalytic reduction of oxygen, it is possible to electrochemically investigate the system with solution phase QZ concentrations as low as 5nM (∼100 ppt). Further, the biologically significant properties of the QZ moiety are probed, specifically, DNA intercalation is demonstrated and in particular the oxidative destruction of the molecule seen.

11.1 Results and Discussion

The reduction of a quinone functionality either by a one or two electron process is known to produce reactive species which are able to readily reduce oxygen (Figure 11.1 system A) either to superoxide ($O_2^{\cdot -}$) or hydrogen peroxide (H_2O_2). When the reduction of the species occurs at an electrode surface this results in a catalytic cycle and voltammetrically, a large *irreversible* redox signal is observed.[13] The reduction of the QZ species upon a BDD electrode was investigated. The voltammetric response of a 2μM aqueous solution of QZ (0.1M KCl, 0.05M phosphate buffer, pH 6.84) was measured. It should be noted that due to the low solubility of the QZ molecule within solution the use of a teflon cell was required to avoid loss of material through adsorption onto glass surfaces, this problem was particularly pronounced at the lower concentrations. Moreover, stock solutions of 0.2 and 0.02 mM QZ in ethanol were prepared. Aliquots of these solutions were added to the aqueous buffer solution to achieve the low QZ concentration required. The potential was swept from -0.2 to -0.85V (vs.SCE) on a BDD electrode at variable scan rates. Figure 11.2 inlay a) depicts the voltammetric response in the presence and absence of QZ, the voltammetric wave at -0.55V (vs SCE) may be attributed as being related to the reversible reduction of the QZ species. It is proposed that due to the low solubility of QZ it readily adsorbs upon the BDD electrode surface. Sig-

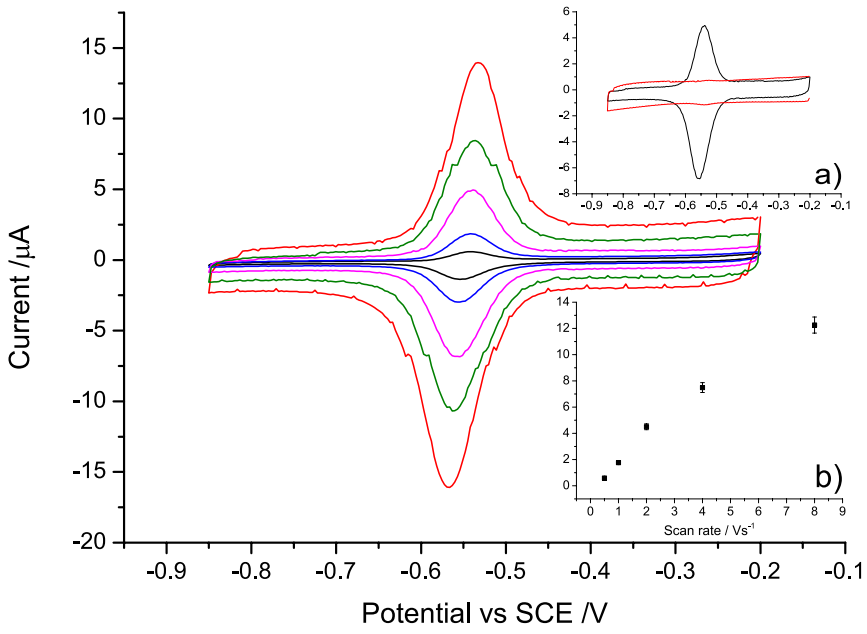

Figure 11.2: The voltammetric response of 2μM quinizarin in a N_2 degassed solution on a BDD electrode at variable scan rate 0.5 (black), 1 (blue), 2 (pink), 4 (green) and 8Vs^{-1} (red). Inlays, a) depicts the voltammetric response in the presence (black) and absence (red) of 2μM quinizarin (2Vs^{-1}), b) peak current of the oxidative wave as a function of scan rate (0.5-8 Vs^{-1}). A voltammetric data recorded in 0.1M PBS, pH 6.84.

nificantly, the forward and reverse peaks are not of equal magnitude, this difference is most prominent at the low scan rates and may be understood in terms of the mediated reduction of the residual oxygen present (estimated as $\sim$10μM) within the solution even after 'degassing.' In order to minimise the error occurring from the catalytic reduction of oxygen, the variable scan rate studies were performed only at relatively high scan rates 0.5-8Vs^{-1}. The variation in the oxidative peak height as a function of scan rate is shown in 11.2 inlay b). As can be seen the peak height varies with near linearity as a function of scan rate, thus implying that the voltammetric response is due to the reduction and oxidation of surface bound groups present upon the BDD surface. Deviations from linearity at high scan rates (8 Vs^{-1}) is likely a combined influence of the electron transfer becoming quasi-irreversible and also due to the influence of uncompensated resistance of the cell, leading to voltammetric distortions. The surface coverage of the QZ species at

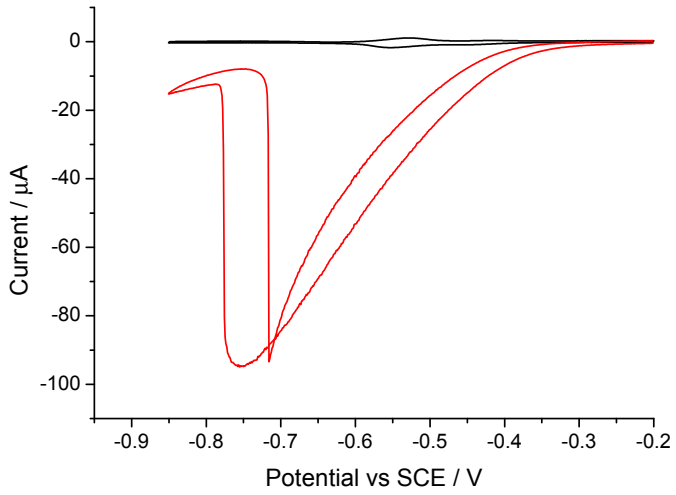

Figure 11.3: Voltammetric response for the reduction of QZ (480nM) in the presence (red) and absence (black) of oxygen, scan rate 0.5 V s^{-1}.

this solution phase concentration of 2μM can be measured as being 1.1±0.2 $\times 10^{13}$ molecules cm^{-2}.

Having ascertained that even at low concentration QZ readily adsorbs to the electrode surface, the influence of oxygen upon the system as investigated at a lower QZ concentration (480nm) where the potential was swept at a scan rate of 0.5Vs^{-1}, between -0.2V and -0.85V (vs SCE), as shown in Figure 11.3. In the absence of oxygen a small surface bound voltammetric peak was observed at -0.54 V (vs SCE) and again is ascribed to being the two-proton, two-electron reduction of the quinone. The direct reduction of adsorbed QZ is measurable until a solution concentration of roughly 200nM. From the charge under the surface bound voltammetric peak in the presence of 480nM QZ it is possible to estimate the surface coverage of the QZ molecule as being roughly 2.5±0.5 $\times 10^{12}$ molecules cm^{-2}. From X-ray crystallographic data the molecular volume is found to be ca. 260 $Å^3$.[14] Using estimated geometric dimensions we can calculate the expected full monolayer coverage of QZ upon the BDD surface to be 1.5-4.0$\times 10^{14}$ molecules cm^{-2}, depending on the orientation of the species (vertical or horizontal). Hence, this suggests that at 480nM the surface coverage of the QZ species, is roughly

0.5-2% of a full monolayer coverage.

In the presence of oxygen a large irreversible voltammetric feature is observed due to the mediated reduction of oxygen (Figure 11.1 system A). In this present study pure oxygen has been used, the application of the following procedures to in vivo studies will likely require the use of lower oxygen concentrations. Significantly, the voltammetric response exhibits a sharp 'switching-off' of the current at -0.776 V (vs SCE). It should be emphasised that the decrease in mediated current for the current example occurs at significantly higher over potentials than observed for the case exemplified by the *solution* phase AQMS. Furthermore, the alteration in the current occurs over a short potential region implying that it is not due to a change in the faradaic process cf. Chapter 10. This rapid shift is indicative of the presence of a phase transition; given that material is known to be adsorbed upon the electrode it is reasonable to conclude that this sharp voltammetric feature is related to a change in the orientation of the surface bound groups at more negative potentials. Further, this phase transition also clearly causes the catalytic redox cycle to become non-operative. This phase transition may be either the desorption of material or a change in alignment of the QZ upon the electrode surface, as is known for quinoline, aniline, and other organic species.[15,16] As the potential is decreased during the reverse scan the material returns to its original orientation switching on the mediated reduction pathway, leading to a rapid increase in current (-0.717 V (vs SCE)). Moreover, the voltammogram exhibits hysteresis in the potentials at which the phase transition occurs upon the forward and reverse scan. Given that the surface coverage of the QZ species is known to be very low (0.5-2%) and that if the QZ distribution upon the surface is assumed to be homogenous the redox centres may be expected to be ca. 2 nm apart. At such large interatomic distance interactions between the redox centres will be minimal, thus the rapidity of the phase change is likely caused by the presence of the 'negative differential

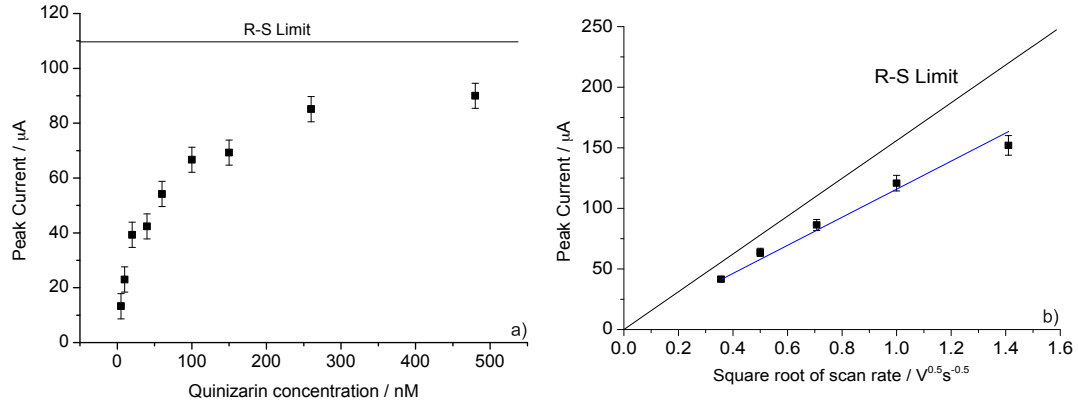

Figure 11.4: (a) variation in the peak current for the mediated oxygen reduction peak as a function of QZ concentration. (b) depicts the variation in the peak current as a function of the square root of scan rate (QZ = 480nM). R-S Limit indicates the classical Randles-Ševčík peak current for a two electron irreversible reduction ((n'+α_{RDS}) = 0.5).

resistance' leading to bistability within the electrochemical system.[17]

The mediated peak current was measured as a function of QZ concentration (Figure 11.4), where it was found that measurable peak currents were found for concentrations as low as 5nM (13.2±3.6 $\times 10^{-6}$A). At higher concentrations the peak current shows a plateau; this limiting of the current is not related to a limitation in the adsorption of the QZ on to the electrode surface. It was found that the voltammetric peak area for the non-mediated process varied linearly with QZ concentration beyond a value of 480nM, such that, as demonstrated above the surface coverage at a solution phase QZ concentration of 2μM is ∼4 times bigger than that found at 480nM. The limitation in the mediated process is more likely related to the consumption of the available oxygen. From literature it is known that the solubility of oxygen within the aqueous solutions is ∼1.24mM[18] and the diffusion coefficient has been measured as 1.77×10^{-5}cm^{2}s^{-1}.[19] Consider the Randles-Ševčík equation for an *irreversible* process,

$$i_p = (2.99 \times 10^5) A D^{0.5} C \nu^{0.5} n (n' + \alpha_{RDS})^{0.5} \tag{11.1}$$

where i_p is the peak current (amperes), A the area of the electrode (cm^2), D

is the diffusion coefficient (cm^2s^{-1}), C is the bulk concentration of the analyte (moles cm^{-3}), ν is the scan rate (Vs^{-1}), n is the total number of electrons, n' is the number of electrons transferred before the rate determining step (RDS) and α_{RDS} is the transfer coefficient for the rate determining step. The value of $(n' + \alpha_{RDS})$ has been set as 0.5 as measured experimentally from Tafel analysis (i.e. the first electron transfer is the rate determining step). The equation predicts that the maximum peak for the reduction of oxygen is $\sim 1.1 \times 10^{-4}$ A (this value is depicted as the horizontal line on the Figure 11.4 (a)). As can clearly be seen at relatively high concentrations of QZ the voltammetric peak current approaches the theoretical maximum. This conclusion is further corroborated by the fact that the peak current for the mediated oxygen reduction peak at 480nM is found to vary with the square root of scan rate (Figure 11.4 (a)). Further, as discussed above the surface coverage of the QZ at the higher concentrations ($\geq$ 200 nM) is known; consequently, it is possible to estimate through measurement of the charge passed for the mediated reduction pathway, that on the forward scan each QZ molecule present upon the surface is on average reduced $\sim$300 times.

Having investigated the fundamentals of the system, we address the QZ chemistry. The main accepted mode of chemotherapeutic action for the anthracycline antibiotics is through intercalation of the quinonal moiety into double stranded DNA and subsequent inhibition of the topoisomerase II enzyme.[20] In order to demonstrate the intercalative abilities of QZ, the voltammetric response of an oxygenated solution containing 60nM QZ was measured, in the presence of increasing concentrations of solution phase DNA, where the DNA is of $\sim$2000 base pairs in length. Figure 11.5 a), depicts the associated voltammograms under conditions in which there is zero (red) and 25μM (black) DNA. Clearly as the DNA concentration increases (Figure 11.5 b)) the measured voltammetric response for the mediated oxygen reduction decreases. This observed decrease is due to the

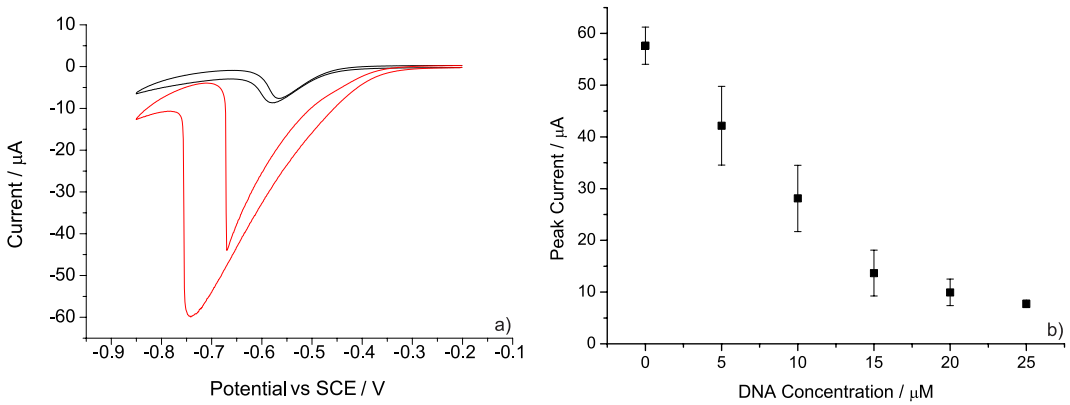

Figure 11.5: (a) depicts representative voltammograms for the mediated oxygen reduction in the presence of 0μM (red) and 25μM (black) DNA, scan rate 0.5 V s^{-1}. (b) depicts the influence of the concentration of DNA present in solution upon the QZ (60 nM) mediated oxygen reduction peak current.

sequestration of the QZ through intercalation. It is to be noted that this decrease in voltammetric response is not due to blocking of the electrode with increasing DNA concentration, as confirmed through the addition of higher concentrations of QZ to a 25μM solution of DNA upon which the mediated voltammetric signal returned.

It is of interest, that given the reported high binding constant for QZ with DNA,[21] a relatively large excess of DNA is required in order to '*titrate*' the QZ. This suggests that the adsorption of the QZ to the electrode surface is causing a decrease in the observed sensitivity of the system. This interference of the BDD electrode may be best understood in terms of both the pre-concentration of QZ on to the electrode surface and also the high number of available adsorption sites present upon the BDD. The pre-concentration of the QZ species upon the electrode increases the local *effective* concentration to roughly 0.6μM (based on an approximate diffusion layer thickness of 10μm). This is consistent with the QZ binding to roughly 1 in 40 DNA base pairs. Moreover, the QZ should not be expected to bind to the DNA in a 1 to 1 ratio due to the likely influence of longer range allosteric effects.[22,23] Further, if we assume that it is possible to attain a near monolayer

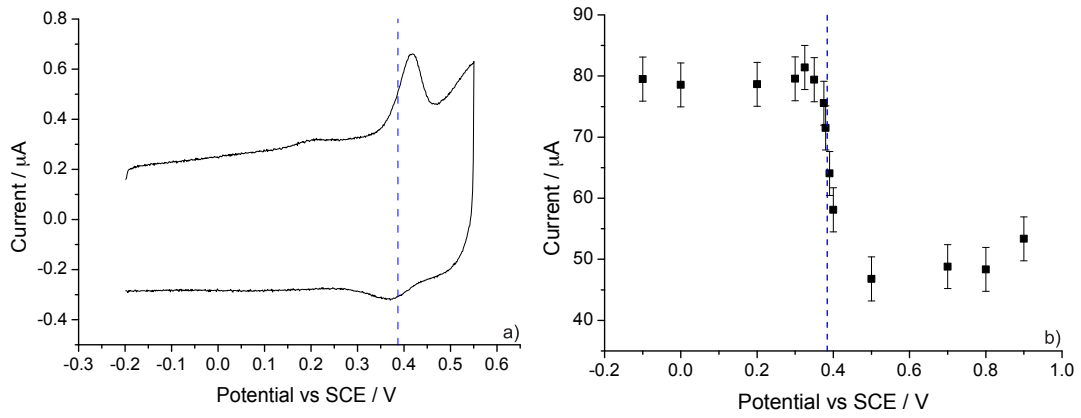

Figure 11.6: (a) depicts the voltammetric direct oxidation of the QZ adsorbed upon the BDD electrode (0.5 Vs^{-1}). (b) plot of the influence of the conditioning potential upon the QZ (480nm) mediated oxygen reduction peak current.

coverage of QZ then within the diffusion layer (10μm), the number of BDD sites as compared to the intercalative sites in the DNA will be greater even at DNA concentrations of 25μM and above. The presence of the non-zero peak current for the mediated oxygen reduction at high concentrations of DNA is also likely a result of the QZ adsorption. Even given this lower sensitivity towards DNA, this current electrochemical method exhibits significantly lower levels of detection than obtainable by comparable UV-Vis based methods,[21,24] this arises predominantly due to the ability to study far lower concentrations of QZ in this present work.

The main metabolic route for the removal of anthracycline antibiotic from the body is via reduction of the carbonyl group (C-13, as labeled on Figure 11.1),[25] but due to the presence of the hydroquinone group within the anthracycline (situated on the quinizarin) the species is also susceptible to oxidative degradation (Figure 11.1 system B). Biologically this reaction is known to occur both directly via oxidation through a peroxidase[26] or alternatively indirectly via the oxidised products of the enzymes.[27,28] Further it has been proposed that the oxidative degradation pathway of the anthracycline species may provide a possible route by which cardiac protection may be attained.[8]

The direct oxidation of the QZ species was investigated at the BDD electrode

in the presence of dissolved oxygen ($0.5 Vs^{-1}$). At relatively high QZ concentrations (480nM) the *irreversible* oxidation of surface bound species is observed with a half-wave potential of +0.386V (vs SCE), Figure 11.6 a), blue dotted line. This voltammetric feature corresponds to the $2e^-$, $2H^+$ oxidation of the hydroquinone group within the QZ structure (Figure 11.1 system B). At most experimentally measured scan rates, no back-peak is observed as the succeeding chemical steps leading the decomposition of the species are rapid. Only at higher scan rates does the evidence of a minimal reverse peak become apparent (as can be seen in Figure 11.6 (a)), this may be due to the direct reduction of the products or may also be related to the presence of electroactive decomposition products. The potential of the *irreversible* oxidative wave was measured as a function of pH where it was confirmed that the peak varied with ∼59mV/pH as such demonstrating that during the oxidation an equal number of protons and electrons are transferred, further corroborating the conclusion that the peak relates to the $2e^-$, $2H^+$ oxidation of the hydroquinone group.

In order to demonstrate that the oxidation of the species is both related to the QZ and further causes loss of the quinone species, the reductive voltammetric scan was performed (cf Figure 11.3) but additionally the system was preconditioned at a more positive potential for 15 seconds prior to running the voltammogram. The results of this can be seen in Figure 11.6 (b), where the conditioning potential has been varied between -0.1 – +0.9 V (vs SCE). As the potential is systematically increased there is a clear decrease in the measured reduction peak current upon the conditioning potential reaching the potential for the oxidation of the QZ species. This decrease occurs over a potential range of 130-170mV, hence it may be concluded that the electron transfer is quasi-reversible in nature. It should be noted that even at high conditioning potentials a non-zero peak current is measured. This current is related to the presence of unreacted QZ present upon

the electrode surface, which accumulates via diffusional replenishment after the oxidative potential has been applied. Furthermore, as demonstrated above only nanomolar quantities of QZ are required for a mediated reduction peak to be observed. Hence, this experiment has demonstrated that the observed voltammetric feature at +0.386 V (vs SCE) corresponds to the *irreversible* oxidation of the QZ species leading to its decomposition.

11.2 Conclusions

The use of electrochemical methods for the investigation of biologically relevant systems is often compromised by levels of low sensitivity and selectivity. We have experimentally demonstrated how, through harnessing the catalytic oxygen reduction mechanism, it is possible to electrochemically observe the presence of the poorly soluble molecule QZ in solution down to 5nM (∼100ppt). Further as QZ forms an active part of the anthracycline antibiotics, the measured electrochemistry gives insight into its biological function. Specifically, this work confirms that oxidation of the quinone functionality cause the degradation of the species and results in the mechanistic pathway which leads to the formation of ROS to be 'switched off.' This oxidation mechanism was found to be pH dependent confirming that the electrochemical mechanism is associated with proton transfer. This work has wider significance in that it provides direct evidence of the redox properties of the quinone functionality present within anthracycline antibiotics, if this oxidative degradation pathway can be exploited biologically and within the heart it has potential to decrease the cardiotoxicity of future chemotherapy treatments.

References

[1] Shi, Y.; Moon, M.; Dawood, S.; McManus, B.; Liu, P. P. *Herz* **2011**, *36*, 296–305.

[2] Outomuro, D.; Grana, D. R.; Azzato, F.; Milei, J. *Int. J. Cardiol.* **2007**, *117*, 6–15.

[3] Minotti, G.; Cairo, G.; Monti, E. *FASEB J.* **1999**, *13*, 199–212.

[4] Gianni, L.; Herman, E. H.; Lipshultz, S. E.; Minotti, G.; Sarvazyan, N.; Sawyer, D. B. *J. Clin. Oncol.* **2008**, *26*, 3777–3784.

[5] Menna, P.; Salvatorelli, E.; Minotti, G. *Chem. Res. Toxicol.* **2009**, *22*, 978–983.

[6] Menna, P.; Salvatorelli, E.; Minotti, G. *J. Pharm. Exp. Ther.* **2007**, *322*, 408–419.

[7] Lown, J. W.; Hsiao-Hsiung, C.; Plambeck, J. A.; Acton, E. M. *Biochem. Pharm.* **1979**, *28*, 2563–2568.

[8] Menna, P.; Salvatorelli, E.; Minotti, G. *Chem. Res. Toxicol.* **2010**, *23*, 6–10.

[9] Bard, A. J.; Faulkner, L. R. *Electrochemical methods: fundamentals and applications*; Wiley, 2001.

[10] Mukherjee, T.; Dodd, N. J. F. *Can. J. Chem.* **1984**, *62*, 1297–1298.

[11] Batchelor-McAuley, C.; Li, Q.; Dapin, S. M.; Compton, R. G. *J. Phys. Chem. B.* **2010**, *114*, 4094–4100.

[12] Guin, P. S.; Das, S.; Mandal, P. C. *J. Phys. Org. Chem.* **2010**, *23*, 477–482.

[13] Li, Q.; Batchelor-McAuley, C.; Lawrence, N. S.; Hartshorne, R. S.; Compton, R. G. *Chem Phys Chem* **2011**, *12*, 1255–1257.

[14] Swaminathan, S.; Nigam, G. D. *Curr. Sci.* **1967**, *36*, 541.

[15] Buess-Herman, C.; Gierst, L. *Electrochim. Acta* **1984**, *29*, 303–309.

[16] Holmqvist, P. *Anal. Chim. Acta* **1977**, *89*, 315–320.

[17] Krischer, K.; N., M.; Grauel, P. *Angew. Chem. Int. Ed.* **2001**, *40*, 850–869.

[18] Millero, F. J.; Huang, F.; Graham, T. B. *J. Solution Chem.* **2003**, *32*, 473–487.

[19] Han, P.; Bartels, D. M. *J. Phys. Chem.* **1996**, *100*, 5597–5602.

[20] Treszezamsky, A. D.; Kachnic, L. A.; Feng, Z.; Zhang, J.; Tokadjian, C.; Powell, S. N. *Cancer Res.* **2007**, *67*, 7078–7081.

[21] Gholivand, M. B.; Kashanian, S.; Peyman, H.; Roshanfekr, H. *Eur. J. Med. Chem.* **2011**, *46*, 2630–2638.

[22] Chaires, J. B. *Biochemistry* **1985**, *24*, 7479–7486.

[23] Chenoweth, D.; Dervan, P. *Proc. Nat. Acad. Sci. USA* **2009**, *32*, 13175–13179.

[24] Guin, P. S.; Das, S.; Mandal, P. C. *J. Sol. Chem.* **2011**, *40*, 492–501.

[25] Skarka, A.; Skarydova, L.; Stambergova, H.; Wsol, V. *Chem-Biol Interact* **2011**, *191*, 66–74.

[26] Reszka, K. J.; McCormick, M. L.; Britigan, B. E. *Free Radical Bio. Med.* **2003**, *35*, 78–93.

[27] Reszka, K. J.; McCormick, M. L.; Britigan, B. E. *Biochemistry* **2001**, *40*, 15349–15361.

[28] Reszka, K. J.; Britigan, L. H.; Britigan, B. E. *J. Pharm. Exp. Ther.* **2005**, *315*, 283–290.

Chapter 12

Voltammetry of Multi-Electron Electrode Processes of Organic Species

Although widely studied, in part due to their ubiquitous presence in the redox behaviour of organic and biological species, multielectron transfer reactions are sometimes poorly analysed. Multi-step processes encompasses a vast number of systems with highly diverse roles and applications, including DNA,[1,2] the nucleobases,[3] numerous pesticides and insecticides[4–6] neurotransmitters such as dopamine (and its derivatives),[7] and quinones,[8] among many others. This chapter aims to present a concise overview of the mechanistic points highlighted through out this thesis. This is undertaken so as to provide a more rigorous than hitherto theoretical basis upon which experimental investigation of multielectron transfer processes may be undertaken allowing greater insight into the commonly complex nature of multielectron redox events. The results and discussion presented herein comprise the majority of the article *Journal of Electroanalytical Chemistry* 2012, 669, 73-81.

Prior to discussing the analysis of voltammetric results we make a brief overview of the factors controlling the thermodynamics and kinetics of electron transfer. For a one electron transfer,

$$\mathrm{A} + \mathrm{e}^- \overset{k_1^o}{\rightleftharpoons} \mathrm{B} \qquad E_{f,1}^{\ominus}$$

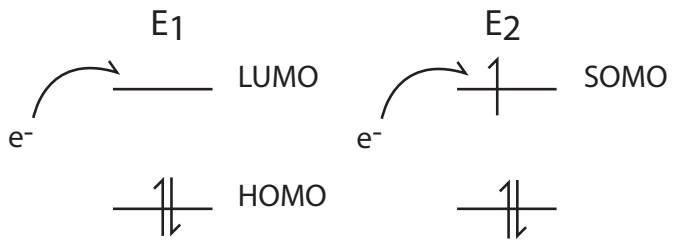

Figure 12.1: Schematic showing the addition of electrons to the frontier orbitals of an electroactive species.

the Nernst equation as shown below (Equation 12.1) describes the variation in the redox electrode potential as a function of the concentration of the oxidised and reduced species,

$$E = E_f^{\ominus} + \frac{RT}{F} ln \frac{[\mathrm{OX}]}{[\mathrm{RED}]} \tag{12.1}$$

where E is the redox potential (V), $E_f^{\ominus}$ is the formal electrode potential (V), R is the gas constant, T is the temperature (K), F is the Faraday constant and, [OX] and [RED] are the activities of the oxidised and reduced species respectively.

In order to gain insight into the relative magnitudes of the formal potentials for two sequential electron transfers to an organic species, consider the schematic of the frontier orbitals involved in the electron transfer as shown in Figure 12.1 for a reduction. It is clear that the first two electron transfer processes whether oxidation or reduction are likely to involve the same molecular orbital. For such a mechanism we may write the following equations;

$$\mathrm{A} + \mathrm{e}^- \overset{k_1^o}{\rightleftharpoons} \mathrm{B} \qquad E_{f,1}^{\ominus} \tag{12.2}$$

$$\mathrm{B} + \mathrm{e}^- \overset{k_2^o}{\rightleftharpoons} \mathrm{C} \qquad E_{f,2}^{\ominus} \tag{12.3}$$

where $\mathrm{E}_{f,1}^{\ominus}$ and $\mathrm{E}_{f,2}^{\ominus}$ are the formal potential for the first and second electron transfers respectively. Without significant structural change the energies associated with these frontier orbitals would remain relatively constant, except for changes

in molecular solvation, which can and often does lead to significant changes in energy.[9] In non-aqueous media the voltammetric difference in potential for the first and second electron is often of the order of 0.5 – 0.8V. This situation is commonly referred to as *normal* ordering of the electrode potentials, where the second electron transfer is significantly thermodynamically more difficult than the first, this is mainly a result of electrostatic repulsion.[10] For experiments in aqueous media this potential difference is commonly significantly compressed, to the extent that only one voltammetric wave may be observed.[11] Beyond the influence of solvation, ion pairing of the electro-active species can lead to significant alterations in the measured formal potentials. This was most clearly demonstrated recently in the systematic study of the role of *weakly coordinating anions* on the measured voltammetry of organometallic species by Geiger *et al.*.[12]

Electrochemical systems in which the electrode potentials are *inverted* i.e. the second electron transfer is thermodynamically easier than the first – even in the absence of a chemical step – are not uncommon. Such a situation has been shown to occur for a number of aromatic species including 3,6-dinitrodurene and derivatives of tetraphenylethylene.[13] The value of $\Delta E_f^{\ominus}$ ($= E_{f,2}^{\ominus}$-$E_{f,1}^{\ominus}$), gives a measure of the magnitude of the potential inversion, in the case of reduction this value is positive whereas for oxidation a negative value is obtained. The cause of such potential inversions is generally ascribed as being due to a change in the molecular structure which leads to a change in the energies of the frontier orbitals[13]. Alternatively, Savéant *et al.* have demonstrated how, for some polyconjugated systems potential inversion may arise solely due to a change in the solvation,[14] similar experimental results have been found by Amatore *et al.* with conjugated ferrocenes.[15] Following the work of Evans, if the potential inversion ($\Delta E_f^{\ominus}$) is greater or equal to 0.4V, then it is likely that the intermediate species is non-existent or is sufficiently short-lived that the electron transfers maybe viewed as being *effectively* concerted. In refer-

ring to the process as being 'concerted' it is implied that the intermediate(s) are non-observable and *not* that the two electrons are tunnelling simultaneously.[16] In regards to this point it is illuminating to look towards some biological systems, in particular enzymes including quinone redox systems. For such processes it would be highly expedient for the electrons to be transferred simultaneously, due to the deleterious effects of reactions involving the intermediates. However, even here evidence exists for the presence of intermediates.[17] Consequently within this current chapter and earlier within the thesis it is assumed that the electron transfers occur in a sequential and not a truly concerted manner.

Classically the rate of electron transfer is described via the well established Butler-Volmer equation, as shown in Equation 12.4 for the one electron process,

$$I = FAk^o \left(exp\left[\frac{+\beta F\eta}{RT}\right][B] - exp\left[\frac{-\alpha F\eta}{RT}\right][A] \right) \tag{12.4}$$

where I is the current (Amperes), F is the Faraday constant, A is the area of the electrode (cm^2), k^o is the standard rate of electron transfer (cm s^{-1}), R is the gas constant, T is the temperature (K), α and β are the transfer coefficients and $[i]$ represents the concentration of species i at the electrode surface. This expression is derived phenomenologically[18] but its routine use within the field reflects its repeated quantitative success in a diversity of applications. More modern approaches towards the understanding of electron transfer processes arose from work developed by Marcus and Hush.[19,20] Originally this work was developed for the description of solution phase electron transfers, where a molecular view of the system was taken. This theory has been adapted so that it is applicable to heterogeneous electron transfer, a significant difference being that due to the continuum of energy levels present within metallic electrodes the 'inverted region' is non-observable.[21] For heterogeneous electron transfer the rate is expected to limit

at high overpotentials; this result has been successfully demonstrated for surface tethered groups.[22] Although the use of Marcus-Hush theory allows the rate of electron transfer to be related to the reorganisation energy of the species involved and hence provides a physical model for understanding electron transfer, in practice its application in its simplest form has demonstrated limited qualitative improvement on the Butler-Volmer theory for solution phase voltammetry. Furthermore, recent work has exemplified cases in which Marcus-Hush theory provides a quantitatively poorer fit than the use of Butler-Volmer kinetics.[23,24] To this end, the present chapter continues in its analysis by only considering the Butler-Volmer model, due in part to its greater simplicity and in part to its established effectiveness.

The models presented throughout the thesis have been described by the nomenclature provided by Testa and Reinmuth, where 'E' (of Equation 12.1) stands to represent an electrochemical process and 'C' represents a chemical step.[25] Moreover, the majority of the model electrochemical systems are presented as reductions, the results obtained here are equally valid for oxidations (β replaces α). A final important comment must be made on the following analysis, in that it is assumed through out that adsorption processes are not significant, consequently the electron transfer process are taken as being 'outer-sphere' in nature. Inner-sphere reaction mechanism are particularly important in a number of electrocatalytic processes.[26] As recently highlighted by Bard, understanding inner-sphere electron transfer processes represents the next major challenge for the development and application of electrochemistry.[27]

12.1 Classical Tafel and Peak Current Analysis

This section aims to provide a résumé of the classical approaches to the analysis of mulielectron voltammetry. Tafel analysis is a powerful tool[28] which has long been utilised in electrochemistry as a means by which the rate determining step

(RDS) for an electrochemical processes may be readily deduced. Analysis of a voltammogram involves plotting $\ln|I|$ versus E (potential) for roughly the lower 50% of the peak current, noting, that the current near the voltammetric peak is influenced by depletion of material adjacent to the electrode and hence is not suitable for simple analysis (without mass transport correction). Furthermore, background correction is imperative so as to remove the non-faradaic contribution to the current from capacitance. In the irreversible limit and using Equation 12.4 we can see that for a one electron reduction a Tafel plot gives a straight line of gradient $-\alpha F/RT$, α is the transfer coefficient and may be viewed as a measure of the position of the transition state relative to the oxidised and reduced products. Conversely, for a fully reversible one electron transfer, it is possible to show through consideration of the Nernst equation that a Tafel plot will yield a straight line of gradient $-F/RT$ i.e. an 'apparent' α value of 1.[29]

Adding a second electron to the mechanism as described by Equations 12.2 and 12.3, leads to the situation becoming significantly more complex. Even in the absence of coupled chemical processes, we are presented with three possible situations. First, both electrons are fully reversible (and assuming the second electron transfer is significantly thermodynamically easier than the first, such that, $|\mathrm{E}^{\ominus}_{f,2}| < |\mathrm{E}^{\ominus}_{f,1}|$[30]), second, the second electron is the rate determining step (RDS), and third, the first electron is the RDS. The Tafel slopes of these three situations are equal to $-(n'+\alpha_{RDS})F/RT$, where n' is the number of electrons transferred prior to the RDS and α_{RDS} is the transfer coefficient of the RDS.[29] In this we are assuming that the steps occurring post the RDS are highly driven and the processes prior to the RDS are at equilibrium. For the three cases outlined above the corresponding values of $(n' + \alpha_{RDS})$ will be 2 (if we observe one voltammetric wave and $|\mathrm{E}^{\ominus}_{f,2}| < |\mathrm{E}^{\ominus}_{f,1}|$[30]), 1.5 and 0.5 respectively. In fact this expression $[-(n' + \alpha_{RDS})F/RT]$ holds for systems in which more than two electrons are passed, hence on this

basis from Tafel analysis we may determine the RDS for a multielectron transfer process. These results are derived on the basis that a macroelectrode is used where the diffusion to the surface is linear (one dimensional). The results for various mechanisms are summarised within Appendix B.1.

The peak current in a linear sweep voltammogram occurs at the potential where the RDS switches from the electron transfer to the mass transport of the species to the electrode. Further, Tafel analysis is a measure of how rapidly the rate of electron transfer increases as a function of potential. It follows that the peak current for a linear sweep voltammogram will reflect in part the gradient of the Tafel slope. This variation in the peak current can be expressed quantitatively via the well known Randles-Ševčík equations for both the reversible and irreversible limits, as derived using the results provided by Nicholson and Shain.[31] These equations parametrically describe the voltammetric peak height and form the basis of a large amount of analysis present within the literature.

$$\text{Reversible :} \qquad I_p = (2.69 \times 10^5) A D^{0.5} C \nu^{0.5} n^{1.5} \tag{12.5}$$

$$\text{Irreversible :} \qquad I_p = (2.99 \times 10^5) A D^{0.5} C \nu^{0.5} n (n' + \alpha_{RDS})^{0.5} \tag{12.6}$$

where I_p is the peak current (Amperes), n is the total number of electrons, A is the area of the electrode (cm^2), C is the bulk concentration of the analyte (moles cm^{-3}), D is the diffusion coefficient of reactant species A ($cm^2\ s^{-1}$), ν is the scan rate ($V\ s^{-1}$), n is the number of electrons transferred before the RDS, and α_{RDS} is the transfer coefficient of the RDS. This equation derives from the use of the Butler-Volmer equation. It should be highlighted that use of Marcusian kinetics does not predict the same dependency of the peak height upon the outlined parameters.[32] Further, in these equations one implicitly assumes that the processes prior to the RDS are at equilibrium and the electron transfer post the RDS are fully driven

(i.e. for a two electron transfer $|\mathrm{E}^{\ominus}_{f,2}| < |\mathrm{E}^{\ominus}_{f,1}|$). These equations show that the variation in the peak current with the number of electrons transferred is non-linear, contrary to what might be initially expected. The actual dependence on the number of electrons transferred reflects the combined influence in the change in charge passed and the increase in the Tafel slope. The variation of the peak current as a function of the number of electrons passed is exemplified for a number of mechanisms within Appendix B.1. The following section considers the influence of two formal potentials occuring at comparable potentials (i.e. $\mathrm{E}^{\ominus}_{f,1} \sim \mathrm{E}^{\ominus}_{f,2}$). This is studied in terms of the relatively simple mechanism of a two electron transfer (EE) and the variation in the peak height is taken as a measure of the change in the voltammetric response.

12.2 EE: the Case of Two Sequential Electron Transfers

For situations in which the transfer of two sequential electrons may be described by Equations 12.2 and 12.3, the corresponding cyclic voltammetric response of the system at a macroelectrode is found to exhibit a strong dependency upon the difference in potential for the first and second electron transfer. The voltammetric peak width, height and peak-to-peak separation is found to vary as a function of this difference in potential ($\Delta E^{\ominus}_{f}$). Historically, the parameters of peak width and peak-to-peak separation have been used as diagnostic criteria to deconvolute the potentials $\mathrm{E}^{\ominus}_{f,1}$ and $\mathrm{E}^{\ominus}_{f,2}$.[9,33] As above, the following two electron mechanism was considered,

$$\mathrm{A} + \mathrm{e}^- \overset{k^o_1}{\rightleftharpoons} \mathrm{B} \qquad E^{\ominus}_{f,1}$$

$$\mathrm{B} + \mathrm{e}^- \overset{k^o_2}{\rightleftharpoons} \mathrm{C} \qquad E^{\ominus}_{f,2}$$

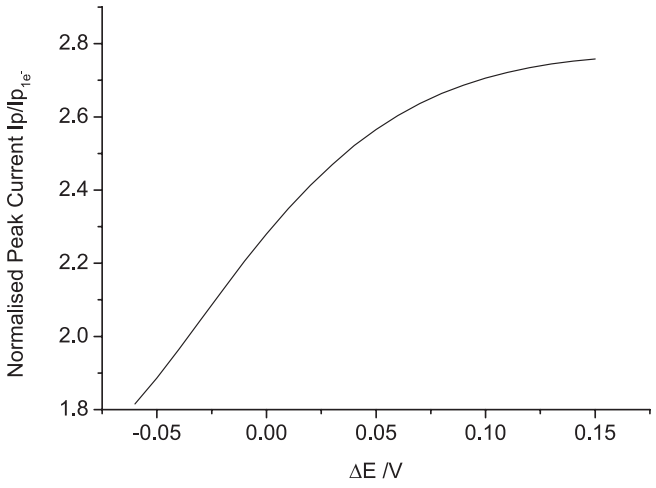

Figure 12.2: The variation in the peak current for a sequential reversible ($\Lambda = 32$) two electron processes as a function of $\Delta E_f^{\ominus}$.

the voltammetric response of this system was simulated using the commercially available software DIGISIM®, where the rate of electron transfer for both of the electron transfer was set as being reversible; $k_1^o = k_2^o = 0.2$ cm s^{-1}, D= 1×10^{-5} cm^2 s^{-1}, at a scan rate of 0.1 V s^{-1} i.e. equivalent to a Matsuda and Ayabe Λ value of 32. For a brief discussion as to what comprises electrochemical reversibility and its measure through Matsuda and Ayabe Λ values, see Appendix B.2. Figure 12.2 demonstrates how the peak height for this simulation, varies as a function of $\Delta E_f^{\ominus}$ (= $E_{f,2}^{\ominus}$ - $E_{f,1}^{\ominus}$). The peak current has been normalised against the peak height of a reversible one electron transfer i.e. it has been divided by $(2.69\times10^5)AD^{0.5}C\nu^{0.5}$. On this scale a two electron transfer is predicted by the reversible Randles-Ševčík equation (Equation 12.5) to have a value of 2.83 ($n^{1.5}$). Negative values of $\Delta E_f^{\ominus}$ imply that the potentials are ordered 'normally' i.e. the second electron transfer is thermodynamically more difficult than the first and positive values imply the the potentials are 'inverted.' For values of $\Delta E_f^{\ominus}$ that are more negative than $\sim$ -60mV a single voltammetric wave is observed but a clear inflection in the current occurs. As can be seen from Figure 12.2, when the value of $\Delta E_f^{\ominus}$ is zero for the given rate of electron transfer ($\Lambda = 32$) the peak current is

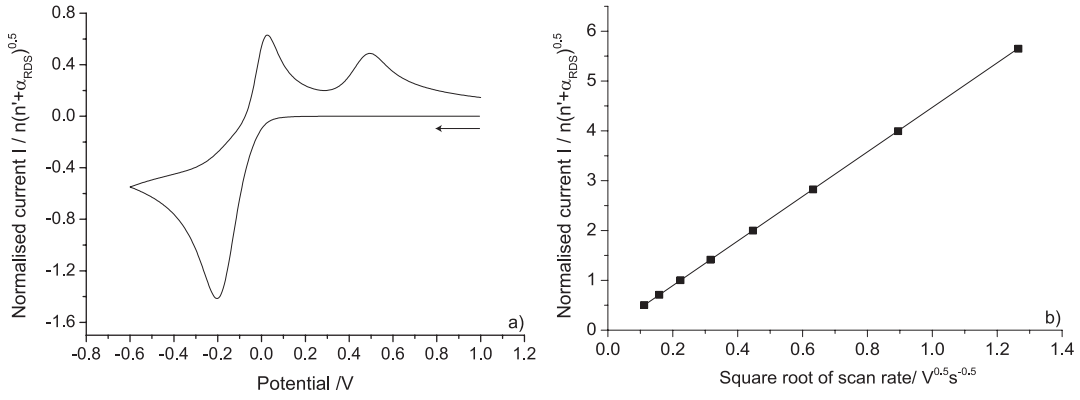

Figure 12.3: (a) depicts the simulated voltammogram for an $E_{irrev}E$ process and (b) depicts the variation of the peak current as a function of scan rate in comparison to the value given by the Randles-Ševčík equation $n = 2$, $n' = 0$ and $\alpha_{RDS} = 0.5$ (Equation 12.6). Arrow indicates scan direction.

ca. 80% of that predicted through the use Equation 12.5. This arises due to the significant probability of the one-electron reduced product (intermediate) diffusing away from the electrode before it is further reduced. Even at relatively high values of potential inversion (+0.15 V) the peak current is still not equivalent to that predicted for a fully reversible two electron process. This result is the first example in this chapter which demonstrates how the use of the Randles-Ševčík for a multielectron process may result in significant errors.

The above discussion views both of the electron transfers as being fully reversible. For the situation in which the first electron is the RDS (i.e. irreversible) then the Randles-Ševčík equation (Equation 12.6) is a reasonable approximation and accurately describes the peak current and its scan rate dependency. It should be noted that in such a situation one would expect to observe a single peak on the forward wave but two reverse peaks as depicted in Figure 12.3, where $E_1 = +0.15$V, $k_1^o = 1 \times 10^{-5}$ cm s^{-1}, $E_2 = 0$V, $k_2^o = 0.2$ cm s^{-1} and $\nu = 0.1$Vs^{-1}. In Figure 12.3 it can be seen that the peak current is equal to ∼1.4 on the normalised scale (current divided by $(2.99\times10^5)AD^{0.5}C\nu^{0.5}$), i.e. equal to $\mathrm{n}(n' + \alpha_{RDS})^{0.5}$ where $n = 2$, $n' = 0$ and $\alpha_{RDS} = 0.5$. Figure 12.3 (b) depicts the variation in the peak

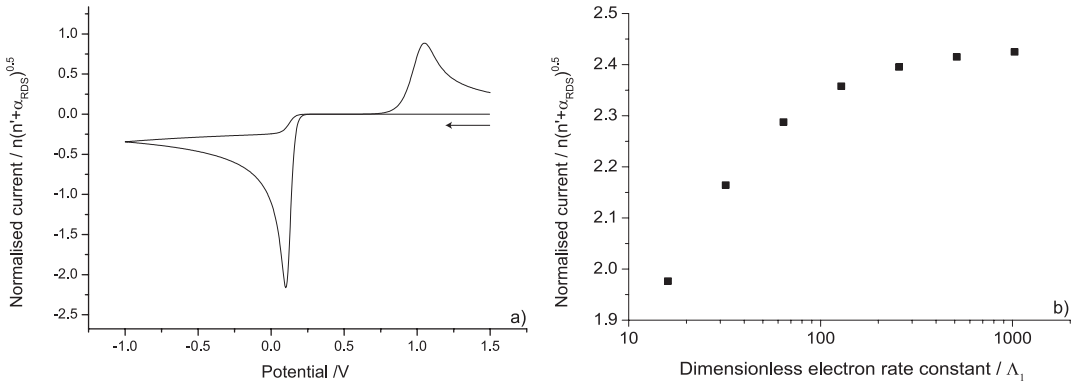

Figure 12.4: (a) the voltammetric response for an EE_{irrev} system and (b) is the variation in the forward peak current as a function of the dimensionless rate constant of the first electron transfer. Arrow indicates scan direction.

height as a function of the square root of scan rate (normalised against 0.1V s^{-1}) where good agreement between the simulation and the Randles-Ševčík equation can be seen.

More complex is the situation where the second electron transfer is the RDS, as depicted in Figure 12.4 (a) where $E_1 = +0.0$V, $k_1^o = 0.2$ cm s^{-1}, $E_2 = +0.7$V, $k_2^o = 1 \times 10^{-5}$ cm s^{-1} and ν=0.1Vs^{-1}. The same current normalisation has been used as in Figure 12.3. It is of note that to achieve a voltammetric system as depicted in Figure 12.4 a very large potential inversion is required due to the large magnitude of the overpotential relating to the second electron transfer. The more physically realistic situation when the potential inversion is less is considered below. The observed voltammetric response shown in Figure 12.4, is sensitive to the rate of electron transfer of the first reversible electrochemical process. Consequently even for values of Λ which are above 15, the simulated voltammetric peak is still significantly less than that predicted by Equation 12.6 as depicted in Figure 12.4 (b). Only at very high values of Λ does the peak tend towards the classical limit of n(n'+α_{RDS})$^{0.5}$ = 2.45. This is the second example of how for many systems the peak current is not described by the Randles-Ševčík equations.

12.3 The Influence of a Subsequent Chemical Step

Equation 12.6 has often been applied to provide expressions for the variation of the peak current in the presence of a chemical process. If the chemical step is rate determining then since the electrode potential does not affect the rate of a chemical reaction the sensitivity of the peak current to the experimental parameters simply reflects the number of electrons transferred before the RDS (ie. n'). Consequently for an ECE reaction where the chemical step is rate determining the Tafel slope ($-(n' + \alpha_{RDS})F/RT$) will have a value of -RT/F.[34] The results for more complex schemes are outlined in Appendix B.1. However, these simplifications can sometimes obfuscate the true dependence of the voltammetric response on the rate and equilibrium constant of the chemical process. In order to more clearly elucidate this matter the following simple electrochemical mechanism is considered;

$$\mathrm{A} + \mathrm{e}^- \overset{k_1^o}{\rightleftharpoons} \mathrm{B} \qquad E_{f,1}^{\ominus} \tag{12.7}$$

$$\mathrm{B} \underset{k_b}{\overset{k_f}{\rightleftharpoons}} \mathrm{C} \qquad K_{eq} \tag{12.8}$$

where k^o is the standard electrochemical rate constant and k_f and k_b are the forwards and backwards rate constants of the chemical step respectively such that $K_{eq} = k_f/k_b$. In an analogous manner to as outlined in Appendix B.2 for electron transfer rates, it is beneficial for the case in question to define a dimensionless parameter for the rate of the chemical step.

$$K_f = \frac{k_f}{\nu}\left(\frac{RT}{F}\right) \tag{12.9}$$

From simulation we can readily determine how the forward peak height for a voltammetric wave varies as a function of both K_{eq} and K_f, as is shown in Figure 12.5 where Λ has been given a value of 32. This value of Λ is equivalent to a k^o

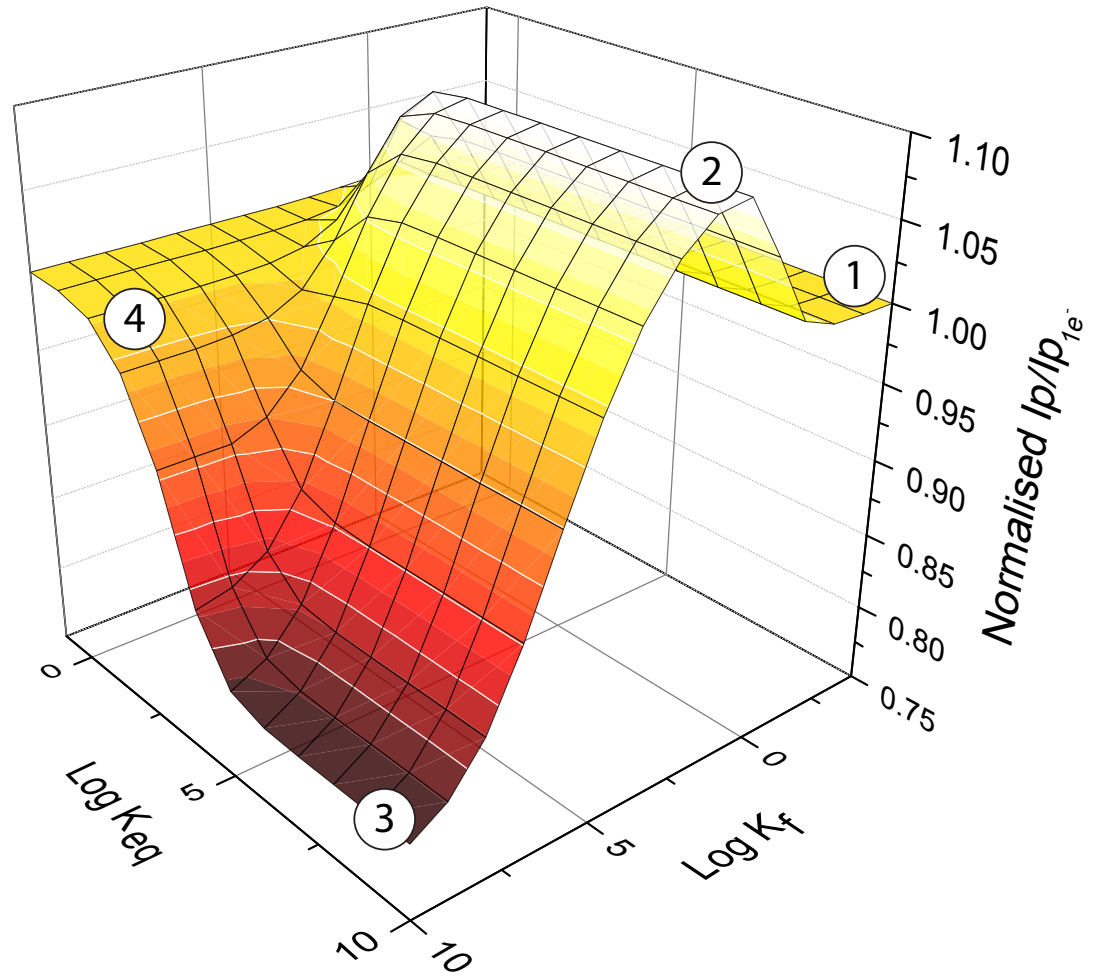

Figure 12.5: Plot demonstrating the variation in the peak current (I_p) for a voltammetric wave as a function of K_{eq} and K_f, $\Lambda = 32$

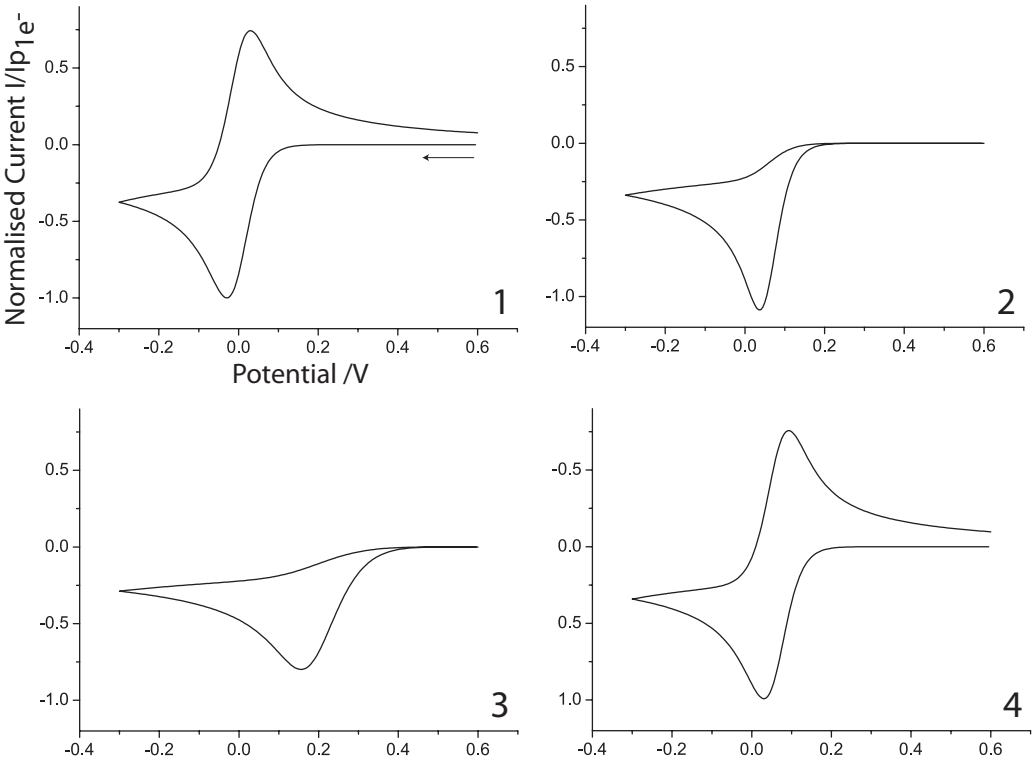

Figure 12.6: Voltammograms of the four representative voltammetric cases where for 1,2, and 3 K_{eq} equals 1×10^{10} and for 4 K_{eq} equals 10. The value of K_f is 1×10^{-4}, 1×10^{2}, 1×10^{10} and 1×10^{10} for cases 1,2,3 and 4 respectively. In all simulations Λ is equal to 32. Arrow indicates scan direction.

of 0.2 cm s^{-1} a D of 1×10^{-5} cm^2 $s^{-1}$and a scan rate of 0.1 Vs^{-1}. Such values are reasonable estimates for a number of organic species which exhibit relatively fast electron transfer kinetics.[35] Four representative cases have been exemplified and the corresponding voltammetric responses depicted in Figure 12.6. For both Figures 12.5 and 12.6 the current has been normalised against that of a reversible one electron transfer i.e. divided by $(2.69\times10^{-5})AD^{0.5}C\nu^{0.5}$. Situation 1 in Figures 12.5 and 12.6 is equivalent to an unperturbed one electron reduction. Hence, although the chemical step is highly driven, the rate of reaction is slow, such that, over the time frame of the voltammetric experiment the amount of B converted to C is negligible. As the rate of the reaction (K_f) increase the voltammetric response

tends towards the 'classical limit' where the peak current is close to equal to Equation 12.6, with n = n' = 1 and α_{RDS} is essentially zero. As the rate of the chemical step increases further and given that the simulations take into account the finite nature of the rate of electron transfer, the variation in the peak current for the EC reaction differs significantly from that predicted classically. This result represents the third example of deviation from the Randles-Ševčík equations, where the peak current decreases and tends towards the irreversible limit, as is shown in Figure 12.6 case 3. Thus for an apparently fully reversible electron transfer reaction, the chemical step may cause the electron transfer to appear electrochemically irreversible.[36] This arises due to the shift in the redox potential (E) to values significantly below the formal potential ($E_f^{\ominus}$) resulting in the rate of electron transfer being significantly below that of the k^o and hence causing the electron transfer to become rate limiting. This apparent electrochemical irreversibility can have a distinct effect on the observed voltammetric response as a function of scan rate, as discussed in the next section. The final example is case 4 in Figure 12.6, where the value of K_f is large but the value of K_{eq} is relatively low, here the peak current is close to that of the reversible one electron reduction but as can be seen in the formal potential for the redox species has been shifted in a Nernstian manner (ca. 59mV at 25°C). The above provides a discussion for an ECE mechanism, similar results would be expected for both DISP 1 and DISP 2. The results presented within this section are in agreement to those provided by Nadjo and Savéant[37] but importantly this text investigates the variation in the peak current, as opposed to the variation in the peak potential as a function of scan rate.

12.4 Non-linear I_p vs. Square root of Scan Rate Plots

For the above mechanistic examples, the peak current is predicted to vary linearly (within experimental error) as a function of square-root of scan rate. For a two

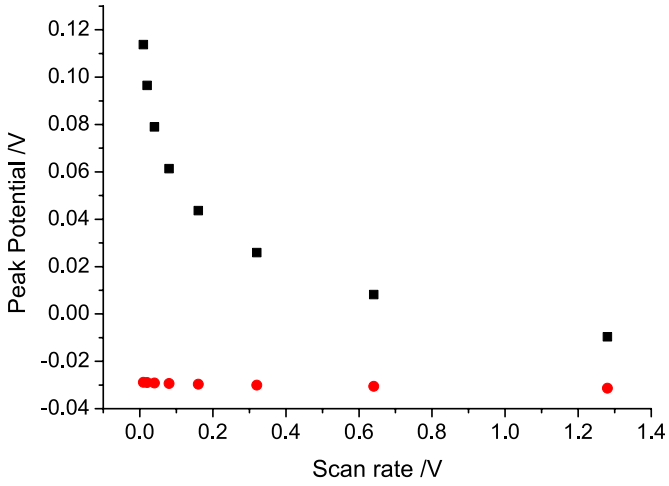

Figure 12.7: Variation in the peak potentials for one electron reversible (E), red circles, and irreversible (EC_{irrev}), black squares, electron transfer processes as a function of scan rate. Arrows indicate scan direction.

electron system in which the second electron transfer is irreversible, the variation in peak current may not be linear with the square root of scan rate. Before considering this situation further it is important to recognise that - unlike for a fully reversible process - for any irreversible electron transfer, as the scan rate is increased the peak potential shifts to higher over potentials. This result is graphically depicted in Figure 12.7, where the forward peak potential for a reversible (E_1= 0.0V and $k_o = 0.2$ cm s^{-1}) and for an irreversible EC_{irrev} reaction ($E_2 = -0.1$, $k_o = 0.2$ cm s^{-1}, $K_{eq} = 1{\times}10^{10}$ and $k_f = 1{\times}10^{10}$) are plotted as a function of scan rate. Further, as demonstrated above for the case of a two electron reversible electron transfer process, the relative potentials at which two voltammetric features occur has a significant influence on the observed voltammetric response. The voltammetric responses depicted in Figure 12.8 shows an example of a EEC_{irrev} process where the two electron transfer processes have the same parameters as given in Figure 12.7, hence due to the scan rate dependence of the second electron transfer the peak current also exhibits a scan rate dependency. This is the fourth example of how the voltammetric response may differ significantly from that described by the

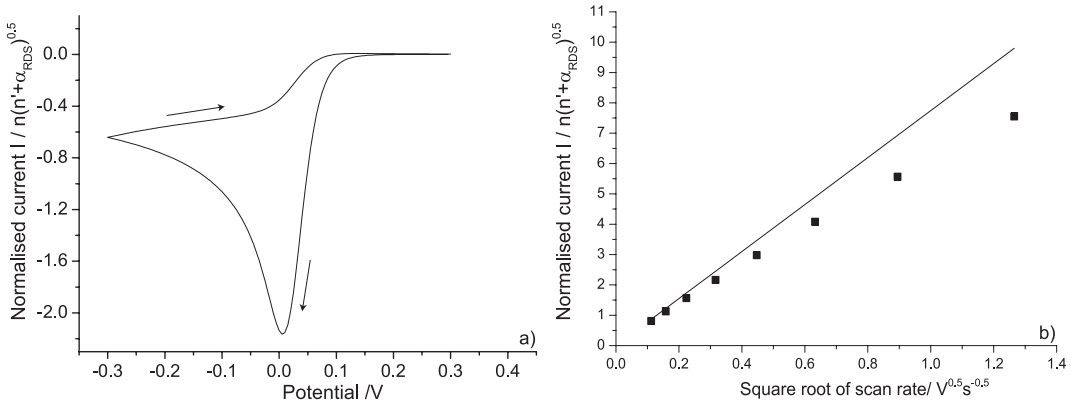

Figure 12.8: (a) the simulated voltammetric response for an EEC_{irrev} process $E^{\ominus}_{f,1}$= 0.0V, $k^o_1 = 0.2$ cm s^{-1}, $E^{\ominus}_{f,2}$ = -0.1V, $k^o_2 = 0.2$ cm s^{-1}, $\nu = 0.1 Vs^{-1}$, $K_{eq} = 1 \times 10^{10}$ and $k_f = 1 \times 10^{10}$. (b) depicts the variation in the peak current as a function of scan rate, where the solid line demonstrates the classically expected value as given by the Randles-Ševčík equation.

Randles-Ševčík equations.

12.5 Beyond the Randles-Ševčík Equations

As demonstrated by the above mechanistic examples, accurate description of the peak current by the Randles-Ševčík equations for multielectron transfers should perhaps be viewed as the exception! Hence, analysis of more complex mechanisms requires the use of simulations in order to extract physically significant information. A number of simulation software programs are commercially available and the results presented within this work were obtained through the use of DIGISIM®. Digisim is based upon a 'fast implicit finite difference' (FIFD) algorithm as developed by Rudolph *et al.*.[38,39] Given that it is necessary to have an accurate measurement of the diffusion coefficients in order to simulate the voltammetric response, a reliable method of measurement, which is independent of the electron transfer kinetics is required. This is best achieved through the use of a microelectrode, where under steady-state conditions the limiting current is fully described by the equation below,

$$I_{ss} = 4nFDCr \tag{12.10}$$

where I_{ss} is the steady state current (Amperes) and r_o is the electrode radius (cm) all other units are as before. Hence, one is able to asses the magnitude of the value of $n \times D$ independently of any influence of electrode kinetics. It should be noted that due to the relatively higher rates of mass-transport to the electrode surface as compared to that found under a linear diffusional regime, the rate of electrode fouling may be significantly greater and hence measurement of the steady-state current may not in some cases be experimentally viable.

12.6 Conclusions

This chapter has provided a résumé of the work presented in this thesis, presenting generalised results that may be applied to other organic electrochemical systems. The analysis has predominantly focused on the assessment of the system through study of the voltammetric peak height but in doing so the author has characterised a wide variety of possible experimental situations. The over riding message being that the Randles-Ševčík equations represent limiting cases and consequently are often unable to accurately describe multielectron processes. This arises mainly due to the fact that experimentally the potentials for multiple electron transfer processes are often comparable ($E^{\ominus}_{f,1} \approx E^{\ominus}_{f,2}$). Consequently subsequent electron transfers after the first are not necessarily highly driven. Four specific cases are highlighted where experimental results deviate significantly from that expected classically, these are as follows.

- When two or more electron transfers occur at comparable potentials the peak current is significantly less than that predicted by the Randles-Ševčík equation.

- For an EE_{irrev} reaction if the first electron is not totally reversible the observed peak current is less than predicted by the Randles-Ševčík equation.

- For an EC reaction, when the chemical step is fast the electron transfer becomes apparently electrochemically irreversible, leading to a distinct decrease in the peak current as predicted by the Randles-Ševčík equation.

- For EE_{irrev} and EEC_{irrev} reactions it is likely that the peak currents will not be linear as a function of the square-root of scan rate due to the scan rate dependency of the irreversible electron transfer.

As a consequence if multielectron transfer processes are to be investigated it is necessary that the voltammetric results are as a matter of routine *simulated* in order to achieve meaningful insights into the processes occurring.

References

[1] Oliveira, S. C. B.; Oliveira-Brett, A. M. *J. Electroanal. Chem.* **2010**, *648*, 60–66.

[2] Paleček, E. *Anal. Biochem.* **1988**, *170*, 421–431.

[3] Oliveira-Brett, A. M.; Piedade, J. A. P.; Silva, L. A.; Diculescu, V. C. *Anal. Biochem.* **2004**, *332*, 321–329.

[4] Fischer, J.; Dejmkova, H.; Barek, J. *Curr. Org. Chem.* **2011**, *15*, 2923–2935.

[5] Brimecombe, R. D.; Limson, J. L. *J. Agri. Food Chem.* **2006**, *54*, 8139–8143.

[6] Oudou, H. C.; Alonso, R. M.; Jiménez, R. M. *Electroanalysis* **2001**, *13*, 72–77.

[7] Bruns, D. *Methods* **2004**, *33*, 312–321.

[8] Hillard, E. A.; De Abreu, F. C.; Ferreira, D. C. M.; Jaouen, G.; Goulart, M. O. F.; Amatore, C. *Chemical Communications* **2008**, 2612–2628.

[9] Savéant, J. *Elements of molecular and biomolecular electrochemistry: an electrochemical approach to electron transfer chemistry*; Baker Lecture Series; Wiley-Interscience, 2006.

[10] Evans, D. H. *Chem. Rev.* **2008**, *108*, 2113–2144.

[11] Quan, M.; Sanchez, D.; Wasylkiw, M. F.; Smith, D. K. *J. Am. Chem. Soc.* **2007**, *129*, 12847–12856.

[12] Barriére, F.; Geiger, W. E. *J. Am. Chem. Soc.* **2006**, *128*, 3980–3989.

[13] Evans, D. H.; Hu, K. *J. Chem. Soc. Farad. Trans.* **1996**, *92*, 3983–3990, cited By (since 1996) 29.

[14] Hapiot, P.; Kispert, L. D.; Konovalov, V. V.; Savéant, J. M. *J. Am. Chem. Soc.* **2001**, *123*, 6669–6677.

[15] Amatore, C.; Gazard, S.; Maisonhaute, E.; Pebay, C.; Schöllhornand, J. L., B. Syssa-Magalé; J., W. *Eur. J. Inorg. Chem.* **2007**, 40354042.

[16] Evans, D. H. *Acta Chemic. Scand.* **1998**, *52*, 194–197.

[17] Cape, J. L.; Bowman, M. K.; Kramer, D. M. *Proc. Nat. Acad. Sci. USA* **2007**, *104*, 7887–7892.

[18] Bard, A. J.; Faulkner, L. R. *Electrochemical methods: fundamentals and applications*; Wiley, 2001.

[19] Marcus, R. A. *J. Chem. Phys.* **1956**, *24*, 966–978.

[20] Hush, N. S. *J. Chem. Phys.* **1958**, *28*, 962–972.

[21] Feldberg, S. W. *Anal. Chem.* **2010**, *82*, 5176–5183.

[22] Chidsey, C. E. D. *Science* **1991**, *251*, 919–922.

[23] Suwatchara, D.; Henstridge, M. C.; Rees, N. V.; Compton, R. G. *J. Phys. Chem. C* **2011**, *115*, 14876–14882.

[24] Henstridge, M. C.; Wang, Y.; Limon-Petersen, J. G.; Laborda, E.; Compton, R. G. *Chem. Phys. Lett.* **2012**, Accepted.

[25] Testa, A.; Reinmuth, W. *Anal. Chem.* **1961**, *33*, 1320–1324.

[26] Koper, M. T. M. *J. Electroanal. Chem.* **2011**, *660*, 254–260.

[27] Bard, A. J. *J. Am. Chem. Soc.* **2010**, *132*, 7559–7567.

[28] Reiger, P. H. *Electrochemistry, 2^{nd} Ed.*; Chapman and Hall, 1994.

[29] Compton, R. G.; Banks, C. E. *Understanding Voltammetry (2nd Edition)*; Imperical College Press, 2011.

[30] This only holds true when both potentials are of the same sign.

[31] Nicholson, R. S.; Shain, I. *Anal. Chem.* **1964**, *36*, 706–723.

[32] Henstridge, M. C.; Laborda, E.; Dickinson, E. J.; Compton, R. G. *J. Electroanal. Chem.* **2012**, *Accepted*.

[33] Myers, R. L.; Shain, I. *Anal. Chem.* **1969**, *41*, 980–.

[34] Fletcher, S. *J. Solid State Electrochem.* **2009**, *13*, 537–549.

[35] Rees, N. V.; Clegg, A. D.; Klymenko, O. V.; Coles, B. A.; Compton, R. G. *J. Phys. Chem. B* **2004**, *108*, 13047–13051.

[36] Streeter, I.; Jenkinson, S. F.; Fleet, G. W. J.; Compton, R. G. *J. Electroanal. Chem.* **2007**, *600*, 285–293.

[37] Nadjo, L.; Savéant, J. M. *J. Electroanal. Chem.* **1973**, *48*, 113145.

[38] Rudolph, M. *J. Electroanal. Chem.* **1994**, *375*, 89–99.

[39] Rudolph, M.; Reddy, D. P.; Feldberg, S. W. *Analytical Chemistry* **1994**, *66*, 589A–600A.

Conclusions

Organic redox species comprise an extensive group of compounds that are of interest for electroanalytical detection and study. One particular area of interest is the detection and quantification of DNA, a review of the current state-of-the-art electrochemical DNA detection methodologies was provided within this thesis. However, the production of highly sensitive electrochemical DNA sensors is commonly hindered due to fact that the associated voltammetric responses of organic species are invariably complicated due to both coupled chemical kinetics and surface interactions. Developing our understanding of the voltammetry of organic redox species is imperative for the development of evermore sensitive and selective analytical methodologies. Through the voltammetric investigation of the quinone moiety as a 'model' organic redox system, this thesis has demonstrated the highly diverse and environment sensitive (i.e. solvent and solute) nature of this class of electroactive species. Quinones play a prominent role in a variety of biological processes including the electron transport chain and as a substituent in a number of chemotherapeutic drugs. An overriding theme of this research is the importance of the relative magnitudes of the formal potentials associated with the electron transfer processes. It is shown that, even under aqueous conditions, the second electron transfer for the reduction of the anthraquinone species is more thermodynamically difficult than the first. Thus, this thesis highlights how the analysis of the voltammetric response through the use of classical equations, such as the Randles-Ševčík for peak height, leads to significant errors.

Chapter 4 investigates the influence of the graphitic substrate upon the experimentally measured electrochemical rate constant, where it is concluded that the rate of electron transfer for a series of outer-sphere redox species is influenced by the electronic properties of the solid. Beyond 'simple' electron transfer processes, coupled homogeneous chemical steps exert a strong influence upon the observed voltammetric response of a redox couple. This effect is illustrated primarily through the study of proton-coupled electron transfer. In Chapter 5 the reduction of anthraquinone is studied in aqueous buffered media across the full pH range. This system is successfully modelled through the use of a 'scheme of squares,' where the variation in both the peak height and position is accurately described. Significantly, to the best of the author's knowledge this was the first reported example of a *complete* scheme of squares for a two-proton two-electron system. Chapter 6 advances this work by studying the system under conditions of low buffer concentration. In a sufficiently low-buffered environment two reduction peaks may be observed for the anthraquinone reduction. These peaks do not correspond to 'two' one-electron transfers but are, instead, related to the consumption of protons at the electrode surface. These split waves were understood further through the application of the model produced in Chapter 5, allowing the variation in the pH adjacent to the electrode surface during the voltammetric experiment to be simulated.

The thermodynamic and kinetic properties of an electroactive species can be significantly altered upon adsorption to an electrode surface. The modification of graphite surfaces is considered in detail. Chapter 7 demonstrates how the pre-modification of a graphitic electrode with an organic solvent can alter the adsorptive nature of the surface without *significantly* altering its electrochemical activity. In Chapter 8, this work is developed further by investigation of the adsorption of anthraquinone-2-monosulfonate in greater detail. It is demonstrated

that the voltammetric response of the surface-bound species can yield information regarding the electrode's surface heterogeneity. Consequently, the conclusion reached is that the rate electron transfer for the 'basal' and 'edge' plane sites on the carbon surface differs by at least 2-3 orders of magnitude, where the rate is significantly slower on the basal plane sites. Chapter 9 takes a different approach towards adsorption and demonstrates how the process may be used in an analytical manner. A procedure is developed allowing the amount of surface adsorbed DNA to be effectively titrated, hence providing a method by which the solution phase DNA concentration may be analysed (LOD = 8.8μM).

It is found experimentally that the rate of electron transfer for a species at a boron-doped diamond surface is significantly less than that found at a metallic electrode. It is therefore possible to selectively electrochemically reduce (or oxidise) 'reversible' species preferentially over 'irreversible' species, and it is this property which allows the anthraquinone mediated reduction of oxygen to be directly investigated. Importantly, the observed voltammetric response for the solution phase species is indicative of the production of significant quantities of the semi-quinone intermediate. This is evidenced by the higher rate of electrocatalytic oxygen reduction at low overpotentials, thus validating the conclusion made in earlier chapters that the first and second electron transfers occur at comparable potentials. This methodology for studying electrocatalysis is later applied in Chapter 11 to the investigation of sparingly soluble antharquinone derivative quinizarin. This work not only permits investigation of the chemistry of quinizarin – namely its interaction with DNA and its oxidation – but also allows it to be electrochemically detected at concentrations as low as 5nM ($\sim$100ppt).

Finally Chapter 12, generalises the conclusions made within the thesis to provide a framework upon which the electrochemistry of other organic redox species may be understood. An important conclusion of this thesis is that, for multi-

electron transfer processes involving organic redox species, if meaningful information is to be extracted then the use of simulation is necessary.

Appendix A

A.1 Fick's Laws of Diffusion

This section addresses the derivation of Fick's second law which allows the concentration at a given point x to be described as a function of time. Given, Fick's first law in one dimension:

$$j = -D\frac{\partial[i]}{\partial x} \tag{A.1}$$

where j is the flux of the species D is the diffusion coefficient, $[i]$ is the concentration of species i and x is a point in one dimensional space. Consider the difference in flux at two different positions, separated by δx i.e. x and $x + \delta x$. Then the change in concentration between these two points can be defined as being equal to:

$$\delta n = [j(x) - j(x + \delta x)]\delta t \tag{A.2}$$

where t is time. Using a Taylor expansion it can be stated that:

$$\delta n \sim -\delta x \left(\frac{\partial j}{\partial x}\right) \delta t \tag{A.3}$$

and given

$$\delta[i] = \frac{\delta n}{\delta x} \tag{A.4}$$

therefore

$$\frac{\partial[i]}{\partial t} = -D\frac{\partial^2[i]}{\partial x^2} \tag{A.5}$$

Equation A.5 is Fick's second law of diffusion.

A.2 The Cottrell Equation

From Fick's second law, it is possible predict the flux at an electrode surface for a diffusion limited system. The is achieved easiest through using a dimensionless variable Γ:

$$\Gamma = \frac{x}{2\sqrt{Dt}} \tag{A.6}$$

In combination with A.5 this gives a second order differential equation, the integration of which yeilds:

$$\frac{d[i]}{d\Gamma} = aexp(-\Gamma^2) \tag{A.7}$$

where a is a constant of integration. Using suitable boundary conditions:

$$[i]_x = [i]\frac{2}{\sqrt{\pi}}\int_0^{\Gamma} \exp(-\Gamma^2)d\Gamma \tag{A.8}$$

this is normally written as:

$$[i]_x = [i]\,\mathrm{erf}\left(\frac{x}{2\sqrt{Dt}}\right) \tag{A.9}$$

The derivative of this equation in accordance with Equation A.1 yields the well known Cottrell equation. Used to describe the current for a chronoampergram at a macroelectrode as a function of time.

A.3 Capacitative Currents as a Function of Varying Potential

Assuming that the electrochemical interface can be modelled as an RC circuit, then using Kirchoff's law, the potential applied (E) to the system can be written as,

$$E = E_c + E_r \tag{A.10}$$

where E_c and E_r are the potentials held across the capacitor and resistor respectively. In a voltammetric experiment the applied potential varies as a function of time, $E = \nu t$, where ν is the scan rate. Using equation 1.1 and Ohm's law then the current may be written as:

$$I = \frac{dq}{dt} = \frac{\nu t}{R_s} - \frac{q}{AC_{dl}R_s} \tag{A.11}$$

where q is the charge passed and R_s is the magnitude of the resistor, for the case in question R_s can be viewed as the solution phase resistance. Equation A.11 is an first-order differential equation, solving this requires the use of an integrating factor. It follows that:

$$I = \nu AC_{dl}\left[1 - \exp\left(\frac{-t}{R_s AC_{dl}}\right)\right] \tag{A.12}$$

Appendix B

B.1 Tafel Plots for Multi-Electron Transfers

The following summary presents the classically expected Tafel slopes ($d\ln \mathrm{I}/d\mathrm{E}$) and the dependence of the peak current (I_p) on the number of electrons transferred for a range of different mechanistic situations. For the multi-electron processes it should be noted that in all cases it is assumed that all electron transfers which follow the RDS are highly driven.

Simple One Electron Transfer

For a one electron transfer the following mechanism can be written:

$$\mathrm{A} + \mathrm{e}^- \rightleftharpoons \mathrm{B}$$

For such a mechanism we predict the following Tafel slopes and dependency of the peak current on electron(s) transferred (see 12.5 and 12.6):

$$n = 1,\ n' = 0 \text{ (necessarily)}$$
$$\text{Tafel slope} = -\frac{RT}{\alpha F}$$
$$I_p \propto n$$

The transfer coefficient α has an 'apparent' value of 1 for an eletrochemically reversible process (fast electron transfer kinetics) and $\alpha \simeq 0.5$ for an irreversible process (slow electron transfer kinetics as compared to mass transport).

Overall Two Electron Transfer

For a two electron process we may write the following mechanism, with the electron transfers occuring sequentially:

$$\mathrm{A} + \mathrm{e}^- \rightleftharpoons \mathrm{B}$$

$$\mathrm{B} + \mathrm{e}^- \rightleftharpoons \mathrm{C}$$

Case (a), both electrons are fully reversible (EE) and assuming the second electron transfer is highly driven such that $|\mathrm{E}^{\ominus}_{f,2}|$ ¡ $|\mathrm{E}^{\ominus}_{f,1}|$?

$$n = 2,\ n' = 0$$

$$\text{Tafel slope} = -\frac{RT}{2F}$$

$$I_p \propto 2^{1.5}$$

Case (b)

i) The first electron transfer is the RDS,

$$n = 2,\ n' = 0$$

$$\text{Tafel slope} = -\frac{RT}{\alpha_1 F}$$

$$I_p \propto 2\sqrt{\alpha_1}$$

ii) The second electron transfer is the RDS,

$$n = 2,\ n' = 1$$
$$\text{Tafel slope} = -\frac{RT}{(1+\alpha_2)F}$$
$$I_p \propto 2\sqrt{1+\alpha_2}$$

Case (c), the E steps are separated by a chemical step (ECE)

$$\mathrm{A} + \mathrm{e}^- \rightleftharpoons \mathrm{B}$$
$$\mathrm{B} \rightleftharpoons \mathrm{B}'$$
$$\mathrm{B}' + \mathrm{e}^- \rightleftharpoons \mathrm{C}$$

The first and second electrochemical transfers are reversible and the chemical step is rate determining.

$$n = 2,\ n' = 1$$
$$\text{Tafel slope} = -\frac{RT}{F}$$
$$I_p \propto 2$$

Overall Four Electron Transfer

For a four electron transfer where after the first two electrons there is a chemical step we can write the following mechanism

$$\mathrm{A} + 2\mathrm{e}^- \rightleftharpoons \mathrm{C}$$
$$\mathrm{C} \overset{k_1}{\rightleftharpoons} \mathrm{C}'$$
$$\mathrm{C}' + 2\mathrm{e}^- \rightleftharpoons \mathrm{E}$$

Case (a), all electrons are fully reversible (EEEE) and the reaction is not limited by the chemical step

$$n = 4,\ n' = 0$$
$$\text{Tafel slope} = -\frac{RT}{4F}$$
$$I_p \propto 4^{1.5}$$

Case (b), A/C step is irreversible

i) 1st electron transfer is the RDS (A to B)

$$n = 4,\ n' = 0$$
$$\text{Tafel slope} = -\frac{RT}{\alpha_1 F}$$
$$I_p \propto n_{eff}\sqrt{\alpha_1}$$

where $2 < n_{eff} < 4$, as determined by the rate of k_1 as compared to the scan rate

ii) 2nd electron transfer is the RDS (B to C)

$$n = 4,\ n' = 1$$
$$\text{Tafel slope} = -\frac{RT}{(1+\alpha_2)F}$$
$$I_p \propto n_{eff}\sqrt{1+\alpha_2}$$

where $2 < n_{eff} < 4$, as determined by the rate of k_1 as compared to the scan rate

Case (c), the chemical step is rate determining

$$n = 4,\ n' = 2$$
$$\text{Tafel slope} = -\frac{RT}{2F}$$
$$I_p \propto n_{eff}\sqrt{2}$$

where $2 < n_{eff} < 4$, as determined by the rate of k_1 as compared to the scan rate

Case (d), C'/E is irreversible

i) 3$^{\text{rd}}$ electron transfer is the RDS (C' to D)

$$n = 4,\ n' = 2$$
$$\text{Tafel slope} = -\frac{RT}{(2+\alpha_3)F}$$
$$I_p \propto 4\sqrt{2+\alpha_3}$$

ii) 4$^{\text{th}}$ electron transfer is the RDS (D to E)

$$n = 4,\ n' = 3$$
$$\text{Tafel slope} = -\frac{RT}{(3+\alpha_4)F}$$
$$I_p \propto 4\sqrt{3+\alpha_4}$$

B.2 The Matsuda-Ayabe parameter

Here it is considered what 'parametrically' defines an electron transfer as being 'reversible' or 'irreversible' for an electron transfer at a macroelectrode. For a fully reversible redox reaction the concentration of the electroactive species at the electrode surface are at equilibrium, as described by the Nernst equation (1.5).

Using the results provided by Matsuda and Ayabe (*Z. Elecktrochem.* 1955, *59*,494) we may designate a dimensionless parameter Λ (for an linear sweep voltammogram) which is dependent upon k^o and is,

$$\Lambda = k^o \sqrt{\frac{RT}{D\nu F}} \tag{B.1}$$

such that, values of Λ greater than 15 signifies the electron transfer to be 'reversible' and values of Λ below 10^{-3} are 'irreversible'. It is clear from B.1 that the definition of the electron transfer as being reversible or irreversible is scan rate dependent. This result reflects the fact that the rate of electron transfer is finite and the extent of reversibility reflects the electron transfer kinetics relative to the rate of mass transport.